STRUCTURAL PERFORMANCE OF HIGH-STRENGTH REINFORCED CONCRETE BEAMS BUILT WITH SYNTHETIC FIBERS

By

Roukaya Bastami

Thesis submitted to the
Faculty of Graduate Studies and Research
in partial fulfillment of the requirements for the degree of
Master of Applied Sciences
in Civil Engineering

uOttawa

Department of Civil Engineering
Faculty of Engineering
University of Ottawa

Abstract

This thesis presents the results of a research program examining the effects of macro-synthetic fibers on the shear and flexural behaviour of high-strength concrete (HSC) beams subjected to static and blast loads. As part of the study, a series of seventeen fiber-reinforced HSC beams are built and tested under either quasi-static four-point bending or simulated blast loads using a shock-tube. The investigated test parameters include the effects of: macro-synthetic fibers, fiber hybridization, combined use of fibers and stirrups and longitudinal steel ratio and type.

The results show that under slowly applied loads, the provision of synthetic fibers improves the shear capacity of the beams by allowing for the development of yield stresses in the longitudinal reinforcement, while the combined use of synthetic fibers and stirrups is found to improve flexural ductility and cracking behaviour. The results also show that the provision of synthetic fibers delays shear failure in beams tested under blast pressures, with improved control of blast-induced displacements and increased damage tolerance in beams designed with combined fibers and stirrups. The study also shows that the use of hybrid fibers was capable of effectively replacing transverse reinforcement under both loading types, allowing for ductile flexural failure. Moreover, the use of synthetic fibers was effective in better controlling crushing and spalling in beams designed with Grade 690 MPa high-strength reinforcement. Furthermore, the results demonstrate that synthetic fibers can possibly be used to relax the stringent detailing required by modern blast codes by increasing the transverse reinforcement hoop spacing without compromising performance. As part of the analytical study, the load-deflection responses (resistance functions) of the beams are predicted using sectional (moment-curvature) analysis, as well as more advanced 2D finite element modelling. Dynamic resistance functions developed using both approaches, and incorporating material strain-rate effects, are then used to conduct non-linear single-degree-of-freedom (SDOF) analyses of the blast-tested beams. In general, the results show that both methods resulted in reasonably accurate predictions of the static and dynamic experimental results.

Acknowledgements

First and foremost, I must thank God Almighty for providing me with this great opportunity and facilitating the completion of this thesis.

I would like to express my sincere gratitude and appreciation to my supervisor Dr. Hassan Aoude for the continuous support throughout my master's study and research program, for his help, patience, motivation, encouragement, guidance and immense knowledge.

I would also like to express my gratitude and appreciation to Dr. Gamal Elnabelsya and Dr. Muslim Majeed for their continuous and precious assistance in the lab.

The advice of Dr. Beatriz Martin-Perez during the modelling process was also greatly acknowledged.

My deepest appreciation also goes to my colleagues Charlemagne Charles, Yang Li, Hyunchul Jung, Wesam Njeem, Jordan Gandia, Adel Barakati and Nima Aghniaey for making this thesis work possible through their continuous help during the construction and testing of the specimens. Without them, none of this would have been possible.

The assistance of Michael Chan and Fawwaz Ibrahim was invaluable.

The financial assistance provided by the National Sciences and Engineering Research Council of Canada (NSERC), the Ontario Graduate Student (OGS) and the University of Ottawa Excellence Scholarship was highly appreciated.

Finally, I would like to thank my mother, my father and my siblings for inspiring me to follow my dreams, for their continuous encouragement and incredible support and for always believing in me. This thesis could not have been completed without them.

Notations

Symbol	Definition
A	Area impacted by the blast pressure
A_b	Area of steel rebar
A_u	Toughness
A_{85}	Toughness corresponding to displacement when load reached 85% of peak load
A_{max}	Toughness corresponding to maximum displacement
d	Section depth
d_b	Steel reinforcement bar diameter
d_f	Fibre diameter
E_c	Modulus of elasticity, plain concrete
E_f	Modulus of elasticity, fiber-reinforced concrete
E_s	Modulus of elasticity, steel
f'_{ct}	Peak fiber-reinforced concrete tensile stress
f'_c	Compressive concrete strength
$f_{e,3}$	Equivalent flexural strength
f_s	Steel stress
f_{sh}	Steel strain hardening stress
f_u	Steel ultimate stress
f_y	Steel yield stress
F_{be}	Bond efficiency of fiber
I_r	Reflected impulse
K	Stiffness
K_{LM}	Load-mass transformation factor
l_f	Fibre length
l_p	Plastic hinge length
m	Total mass of the system
M_{fl}	Moment capacity
P_d	Driver pressure
P_r	Reflected pressure
P_{anls}	Analytical ultimate load
P_{fl}	Flexural load capacity
P_v	Shear load capacity
P_{max}	Experimental ultimate load
R	Resistance of the member
t_P	Positive phase duration
u	Deflection at mid-height
$\ddot{u}$	Acceleration at mid-height

V_f	Fibre volume ratio
ε_y	Steel yield strain
ε_r	Steel rupture strain
ε_{sh}	Steel hardening strain
ε_u	Steel ultimate strain
ε_y	Steel yield strain
$\dot{\varepsilon}$	Dynamic strain rate
$\dot{\varepsilon}_s$	Static strain rate
δ_{anls}	Analytical mid-span displacement
δ_{max}	Experimental mid-span displacement
θ_{max}	Maximum support rotation
ϕ	Curvature
τ_{bond}	Matrix bond strength
Δ_y	Displacement at yielding of reinforcing bar
Δ_{85}	Displacement when load reached 85% of peak load
Δ_{res}	Residual displacement
Δ_{max}	Maximum displacement

Acronyms

Acronym	Definition
ACI	American Concrete Institute
ASTM	American Society of Testing and Materials
CMOD	Crack mouth opening displacement
CSA S850	Canadian Standards Association for the design and assessment of buildings subjected to blast loads
CTOD	Crack tip opening displacement
DIF	Dynamic increase factor
F	Flexural crack width
FE	Finite element
FEA	Finite element analysis
FRC	Fiber-reinforced concrete
FRP	Fibre-reinforced polymer
HS	High-strength (steel reinforcement)
HSR	High-strength reinforcement
HSC	High-strength concrete
HSFRC	High-strength fiber-reinforced concrete
HSS	Hollow steel section
HYB	Hybrid fibers
HYFRC	Hybrid fiber-reinforced concrete
LTD	Load transfer device
LVDT	Linear variable displacement transducer
MASF	Macro-synthetic fibers
MISF	Micro-synthetic fibers
MMFX	Microcomposite multistructural formable steel
NS	Normal-strength (steel reinforcement)
NSC	Normal-strength concrete
PP	Polypropylene
PVA	Polyvinyl alcohol
SA	Sectional analysis
SCC	Self-consolidating concrete
SDOF	Single-degree-of-freedom
SFRC	Steel fiber-reinforced concrete
SNFRC	Synthetic fiber-reinforced concrete
SHPB	Split Hopkinson Pressure Bar
TNT	Trinitrotoluene

Table of Contents

List of Figures

List of Tables

Chapter 1: Introduction

1.1 General

Concrete structures subjected to severe loads such as blast, impact or earthquakes are vulnerable to fail suddenly without warning. Indeed, many recent earthquakes (e.g. Haiti, Mexico City and others) as well as terrorist attacks (e.g. Oklahoma City Bombing) have demonstrated the devastating effects of extreme loads on concrete structures, which can lead to loss of life as well as severe economic losses. Design considerations accounting for the mitigation of blast loads on such structures have become a major concern in order to ensure the public's safety.

High-strength concrete (HSC) is a material that has seen rapid growth in the past few decades, and is now commonly used in building and bridge applications. HSC may be defined as concrete which has a compressive strength greater than 60 MPa. Despite its advantages which include enhanced strength and stiffness, HSC also has negative features, which include brittle behavior in compression and poor tensile resistance. These brittle properties, along with HSC's poor fragmentation resistance, can raise concerns about the safety and ductility of structures built with this material when exposed to extreme loading. The use of fibers is one potential solution to increase HSC's toughness in compression, while also allowing for increased tensile resistance and improved fragmentation resistance. These enhanced qualities make high-strength fiber-reinforced concrete better suited for the design of structures exposed to impact and blast loads.

While important research is available on the impact and blast performance of fiber-reinforced concrete, most previous tests have focussed on steel fibers. Recently, there has been increased interest in the potential of using synthetic fiber-reinforced concrete (SNFRC) in structural applications. Macro-synthetic fibers, which are larger and coarser than traditional micro-synthetic fibers, can provide concrete with similar toughness and resistance to steel fibers. The improved toughness and fragmentation resistance of SNFRC make it well-suited to increase the damage tolerance of high-strength reinforced concrete members subjected to blast loads.

This thesis presents the results of a combined experimental and analytical study which aims at better understanding the influence of macro-synthetic fibers on the behaviour of high-strength reinforced concrete structures exposed to both static and dynamic loads, with a particular focus on high-strength concrete beams.

1.2 Research Objectives

This thesis aims at examining the potential of using macro-synthetic fibers to improve the flexural and shear behavior of high-strength concrete beams subjected to both quasi-static and extreme blast loading. This objective is achieved by testing a series of large-scale beams built with fiber-reinforced high-strength concrete under four-point bending and simulated blast loads using a shock-tube. The study also examines the influence of various design variables including the

ability of fibers to replace transverse reinforcement, the combined use of fibers and stirrups, as well as the effects of hybrid fibers, longitudinal steel ratio and longitudinal steel type. In addition, the research aims at examining the ability of both sectional analysis and more advanced finite element modelling to predict the static and dynamic responses of reinforced concrete beams built with macro-synthetic fibers.

1.3 Scope

As part of this study, seventeen beams are built and tested. Nine beam specimens are tested under quasi-static four-point bending, while the remaining eight beams are tested under simulated blast loads using the University of Ottawa shock-tube. The design parameters investigated in the study include:

- The effect of macro-synthetic fibres, with companion beams built with and without fibers;
- The effect of hybrid fibers, with beams built with 0.75% synthetic fibers or a hybrid mix of 0.75% synthetic fibers and 0.25% steel fibers;
- The effect of combined use of fibers and stirrups, with companion beams built with and without shear reinforcement;
- The effect of longitudinal reinforcement ratio, with beams constructed with either 2-15M or 2-20M normal-strength (400 MPa) bars;
- The effect of steel reinforcement type, with companion beams built with normal-strength (400 MPa) and high-strength (690 MPa) steel bars;
- The ability of macro-synthetic fibers to relax blast detailing, with companion beams detailed with different hoop spacings (s = 100 mm and s = 50 mm).

For the static tests, the responses of the specimens are assessed in terms of: failure mode, maximum load-carrying capacity, maximum displacement, ductility and toughness. The performance criteria for the dynamic tests are assessed based on: maximum and residual mid-span displacements, magnitude of blast pressure at failure and failure mode, and damage tolerance including crack control and secondary fragmentation.

This research also includes a comprehensive analytical study which aims at: 1) predicting the flexural and shear capacities of the beams using various equations proposed in the literature, 2) simulating the static and dynamic resistance functions of the beams using sectional analysis and finite element modelling, and 3) predicting the dynamic responses of the beams using non-linear single-degree-of-freedom (SDOF) analysis.

1.4 Thesis Breakdown

This thesis contains nine chapters as shown in **Figure 1-1**, and is divided as follows:

Chapter 1 – Introduction

- Introduces the significance of the thesis, presents the research objectives, and defines the scope.

Chapter 2 – Literature Review

- Provides background information regarding the thesis topic and summarizes previous research on the static, impact and blast performance of reinforced concrete beams and structural components constructed with synthetic fibers and fiber-reinforced concrete materials.

Chapter 3 – Experimental Program

- Describes the experimental program, including an overview of the test matrix, specimen design details, material parameters, test setups and testing protocols.

Chapter 4 – Experimental Results of the Static Tests

- Presents and describes the individual behaviour of each of the beams tested under quasi-static loading with the results presented in terms of load-deflection response.

Chapter 5 – Experimental Results of the Shock-Tube Tests

- Summarizes the detailed results from the dynamic experimental program with the results presented in terms of pressure-displacement time histories.

Chapter 6 – Discussion of Static Experimental Results

- Discusses the effects of various parameters including the effects of macro-synthetic fibers, hybrid fibers and steel reinforcement type on the quasi-static behaviour of the FRC beams.

Chapter 7 – Discussion of Dynamic Experimental Results

- Summarizes key observations from the blast tests regarding the effects of macro-synthetic fibers, hybrid fibers, longitudinal reinforcement ratio and type.

Chapter 8 – Prediction of Static & Dynamic Response

- Compares the flexural and shear strength predictions performed using various models;
- Explains the procedure implemented to predict the static and dynamic response of the specimens using sectional analysis, finite element analysis (FEA) and single-degree-of-freedom (SDOF) modelling;

- Summarizes the analytical predictions along with a comparison between the experimental and analytical response regarding various aspects.

Chapter 9 – Conclusion & Recommendations

- Summarizes the conclusions from the research program and proposes recommendations for further research.

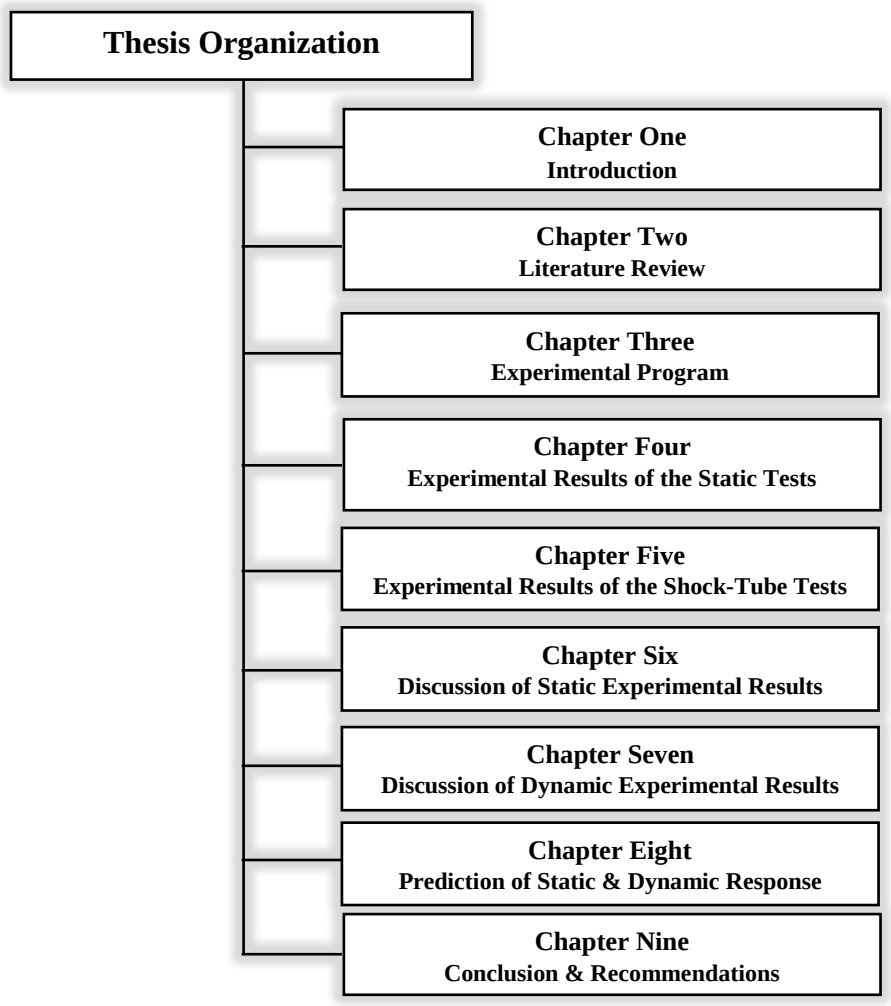

Figure 1-1 Thesis organization

Chapter 2: Literature Review

2.1 Chapter Overview

This chapter provides a literature review related to the thesis research topics. The first section presents an introduction to macro-synthetic fibers (MASF) and the effect of such fibers on key concrete properties. The next section reviews previous research on the shear and flexural behaviour of synthetic fiber-reinforced concrete (SNFRC) beams under static loading. The final section reviews previous research which has examined the effects of synthetic fibers on the material and structural response of concrete under impact and blast loads.

2.2 Macro-Synthetic Fiber-Reinforced Concrete

2.2.1 Synthetic Fibers

The addition of fibers in concrete improves many of its properties, including its tensile resistance, post-cracking capacity and flexural toughness. Over the years, extensive research has examined the behavior of fiber-reinforced concrete (FRC), both at the material and structural level. As result of this research, several codes worldwide (ACI 318, fib Model Code) now include provisions that allow for the use of fibers in certain structural applications, including in beams. However, the majority of this research has focussed on steel fibers.

Recently, there has been renewed interest in the use of synthetic fibers in concrete structures. Synthetic fibers can be varied in their composition (e.g. polyethene (PE), polypropylene (PP), polyvinyl alcohol (PVA), polyester (PES), acrylics (PAN), polyamides (PA), aramid and carbon), geometry and physical characteristics (Zheng & Feldman, 1995). The physical properties corresponding to the different types of synthetic fibers are summarized in **Table 2-1**. **Table 2-2** shows the properties related to durability. Among the mentioned types, polypropylene (PP) fibers are the most widely used as they don't influence concrete water requirements.

These fibers are available in three physical forms: monofilament, fibrillated or both as shown in **Figure 2-1**. Unlike monofilament fibers which are smooth, fibrillated fibers can provide efficient mechanical anchorage to the cement paste due to their ability to evenly disperse (Laning, 1992). Synthetic fibers can be further classified into two categories based on dimensions: micro-synthetic fibers and macro-synthetic fibers (MISF and MASF). Micro-synthetic fibers are typically less than 19 mm long and are used to resist cracks formed due to plastic shrinkage (Euclid, n.d.). Macro-synthetic fibers (also known as "structural" fibers) are larger and coarser than traditional micro-synthetic fibers (as shown in **Figure 2-2**) and can provide concrete with similar toughness and resistance to steel fibers and light gage steel reinforcement (Mahoney, 2005).

2.2.2 Effects of Synthetic Fibers on Concrete Properties

The addition of synthetic fibers to concrete affects many of its properties, both in the fresh state and hardened state, including: workability, plastic/drying shrinkage, compressive strength, tensile strength, flexural strength and post-cracking resistance. A comprehensive review of the effects of synthetic fibers on these properties is provided in Yin et al. (2015).

Compressive strength:

A review of the literature indicates that although the provision of synthetic fibers has no significant effect on the peak compressive strength of concrete, the benefit is more pronounced when examining the post-peak performance (see **Figure 2-3a**). Carnovale (2013) studied the effects of both macro-synthetic (2-3%) and steel fibers (0.5-1%) on the compressive behaviour of high-strength concrete cylinders having compressive strengths ranging from 51 to 72 MPa. Typical stress-strain curves for HSC and high-strength fiber-reinforced concrete (HSFRC) are shown in **Figure 2-3b**. The results show that the peak stress was not significantly affected by the fibers, although the fibers increased the strain at peak stress. However, both the steel and synthetic fibers improved the toughness and post-peak capacity of HSC in compression.

Tensile strength:

The addition of fibers significantly affects the post-cracking tensile resistance of concrete. Amin et al. (2017) studied the post-cracking response of FRC with macro-synthetic PP fibers using a series of matched direct uniaxial and indirect three-point prism and round-panel tests. The direct tensile tests were conducted on hourglass specimens (see **Figure 2-4b**), with two different fiber dosages investigated (4 and 8 kg/m^3: labelled as FRC4 and FRC8). The results from the tests are shown in **Figure 2-4c**. It can be observed the that the PP-FRC specimens show a sharp decrease in stress after peak, with significant opening of the main dominant crack. After crack stabilization, the specimens show an increase in stress with increasing crack opening. It can also be observed that the direct tensile response remains relatively constant at larger crack widths ($w > 2.5$ mm).

Flexural strength:

Due to the difficulties in conducting direct tensile tests, indirect tests (on prims or round panels) are typically used to determine the post-cracking properties of FRC. Examples of standardized tests include the European Standard EN14651 and ASTM C1609 three and four-point prism bending tests. Reddy & Subramaniam (2017) investigated the flexural response of macro-synthetic fibers on the flexural response of 150 mm × 150 mm × 500 mm prims tested under three-point bending. Parameters investigated include the effects of fiber type (polypropylene and polyolefin-based macro fibers) and fiber content (4, 6 and 8 kg/m3). When compared to conventional concrete, SNFRC showed improved toughness with increasing fiber content as shown in **Figure 2-5b**. This same result can also be observed in Amin et al. (2017) tests presented previously (compare results for FRC4 and FRC8).

Table 2-1 Physical properties of synthetic fibers (Adapted from Zheng & Feldman, 1995)

Fibre type	Specific gravity	Tensile strength (MPa)	Elastic modulus (GPa)	Ultimate elongation (%)
Acrylic	1.17	207–1000	14.6–19.6	7.5–50.0
Aramid I	1.44	3620	62	4.4
Aramid II (high modulus)	1.44	3620	117	2.5
Nylon	1.16	965	5.17	20.0
Polyester	1.34–1.39	896–1100	17.5	
Polyethylene	0.96	200–300	5.0	3.0
Polypropylene	0.90–0.91	310–760	3.5–4.9	15.0

Table 2-2 Properties related to durability for synthetic fibers (Adapted from Zheng & Feldman, 1995)

	Environmental durability		Thermal resistance	
Fibre type	Water resistance	Alkali resistance	Behaviour at high temperature	Temp. at which all strength is lost (°C)
Aramid	Good	Good	Progressive loss in tensile strength at 200°C or higher	400–500
Nylon	Good	Good	Progressive loss in tensile strength at 100°C or higher	180–200
Polyethylene	Good	Good	Progressive loss in tensile strength at 100°C or higher	100–130
Polypropylene	Good to fair	Good	Progressive loss in tensile strength at 100°C or higher	120–150
Poly(vinyl alcohol)	Good	Good	Progressive loss in tensile strength at 100°C or higher	200–240
Pitch-based carbon	Good	Good	Gradual decrease in tensile strength at 300–350°C	500–600
PAN-based carbon	Good	Good	Gradual decrease in tensile strength at 300–350°C	500–600

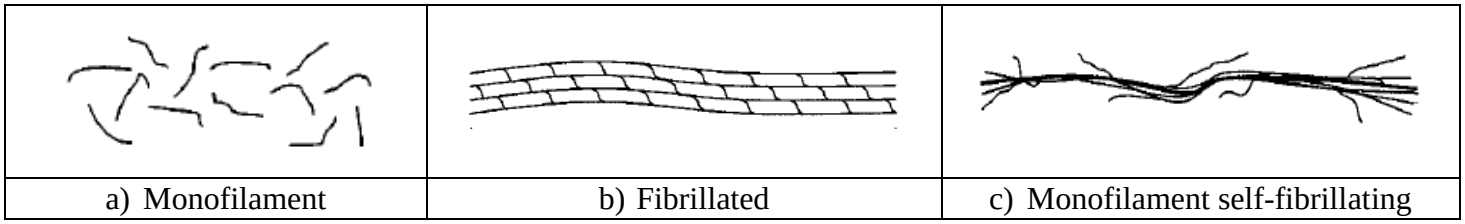

a) Monofilament	b) Fibrillated	c) Monofilament self-fibrillating

Figure 2-1 Physical forms of synthetic fibers (Adapted from Trottier et al., 2002)

a) Micro	b) Macro

Figure 2-2 Synthetic fibers (Adapted from Euclid Chemical, n.d.)

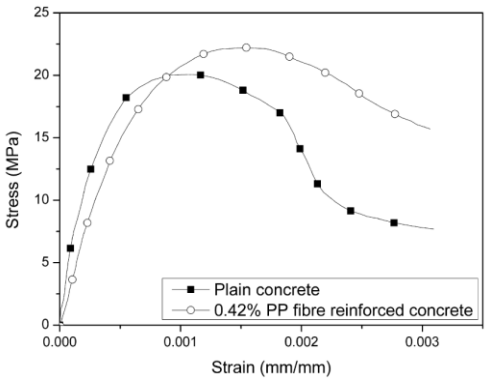

a) Yin et al. (2015)

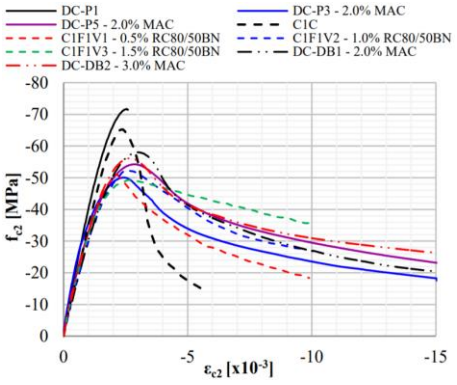

b) Carnovale (2013)

Figure 2-3 Average stress-strain curves of compressive test

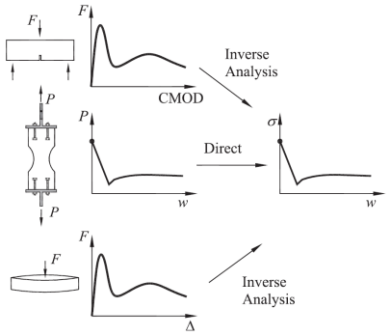

a) Methods to determine the tensile properties of PPFRC

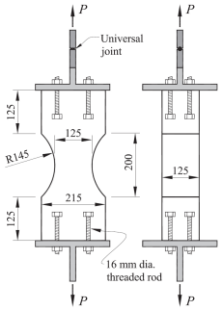

b) Details of uniaxial tension test specimens

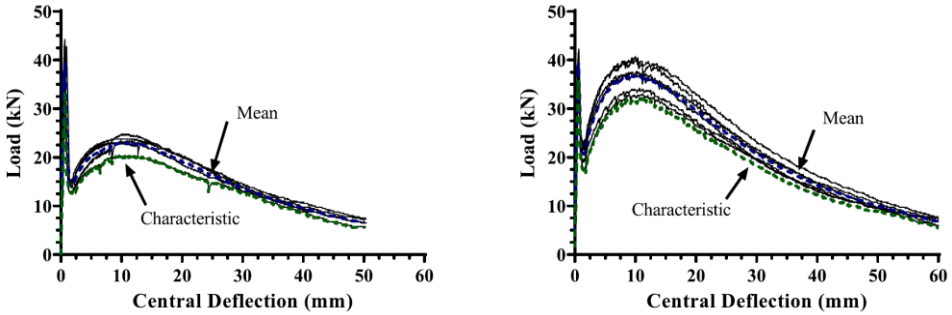

c) Round panel test results for FRC4 and FRC8 respectively

Figure 2-4 Amin et al. (2017)

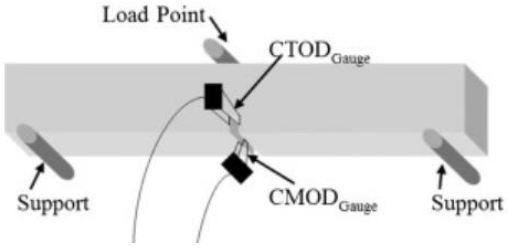

a) Test setup

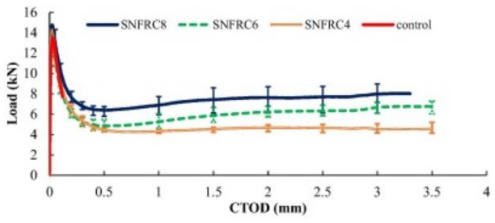

b) Load vs. CTOD response of SNFRC beams

Figure 2-5 Reddy & Subramaniam (2017)

2.3 Previous Research on Behaviour of FRC Beams under Static Loading

2.3.1 Overview of Previous Tests

Extensive research over the past three decades has examined the effect of steel fibers on the shear and flexural behaviour of beams (Parra-Montensinos, 2006). Published research on the shear and flexural behaviour of synthetic fiber-reinforced concrete (SNFRC) beams is more limited. **Table 2-3** and **Table 2-4** present a summary of some of these studies. It can be observed that limited studies have focused on high-strength SNFRC beams ($f_c' \geq 60$ MPa).

2.3.2 Shear Response of SNFRC Beams

Li et al. (1992) conducted an early study which examined the shear response of 60 steel and synthetic fiber-reinforced mortar beams with cross-sections of 127×64 mm and 228×127 mm under center-point loading (**Figure 2-6a**). Both macro-steel fibers and micro-synthetic fibers (acrylic, aramid, and high-strength polyethylene) were investigated in beams having varied fiber contents, tension steel ratios and shear span-effective depth (a/d) ratios. **Figure 2-6b** shows mortar prism test results for different fibers. The beam results showed that using 1% steel, polyethylene or aramid fibers increased shear resistance by 100-200%. The authors noted that the steel and polyethylene fibers were most effective when compared to the aramid and acrylic fibers. The responses of the beams were also affected by both the a/d ratio and beam depth.

Majdzadeh et al. (2006) investigated the shear capacity of fourteen 150 mm × 150 mm × 1000 mm FRC beams under four-point load as illustrated in **Figure 2-7a**. The main parameters investigated were the fiber volume (0.5-1.5%) and fiber type, with one type of hooked-end steel fiber and two types of macro-synthetic fibers (self-fibrillating and straight), investigated. Results showed that as the fiber volume increased, the shear strength also increased for all fiber types. The optimal volume fraction for the three types of fibers used was found to be 1%, with no improvements beyond this value. In general, the authors concluded that, at a given fiber volume fraction, steel fibers were better than synthetic fibers. However, with a specific range of material shear strength, synthetic fibers were found to be more efficient (**Figure 2-7b**). Energy absorption capacity (area under the load-deflection curves) also improved upon adding fibers. The authors noted that steel fibers performed best, though synthetic fibers were still effective. Finally, beams with either steel fibers and stirrups or straight synthetic fibers and stirrups showed synergistic effects. **Figure 2-7c** shows the results for the FRC beams with straight synthetic fibres.

Conforti et al. (2015) presented another study which investigated the shear behaviour of FRC beams reinforced with macro-synthetic fibers. A total of 22 deep (430 mm × 890 mm × 3000 mm) and 14 wide-shallow (250 mm × 330 mm × 6000 mm) beams were tested under four-point bending as shown in **Figure 2-8a**. Three types of members were used in both types of beams: members without shear reinforcement, members with minimum shear reinforcement, and members with only polypropylene (PP) fibers as shear reinforcement (at a volume fraction of 1.45%). **Figure 2-8b** and **Figure 2-8c** summarize the results for both types of beams. Results showed that

in wide-shallow beams, PP fibers can completely substitute the shear reinforcement. However, in deep beams, PP fibers can only substitute the minimum shear reinforcement. Nonetheless, the use of 1.45% of PP fibers caused a 100% increase in the shear strength of the deep beams. Fibers also had a positive impact on cracking, resulting in a more diffused crack pattern where the cracks are smaller and more closely spaced.

Altoubat et al. (2009) investigated the effect of macro-synthetic fibers on the shear strength of beams built without stirrups. A total of 27 beam specimens with cross-sections of 280×460 mm (Phase 1: 13 beams) and 230×390 mm (Phase 2: 14 beams) were tested under center-point bending as shown in **Figure 2-9a**. The length of the beams varied between 1.9 and 3.2 m. The shear span-depth ratio (a/d = 2.3 and 3.5 for short and slender beams, respectively) and synthetic fiber content (0.5, 0.75 and 1%) were varied in both beam sets. Results show that macro-synthetic fibers significantly improved the shear strength, ductility, and toughness of both the short and slender beams (see **Figure 2-9b**). The use of 0.5%, 0.75% and 1% fibers increased shear resistance by 14%, 23%, and 30% for slender beams. Similarly, for the short beams, adding 0.5% and 0.75% fibers increased shear strength by 20% and 28%. The fibers also affected the cracking pattern and failure mode. Adding macro-synthetic fibers at volume fractions of 0.5-0.75-1% also increased the deflection at maximum load by 63-93-100% for the slender beams. Similarly, for the short beams and fiber volumes of 0.5% and 0.75%, the deflection increased by 103% and 138%. In the RC beams, a single diagonal crack occurred at failure, whereas multiple diagonal cracks and improved arching action were observed in the slender beams. Similarly, adding fibers in the short beams changed the mode of failure from web-shear cracking (in the control beams) to flexural-shear cracking (in the FRC beams). Moreover, while fibers did not change the load that caused the first diagonal crack, they slowed the propagation and widening of the major diagonal crack. Thus, the provision of synthetic fibers effectively redistributed stresses in the beam and improved the strain capacity.

In a related study, Altoubat et al. (2012) compared the results of short and slender SNFRC beams with 230×390 mm cross-sections, built with and without stirrups (**Figure 2-10a**). Each group had 4 types of beams: one control with no fibers, one with minimum stirrups, one with fibers, and one with hybrid reinforcement (fibers and minimum stirrups). By using fibers alone, the shear strength of short and slender beams increased by 18 and 14% respectively. Similarly, using minimum stirrups alone increased the shear strength of short and slender beams by 19%. However, hybrid reinforcement increased the shear strength of short and slender beams by 42 and 69% respectively, which means that hybrid reinforcement had a synergistic effect on shear strength. This effect was more significant in long (slender) beams suggesting that it depends on the slenderness of beams. For ductility, beams with either fibers or minimum stirrups were more ductile than the control beams without stirrups. Moreover, beams with hybrid reinforcement showed a significant improvement in ductility. **Figure 2-10b** shows the test results for short beams.

In a further paper presented by the same research group, Yazdanbakhsh et al. (2015) assessed the ability of 11 analytical shear models originally developed for steel FRC beams to

predict the shear capacity of the tested macro-synthetic FRC beams. It was shown that the fib-MC2010, RILEM, Swamy et al., Mansur et al., and Ashour et al. equations predicted the shear strength of the slender SNFRC beams accurately, although more conservative results were obtained for the short beams. Finally, the authors used a statistical method to calibrate the original RILEM model for predicting the shear resistance of the SNFRC beams.

Karthik & Maruthachalam (2015) examined the shear behaviour of 10 hybrid fiber-reinforced concrete beams with length of 1700 mm under four-point bending as shown in **Figure 2-11a**. In addition to investigating the benefits of adding scrim bled steel (ST) fibers and synthetic fibers (recycled polyethylene terephthalate – RPET and polypropylene – PP) to plain concrete, different hybrid fiber combinations were also studied: ST + RPET and ST + PP. The fiber dosage ranged from 0.12-0.5% for all types of fibers. Results show that beams containing hybrid fibers (ST + PP) provided the best performance (see **Figure 2-11b**) due to the synergy effect, where steel fibers contributed in bridging the cracks while synthetic fibers delayed the formation of micro cracks.

A few studies have also investigated the benefits of implementing synthetic fibers in self-compacting concrete (SCC) beams, including: Grenough & Nehdi (2008), Conforti et al. (2017) and AbdelAleem et al. (2018). Several recent studies have also compared the effects of steel and macro-synthetic fibers on the shear resistance of FRC beams, as well as the synergy of transverse reinforcement and fibers in SNFRC beams, including: Joshi et al. (2018), Navas et al. (2018) and Arslan & Keskin (2019). However, as shown in **Table 2-3**, most of these studies were conducted on normal-strength concrete beams, with f_c' < 60 MPa.

Table 2-3 Summary of previous shear tests on SNFRC beams

Authors	No. of beams		Test method	Type of concrete	Beam dimensions (mm)				f_c' (MPa)	Tension steel		Transverse steel		Fibers						
					B	H	L	a/d ratio		Yield strength f_y (MPa)	Steel ratio ρ (%)	Spacing s (mm)	Steel ratio (%)	Type	Content (%)	Micro-synthetic	Macro-synthetic	L_f (mm)	d_f (mm)	Aspect ratio
Arslan & Keskin (2019)	23		3P bending	SNFRC	150	240	1400-2200	2.5-4.5	21	492	1.28	15-20	0.34-0.45	PP	0-3		×	39	-	78
AbdelAleem et al. (2018)	12		4P bending	SCC	250	250	1500	2.5	38-65	417	2.03	-	-	-	-	N/A		-	-	-
				SNFRC (VC)					28-34					SN	0.2-1	×		19	0.66	29
														SN	0.2-1		×	38-54	0.64-0.8	29-76
Joshi et al. (2018)	11	1	4P bending	OPC	200	300	3500	5	58	1860	0.4	-	-	-	-	N/A		-	-	-
		5		SFRC										SF	0.35-1	N/A		30	0.6	50
		5		SNFRC										PO	0.35-1		×	50	0.5	100
Navas et al. (2018)	16		3P bending	SNFRC	229-305	552	5060-5970	3.8-4.87	42.17	579	1.67-2.25	None, 300 or 330	0-0.15	PO	0-1.1		×	48	0.85	57
Conforti et al. (2017)	6	2	3P bending	SCC	2490	500	6000	3.1	70	1790	0.89	200	0.16	-	-	N/A		-	-	-
		4		SNFRC								None or 200	0-0.16	PP	0-1.1		×	40	0.75	53
Conforti et al. (2015)	36	14 wide-shallow	4P bending	SNFRC	430-890	250-330	3000	2.5	26-31	-	1.15-1.3	None or 150	0-0.1	PP	1.5		×	40	0.75	58.3
		22 deep			150-300	600-800	6000	2.5	30-34		1-1.12	None or 200	0-0.32							
Karthik & Maruthachalam (2015)	10		4P bending	OPC, SFRC, SNFRC, HYFRC	-	200	1700	3.85	40	-	-	-	-	C	0.12-0.5	N/A		50	1	50
														RPET	0.12-0.5		×	38	0.02	1900
														PP	0.12-0.5		×	38	0.1	380
Altoubat et al. (2012)	16	8 slender	3P bending	SNFRC	230	390	2700	3.5	42	-	3.18	None or min.	0-0.17	PM	0-0.5		×	40	-	90
		8 short					1900	2.3												
Parmentier et al. (2012)	28	4	4P bending	OPC	200	300	2500	0.5-2.5	52	-	1.21	-	-	-	-	N/A		-	-	-
		24		SFRC										UN	0.3-0.5		×	50	1	50
				SFRC										CEA			×	54	1	54
				SNFRC										PM	0.5		×	50	-	-
Altoubat et al. (2009)	27	13 slender	3P bending	SNFRC	280	460	1900-3200	3.5	41	-	2.15	-	-	PM	0.5-1		×	40	-	90
		14 short			230	390	1901-3200	2.3			3.18				0.5-2					
Greenough & Nehdi (2008)	13	1	4P bending	SCC	200	300	2400	3	40	400	1.7	-	-	-	-	N/A		-	-	-
		9		SFRC										SF	0.5-1	N/A		50	0.7-1	43-50
		3		SNFRC										PP	0.5-1		×	50	0.83	63
Majdzadeh et al. (2006)	14		4P bending	SFRC	150	150	1000	3	43	-	-	None or 75	0-0.28	HE	0-1.5	N/A		60	-	80
				SNFRC										PP-FB			×	54		360
														PP			×	50		85
Li et al. (1992)	60	51 small	3-point bending	SFRC	63.5	127	280-1300	1~3	23	440-460	1.1-2.2	-	-	HE	1	N/A		30-50	-	60-100
		9 large		SNFRC	127	228								PE	1	×		12.7		334

Fiber type: SF = steel fiber, SN = synthetic fiber, HY = hybrid fiber; HE = hooked-end, C = Crimped, UN = undulated, CEA = conical end anchorage; PM = polymeric mix, PP = polypropylene, PE = polyethylene, PP-FB = polypropylene-fibrillated, PM = polymeric, PO = polyolefin , RPET = recycled polyethylene terephthalate

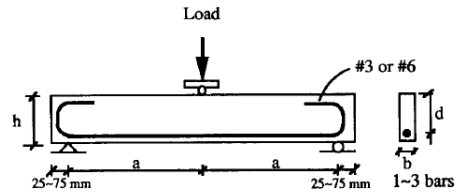

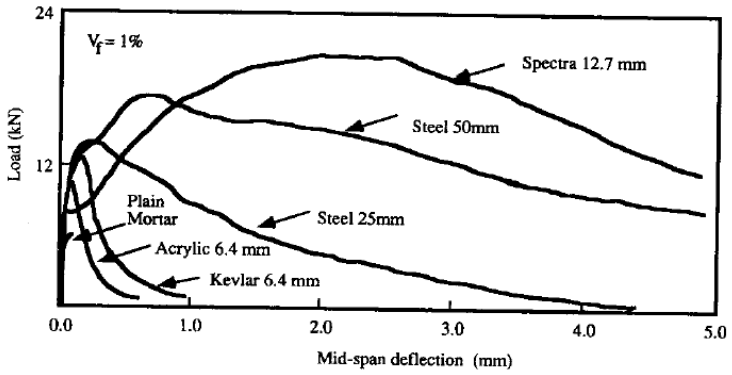

a) Test setup

b) Load vs. deflection curve for mortar reinforced beams with different types of fibers

Figure 2-6 Li et al. (1992) research

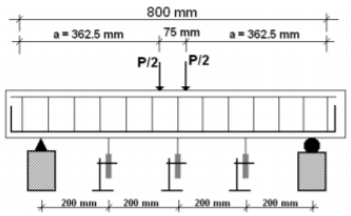

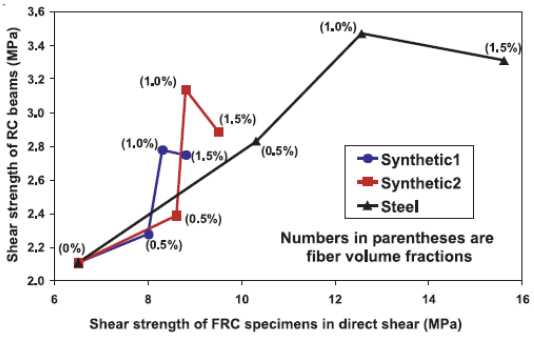

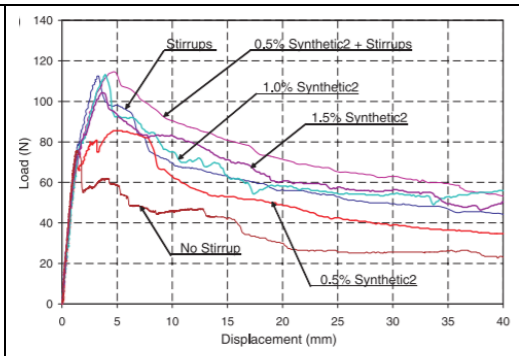

a) Test setup

b) Shear strength of RC beams vs. material shear strength of FRC

c) Load vs. displacement for FRC beam with synthetic 2

Figure 2-7 Majdzadeh et al. (2011) research

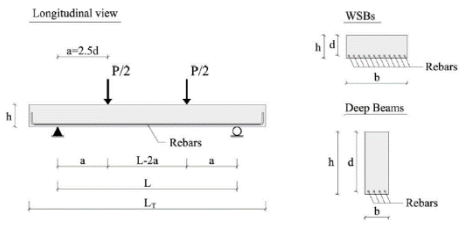

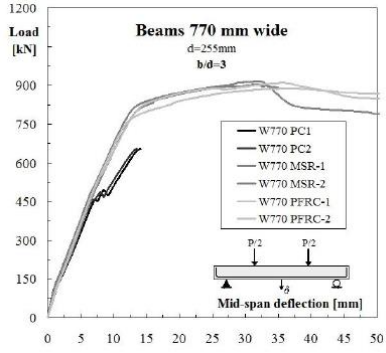

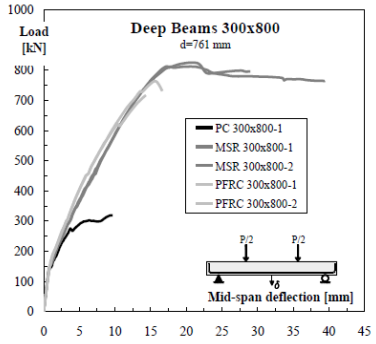

a) Geometry of beams

b) Load vs. mid-span deflection of wide-shallow beams

c) Load vs. mid-span deflection of deep beams

Figure 2-8 Conforti et al. (2015) research

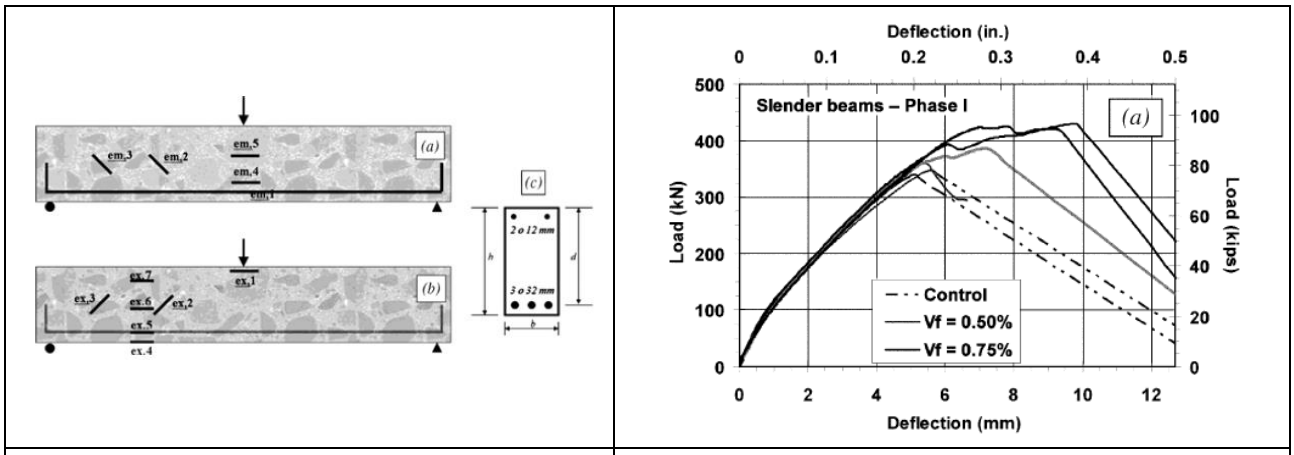

a) Test setup | b) Load-deflection curves for slender beams

Figure 2-9 Altoubat et al. (2009) research

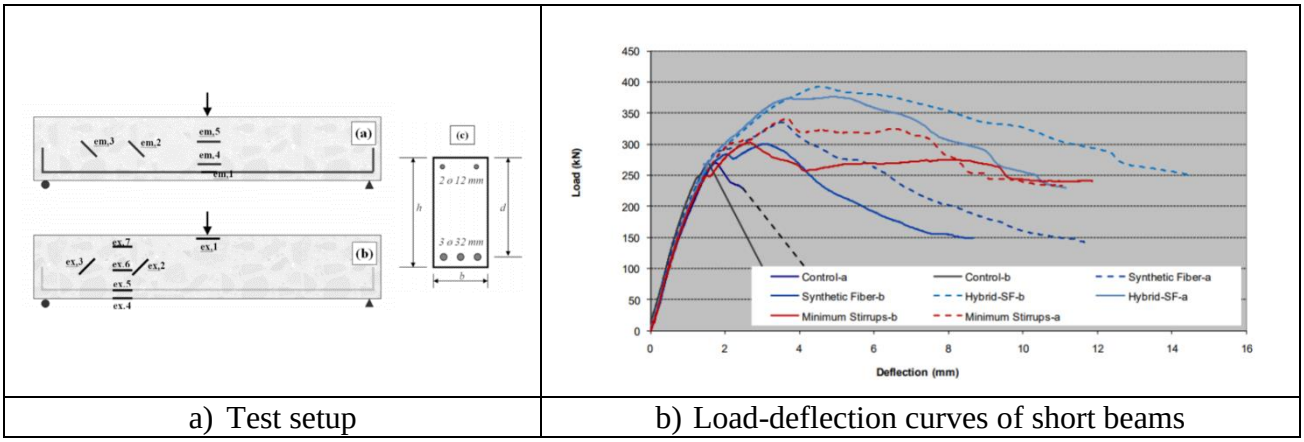

a) Test setup | b) Load-deflection curves of short beams

Figure 2-10 Altoubat et al. (2012) research

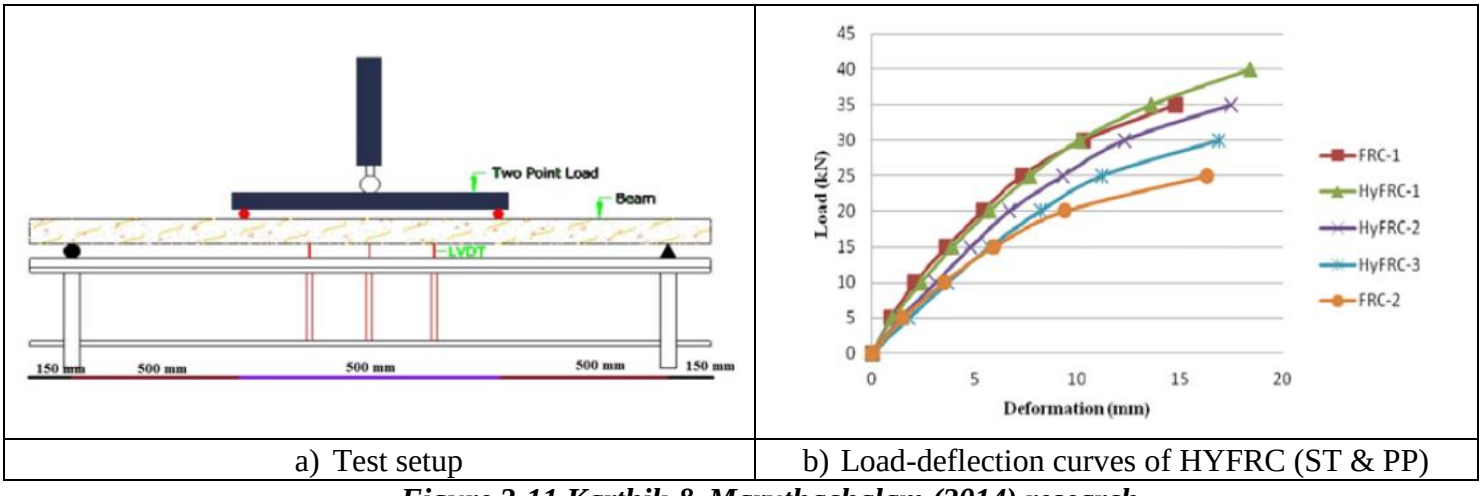

a) Test setup | b) Load-deflection curves of HYFRC (ST & PP)

Figure 2-11 Karthik & Maruthachalam (2014) research

2.3.3 Flexural Response of SNFRC Beams

In addition to the studies on shear resistance, a few studies have also examined the flexural behavior of FRC beams built with synthetic fibers (see **Table 2-4**).

Wang & Belarbi (2005) examined the flexural behaviour of 12 FRC beams reinforced with glass or carbon fiber-reinforced polymer (GFRP, CFRP) bars and polypropylene (PP) fibers under four-point flexural loading and cyclic loading as shown in **Figure 2-12a**. Three types of FRP bars were used, including No.4 CFRP and No.4 or No.8 GFRP bars. Results show that, at service load, the beams with 0.5% PP fibers had smaller crack widths when compared to plain concrete as shown in **Figure 2-12b**. Moreover, the ultimate strain in the FRC beams was significantly larger than that of plain concrete. Finally, the ductility index was improved upon the addition of fibers.

Suji et al. (2007) examined the flexural performance of 12 PFRC (polypropylene fiber-reinforced concrete) beams under four-point bending as shown in **Figure 2-13a**. The beams were reinforced with 6 mm diameter stirrups, with 10 and 8 mm bars as tension and compression reinforcement. The main parameter investigated was the volume of PP fibers (0.1, 0.2, 0.3%). Results show that fibers improved the ductility of beams with 0.2% of fibers being the ideal dosage. Fibers also reduced the crack width but didn't change the crack pattern. Moreover, the load capacity of fiber-reinforced concrete beams increased when compared to the control beams, but the increase was in minor increments. Finally, fibers increased the rigidity of the beams. **Figure 2-13b** shows a summary of the results obtained.

Yang et al. (2012) studied the effect of synthetic fibres on the flexural response of high-strength concrete beams, however the HSC beams in this study were reinforced with FRP bars. The geometry of the tested beams can be seen in **Figure 2-14a**. Two types of FRP reinforcement were used: 9 mm CFRP bars and 13 mm GFRP bars. In addition, both steel fibers (at a volume percentage of 1%) and macro-synthetic fibers (at a volume percentage of 2%) were investigated. Results show that both types of fibers decreased the crack widths, as shown in **Figure 2-14b**, and delayed the initiation of flexural cracks. **Figure 2-14c** shows that the failure of CFRP beams with synthetic and steel fibers was brittle due to FRP bar rupture. However, GFRP beams with synthetic and steel fibers showed improved ductility as shown in **Figure 2-14d**, due to the increased ultimate compressive strain capacity and improved post-peak behaviour of FRC. In terms of cracking response, synthetic fibers at 2% by volume were better than steel fibers at 1% by volume in CFRP beams. However, steel fibers performed better in terms of restraining the depth of the cracks.

Rajkumar & Vasumathi (2013) presented a further study which investigated the flexural performance of 12 FRC beams confined with FRP. **Figure 2-15a** shows the test setup. The beams had a cross-section of 150×230 mm and were 2000 mm long. The main parameter investigated was the volume fraction of macro-synthetic fibers (0.3, 0.5, and 0.7%). Results show that the beam with 0.7% fibers gave the best behaviour compared to the other beams as demonstrated in **Figure 2-15b**. Moreover, the cracking behaviour of the beams improved with the addition of fibers. Similar conclusions have been reported by Bernard (2019), where the the provision of synthetic

fibers was found to reduce the mean spacing between cracks as well as the mean flexural crack widths.

Athiappan & Vijaychandrakanth (2014) tested the flexural performance of 6 concrete beams, including 3 control beams and 3 with 0.3% sisal fibers (by weight of cement) as shown in **Figure 2-16a**. Sisal fiber is a hard and tough fiber extracted from the leaves of sisal plants. The beams had a cross-section of 150×300 mm and were 1500 mm long. Results show that the flexural strength of beams increased with the addition of fibers as shown in **Figure 2-16b**. Moreover, adding 0.3% by volume of sisal fiber improved the ductility of beams.

Sahoo et al. (2014) examined the flexural response of 6 FRC beams with dimensions of 150 mm ×150 mm × 2000 mm. The beams were doubly-reinforced with 12 mm bars for the tensile and compressive reinforcement, and 8 mm stirrups as shown in **Figure 2-17a**. Two types of fibers were used in the experiment: steel fibers and polypropylene fibers, with volume fractions of 0.5 or 1%. The effect of combined (hybrid) fibers was also investigated. Results show that both fibers improved the post-peak resistance with steel fibers being more effective. Moreover, the post-yield strain-hardening behavior was improved by using 1% volume fraction of both types of fibers. However, both fibers didn't significantly improve the ultimate flexural resistance of the beams. As for ductility, polypropylene fibers were more effective than steel fibers. Steel FRC specimens had a lower stress level in the longitudinal bars compared to RC specimen. However, PFRC (polypropylene fiber-reinforced concrete) and CFRC (combined fiber-reinforced concrete) specimens had high strain levels in the longitudinal bars due to the low-modulus polypropylene fibers. Adding fibers also improved the post-peak residual strength response of the beams as shown in **Figure 2-17b** and **Figure 2-17c**. Finally, results show that to get a better flexural response and reduce costs, a percentage of steel fibers can be replaced by polypropylene fibers.

Aulia & Rinaldi (2015) investigated the bending capacity of 4 high-strength fiber-reinforced concrete beams as shown in **Figure 2-18a**. The beams had a cross-section of 150×300 mm and were 2200 mm long. The beams were doubly-reinforced with 16 mm and 12 mm tension and compression bars, and 12 mm stirrups. Three environmentally friendly synthetic fibers were used in the analysis: polypropylene fiber (at 0.2% concrete volume), tie wire fiber (at 2% concrete volume), and used rubber tie fiber (at 0.75% concrete volume). The main parameter investigated was the effect of fiber type on the bending capacity of high-strength concrete beams. Results show that both the bending capacity and the failure behavior were improved with the addition of synthetic fibers. Fibers also enhanced the ultimate deflections of the beams leading to an increase in ductility. Tie wire fiber gave the highest increase in flexural capacity. Moreover, this type of fiber contributed the most to the delay of reinforcement yield strains at a higher load. However, polypropylene fibers had the highest contribution in terms of ultimate deflection and ductility. **Figure 2-18b** shows the test results for all the tested beams.

Sundar et al. (2017) tested the flexural strength of 4 reinforced concrete beams containing synthetic fibers. The test setup is shown in **Figure 2-19a**. The beams had a cross-section of

150×200 mm and were 1200 mm long. Two types of polypropylene fibers, with 2 different lengths of 12 and 24 mm, were used, at 0.5% volume by weight. Results show that fibers improved the flexural strength of concrete as shown by the red curve in **Figure 2-19b**.

Zhang et al. (2018) investigated the performance of twelve 150 mm × 150 mm × 1100 mm reinforced self-consolidating concrete (SCC) beams containing hybrid fibers under four-point bending as illustrated in **Figure 2-20a**. The main parameters investigated were the fiber type (steel fiber – SF, micro & macro polypropylene – PP fibers and their combinations), fiber content (SF: 20 – 50 kg/m^3, micro PP: 0.5 – 1 kg/m^3, macro PP: 2 – 6 kg/m^3) and longitudinal steel ratio. Results show that the hybrid use of SF and macro PP provides significant enhancements in the overall performance of the beams including: enhanced ultimate flexural bearing capacity, reduced deflection, reduced steel reinforcement strain and stress and localized cracks (see **Figure 2-20b**). However, these enhancements become less significant with the increase in longitudinal steel ratio.

Table 2-4 Summary of previous flexural tests on SNFRC beams

Authors	No. of beams		Test method	Type of concrete	Beam dimensions (mm)			f_c' (MPa)	Tension reinforcement			Transverse steel			Fibers						
					B	H	L		Bar diameter (mm)	Yield strength (MPa)	Reinforcement ratio (%)	Yield strength (MPa)	Spacing (mm)	Reinforcement ratio (%)	Type	Content (kg/m^3 or %)	Micro-synthetic	Macro-synthetic	L_f (mm)	d_f (mm)	Aspect ratio
Bernard (2019)	12		4P bending	SNFRC	300	300	3600	32	16	500	-	-	-	-	PP	4.0-4.5 kg/m^3		×	54-58	-	27-580
Zhang et al. (2018)	12		4P bending	SFRC/ SNFRC/ HYFRC (SCC)	150	150	1100	65	8-10	475-491	0.56-1.31	278	60-120	0.38-0.76	HE	20-50 kg/m^3	N/A		60	0.75	80
															PP	0.5-1.0 kg/m^3	×		9	0.018	500
															PP	2-6 kg/m^3		×	45	0.74	61
Sundar et al. (2017)	4		4P bending	SNFRC	150	200	1200	33-38	12	415	-	415	150	0.45	PP	0.5%		×	12-24	-	~800
Aulia & Rinaldi (2015)	4		4P bending	SNFRC (HSC)	150	300	2200	64	15.8	407	2.8	412	80	1.85	PP	0.2%	×		12	0.018	66.7
															TW	2%		×	50	1	50
															URT	0.75%		×	60	-	-
Sahoo et al. (2014)	7		4P bending	SFRC	150	200	2000	32-39	12	500	1.35	500	End: 65 Middle 1/3 span: 130	0.52-1.03	HE	0.5-1%	N/A		60	0.75	8
				SNFRC											PP	1%		×	40	0.5	-
Athiappan & Vijaychandrakanth (2014)	6	3	4P bending	OPC	150	300	1500	40	12	-	0.65	-	200	0.34	-	-	N/A		-	-	-
		3		SNFRC											SI	0.3%	-				
Rajkumar & Vasumathi (2013)	12	4	4P bending	OPC	150	230	2000	55	-	-	-	-	-	-	-	-	N/A		-	-	-
		8		SNFRC											PP	0-0.7%		×	42	0.24	175
Yang et al. (2012)	6	CFRP	4P bending	SFRC (HSC)	230	250	2300	76-104	9	-	0.15	477	80	0.85	HE	1%	N/A		30	0.5	60
		GFRP		SNFRC (HSC)					13		0.31				PO-C	1%		×	40	-	35.8
Suji et al. (2007)	12	4	4P bending	SNFRC	100	200	1800	48	10	415	0.98	-	130	0.43	PP-FB	0-0.3%		×	24	-	-
		4						52													
		4						57													
Wang & Belarbi (2005)	12	2-#4 GFRP	4P bending	OPC	178	229	2032	48	13	690	3.51	-	89	0.9	-	-	N/A		-	-	-
		2-#8 GFRP							25	552	3.6										
		2-#4 CFRP							13	2069	3.16										
		2-#4 GFRP		SNFRC				30	13	690	4.71				PP	0.5%		×	57	-	-
		2-#8 GFRP							25	552	4.83										
		2-#4 CFRP							13	2069	4.24										

Fiber type: SF = steel fiber, SN = synthetic fiber, HY = hybrid fiber; HE = hooked-end; PP = polypropylene, PO-C = polyolefin-crimped, PP-FB = polypropylene-fibrillated, TW = tie wire, URT = used rubber tires, SI = sisal

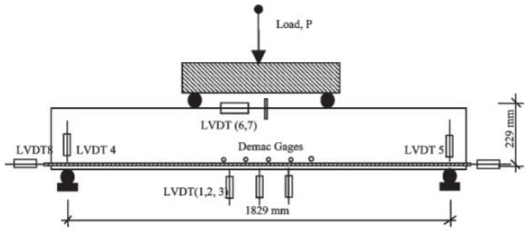

Specimen I.D.	P4C	P4G	P8G	F4C	F4G	F8G
Crack Width (mm)	0.60	0.49	0.45	0.54	0.41	0.36
% decrease relative to respective plain concrete	---	---	---	10%	16%	20%

a) Test setup

b) Crack width of plain and FRC beams

Figure 2-12 Wang & Belarbi (2005) research

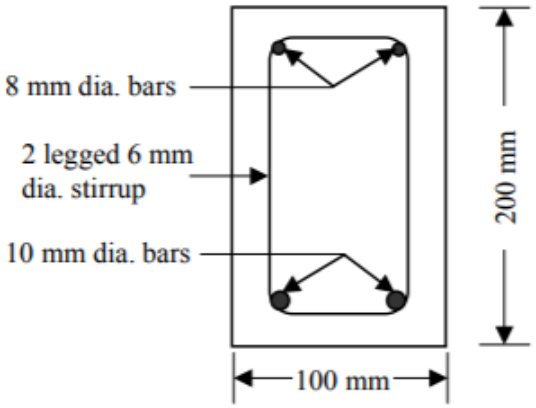

Beam designation	Mix type	v_f (%)	Fiber addition (kg/m^3)	Ultimate load (kN)	Initial crack load (kN)	Maximum mid-span deflection (mm)
AC	I	0.0	–	51	18	11.51
API	I	0.1	0.9	54	19	22.80
APII	I	0.2	1.8	57	21	46.44
APIII	I	0.3	2.7	60	20	43.81
BC	II	0.0	–	57	19	16.68
BPI	II	0.1	0.9	60	18	23.41
BPII	II	0.2	1.8	60	20	44.79
BPIII	II	0.3	2.7	61	21	33.68
CC	III	0.0	–	67	20	29.93
CPI	III	0.1	0.9	63	19	31.39
CPII	III	0.2	1.8	67	21	46.09
CPIII	III	0.3	2.7	64	20	27.01

a) Beam cross-section

b) Summary of test results

Figure 2-13 Suji et al. (2007) research

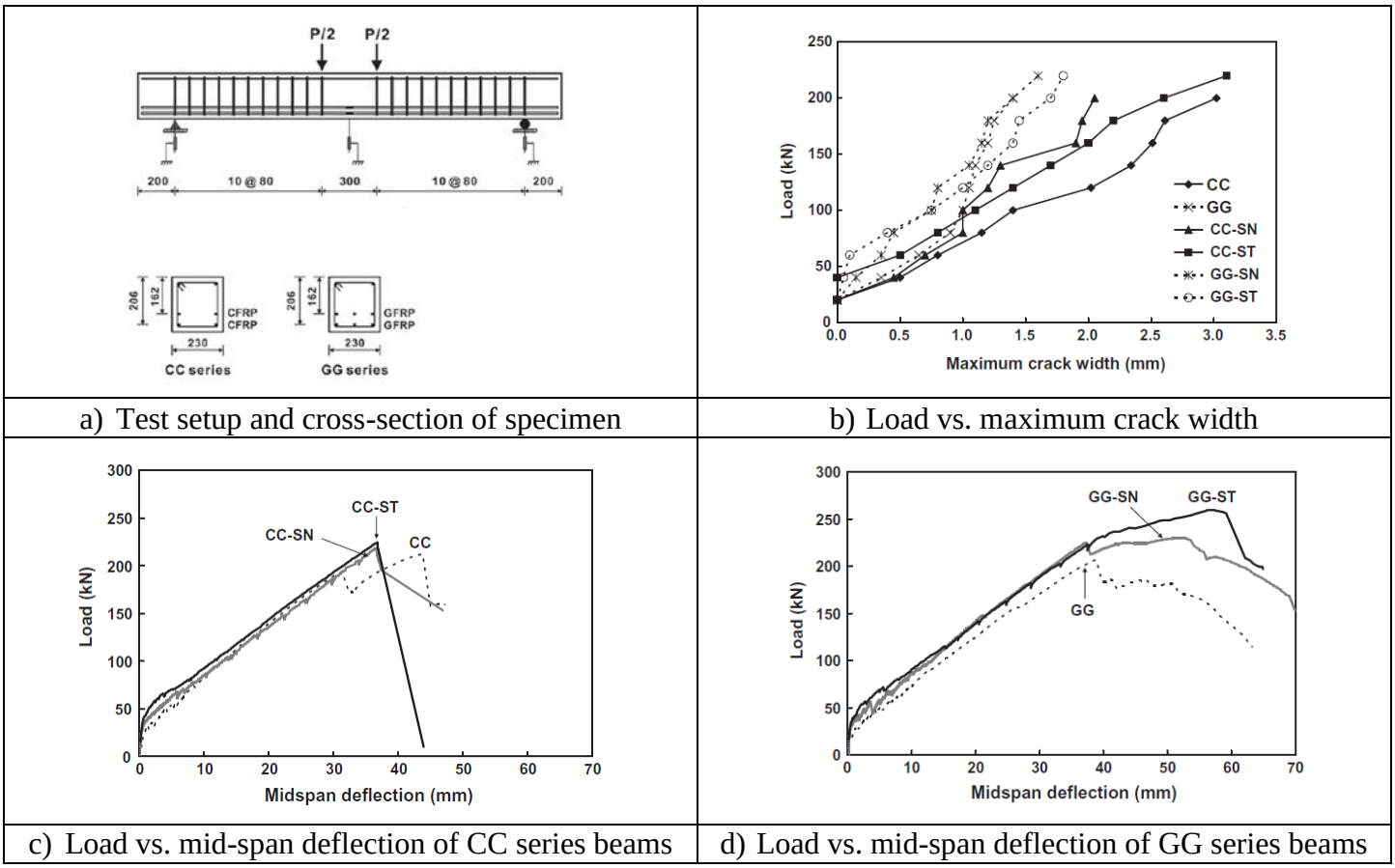

a) Test setup and cross-section of specimen

b) Load vs. maximum crack width

c) Load vs. mid-span deflection of CC series beams

d) Load vs. mid-span deflection of GG series beams

Figure 2-14 Yang et al. (2012) research

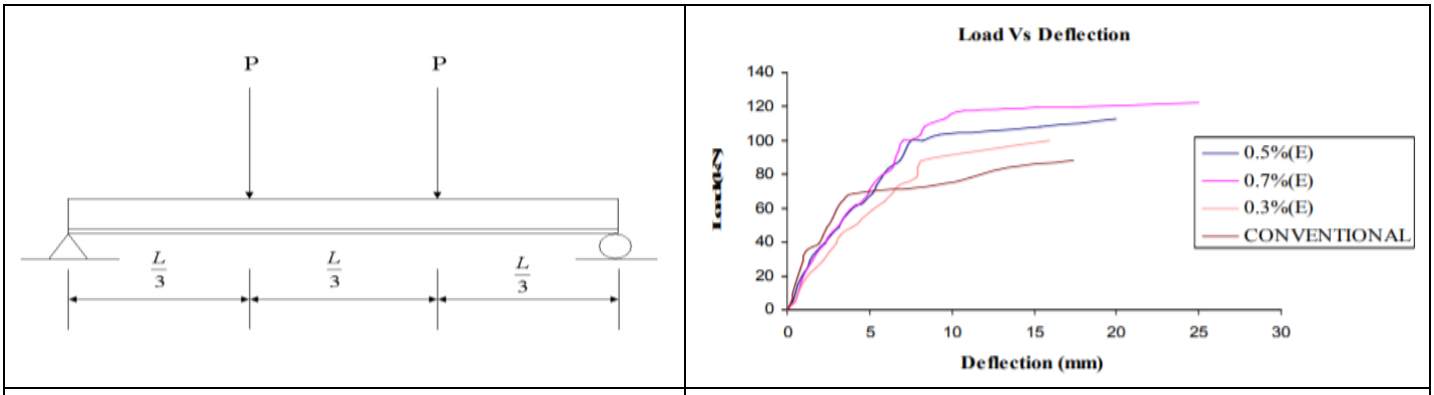

a) Test setup

b) Load vs. deflection curve for different beams

Figure 2-15 Rajkumar & Vasumathi (2013) research

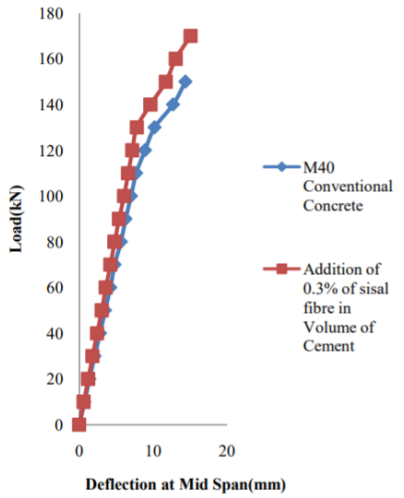

a) Test setup | b) Load vs. deflection curve for tested beams

Figure 2-16 Athiappan & Vijaychandrakanth (2014) research

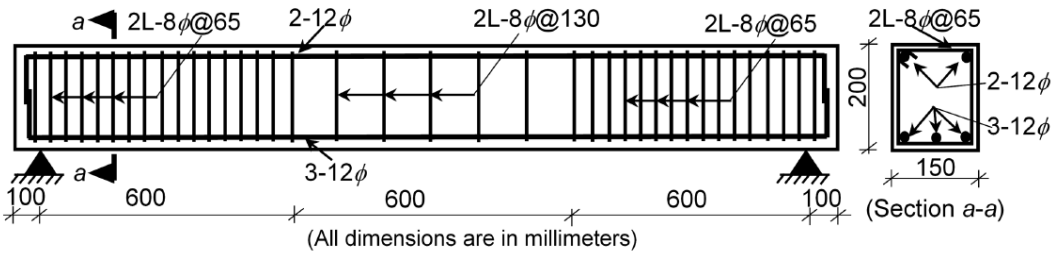

a) Geometry of specimens

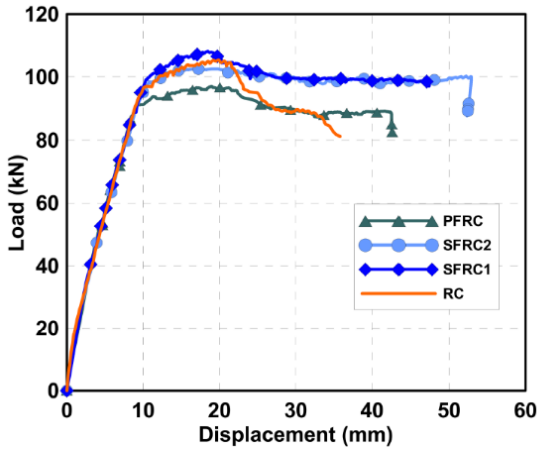

b) Load vs. displacement curve for beams with single fiber

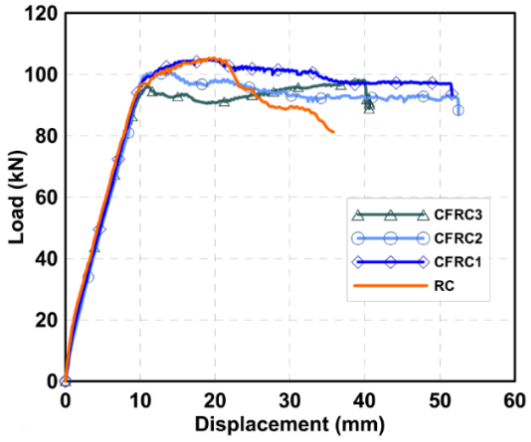

c) Load vs. displacement curve for beams with combined fibers

Figure 2-17 Sahoo et al. (2014) research

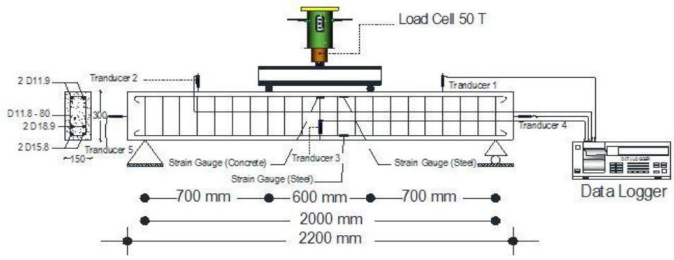

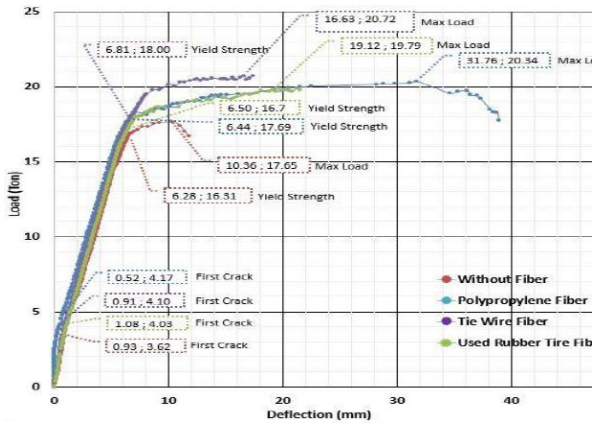

a) Test setup | b) Load vs. deflection curve for different beams

Figure 2-18 Aulia & Rinaldi (2015) research

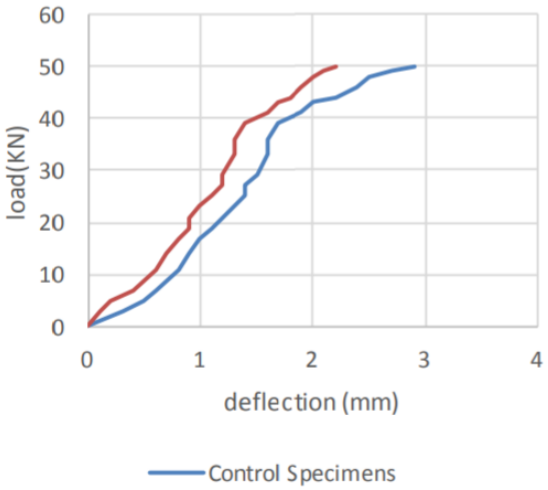

a) Detail of reinforcement used | b) Load vs. deflection curve

Figure 2-19 Sundar et al. (2017) research

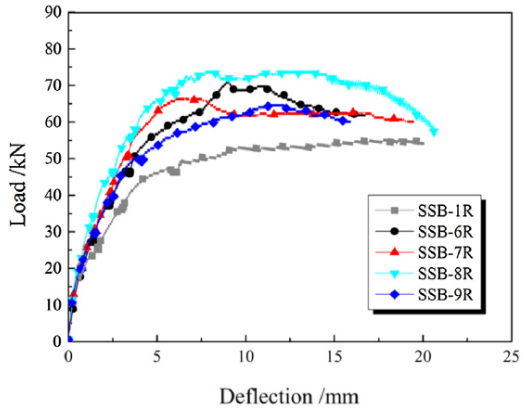

a) Test setup | b) Load vs. deflection curve

Figure 2-20 Zhang et al. (2018) research

2.4 Previous Research on Impact and Blast Performance of SNFRC

2.4.1 Previous Impact tests

This section summarizes previous studies which have examined the effect of synthetic fibers on the dynamic properties of concrete under impact, including tests on smaller-scale cylinders/prisms, panels/plates and beams (see **Table 2-5**).

Small-scale tests on cylinders and prisms:

Wang et al. (1996) tested 9 small concrete beams under impact tests (1 with no fibers, 2 with fibrillated polypropylene fibers, 5 with hooked-end steel fibers, and 1 with long crimped steel fibers) using a drop-weight setup. The fiber content used in the specimens ranged between 0.25-1.5%. The beams had a cross-section of 102×102 mm and were 355 mm long. Cumulative impact tests were conducted using a 60 kg impact hammer held at a 150 mm drop-height as shown in **Figure 2-21a**. Sample results for 0.25% and 0.5% PP fibers are shown in **Figure 2-21b**. Results show that adding 0.5% of polypropylene fibers by volume increased the fracture energy by only 21%. Hence, this type of fiber wasn't as effective under dynamic loading. Beams with 0.75% crimped steel fiber had a similar result to beams with 0.75% hooked steel fibers. Findings show that as the volume of hooked steel fibers increases, the fracture energy increases. However, there is a critical value of fibers at which this fracture energy increases. This value was found to be between 0.5% and 0.75% for hooked steel fibers.

Zhang (2008) conducted impact tests on FRC cylinders in compression and beams in flexure. The cylinders had a diameter of 100 mm and a height of 200 mm. The beams had a cross-section of 100×100 mm and were 350 mm long. For the compression tests, a 578 kg mass was dropped with a maximum drop-height of 2.5 m. **Figure 2-22a** shows the setup. For the impact flexural tests, a drop-weight of 60 kg was used with a maximum drop-height of 2 m. Two types of fibers were used in the analysis: a steel fiber with flattened ends (at 0.5% volume fraction) and a synthetic fiber made of a blend of polypropylene and polyethylene (at 1% volume fraction). The main parameters investigated were the type and volume of fibers used. For the flexural impact test, PP fibers showed more efficient energy absorption capacity at low drop heights while steel fibers were more efficient at higher drop heights. Moreover, the stress rate sensitivity of concrete was reduced when the fiber content was high. For the compressive impact tests, results show that the strength increased as the drop-height increased, for both the PP and steel FRC. Moreover, the compressive strength under impact was higher for steel FRC, while the PP-FRC had a large scatter of results. **Figure 2-22b** shows the result for synthetic FRC.

Nia et al. (2012) conduced a further impact study on twelve 150×64 mm cylindrical specimens using a drop-weight setup. In the tests, a mass with a weight 4.54 kg at a height of 457 mm was released repeatedly hitting a steel ball which in turn hit the concrete sample. **Figure 2-23a** shows the test setup. The specimens tested were as follows: 2 plain concrete, 6 polypropylene FRC, and 4 steel FRC. The fiber content ranged from 0.5-1% for steel fibers and from 0.2-0.5%

for synthetic fibers. The specimens were also prepared with 2 water-cement ratios: 0.36 and 0.46. Results show that even though both types of fibers improved the impact strength of concrete, steel fibers performed better than polypropylene fibers. This is due to their hooked ends, which provided more cohesion, and their larger length. Moreover, fibers improved the energy absorption capacity of concrete regardless of the water-cement ratio. **Figure 2-23b** shows the results obtained.

Weidner et al. (2012) investigated the effect of impact loading on 100×200 mm cylinders under low-velocity impacts using a drop hammer setup as shown in **Figure 2-24a**. The main parameters investigated were: concrete composition (normal weight concrete – NWC vs. fiber-reinforced concrete – FRC), drop heights, and loading types (room temperature vs. elevated temperature, up to 400˚F). Macro-synthetic fibers were added at 1% by volume of the FRC. Results show that, for compression tests at room temperature, the DIF and strain rates were higher for the FRC specimens compared to that of the NWC for both 8 ft and 16 ft drop heights. On the other hand, for tension tests, the FRC specimens had lower DIF than NWC. At elevated temperatures, the DIF and strain rates were lower for the FRC when compared to NWC for both compression and tension. Compared to room temperature, elevated temperatures caused a decrease in DIF and strain rates in FRC for both 8 ft and 16 ft drop heights. **Figure 2-24b** summarizes the test results for several samples.

Saadun et al. (2016) examined the dynamic response of nine 50×50 mm cylindrical concrete specimens under high-velocity impact loads. The main parameter investigated was the effect of adding macro-synthetic polypropylene (PP) fiber on dynamic compressive strength and dynamic increase factor (DIF) of concrete. Three samples were casted for three mix types: plain concrete (SC3) and concrete mixed with varying amounts of PP fibers (SC1: 1 kg/m^3 and SC2: 2 kg/m^3). Specimens were tested using a Split Hopkinson Pressure Bar (SHPB) setup under a strain rate of 10 s^{-1} as shown in **Figure 2-25a**. Results show that the ultimate dynamic compressive strength of concrete was increased significantly when PP fibers were added, with the increase observed being proportional to the volume of PP fibers. In addition, PP fibers at 2 kg/m^3 were better able to absorb impact, recording lower critical strains when compared to plain concrete. Finally, results show that the DIF is directly proportional to the increase in volume of PP fibers as shown in **Figure 2-25b**. **Figure 2-25c** to **Figure 2-25e** compares the stress-strain curve for the three samples tested under dynamic load.

Zhang et al. (2019) investigated the behaviour of 37×74 mm hybrid fiber-reinforced concrete cylinders under impact loads using a Split Hopkinson Pressure Bar (SHPB) apparatus as shown in **Figure 2-26a**. The main parameters investigated were: fiber hybrid ratio (V_f = 0.05, 0.075, 0.1% for basalt fiber – BF and V_f = 0.15, 0.25, 0.35, 0.5% for macro-synthetic polypropylene fiber – SF) and strain rate. Results show that a ratio of 0.075%-0.35% (BF-SF) was considered optimal as it provided the best impact resistance with different fiber enhancement contributions. For instance, BF was effective in enhancing the impact strength while SF improved impact toughness as illustrated in **Figure 2-26b**. Finally, increasing the strain rate was found to improve the overall impact response.

Tests on panels and plates (slabs):

Mindess & Yan (1993) tested small circular concrete and FRC plates under low velocity impact loading as shown in **Figure 2-27a**. A drop-weight with a mass of 345 kg was used with impact velocities ranging from 1.34 to 2.67 m/s. The specimens had a diameter of 245 mm and a thickness of 25 mm. Two concrete mix designs were tested: normal-strength (40 MPa) and high-strength (75 MPa). The fibers used in the analysis were fibrillated polypropylene fibers (0.5% by volume) or hooked steel fibers (1% by volume). Results show that both fibers increased the peak load and fracture energy of concrete as shown in **Figure 2-27b**. However, steel fibers had a greater effect compared to polypropylene fibers. This was attributed to the fact that they not only had a larger volume but also their elastic modulus was higher. Nonetheless, both fibers reduced the damage on the back faces of the specimens.

Xu et al. (2004) tested 5 centrally loaded round panels under low velocity impact loading as shown in **Figure 2-28a**. The tested panels were as follows: 1 plain HSC, 2 HSC with steel fibers and 2 HSC with a blend of polypropylene and polyethylene synthetic fibers. The panels had a diameter of 650 mm and a thickness of 60 mm, while the fiber content ranged between 0.5-1%. Results show that the peak load increased with the addition of fibers, however the increase in strength was slightly lower for the panels with synthetic fibers when compared to steel fibers. All panels with fibers showed a more ductile behaviour when compared to plain panels. For the synthetic fiber panels, fibers tended to break under low-velocity impact loading due to reduced impact resistance contribution. For the steel fiber panels, fibers pulled-out during loading leading to more impact resistance. The effect of the loading rate was also analyzed. Results show that panels tested at 300 mm drop-height showed less toughness when compared to companion panels tested at a lower drop-height of 150 mm. Finally, as the fiber volume increased, the toughness under impact resistance increased with steel fibers being more effective than synthetic fibers as shown in **Figure 2-28b**.

Horska et al. (2015) examined the performance of 9 FRC plates under impact loading using the setup shown in **Figure 2-29a**. The square slabs had dimensions of 300×300 mm with variable thicknesses (30/60/120 mm). The fibers used in the study were polypropylene and steel fibers at a fiber content of 9 and 80 kg/m^3 respectively. The main parameters investigated were the effects of fiber type, fiber content, and slab thickness. Results show that slabs reinforced with steel fibers were able to slow the burden of the impact the most. Moreover, samples with a depth of 120 mm were almost able to stop the burden. On the other hand, slabs with 30 mm depth had the least impact resistance. **Figure 2-29b** summarizes the static and dynamic strength of different slabs.

Ong et al. (1999) investigated the resistance of 10 square slabs under low velocity projectile impact. The test was achieved by dropping a 43 kg projectile from a height of 4 m as shown in **Figure 2-30a**. The slabs had a size of 1 m × 1 m and were 50 mm thick. The main parameters investigated were the fiber type and volume. Studied fiber types included: polyolefin, polyvinyl alcohol (PVA) and steel, while the volume fraction was either 1% or 2%. Results show that concrete slabs reinforced with steel fibers had the best performance in terms of energy absorption

and cracking characteristics. Moreover, for the same fiber volume, slabs with PVA fibers had higher fracture energy and energy absorption capacities compared to polyolefin fiber-reinforced slabs as shown in **Figure 2-30b**. Finally, the mode of failure for both PVA and steel fibers was pullout while that of polyolefin fibers was pullout and rupture.

Tests on larger-scale beams:

Several previous studies have examined the effect of steel fibers on the impact performance of larger-scale reinforced concrete beams, including: Min et al. (2014), Jin et al. (2017), Ulzurrun & Zanuy (2017) and Lee et al. (2018). In comparison, research on the impact performance of reinforced concrete beams built with synthetic fibers is scarce.

Banthia et al. (1987) assessed the impact performance of 50 beams using an instrumented drop-weight test setup as shown in **Figure 2-31a**. The specimens tested were as follows: 19 normal-strength concrete beams, 19 high-strength concrete beams, 6 fiber-reinforced concrete beams with 1.5% by volume steel fibers, and 6 fiber-reinforced concrete beams with 0.5% by volume polypropylene fibers. The beams had a cross-section of 100×125 mm and were 1400 mm long. A 345 kg impact hammer was dropped from various heights at the midpoint of the simply supported beams. Results show that for both normal-strength and high-strength concrete, the impact strengths and fracture energies increased with the increase in stress rate. Under dynamic loading, fiber-reinforced concrete was found to have improved impact resistance when compared to plain concrete due to its increased ductility. However, steel fibers gave better results than polypropylene fibers as they had multiple peaks in the load vs. deflection plot. **Figure 2-31b** shows a sample result for the polypropylene fiber-reinforced concrete.

Chorzepa et al. (2017) presented a further study which investigated the behavior of 14 reinforced concrete beams using a drop-weight impact test setup. The beams had a cross-section of 150×254 mm and were 2286 mm long. **Figure 2-32a** and **Figure 2-32b** show the beam details and test setup respectively. Four types of fibers were used: microscale polyvinyl alcohol (PVA) (0.5% by volume), carbon nanofibers (CNF) (0.01% by volume) and macroscale polypropylene and steel fibers (0.5% by volume). The main focus of the study was the effect of combining multiscale fibers on the impact performance of the beams. Results show that beams with CNF alone didn't show any enhancements as the failure mode was brittle. On the other hand, macroscale polypropylene and steel fibers improved ductility and toughness. Moreover, using multiscale fibers noticeably altered the mechanism of impact energy dissipation by reducing spalling damage. For example, combining microscale PVA and macroscale fibers was effective in minimizing the local crushing damage. **Figure 2-32c** shows the mid-span deflection-time history for several specimens.

Table 2-5 Summary of previous impact tests

Study	Test method	No. of specimens	Specimen type	Reinforced	Specimen dimension (mm)				Type of concrete	Drop-height (mm) or Strain rate (s^{-1})	f_c' (MPa)	Fibers						
					B	H	L	D				Type	*Content* (kg/m^3 or %)	Micro-synthetic	Macro-synthetic	L_f (mm)	d_f (mm)	Aspect Ratio
Zhang et al. (2019)	SHPB	12	Cylinder	No	-	37	-	74	HYFRC	10^1-10^2	42.5	BF	0.05-0.1%	×		12	0.015	800
												PP	0.15-0.5%		×	15	0.8	19
Chorzepa (2017)	Drop weight (flexure)	14	Beam	Yes	150	254	2286	-	SNFRC	6096	41.1-51	CNF	0.01%	N/A		0.05-0.2	0.0001	500-2000
									SNFRC			PVA	0.5%	×		8	0.038	211
									SNFRC			PP	0.5%		×	54	0.5	108
									SFRC			HE	0.5%	N/A		30	0.55	55
Saadun et al. (2016)	Drop weight (compressive)	3	Cylinder	No	-	50	-	50	OPC	10 s^{-1}	33	-	-	N/A		-	-	-
		6									28-35	PP	1-2 kg/m^3		×	38 & 54		
Horska et al. (2015)	Drop weight (flexure)	9	Tile	No	300	30-120	300	-	OPC	4100	-	-	-	N/A		-	-	-
									SNFRC			PP	9 kg/m^3		×	54		
									SFRC			FE	80 kg/m^3	N/A		13 & 60		
Weidner et al. (2012)	Drop weight (comp. & tensile)	89	Cylinder	No	-	203.2	-	101	OPC	2438-4877 mm	75	-	-	N/A		-	-	-
									SNFRC			PP	1		×	50.8		
Nia et al. (2012)	Drop weight (compressive)	2	Cylinder	No	-	64	-	150	OPC	457 mm	-	-	-	N/A		-	-	-
		4							SFRC			HE	0.5-1%	N/A		60	0.75	80
		6							SNFRC			PP	0.2-0.5%	×		12	0.02	600
Zhang (2008)	Drop weight (compressive)	160	Cylinder	No	-	200	-	100	SFRC (HSC)	250-1000 mm	54-121	FE	0.5-1%	N/A		30	-	-
	Drop weight (flexural)	192	Beam	No	100	100	350	-	SNFRC (HSC)	250-1500 mm		PM	0.5-1%		×	50		
Xu et al. (2004)	Drop weight (flexural)	1	Round panel	No	-	6012	-	650	HSC	150-300 mm	80	-	-	N/A		50	-	-
		2							SFRC (HSC)			SF	0.5-1%	N/A		50		
		2							SNFRC (HSC)			PM	0.5-1%		×	50		
Ong et al. (1999)	Drop weight (flexure)	10	Slab	No	1000	50	1000	-	SNFRC	4000	-	PO	0-2%		×	50	0.63	79
									SNFRC			PVA		×		12	0.2	60
									SFRC			HE		N/A		30	0.5	60
Wang et al. (1996)	Drop weight (flexural)	1	Beam	No	102.4	102.4	355.6	-	OPC	150 mm	-	-	-	N/A		-	-	-
		2							SNFRC	151 mm		PP-FB	0.25-0.5%		×	38	0.5	76
		5							SFRC	152 mm		HE	0.25-1.5%	N/A		30	0.5	60
		1							SFRC	153 mm		LC	0.75%	N/A		50	1	50
Mindess & Yan (1993)	Drop weight (flexural)	14	Circular plates	No	-	25.4	-	245	SNFRC	2500 mm	40-75	PP	0.5%	×		-	-	-
									SFRC			HE	1%	N/A		30	0.5	60
Banthia et al. (1987)	Drop weight (flexure)	50	Beam	Yes/No	100	125	1400	-	OPC (SFRC & SNFRC)	0.15-0.5	42	-	-	N/A		-	-	-
												HE	1.5	N/A		50		
									HSC (SFRC & SNFRC)		82	PP-FB	0.5		×	37		

Fiber type: SF = steel fiber, SN = synthetic fiber, HY = hybrid fiber; HE = hooked-end, FE =flattened ends, LC = long crimped; BF = basalt, PP = polypropylene, CNF = carbon nanofiber, PP-FB = polypropylene fibrillated, PO = polyolefin, PVA = polyvinyl alcoholic, PM = polymeric mix

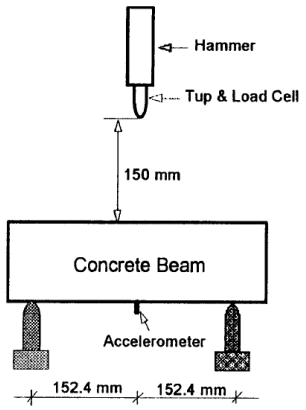

a) Test setup

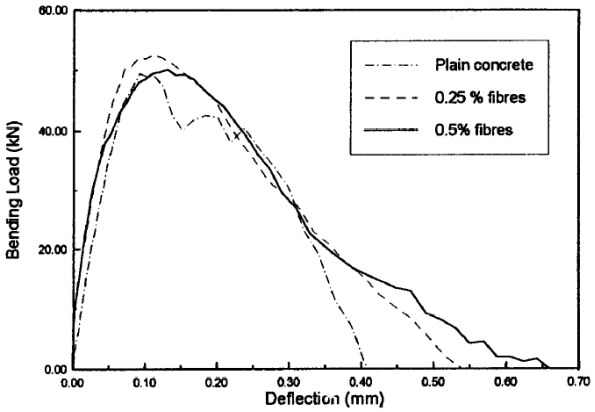

b) Bending load vs. deflection for polypropylene FRC

Figure 2-21 Wang et al. (1996) research

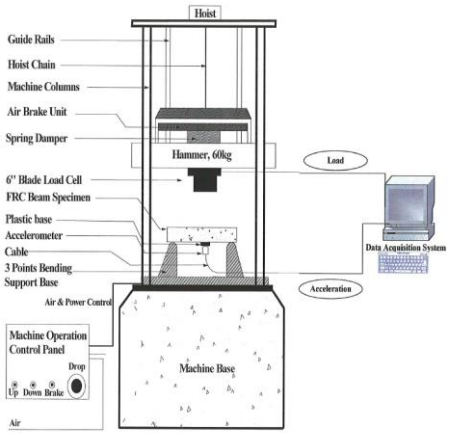

a) Drop-weight impact machine

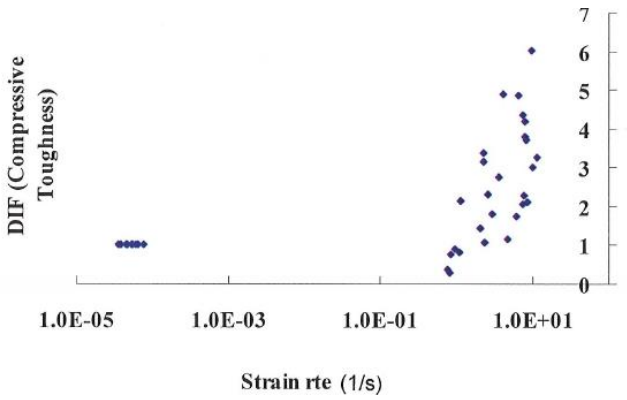

b) Toughness improvement with increasing strain rate for synthetic FRC

Figure 2-22 Zhang (2008) research

a) Specimen test setup

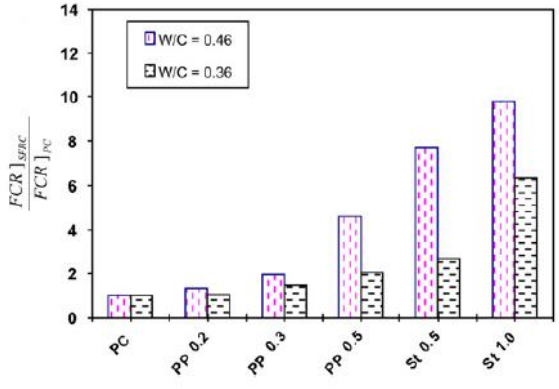

b) Ratio of impact strengths of FRC (with different types of fibers and volumes) to that of PC for 1st crack

Figure 2-23 Nia et al. (2012) research

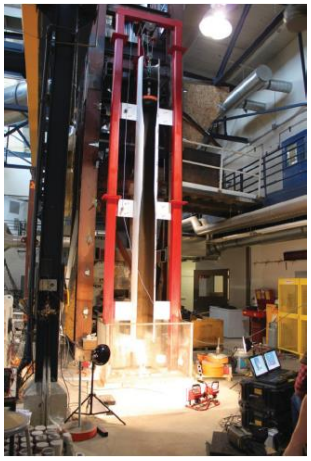

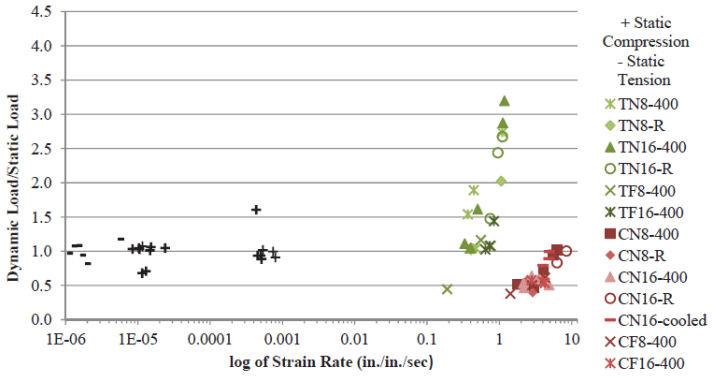

a) Test setup | b) Dynamic increase factor vs. strain rate

Figure 2-24 Weidner et al. (2012) research

Code	Dynamic Compressive Strength (MPa)	Static Compressive Strength (MPa)	DIF
SC1	74.5	34.87	2.14
SC2	116.4	28.08	4.15
SC3	65.8	33.4	1.97

a) SHPB setup | b) Experimental results

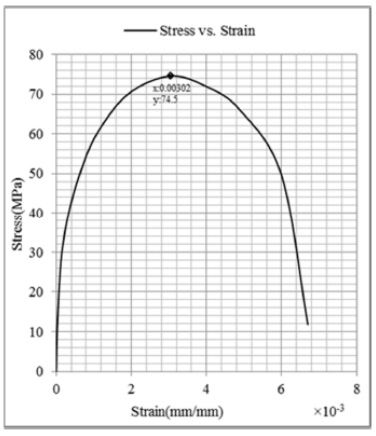

c) Stress-strain for SC1 under dynamic load

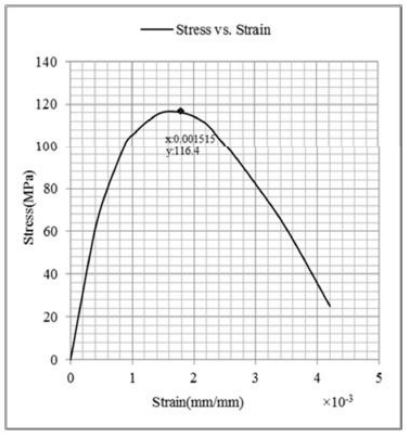

d) Stress-strain for SC2 under dynamic load

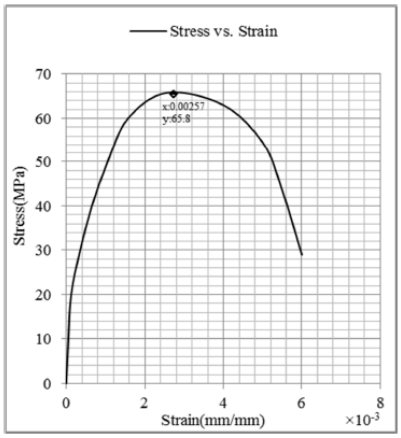

e) Stress-strain for SC3 under dynamic load

Figure 2-25 Saadun et al. (2016) research

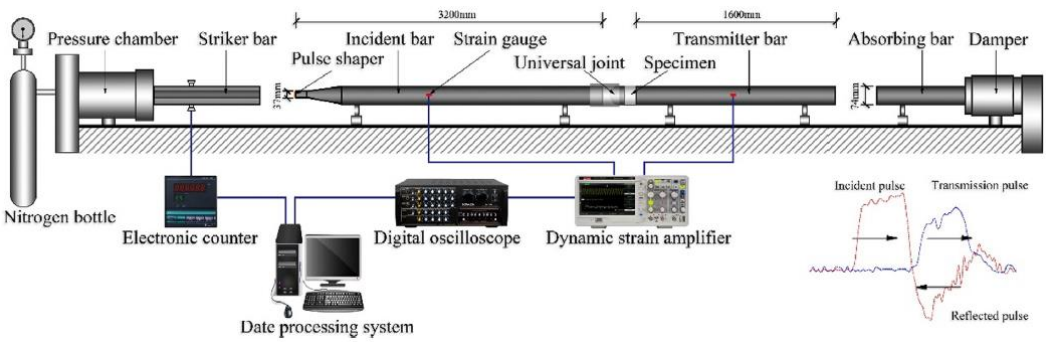

a) SHPB apparatus

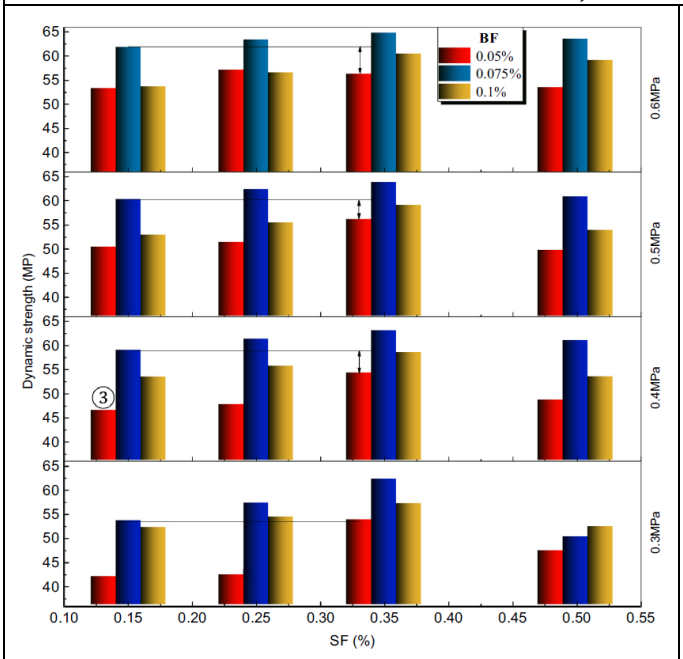

b) Fiber hybrid ratio effect on impact strength

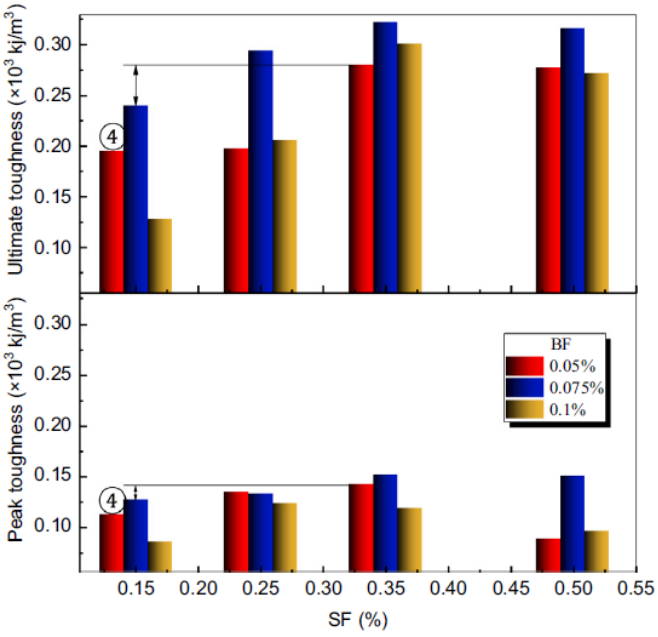

c) Fiber hybrid ratio effect on impact toughness

Figure 2-26 Zhang et al. (2019) research

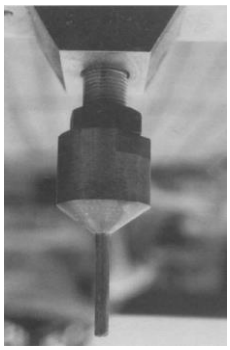

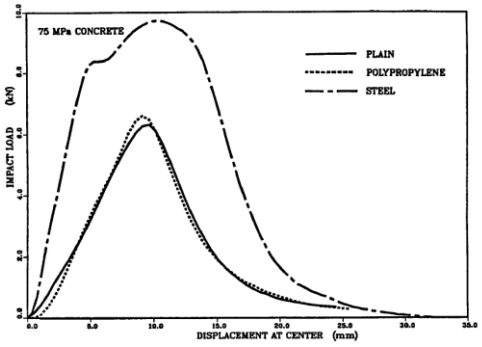

a) Tip of test setup

b) Load vs. deflection curve for different plates under impact (for 75 MPa concrete)

Figure 2-27 Mindess & Yan (1993)

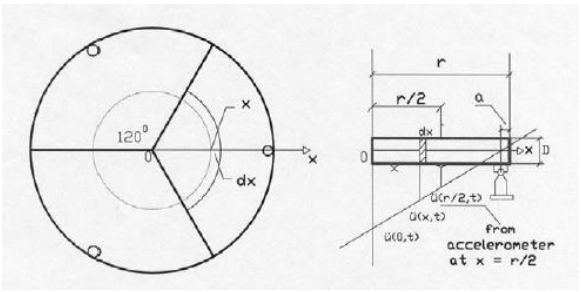

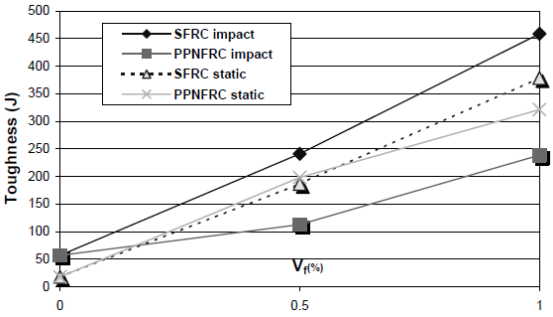

a) Round panel setup

b) Effect of fiber type and volume on panel toughness at 40 mm deflection

Figure 2-28 Xu et al. (2004) research

Concrete mixtures	h [mm]	Burden [kg]	F_{dyn} [kN]	F_{stat} [kN]	F_{dyn}/F_{stat}
NSC	30	20.6	5.2	4.4	**1.18**
NSC	30	46.4	6.2	4.4	**1.41**
NSC	60	46.4	15.5	17.2	**0.90**
NSC	60	75.2	20.7	17.2	**1.20**
NSC	120	46.4	74.2	81.0	**0.92**
NSC	120	75.2	75.2	81.0	**0.93**
NSC-PP-9	30	20.6	6.9	5.7	**1.21**
NSC-PP-9	30	46.4	7.7	5.7	**1.35**
NSC-PP-9	60	46.4	23.2	23.5	**0.99**
NSC-PP-9	60	75.2	30.1	23.5	**1.28**
NSC-PP-9	120	46.4	116.0	92.2	**1.26**
NSC-PP-9	120	75.2	120.2	92.2	**1.30**
NSC-FE-80	30	20.6	8.2	6.5	**1.26**
NSC-FE-80	30	46.4	7.7	6.5	**1.18**
NSC-FE-80	60	46.4	23.2	24.5	**0.95**
NSC-FE-80	60	75.2	33.8	24.5	**1.38**
NSC-FE-80	120	46.4	102.1	109.0	**0.94**
NSC-FE-80	120	75.2	137.8	109.0	**1.26**

a) Test setup

b) Static and dynamic strength of different slabs

Figure 2-29 Horska et al. (2015)

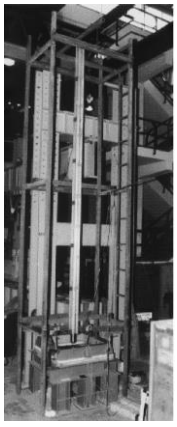

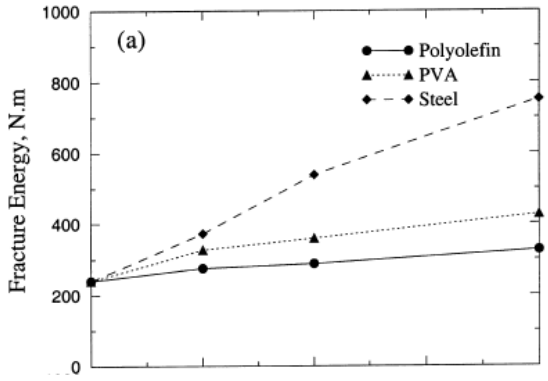

a) Test setup

b) Effect of fiber type and volume on fracture energy

Figure 2-30 Ong et al. (1999) research

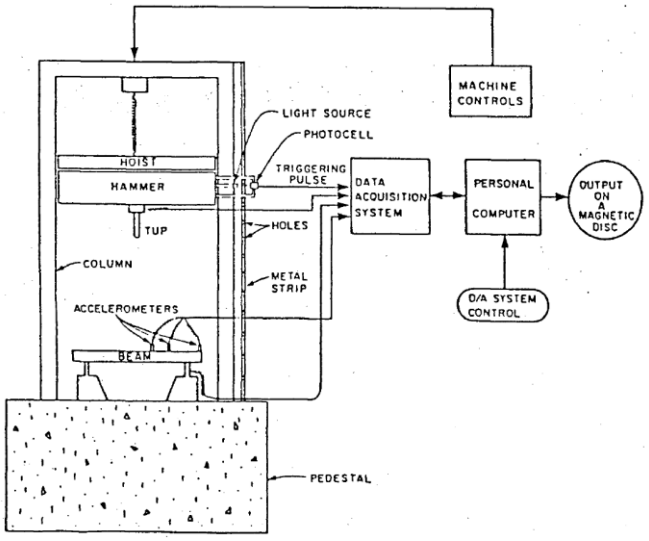

a) Test setup

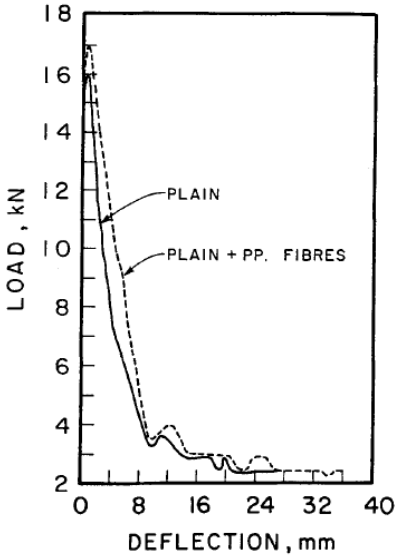

b) Load vs. deflection curve for plain and polypropylene FRC beams

Figure 2-31 Banthia et al. (1987) research

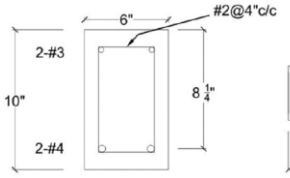

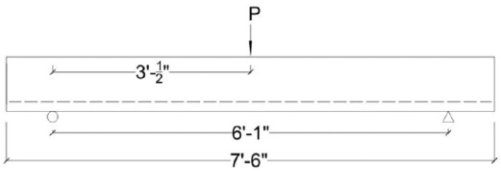

a) Beam details

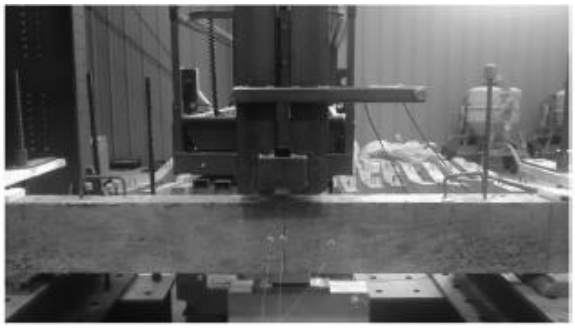

b) Drop-weight impact test setup

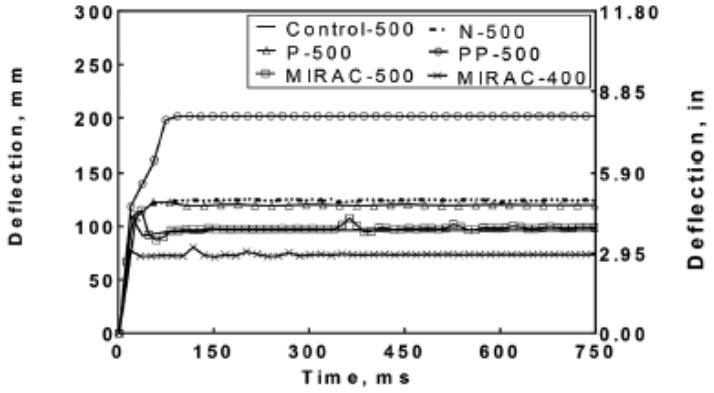

c) Mid-span deflection-time history

Figure 2-32 Chorzepa et al. (2017) research

2.4.2 Previous Blast Tests on SNFRC Structures

As shown in **Table 2-6**, limited studies have examined the effect of synthetic fibers on the blast performance of concrete structures, with most previous tests conducted on panel and slab type elements (see **Table 2-6**) as discussed in this section.

Previous tests on panels and slabs:

Ohtsu et al. (2007) examined the dynamic failure of 4 slabs (reinforced concrete (RC), polyvinyl alcoholic fiber-reinforced concrete (PVAFRC) with 5% fiber volume fraction, polyethylene fiber-reinforced concrete (PEFRC) with 4% fiber volume fraction, and polypropylene fiber-reinforced concrete (PPFRC) with 1.5% fiber volume fraction) under blasting as shown in **Figure 2-33a**. The slabs had dimensions of 60 cm × 60 cm × 10 cm. The main parameter investigated was the effect of fiber addition on the flexural toughness of concrete exposed to blast. Results show that RC slab (with 0.2 kN·m flexural toughness) had the largest spall area, while the PEFRC slab (with 45.9 kN·m toughness) had the smallest spall area (**Figure 2-33b**). Hence, adding polymeric fiber reinforcement improves the flexural toughness of concrete which in turn decreases the damaged volume.

Foglar & Kovar (2013) investigated the blast resistance of 5 bridge decks (3 FRC and 2 RC) using 25 kg of TNT charges placed at a distance from the slab. **Figure 2-34a** shows the experimental setup. The specimens were 6 m long, 1.5 m wide and 0.3 m thick. Polypropylene synthetic fibers were used at a volume fraction of 0.5% and 1%. Slabs were reinforced longitudinally and transversally. The compressive strength of concrete used in the specimens was either 30 or 55 MPa. The main parameters investigated were the effects of fiber volume, concrete compressive strength and the combination of both on blast resistance. Results show that fibers changed the failure mode from brittle to ductile. Moreover, debris was more attached by the fibers making it harder to eject during the tests, with the volume of debris reduced. Specimens with higher compressive strength performed better and were less damaged. Combining fibers and high-strength concrete improved the blast performance of slabs significantly. **Figure 2-34b** shows a comparison of the blast performance of the different specimens.

Tabatabaei et al. (2013) tested 7 panels (3 RC and 4 FRC) using 34 kg of TNT at a standoff distance of 1675 mm and zero angle of incidence as shown in **Figure 2-35a**. The panels measured 1830×1830 mm and were 165 mm thick. Two types of fibers were used in the analysis (long carbon fiber Type A and long carbon fiber Type B). The fiber was added at 1.5% and 1% by volume for Type A and B respectively. The main parameter investigated was the effect of fiber on blast performance of panels. Results show that the spalling resistance of concrete increased significantly with the addition of long carbon fibers (either Type A or B). Moreover, fibers reduced the degree of cracking and increased blast resistance. **Figure 2-35b** shows the surface damage of panels. It was also found that fibers contributed to a significant decrease in flying debris.

Pantelides et al. (2014) tested eighteen 1.2 m square panels (RC and FRC) with different thicknesses under blast detonations as shown in **Figure 2-36a**. **Figure 2-36b** shows the specimen

details. Macro-synthetic polymer fibers were used in this study at a volume of 1% for the FRC specimens. Reinforcement consisted of steel and/or GFRP (glass fiber-reinforced polymer) bars. **Figure 2-36c** provides a description of the panels. The main parameters investigated were the effects of macro-synthetic fibers, GFRP bars and their combination on the blast resistance of concrete. Results show that in RC panels, GRFP bars caused a brittle failure when compared to the ductile failure caused by steel bars. Reinforcing FRC panels with steel bars was found to enhance the blast performance when compared to FRC panels without steel bars. Among the panels tested, the FRC panel with steel bars (C4) showed the best results as shown in **Figure 2-36d**.

Drdlova et al. (2018) examined the blast resistance of 500×500×40 mm hybrid fiber-reinforced high-performance concrete panels exposed to explosives at 100 mm from the specimen as illustrated in **Figure 2-37a**. The main parameter investigated was the effect of combining fibers with various geometries (high-modulus steel/middle-modulus PVA and high-modulus steel/low-modulus PP). Results show that hybrid reinforcement significantly enhances the overall blast resistance in terms of reduced spalling and fragmentation. The performance of the steel-PVA (50 mm and 12 mm respectively) fiber-reinforced panel significantly outperformed that of the companion specimen containing steel-PP fibers due to the high tensile strength and modulus of elasticity of PVA, which further strengthened the fiber-matrix bond strength (see **Figure 2-37b** and **Figure 2-37c**).

Previous tests on vehicle barriers:

Coughlin et al. (2010) tested the behaviour of 5 portable concrete vehicle barriers under satchel sized contact charge explosives as shown in **Figure 2-38a**. One barrier was a control barrier with normal concrete. Two other barriers were fiber-reinforced, one had nylon fibres while the second had carbon fibers. Both had 1.5% fibers by volume. The final two barriers were constructed with a mix of steel and synthetic fibers each with a different fiber volume (3.8% and 5%). The barriers had a rectangular shape with dimensions of 3050×1070×610 mm. The main parameters investigated were the type of fiber and the fiber content. Results show that using fiber-reinforced concrete reduced damage and helped keep damaged concrete more intact. Both the 3.8% and 5% steel/synthetic fiber mixes had similar performance. In other words, when a certain level of fiber volume is reached, adding more fibers won't affect the results. Finally, fibers with high surface area, like carbon fibers, gave fragments greater cohesiveness resulting in larger fragments. **Figure 2-38b** shows the percentage of barrier fragment ejected during blast.

Previous tests on beams:

To the knowledge of the author there exists no research on the blast behavior of SNFRC beams. However, a limited number of studies have focussed on steel FRC.

Magnusson et al. (2010) examined the blast performance of plain and steel fiber-reinforced concrete beams with dimensions of 300 mm × 160 mm × 1720 mm under air blast loading, which was applied at a standoff distance of 10 m (see **Figure 2-39a**). The beams were constructed with NSC or HSC and were reinforced with varying longitudinal ratios and stirrups spaced at 200 mm. Results show that the use of steel fibers prevented brittle failures under dynamic loading while ensuring a ductile failure mode due to the enhanced shear strength and ductility as shown in **Figure 2-39b**.

Among these studies, four were conducted at the University of Ottawa. The test program involved beams having similar characteristics in terms of specimen detail and test setup in order to allow for comparison between the results. Algassem (2016) tested the behaviour of plain and steel fiber-reinforced high-strength concrete beams with dimensions of 125 mm × 250 mm × 2440 mm under dynamic blast loads using a shock-tube as illustrated in **Figure 2-40a**. The results show that the use of steel fibers led to significant improvements including: increased shear capacity, reduced maximum and residual mid-span displacements, reduced blast fragments and increased damage tolerance. Fibers at a volume of 1% were also sufficient to replace transverse reinforcement (see **Figure 2-40d** and **Figure 2-40e**).

Li (2016) examined the static and dynamic behaviour of 125 mm × 125 mm × 2440 mm HSC beams detailed with high-strength reinforcement. Results show that reinforcing the beams with high-strength bars increased blast capacity and controlled maximum and residual displacements. Adding steel fibres was found to be effective in controlling crack width, increasing fragmentation resistance, reducing displacements and further increasing blast load capacity. Despite these enhancements, the combined use of HSC and high-strength steel led to a more brittle failure as illustrated in **Figure 2-40b** and **Figure 2-40c**.

Castonguay (2017) investigated the behaviour of 18 steel fiber-reinforced concrete beams under quasi-static (see **Figure 2-40h**) and simulated blast loading using the shock-tube. The 125 mm × 125 mm × 2440 mm beams were cast with normal-strength self compacting concrete. The results illustrated in **Figure 2-40i** show the significant effect of steel fibers in improving shear and flexural capacity of the beams. Furthermore, increasing fiber content to a certain volume fraction was found to improve the overall blast response by reducing mid-span displacement, improving damage tolerance and reducing fragmentation. Further increases in fiber content was found to negatively affect workability without any noticeable enhancements in performance.

Charles (2019) examined the effect of reinforcement detailing by testing 17 HSC beams under static and dynamic loading. Results show that the provision of compression bars and closely spaced ties improved the blast performance by controlling displacement, increasing blast capacity and minimizing damage (see **Figure 2-40f** and **Figure 2-40g**).

Table 2-6 Summary of previous blast tests

Study	Test method	No. of specimens		Specimen type	Kg of TNT	Standoff distance (mm)	Cross-section dimension (mm)			f_c' (MPa)	Tension steel				Transverse steel			Fibers						
							B	H	L		Diameter (mm)	Spacing (mm)	Yield strength (MPa)	Reinforcement ratio (%)	Spacing (mm)	Yield strength (MPa)	Reinforcement ratio (%)	Type	Content (%)	Micro-synthetic	Macro-synthetic	L_f (mm)	d_f (mm)	Aspect ratio
Drdlova et al. (2018)	Live test	11		Panel	0.1-0.15	100	500	40	500	114	-	-	-	-	-	-	-	SF	3	N/A		30-50	0.6-0.8	50-63
																		PP		×		6-12	0.018	333-667
																		PVA		×		6-12	0.04-0.1	120-150
Pantelides et al. (2014)	Live test	18	Normal steel	Panel	6.2-15.6	1000	1200	152-356	1200	46-51	10 - 16	152-305	420	0.61-1.72	152-305	420	-	-	-	N/A		-	-	-
			GFRP								10 - 16	152-305	717-758	0.61-1.72	152-305	717-758	-	P	1		×	50	0.9	56
Foglar & Kovar (2013)	Live test	5		Bridge deck	25	450	1500	300	6000	30 or 55	16	140	500	0.5	150	-	0.07	PP	0.5-1		×	54	-	-
Tabatabaei et al. (2013)	Live test	7		Panel	34	1675	1830	165	1830	45-54	13	150	407	0.82	300	-	0.03	LC	1-1.5		×	100	-	-
Coughlin et al. (2010)	Air blast loading using C-4 explosives	5		Vehicle barrier	Can't be disclosed due to sensitive nature of research	-	610	1070	3050	~35	-	-	-	-	-	-	-	N	1.5		×	75	-	-
																		C	1.5		×	75		
																		FE	2-2.5	N/A		30		
																		PP	0.066	×		Variable		
																		PP/PE	0.4-1.8		×	Variable or 50		
Ohtsu et al. (2007)	Close-in	4		Slab	0.01 of SEP	-	600	100	600	39-63	10	120	-	1.2	120	-	0.22	PVA/PE/PP	1.5-5		×	30	-	-

Fiber type: SF = steel fiber, SN = synthetic fiber; FE = flattened ends; P = polymer, PP = polypropylene, PE = polyethylene, PVA = polyvinyl alcoholic, LC = long carbon, N = nylon, C = carbon

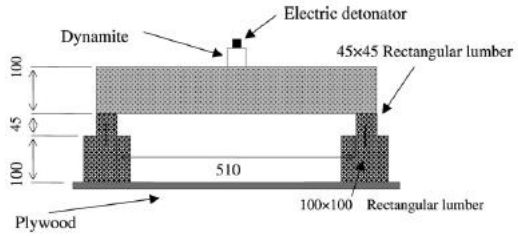

a) Test setup

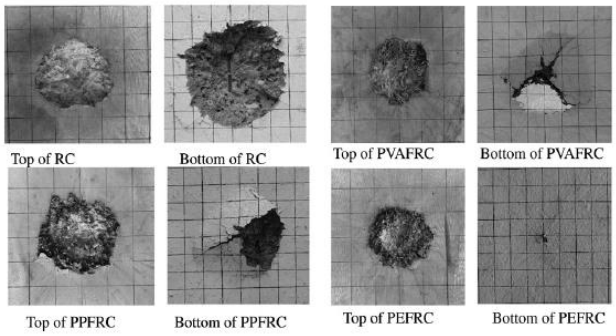

b) Damage patterns for each specimen

Figure 2-33 Ohtsu et al. (2007) research

a) Experimental setup

Specimen No.	1	2	3	4	5
Concrete	C30/37	C30/37	C55/67	C55/67	C30/37
Fibers	–	4.5 kg/m^3	–	4.5 kg/m^3	9.0 kg/m^3
Puncture – top surface	0.43 m^2	0.26 m^2	0.02 m^2	–	–
Concrete spalling (soffit) – <concrete cover	2.35 m^2	1.89 m^2	1.51 m^2	0.73 m^2	0.61 m^2
Concrete spalling (soffit) – >concrete cover	1.71 m^2	1.09 m^2	1.2 m^2	0.44 m^2	0.37 m^2
Concrete spalling (top surface) – <concrete cover	0.43 m^2	0.26 m^2	0.89 m^2	0.68 m^2	0.66 m^2
Concrete spalling (top surface) – >concrete cover	0.43 m^2	0.26 m^2	0.29 m^2	0	0.08 m^2
Concrete spalling (left side) – <concrete cover	0.52 m^2	0.05 m^2	0.08 m^2	0	0
Concrete spalling (left side) – >concrete cover	0.35 m^2	0	0.02 m^2	0	0
Concrete spalling (right side) – <concrete cover	0.34 m^2	0.16 m^2	0.08 m^2	0	0
Concrete spalling (right side) – >concrete cover	0.23 m^2	0.11 m^2	0.02 m^2	0	0
Volume of crushed concrete	0.23 m^3	0.15 m^3	0.20 m^3	0.05 m^3	0.06 m^3
Permanent deflection	0.31 m	0.37 m	0.28 m	0.30 m	0.26 m

b) Blast performance of different specimens

Figure 2-34 Foglar & Kovar (2013) research

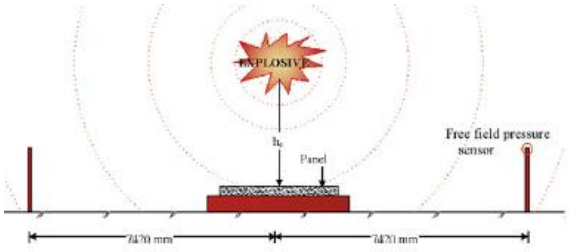

a) Blast test setup

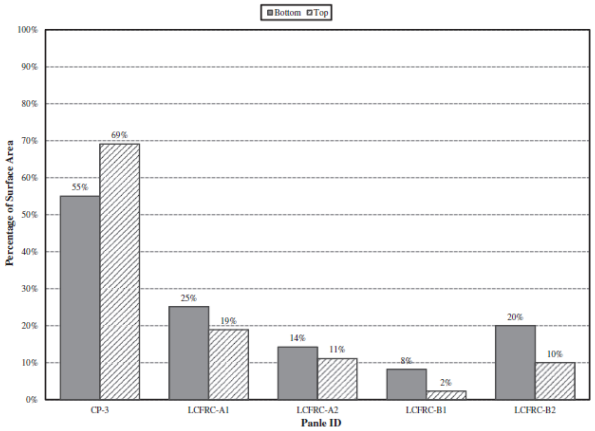

b) Surface damage of panels from both front and back

Figure 2-35 Tabatabaei et al. (2013) research

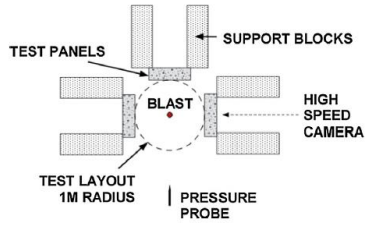

a) Test setup

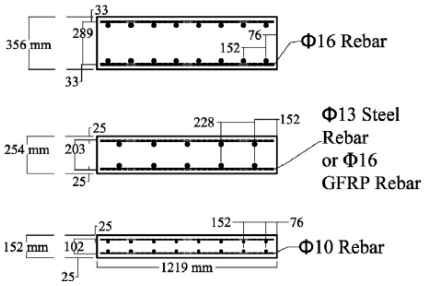

b) Specimen details

1.2 m × 1.2 m panels	
Type	Description
A4	RC (steel bars)
B4	FRC
C4	FRC + steel bars
D4	RC (GFRP bars)
E4	RC (steel bars) + GFRP laminate
COND	RC (GFRP bars)
CONB	FRC

c) Detailed description of panels

Specimen	Crack width	Deflection (mm)	Mass loss (%)	Level of protection (mm)
A4-6	16	82	30	Below AT[a] standards
A4-10	13	31	22	Below AT standards
B4-6	NA	NA	50	Below AT standards
B4-10	NA	NA	50	Below AT standards
C4-6[b]	2	5	0	Medium
C4-10	1.3	2	1	Medium
C4-14	0.1	1	5	Medium
D4-6	2	9	5	Very low
D4-10	13	12	20	Below AT standards
D4-14	6	2	10	Very low
E4-6	3	8	8	Very low
E4-10	13	3	5	Very low
E4-14	3	1	3	Medium
CON-1[c]	10	11	15	Below AT standards
CON-3[c]	16	43	40	Below AT standards

d) Test results

Figure 2-36 Pantelides et al. (2014) research

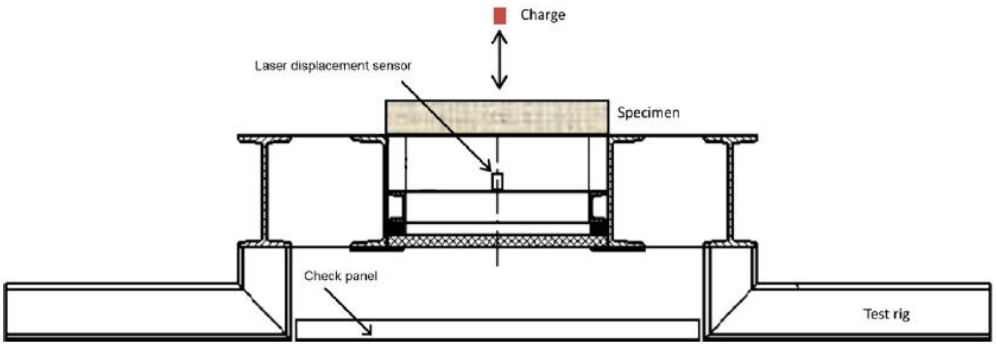

a) Blast setup

b) Steel + PP

c) Steel + PVA

Figure 2-37 Drdlova et al. (2018) research

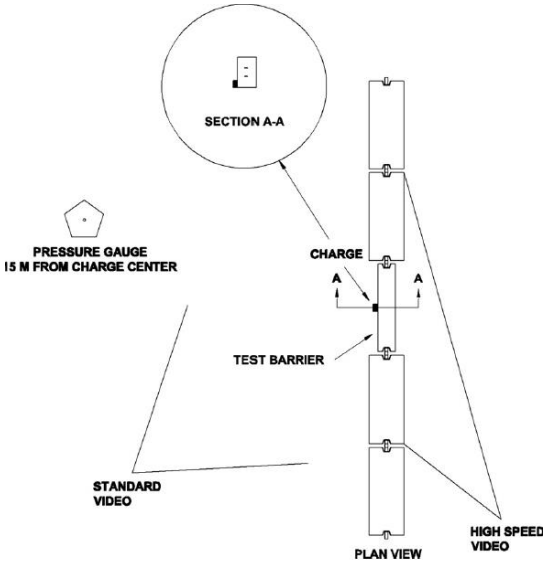

a) Test setup (plan view)

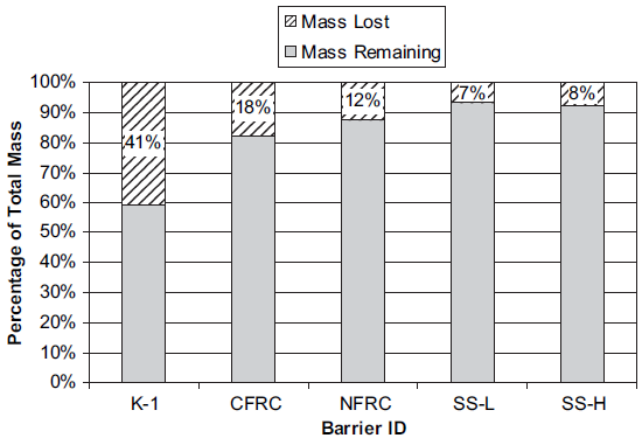

b) Percentage of barrier fragment ejected during blast

Figure 2-38 Coughlin et al. (2010) research

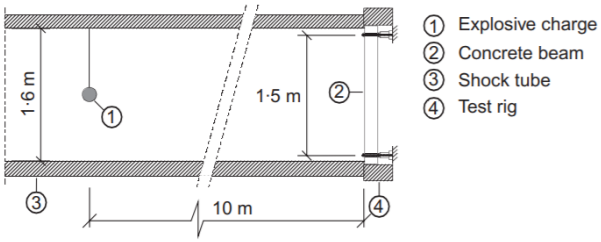

a) Test setup

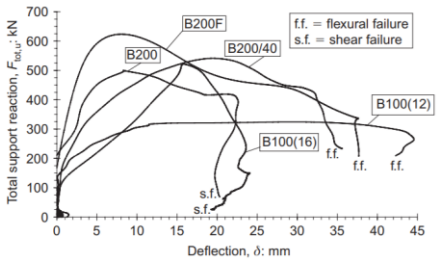

b) Sample support reaction-deflection curves of tested beams

Figure 2-39 Magnusson et al. (2010) research

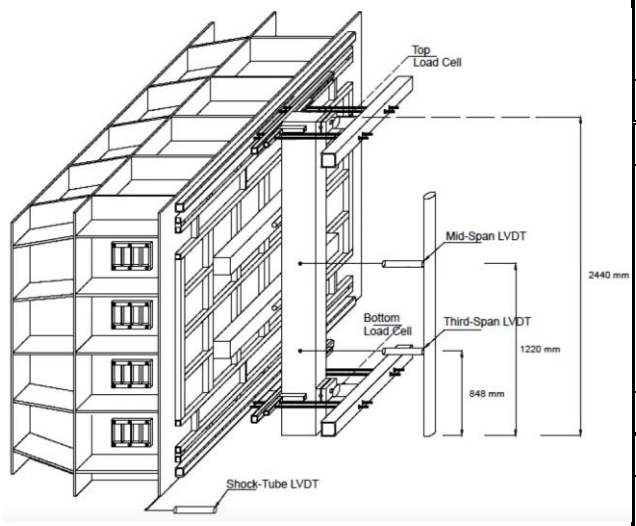

a) Blast test setup

Algassem (2016)

b) Plain HSC

c) HSC with 1% steel fibers

Li (2016)

d) Plain HSC + HSR

e) HSC with 1% steel fibers + HSR

Charles (2019)

f) Plain HSC + 10M + d/2

g) Plain HSC + 10M + d/4

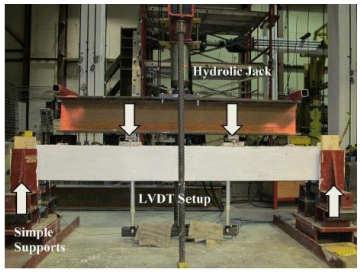

h) Static test setup

Castonguay (2017)

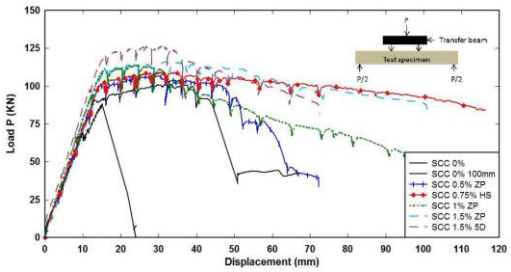

i) Load vs. displacement curves

Figure 2-40 Previous research performed at uOttawa

2.5 Summary

This chapter presented a literature review related to the shear and flexural behaviour of synthetic fiber-reinforced concrete beams under static loading. It also reviewed previous studies on the effect of synthetic fibers on the structural response of concrete under impact and blast loads. Based on these studies, the following conclusions can be summarized below:

- Material studies on SNFRC show that the use of synthetic fibers improves the post-peak capacity of concrete in compression with no significant effect on peak compressive strength. Moreover, the addition of synthetic fibers significantly affects the post-cracking tensile resistance of concrete with improved toughness;
- A limited number of studies have investigated the shear and flexural behaviour of SNFRC beams, especially in the case of high-strength concrete ($f_c^{'} \geq 60$ MPa). Based on these studies, the use of macro-synthetic fibers improved the shear strength, ductility and toughness of beams while also resulting in a more diffused cracking pattern with reduced crack widths;
- Research on the dynamic properties of concrete tested under impact indicates that the addition of synthetic fibers improves the impact resistance and toughness of concrete under dynamic loading, though the energy absorption capacity of synthetic fibers is greater at lower drop heights (strain-rates). Some studies also indicate that synthetic fibers are less effective under impact when compared to steel fibers;
- The behaviour of SNFRC under blast loads is not well understood, especially in the case of beams and elements built with high-strength concrete. Moreover, most previous research has focused on elements subjected to near-field blasts. Nonetheless, previous tests conducted on panels and slabs indicate that adding synthetic fibers improves the flexural toughness which in turn leads to a reduction in the volume of damage.

In summary, limited research exists on the response of high-strength concrete beams reinforced with macro-synthetic fibers. Moreover, the ability of macro-synthetic fibers to improve the blast resistance of concrete requires further study, especially in the case of beams and elements subjected to far-field type blasts. Furthermore, there is a need to examine the potential of using macro-synthetic fibers to relax stringent blast detailing requirements in modern blast codes.

Chapter 3: Experimental Program

3.1 Chapter Overview

The experimental research program includes seventeen beams built with macro-synthetic fiber-reinforced concrete which are tested under static and dynamic loads. Parameters investigated include the effects of: macro-synthetic fibers, hybrid fibers, combined use of fibers and stirrups, longitudinal reinforcement type and ratio. This chapter summarizes the details regarding beam specimen designs, material properties, specimen construction, experimental setups and testing procedures.

3.2 Specimen Specifications

A total of seventeen beams were constructed and tested in this research program. Nine of the beams were tested under quasi-static four-point bending, and eight were tested under simulated blast loading using the University of Ottawa's shock-tube. Most of the beams were cast using either plain high-strength concrete (HSC) or high-strength macro-synthetic fiber-reinforced concrete (HSFRC), with two beams casted with normal-strength self-consolidating concrete (SCC). The beam design details are summarized in **Figure 3-1**.

All specimens had dimensions of 125 mm × 250 mm × 2440 mm and were tested over a simply-supported span of 2232 mm, with a constant moment region of 750 mm and shear spans of 741 mm, resulting in a shear span to depth ratio (*a/d*) of 3.7. The longitudinal reinforcement consisted of either: 2-15M or 2-20M (Canadian size) normal-strength bars, or 2-No.5 (US size) ASTM A1035 Grade 690 MPa high-strength bars. The No.5 and 15M bars were detailed with 90° hooks (except for the 15M used for the SCC specimens), while the 20M bars were detailed with 180° hooks to provide adequate development of the tension steel. Eight of the seventeen beams were designed with transverse reinforcement which consisted of either U-shaped stirrups spaced at 100 mm in the shear spans (minimum stirrups required by the CSA A23.3 standard) or closed hoops spaced at 100 mm along the span of the beam (relaxed blast detailing at s = d/2 rather than the d/4 spacing required in the CSA S850 standard). Stirrups and hoops were made from 6.35 mm smooth steel wire. To facilitate construction, 2-6.35 mm bars were also provided in the shear spans of most beams (the exception was the doubly-reinforced beam which was provided with 2-10M top bars over the full span). The clear cover to the longitudinal bars was kept at 41 mm for all beams. Macro-synthetic fibers were implemented in all the fiber-reinforced concrete beams at a fiber content of 0.75% by volume of concrete (6.8 kg/m^3), with two specimens having a hybrid mix of 0.75% macro-synthetic fibers and 0.25% smooth straight steel fibers (19.5 kg/m^3).

The specimens can be divided into three categories based on longitudinal steel ratio (rebar size), which include the: 15M series, 20M series and No.5 high-strength steel series. **Table 3-1** shows a summary of the design details for the various beams within each series, including

specimen ID, concrete mix type, fiber type and volumetric ratio (V_f), steel reinforcement properties and loading type. The specimen nomenclature follows this logic:

CONCRETE TYPE - FIBER % and TYPE - STEEL REBAR SIZE - STIRRUPS

For instance, HSC-0.75%S1-15M-0 is the label for a beam constructed with high-strength concrete (HSC) having 0.75%S1 fibers and reinforced with 15M normal-strength longitudinal reinforcement with no stirrups, while HSC-0.75%S1-15M-S is the companion beam with stirrups. Similarly, HSC-0.75%S1-No.5(HS)-S is the label for the companion beam constructed with No.5 high-strength bars and stirrups.

The following nomenclature was used for one of the beams with top continuity bars:

CONCRETE TYPE - FIBER % and TYPE - STEEL REBAR SIZE (BOTTOM - TOP) - STIRRUPS

HSC-0.75%S1-20M-10M-d/2 is the ID for a beam built with high-strength concrete containing 0.75% macro-synthetic fibers and reinforced with 20M normal-strength longitudinal reinforcement, 10M compression bars at the top and closed ties spaced at 100 mm all the way.

Table 3-1 Specimen designation and main properties

Series	Beam ID	Concrete Type	Fibers		Steel Reinforcement Properties				Test Type[1]
			Type	V_f (%)	Type	Grade (MPa)	Amount & Size	Stirrup Spacing (mm)	
Series 15M	SCC-0.75%S1-15M-0	SCC	Synthetic (S1)	0.75	NS	400	2-15M	-	S
	SCC-0.75%S1-15M-S	SCC	Synthetic (S1)	0.75	NS	400	2-15M	100	S
	HSC-0%-15M-0	HSC	-	-	NS	400	2-15M	-	S/D
	HSC-0.75%S1-15M-0	HSFRC	Synthetic (S1)	0.75	NS	400	2-15M	-	S/D
	HSC-0.75%S1-15M-S	HSFRC	Synthetic (S1)	0.75	NS	400	2-15M	100	S/D
Series 20M	HSC-0.75%S1-20M-0	HSFRC	Synthetic (S1)	0.75	NS	400	2-20M	-	S/D
	HSC-0.75%S1-20M-S	HSFRC	Synthetic (S1)	0.75	NS	400	2-20M	100	S/D
	HSC-0.75%S1-20M-10M-d/2	HSFRC	Synthetic (S1)	0.75	NS	400	2-20M	100*	D
	HSC-HYB-20M-0	HSFRC	Synthetic (S1)	0.75	NS	400	2-20M	-	S/D
			Steel (OL)	0.25					
Series No.5	HSC-0.75%S1-No.5(HS)-S	HSFRC	Synthetic (S1)	0.75	HS	690	2-No.5	100	S/D

[1]: S: Static Test; D: Dynamic Test

*: Closed hoops provided over the full span

	Steel Reinforcement Details	Cross-Section
Without Stirrups	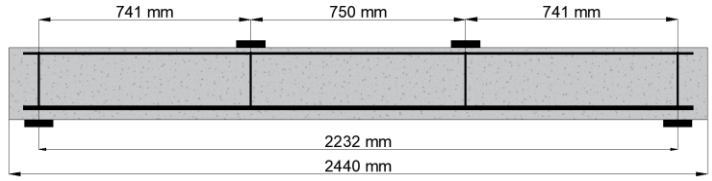 a) SCC beams with 0.75%S1 fibers	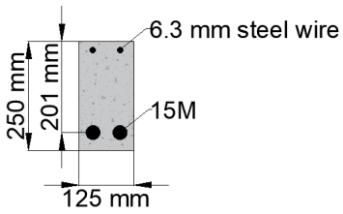
	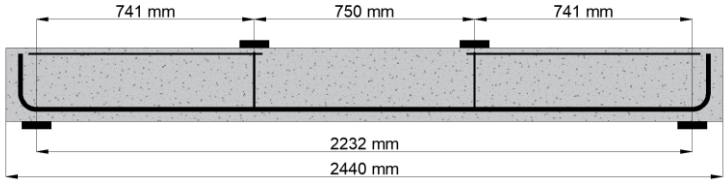 b) HSC beams with no fibers or 0.75%S1 fibers	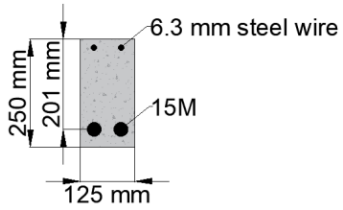
	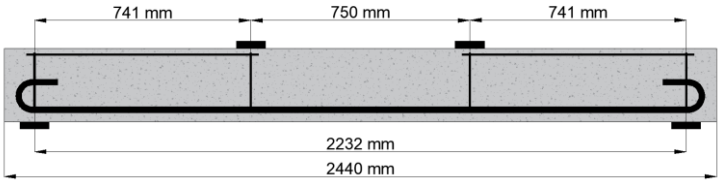 c) HSC beams with 0.75%S1 fibers or hybrid fibers	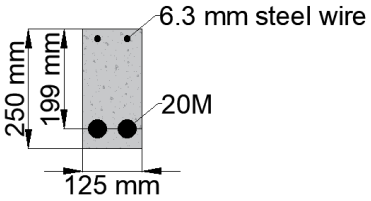
With Stirrups	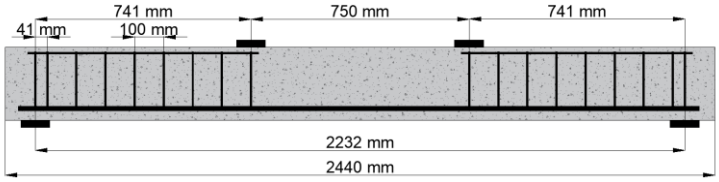 d) SCC beams with 0.75%S1 fibers and stirrups	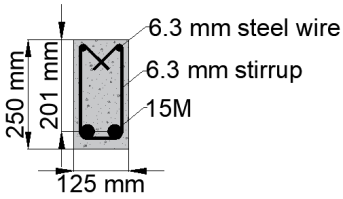
	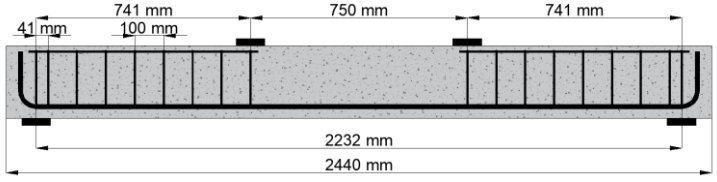 e) HSC beams with 0.75%S1 fibers and stirrups	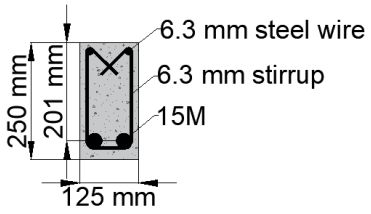
	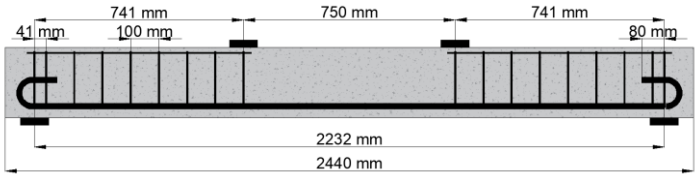 f) HSC beams with 0.75%S1 fibers and stirrups	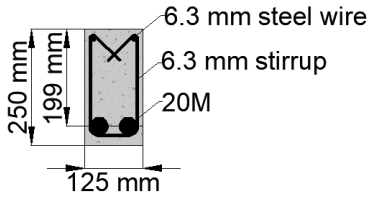
	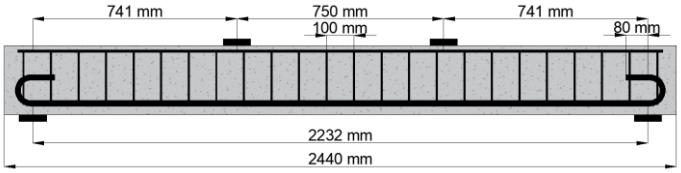 g) HSC beams with 0.75%S1 fibers and closed hoops	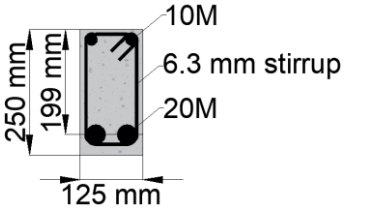

Figure 3-1 Beam dimensions and reinforcement details

3.2.1 Series 15M

A total of eight specimens were constructed using 15M normal-strength reinforcement. The beams can be divided into two groups, with two beams casted with self-consolidating concrete (SCC) and the remaining six beams casted with high-strength concrete (HSC). Both SCC specimens were tested under quasi-static loading. Three of the HSC specimens were tested under static four-point bending while the three companion beams were tested under dynamic loading. This series included beams with either stirrups, macro-synthetic fibers, or both.

3.2.2 Series 20M

This series included seven high-strength concrete beams reinforced with 20M normal-strength bars. Four of the specimens had macro-synthetic fibers incorporated at a volumetric ratio of 0.75%, two of which had no stirrups (one for static loading and one for dynamic loading) and the other two were detailed with stirrups spaced at 100 mm in the shear spans (one for static loading and one for dynamic loading). One of the specimens constructed for dynamic loading and reinforced with 0.75% macro-synthetic fibers had 10M bars at the top of the beam section with closed stirrups spaced at 100 mm all the way. The last two beams in this series had no stirrups and included hybrid fibers. The two types of fibers used for this specimen were macro-synthetic fibers with a fraction volume of 0.75% and smooth straight steel fibers with a volume of 0.25%.

3.2.3 Series No.5

The last series included two beams (one for static and one for blast) which were built with American Size No.5 high-strength bars. Both beams were detailed with stirrups spaced at 100 mm in the shear spans and were reinforced with 0.75% macro-synthetic fibers.

3.3 Materials

This section describes the materials used for this research, which include: concrete mixes, steel reinforcement bar types and fiber types.

3.3.1 Concrete Parameters

Three types of concrete were used in this study: self-consolidating concrete (SCC), high-strength concrete (HSC) and high-strength fiber-reinforced concrete (HSFRC). The concrete was mixed using the large pan-mixer at the University of Ottawa Structures Laboratory.

The SCC used consisted of a pre-packaged mix, shown in **Figure 3-2**, with a specified strength of 40 MPa. The mix contained a maximum aggregate size of 10 mm with a sand-to-aggregate ratio of roughly 0.45 and a water-cement ratio of approximately 0.42. An air-entraining admixture, a super-plasticizer and a viscosity-modifying admixture (VMA) were incorporated into the blend in the form of dry powder. **Table 3-2** shows the properties of the pre-packaged MS-S10 SCC mix provided by the manufacturer (*King Packaged Materials Company*). **Table 3-3** shows the properties of the HSC and HSFRC mixtures. The high-strength concrete mix in this study

contained Portland cement, slag, silica fume, two sizes of coarse aggregate (9.5 mm and 19 mm), sand and liquid admixtures (a super-plasticizer and a set retarder) and had a target strength of 100 MPa. **Figure 3-3** presents the materials used for the HSC base mix. The HSFRC mix was constructed with a similar HSC base mix, with the addition of fibers.

Table 3-2 KING SCC mix properties

Mix Component	**Content (kg/m^3)**
HSF Cement	500
Fine Aggregate	915
Coarse Aggregate	765
Mass Density	2300

Table 3-3 HSC and HSFRC mix properties

Solid Component	**Content (kg/m^3)**		
	Plain HSC	**HSFRC (Synthetic)**	**HSFRC (Hybrid)**
Type GU Cement	373	373	373
Slag	164	164	164
Silica Fume	48	48	48
Sand	740	740	740
Fine Aggregate (9.5 mm)	560	1120	1120
Coarse Aggregate (19 mm)	560	-	-
Fiber Content (S1, OL)	-	6.8 (S1)	6.8 (S1) + 19.5 (OL)
Liquid Component	**Content (L/m^3)**		
Water	176	176	176
Super-Plasticizer	7.5	10	11
Retarder	1.9	1.9	1.9

Figure 3-2 KING SCC

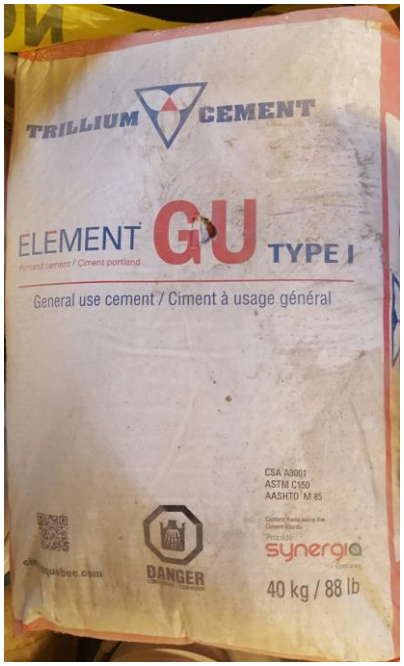

a) Type GU Cement

b) Silica Fume

c) Slag

d) Coarse Aggregate (19 mm)

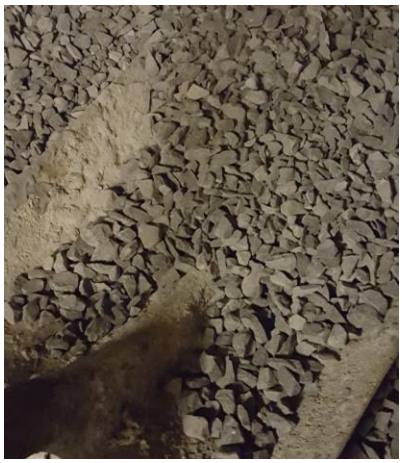

e) Fine Aggregate (9.5 mm)

f) Sand

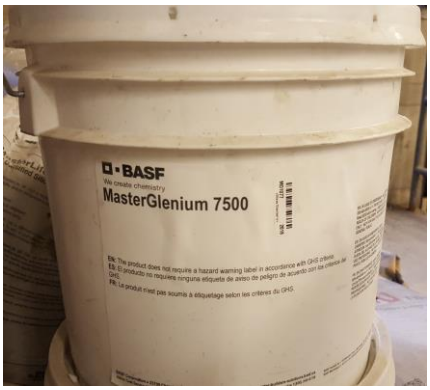

g) Super-Plasticizer

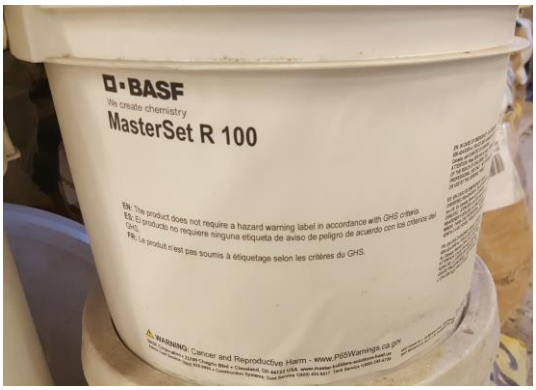

h) Retarder

Figure 3-3 Materials for HSC mix

3.3.2 Steel Reinforcement Parameters

Five types of steel reinforcement were used in this study. The first type was smooth non-deformed wire which had a diameter of d_b = 6.35 mm and a cross-section of A_b = 32 mm^2 and was used as either the transverse reinforcement or the compression reinforcement in the shear spans (for easier construction of the cages). The second type, which was used as compression steel for one of the dynamic specimens, consisted of deformed normal-strength steel (10M) with a diameter of d_b = 11.3 mm and a cross-section of A_b = 100 mm^2. The remaining three types of deformed steel were used for the tension longitudinal reinforcement and consisted of either normal-strength steel (15M and 20M) or high-strength ASTM A1035 bars (No.5). The 15M and No.5 rebars had diameters of d_b = 16.0 mm and d_b = 15.9 mm, respectively, with a cross-section of A_b = 200 mm^2, while the 20M rebar had a diameter of d_b = 19.5 mm and a cross-section of A_b = 300 mm^2.

Steel coupons were tested using the GALDABINI SUN 60 Universal Floor Standing Testing Machine shown in **Figure 3-4**. **Table 3-4** summarizes the properties of all five types of steel used, including steel ID, bar diameter and area, yield strain and strength, ultimate strain and strength and strain at rupture. **Figure 3-5**, **Figure 3-6** and **Figure 3-7** show the stress-strain curves for each type of steel. A comparison of the stress-strain relationship of all steel reinforcement used is demonstrated in **Figure 3-8**.

Table 3-4 Steel reinforcement mechanical properties

Steel ID	**Steel Reinforcement**	**Bar Diameter d_b (mm)**	**Bar Area A_b (mm^2)**	**Yield**		**Ultimate**		**Rupture**
				ε_y	f_y (MPa)	ε_u	f_u (MPa)	ε_r
6.3NS	Non-deformed	6.35	32	0.0031	559	0.063	617	0.069
10M	Regular	11.3	100	0.0026	477	0.149	569	0.173
15M	Regular	16.0	200	0.0027	434	0.137	586	0.209
20M	Regular	19.5	300	0.0030	426	0.143	568	0.202
No.5	MMFX2	15.9	200	0.0065	886	0.049	1144	0.107

Figure 3-4 GALDABINI Universal Floor Standing Testing Machine; testing steel rebar

Coupon Test	Stress-Strain Relationship
	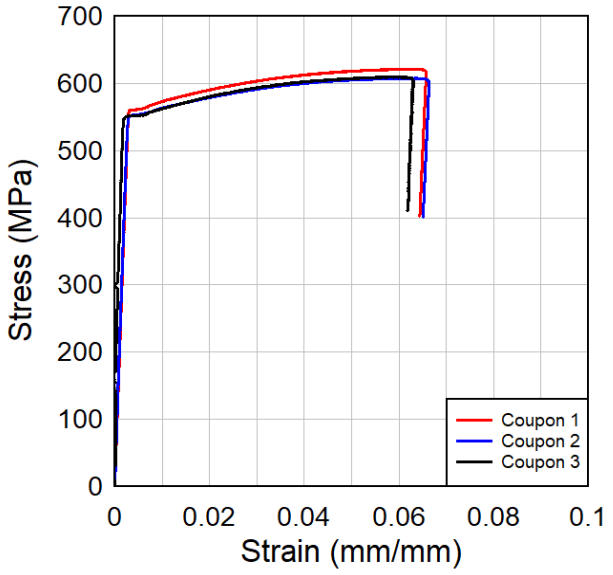
a) Rebar size 6.35 mm (Non-deformed)	
	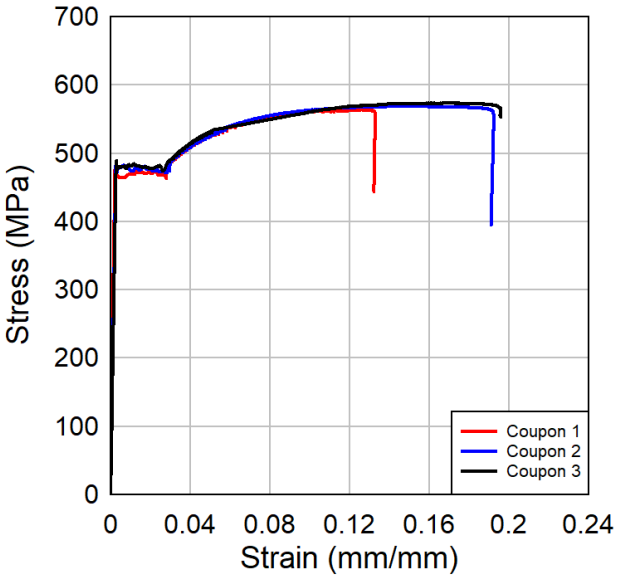
b) Rebar size 10M	

Figure 3-5 Stress-strain relationships for different types of steel bars with photographs

Coupon Test	Stress-Strain Relationship
	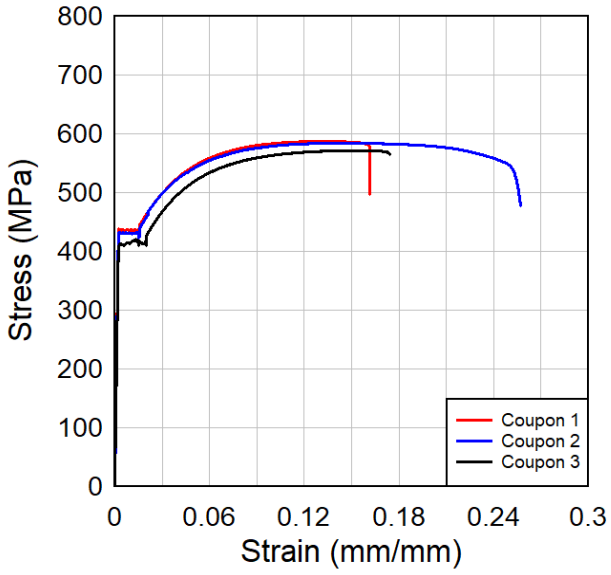
a) Rebar size 15M	
	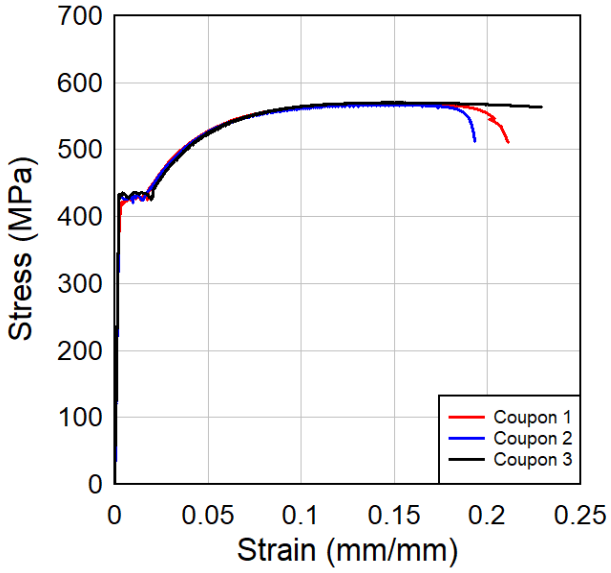
b) Rebar size 20M	

Figure 3-6 Stress-strain relationships for different types of steel bars with photographs

Coupon Test	Stress-Strain Relationship
	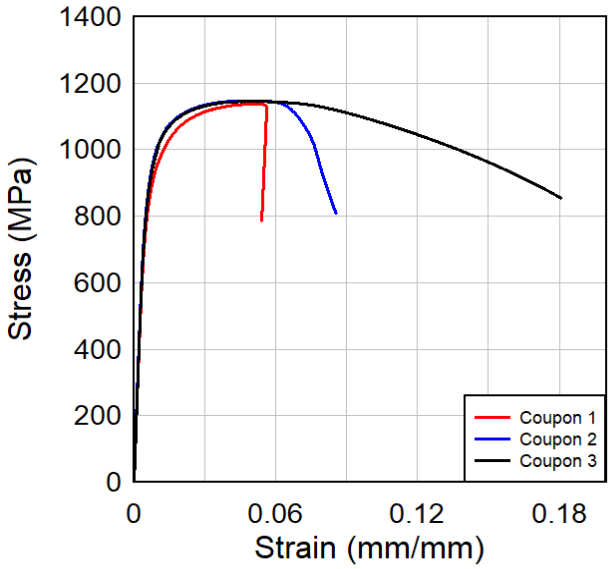
a) Rebar size No.5	

Figure 3-7 Stress-strain relationships for different types of steel bars with photographs

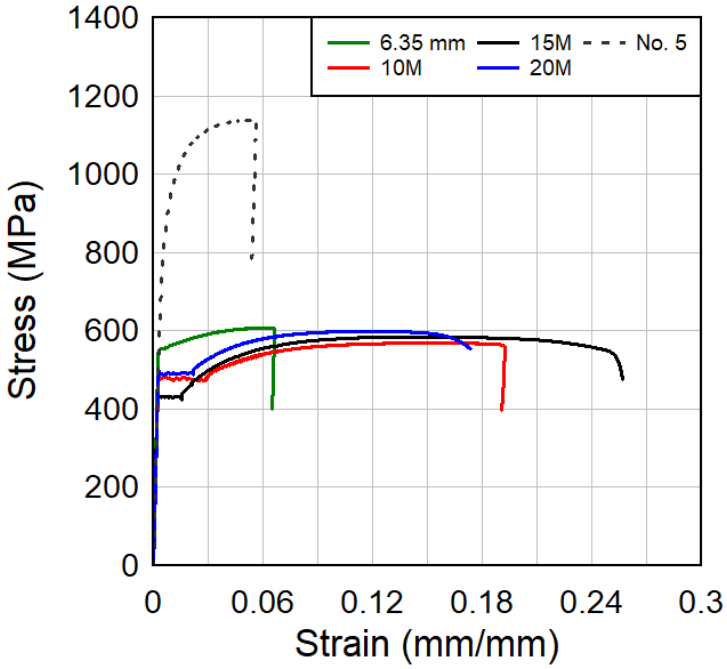

Figure 3-8 Comparison of stress-strain relationships for different types of steel bars used

3.3.3 Fibers Parameters

Two types of fibers were used in this research. The main fiber used in all the fiber-reinforced concrete beams was macro-synthetic fibers designated as "S1" fibers. These polypropylene fibers had a length of 50 mm, with a tensile strength of 625 MPa, and partially fibrillate when mixed in concrete. The other fiber used for the hybrid mix was smooth straight steel fibers having a length of 13 mm and a tensile strength of 2750 MPa (designated as "OL" fibers). **Table 3-5** summarizes the properties for both types of fibers, while **Figure 3-9** shows sample photos. The synthetic fiber-reinforced concrete beams were built with HSC containing 0.75% (V_f = 6.8 kg/m3) of macro-synthetic fibers. The smooth straight steel fibers were used in the hybrid mix at a volumetric ratio of 0.25% (V_f = 19.5 kg/m^3).

Table 3-5 Fiber properties

Fiber ID	Fiber Name	Length l_f (mm)	Diameter d_f (mm)	Cross-Section (mm × mm)	Aspect Ratio (mm/mm)	Tensile Strength (MPa)
S1	TUF-STRAND	50	-	0.37 × 1.1	74	625
OL	OL 13/.20	13	0.21	-	62	2750

a) S1

b) OL

Figure 3-9 Photographs of fibers

3.4 Construction of Test Specimens

The construction of the seventeen beams was accomplished at the University of Ottawa Structures Laboratory. The following procedures were followed: preparing the formwork, bending the steel bars, building the steel cages, applying the strain gauges, casting of the concrete and finally curing the beams.

3.4.1 Preparation

The first step was to build a wood formwork to be used for casting the beams. 4'× 8' sheet of 1/2" thick plywood was used as the base of the form with 2" × 4" studs placed on the sides to provide lateral support when casting the specimens. The form was able to fit seven specimens at a

time with 3/4" thick plywood being installed as a separator. **Figure 3-10** shows the formwork after it was ready to be used.

The steel cages were built either with or without stirrups. The transverse reinforcement consisted of either U-shaped stirrups or closed stirrups made from 6.35 mm wire and bent using a manually operated jig. The U-shaped stirrups were spaced at 100 mm in the shear spans for beams with shear reinforcement. Two top 6.35 mm wires were also provided in the shear spans to facilitate construction. The closed stirrups were used in only one of the 20M specimens tested under dynamic loading and were spaced at 100 mm throughout the entire length. Both the No.5 high-strength steel and 15M normal-strength steel were bent to have a 90° hook at both ends (except for the 15M used for the SCC specimens where the bars were kept straight). The 20M normal-strength bars were bent to have a 180° hook at both ends. **Figure 3-11** to **Figure 3-15** show photographs of the different steel cages after construction. Once the cages were ready, a strain gauge was installed at the mid-span of the longitudinal steel bar. A 120 Ω strain gauge was used on one of the bars for the static specimens and a 350 Ω strain gauge was used on both bars for the dynamic specimens. To prevent concrete from adhering to the form and allow for an easier removal of the beams, oil was applied into each row of the form using a brush. This also allows the reuse of the formwork. After oiling, 41 mm plastic chairs were placed inside the form to provide adequate clear cover. Finally, the steel cages were inserted inside the formwork.

Figure 3-10 Beam wood formwork

Figure 3-11 20M rebar with 10M compression bar and closed stirrups all the way

Steel cages with 90° hooks (no stirrups)

Figure 3-12 15M rebar without stirrups

Steel cages with 90° hooks (with stirrups)

Figure 3-13 15M & No.5 rebars with stirrups

Steel cages with 180° hooks (no stirrups)

Figure 3-14 20M rebar without stirrups

Steel cages with 180° hooks (with stirrups)

Figure 3-15 20M rebar with stirrups

3.4.2 Mixing and Curing

Concrete was mixed at the University of Ottawa Structures Laboratory using a 420-volt electric pan-mixer, as shown in **Figure 3-16**, with a capacity of 225 L. Once the mix was ready, the concrete was poured inside the form in layers and a vibrator was used throughout for both the HSC and HSFRC mix to ensure the concrete is well consolidated. The remaining mix was used to cast concrete cylinders and flexural beam prisms. After levelling the beams and allowing the concrete to dry for around three hours, all the specimens (beams, cylinders and prisms) were covered with a wet burlap sheet (as shown in **Figure 3-17**) and then a plastic sheet on top (to keep moisture) and cured for seven consecutive days. The beams were then removed from the form and air-cured until the day of testing.

Figure 3-16 Concrete pan mixer

Figure 3-17 Curing of beams

3.4.3 Fresh State Properties

The fresh state properties of most beams were recorded using a standard slump test. The ASTM C1611 “Standard Test Method for Slump Flow of Self-Consolidating Concrete” was used for the SCC mix. For this test, fresh concrete mix was poured into a metal cone. The cone is then raised. Once the concrete stopped flowing, the maximum diameters in any two perpendicular directions were measured and the average was taken as the slump. For the HSC and HSFRC mix, the ASTM C143 “Standard Test Method for Slump of Hydraulic-Cement Concrete” was

conducted. Like the previous test, concrete is poured into a metal cone but this time in three layers, where each layer is rodded twenty-five times before pouring the next layer. The top of the mould is then levelled and carefully raised. The difference in level between the top of the concrete and the top of the upturned cone is recorded as the slump. The slump test values are summarized in **Table 3-6**. Sample photographs are included in **Figure 3-18**.

Table 3-6 Concrete fresh state properties

Series	Beam ID	Concrete Type	Fibers		Test Type[1]	Slump (mm)
			Type	V_f (%)		
Series 15M	SCC-0.75%S1-15M-0	SCC	Synthetic (S1)	0.75	S	510*
	SCC-0.75%S1-15M-S	SCC	Synthetic (S1)	0.75	S	510*
	HSC-0%-15M-0	HSC	-	-	S/D	230
	HSC-0.75%S1-15M-0	HSFRC	Synthetic (S1)	0.75	S	120
	HSC-0.75%S1-15M-0	HSFRC	Synthetic (S1)	0.75	D	120
	HSC-0.75%S1-15M-S	HSFRC	Synthetic (S1)	0.75	S	-
	HSC-0.75%S1-15M-S	HSFRC	Synthetic (S1)	0.75	D	130
Series 20M	HSC-0.75%S1-20M-0	HSFRC	Synthetic (S1)	0.75	S	120
	HSC-0.75%S1-20M-0	HSFRC	Synthetic (S1)	0.75	D	120
	HSC-0.75%S1-20M-S	HSFRC	Synthetic (S1)	0.75	S	130
	HSC-0.75%S1-20M-S	HSFRC	Synthetic (S1)	0.75	D	130
	HSC-0.75%S1-20M-10M-d/2	HSFRC	Synthetic (S1)	0.75	D	110
	HSC-HYB-20M-0	HSFRC	Synthetic (S1)	0.75	S	110
			Steel (OL)	0.25		
	HSC-HYB-20M-0	HSFRC	Synthetic (S1)	0.75	D	145
			Steel (OL)	0.25		
Series No.5	HSC-0.75%S1-No.5(HS)-S	HSFRC	Synthetic (S1)	0.75	S	198
	HSC-0.75%S1-No.5(HS)-S	HSFRC	Synthetic (S1)	0.75	D	110

[1]: S: Static Test; D: Dynamic Test
*: Slump flow

a) SCC-0.75%S1

b) HSC-0%

c) HSC-0.75%S1

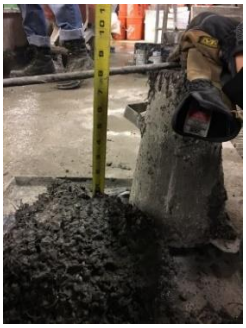

d) HSC-1%ZP

e) HSC-HYB

Figure 3-18 Slump test photographs

3.4.4 Hardened State Properties

This section summarizes the hardened state properties of the different concrete casts performed. These properties include: compressive strength, stress-strain relationship and flexural strength and toughness.

3.4.4.1 Compressive Cylinder Test

Six 100 mm × 200 mm cylinders were cast for each mix. Three of these cylinders were tested to get the compressive strength (at 7 days, 14 days and 28 days) in accordance to ASTM C39 "Standard Test Method for Compressive Strength of Cylindrical Concrete Specimens". The results are reported and summarized in **Figure 3-19** and **Table 3-7**. Among these values, the concrete in beam HSC-0.75%S1-15M-S recorded a relatively low compressive strength value (it is noted that the concrete batch was very stiff with almost no slump which caused difficulties in fabricating the cylinders). The three remaining cylinders were tested using the 1000 kN PILOT CONTROL machine which was connected to a StrainSmart data acquisition system to record the data as shown in **Figure 3-20**. **Figure 3-21** shows typical stress-strain curves. Photographs of cylinders after failure are shown in **Figure 3-22**.

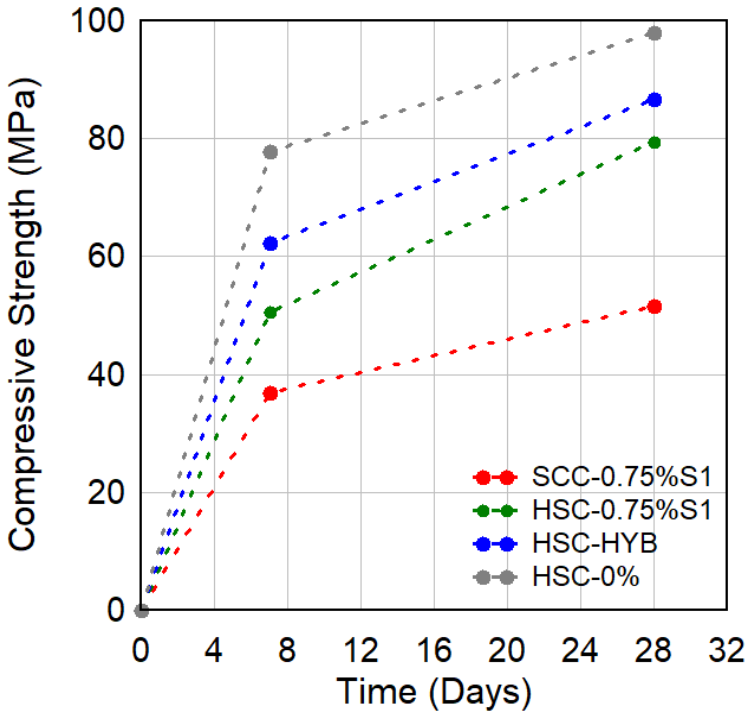

Figure 3-19 Concrete compressive strength with time

Table 3-7 Concrete compressive strength summary

Series	Beam ID	Concrete Type	Fibers		Cylinder Test Compressive Strength (MPa)	Test Type *
			Type	V_f (%)	Avg. strength at 28 days / day of beam test	
Series 15M	SCC-0.75%S1-15M-0	SCC	Synthetic (S1)	0.75	51.6	S
	SCC-0.75%S1-15M-S	SCC	Synthetic (S1)	0.75	51.6	S
	HSC-0%-15M-0	HSC	-	-	101.0	S
	HSC-0%-15M-0	HSC	-	-	96.5	D
	HSC-0.75%S1-15M-0	HSFRC	Synthetic (S1)	0.75	71.4	S
	HSC-0.75%S1-15M-0	HSFRC	Synthetic (S1)	0.75	89.6	D
	HSC-0.75%S1-15M-S	HSFRC	Synthetic (S1)	0.75	57.0	S
	HSC-0.75%S1-15M-S	HSFRC	Synthetic (S1)	0.75	89.9	D
Series 20M	HSC-0.75%S1-20M-0	HSFRC	Synthetic (S1)	0.75	78.3	S
	HSC-0.75%S1-20M-0	HSFRC	Synthetic (S1)	0.75	89.6	D
	HSC-0.75%S1-20M-S	HSFRC	Synthetic (S1)	0.75	89.2	S
	HSC-0.75%S1-20M-S	HSFRC	Synthetic (S1)	0.75	89.9	D
	HSC-0.75%S1-20M-10M-d/2	HSFRC	Synthetic (S1)	0.75	86.4	D
	HSC-HYB-20M-0	HSFRC	Synthetic (S1)	0.75	90.8	S
			Steel (OL)	0.25		
	HSC-HYB-20M-0	HSFRC	Synthetic (S1)	0.75	86.7	D
			Steel (OL)	0.25		
Series No.5	HSC-0.75%S1-No.5(HS)-S	HSFRC	Synthetic (S1)	0.75	91.6	S
	HSC-0.75%S1-No.5(HS)-S	HSFRC	Synthetic (S1)	0.75	86.4	D

*: S: Static Test; D: Dynamic Test

Figure 3-20 Cylinder testing setup

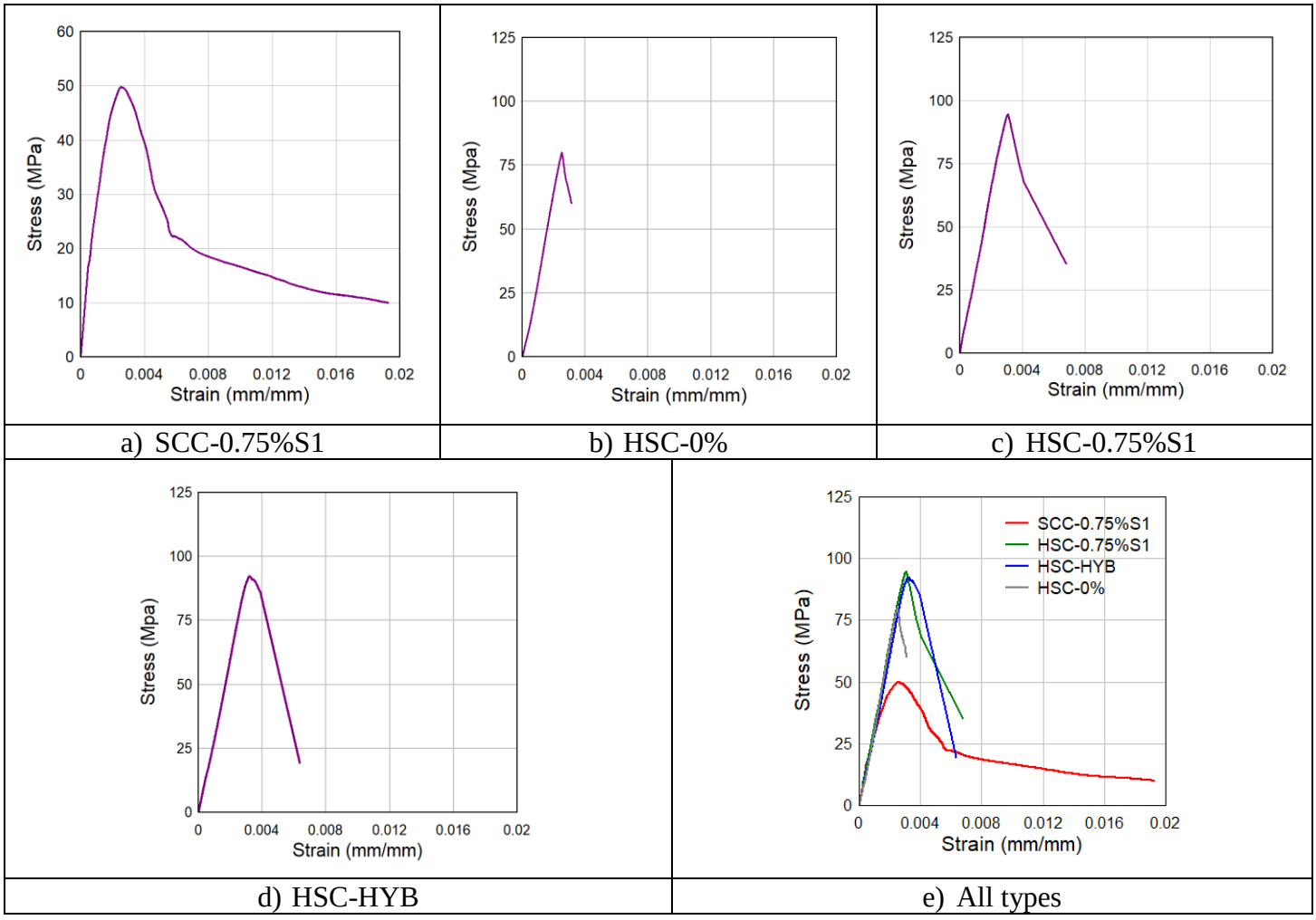

a) SCC-0.75%S1 | b) HSC-0% | c) HSC-0.75%S1

d) HSC-HYB | e) All types

Figure 3-21 Concrete stress-strain curves

a) SCC-0.75%S1 b) HSC-0.75%S1 c) HSC-HYB

d) HSC-0%

Figure 3-22 Sample concrete cylinder testing failures

3.4.4.2 Flexure Toughness

Flexural strength and toughness were assessed by testing 100 mm × 100 mm × 400 mm prisms (casted from each mix) in accordance with the ASTM C1609 standard. The beams were tested under four-point loading over a span of 300 mm using the GALDIBINI SUN 60 Universal Floor Standing Testing Machine, with deflections captured using a pair of LVDTs as shown in **Figure 3-23**. **Table 3-8** summarizes the toughness properties obtained. It is important to note that the numbering next to the concrete mix label designates the different prisms tested in this study since casting took place at different times. As can be seen, the hybrid mix shows larger average peak stress and toughness when compared to the mix containing 0.75%S1 only. Sample load-

deflection curves and photographs of prisms after failure are shown in **Figure 3-24** and **Figure 3-25** respectively.

Figure 3-23 Flexural prism testing setup

Table 3-8 Results from the ASTM C1609 toughness tests

Concrete Mix	ASTM C1609										
	P_1	δ_1	P_p	δ_p	f_1	f_p	P_{600}	f_{600}	P_{150}	f_{150}	T_{150}
SCC-0.75%S1	15.72	0.09	15.72	0.09	4.72	4.72	4.87	1.46	5.90	1.77	11.97
HSC-0%	-	-	20.83	0.05	-	6.25	-	-	-	-	-
HSC-0.75%S1 (1)	12.60	0.03	12.60	0.03	3.78	3.78	7.60	2.28	7.99	2.40	16.42
HSC-0.75%S1 (2)	18.74	0.03	18.74	0.03	5.62	5.62	14.34	4.30	14.90	4.47	29.28
Average	15.67	0.03	15.67	0.03	4.70	4.70	10.97	3.29	11.45	3.44	22.85
HSC-HYB (1)	28.30	0.04	28.30	0.04	8.49	8.49	15.08	4.52	12.10	3.63	29.59
HSC-HYB (2)	24.20	0.05	24.20	0.05	7.26	7.26	18.13	5.44	23.90	7.17	42.22
Average	26.25	0.05	25.88	0.05	7.88	7.88	16.61	4.98	18.00	5.40	35.91

L = Span Length (300 mm), (L/600 = 0.5, L/150 =2)
P_1= First-Peak Load (kN)
δ_1= Net Deflection at First-Peak Load (mm)
P_p= Peak Load (kN)
δ_p= Net Deflection at Peak Load (mm)
f_1= First-Peak Strength (MPa)
f_p= Peak Strength (MPa)
P_{600}= Residual Load at net deflection of L/600 (kN)
f_{600}= Residual Strength at net deflection of L/600 (MPa)
P_{150}= Residual Load at net deflection of L/150 (kN)
F_{150}= Residual Strength at net deflection of L/150 (MPa)
T_{150}= Area under load vs. net deflection curve (0 to L/150), (kN*mm)
FT = Flexural Toughness Factor = (T_{150}*L)/ (L/150 *b*d^2)

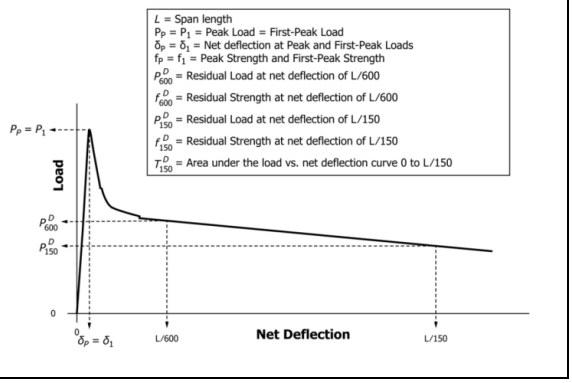

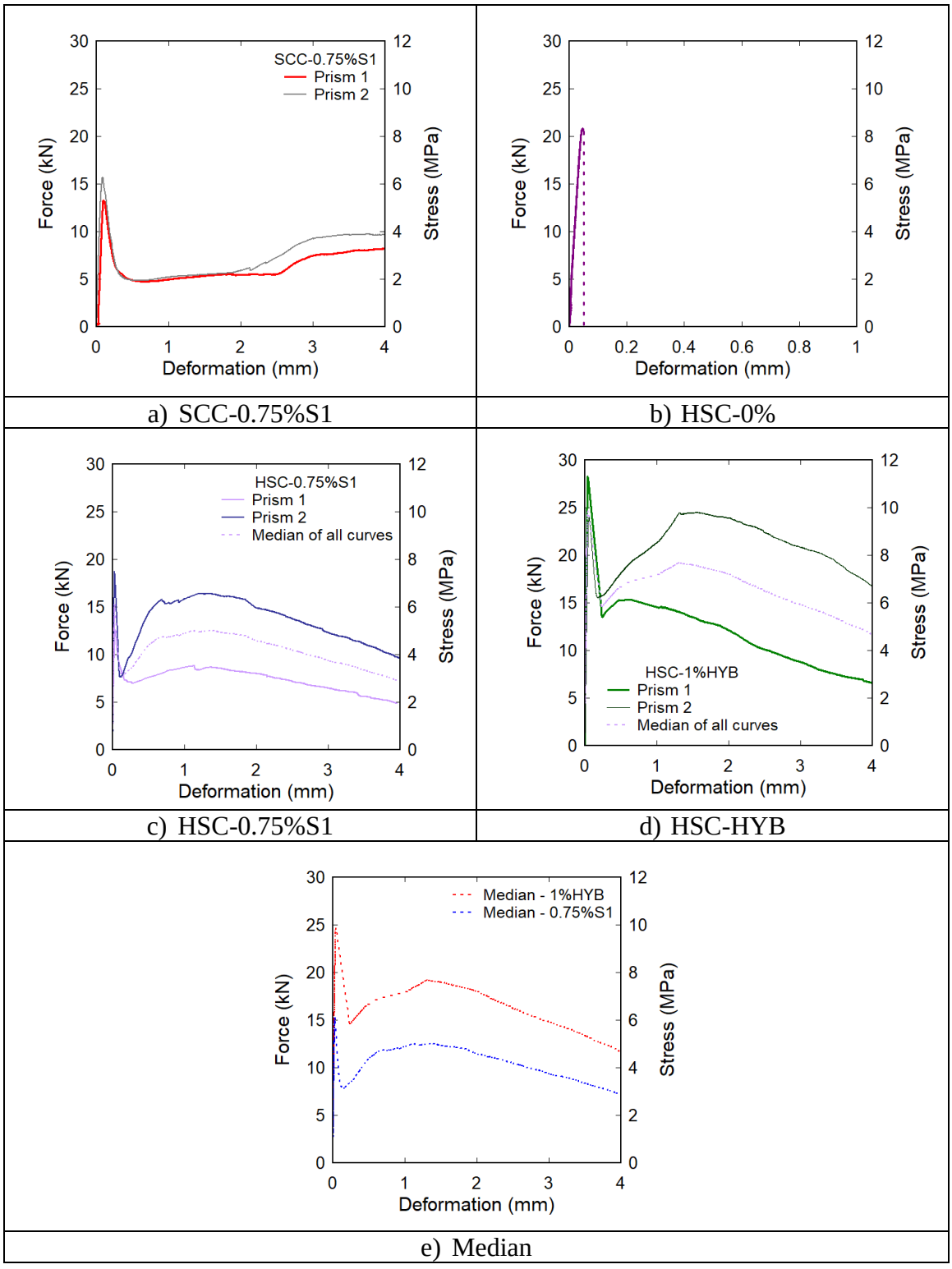

Figure 3-24 Flexural beam load-deflection curve samples

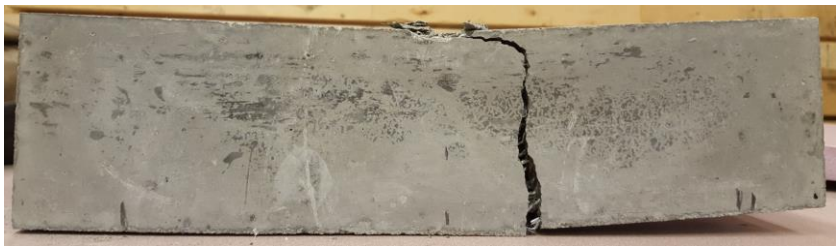

a) SCC-0.75%S1

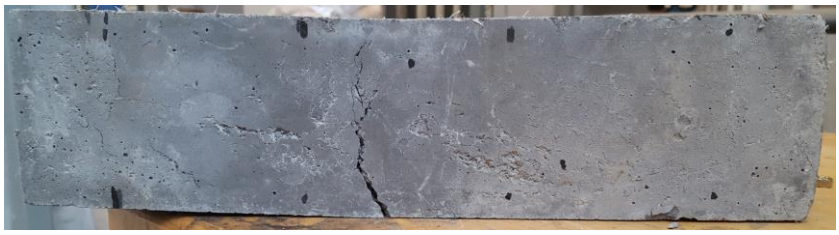

b) HSC-0.75%S1

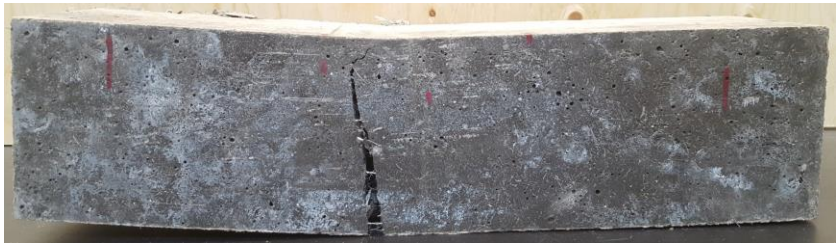

c) HSC-HYB

d) HSC-0%

Figure 3-25 Photographs of prism failure

3.5 Experimental Setup

This section describes the experimental setup for both the static loading test and the dynamic blast testing. The various elements used (load transfer device, high-speed cameras, etc.) are discussed.

3.5.1 Static Loading Test

3.5.1.1 Load Setup and Instrumentation

The setup shown in **Figure 3-26** was used to test all beams under quasi-static four-point bending. The beams were simply supported over a span of 2232 mm, with a constant moment region of 750 mm and two equal shear-spans of 741 mm. A manually operated hydraulic jack was used to apply the loading which was then transferred to the specimens as two-point loads using a steel spreader beam. Load was recorded using a load-cell placed below the hydraulic jack, with displacement at mid-span captured using a cable displacement transducer. Strains in the reinforcing bars were monitored using strain-gages which were applied on the tension steel at mid-span. **Figure 3-27** provides the detailed geometry of the setup.

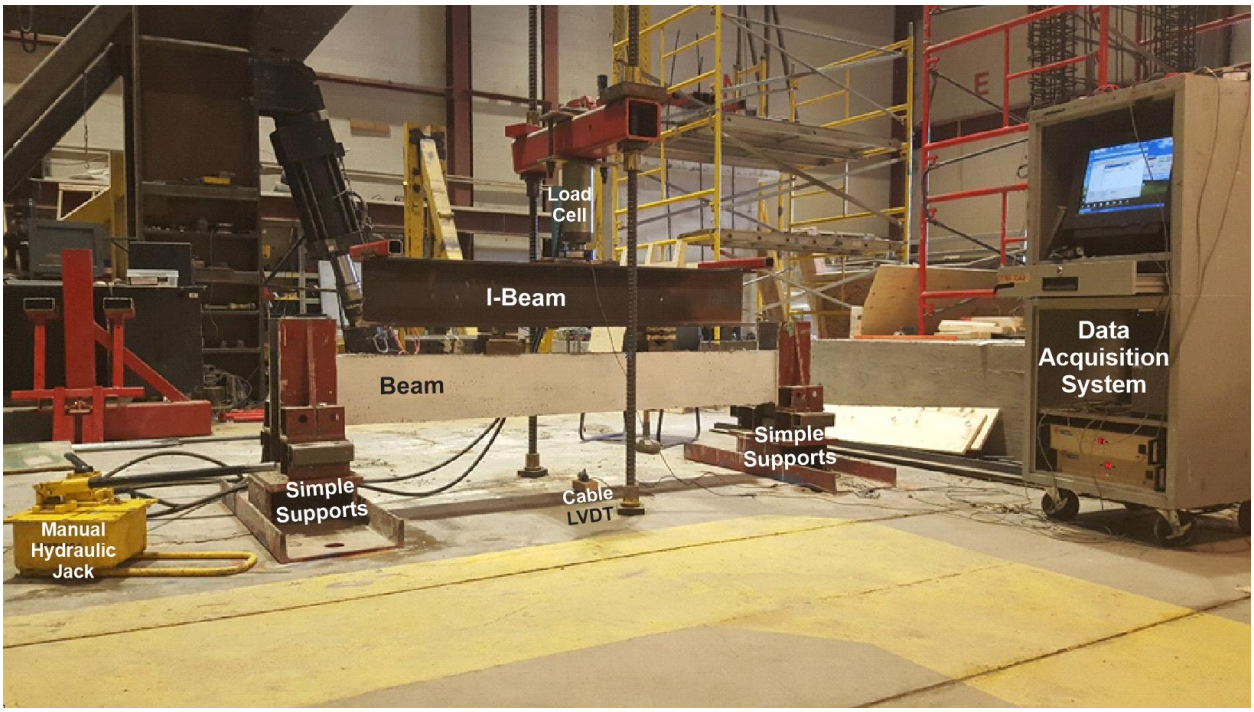

Figure 3-26 Beam test setup

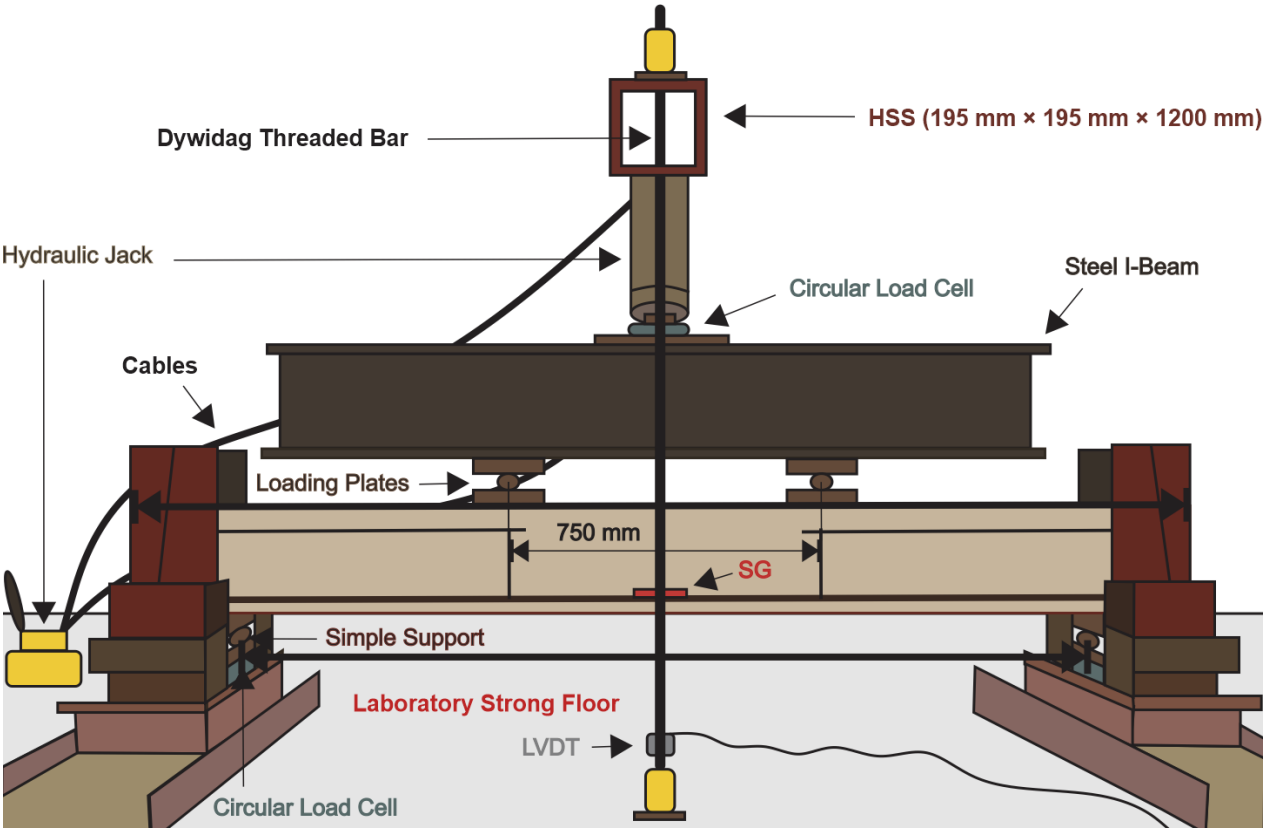

Figure 3-27 Static test setup geometry

3.5.1.2 Testing Sequence

Loading of the beams began under load-control (with load increments of 10 kN) until signs of yielding were detected. Upon yielding, loading continued under displacement-control (with 5 mm increments) until failure of the specimens (concrete crushing or shear collapse).

3.5.2 Dynamic Blast Testing

3.5.2.1 Shock-Tube

Blast testing was conducted using the shock-tube facility at the University of Ottawa. As shown in **Figure 3-28**, the shock-tube consists of four main components: (1) a variable length driver section, (2) a spool section, (3) an expansion section and (4) a rigid end test frame. The driver section generates the blast energy, while the firing of the shockwave is controlled using the double-diaphragm spool section. The rigid end test frame has a 2 m × 2 m square opening where test specimens can be attached. **Figure 3-29** shows a typical beam prior to testing along with the blast test setup.

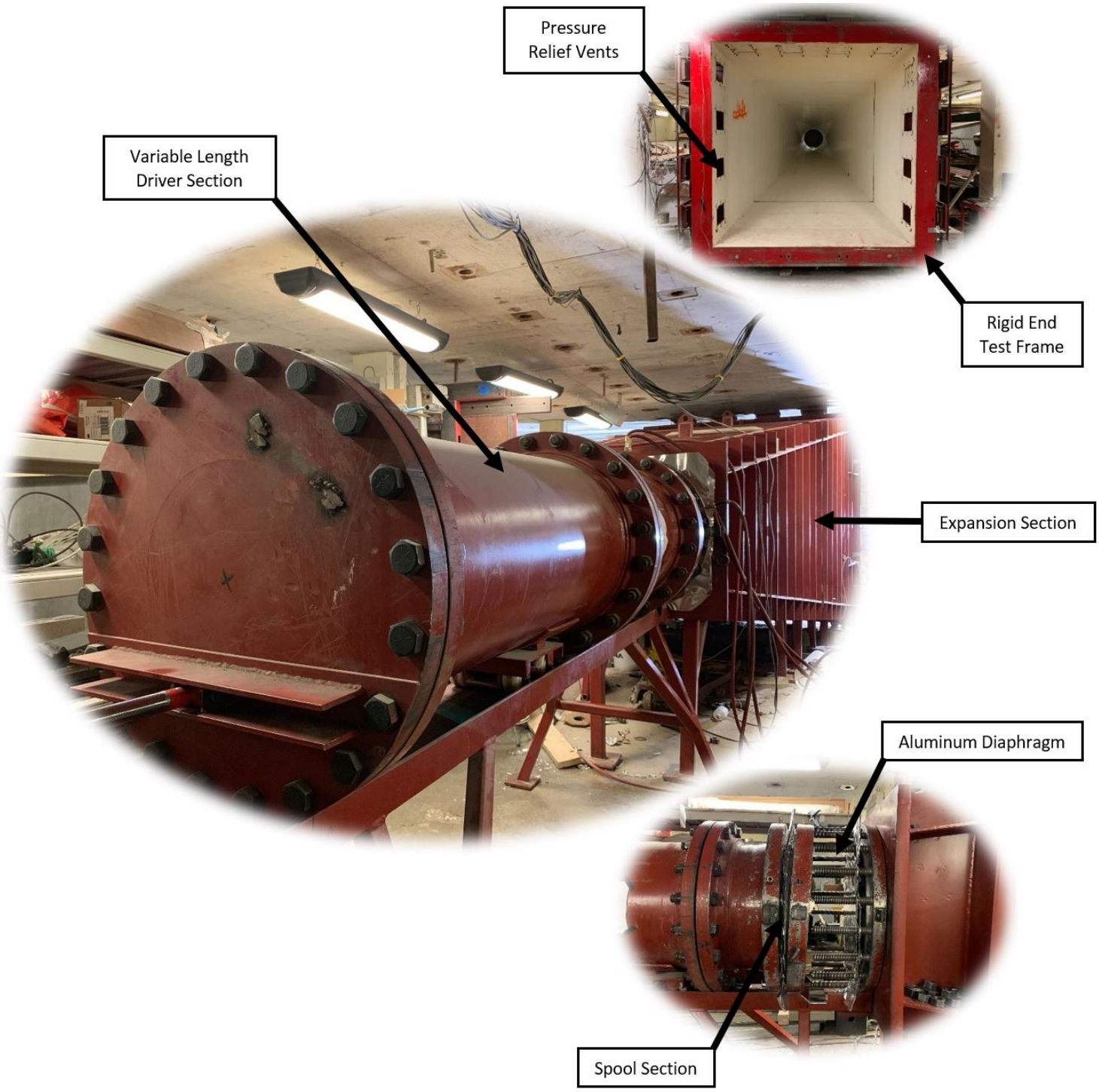

Figure 3-28 Shock-tube

Figure 3-29 Blast setup

3.5.2.2 Lateral Load Transfer Device

A load transfer device (LTD) was used to collect the shockwave pressure at the shock-tube opening and redirect it onto the non-planar beam specimens since these components don't cover the entire opening of the shock-tube. The LTD resulted in the application of blast loading under four-point bending, which closely matched the loading configuration used in static testing. This is achieved by two I-steel load transfer beams (160 mm × 165 mm × 1200 mm) attached to the LTD. The LTD in turn covers the 2 m × 2 m rigid end test frame square opening and is composed of two side-by-side rigid steel panels (2032 mm × 1000 mm). To allow for free lateral movement of the middle portion of the LTD without causing reactions at the hinge locations, sliding hinges are provided near the top and bottom supports. **Figure 3-30** and **Figure 3-31** show the lateral load transfer device in detail.

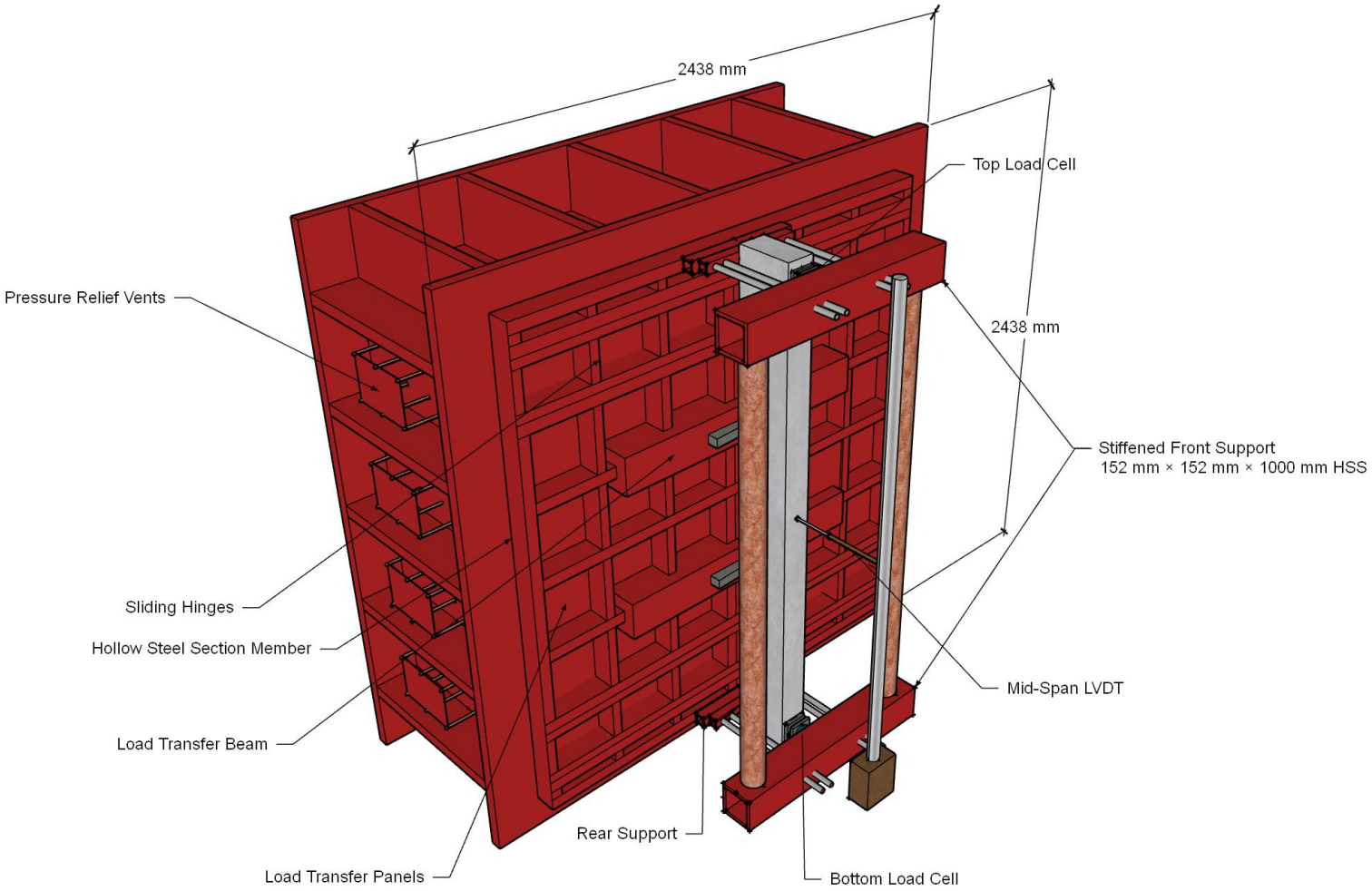

Figure 3-30 Isotropic view of lateral load transfer device

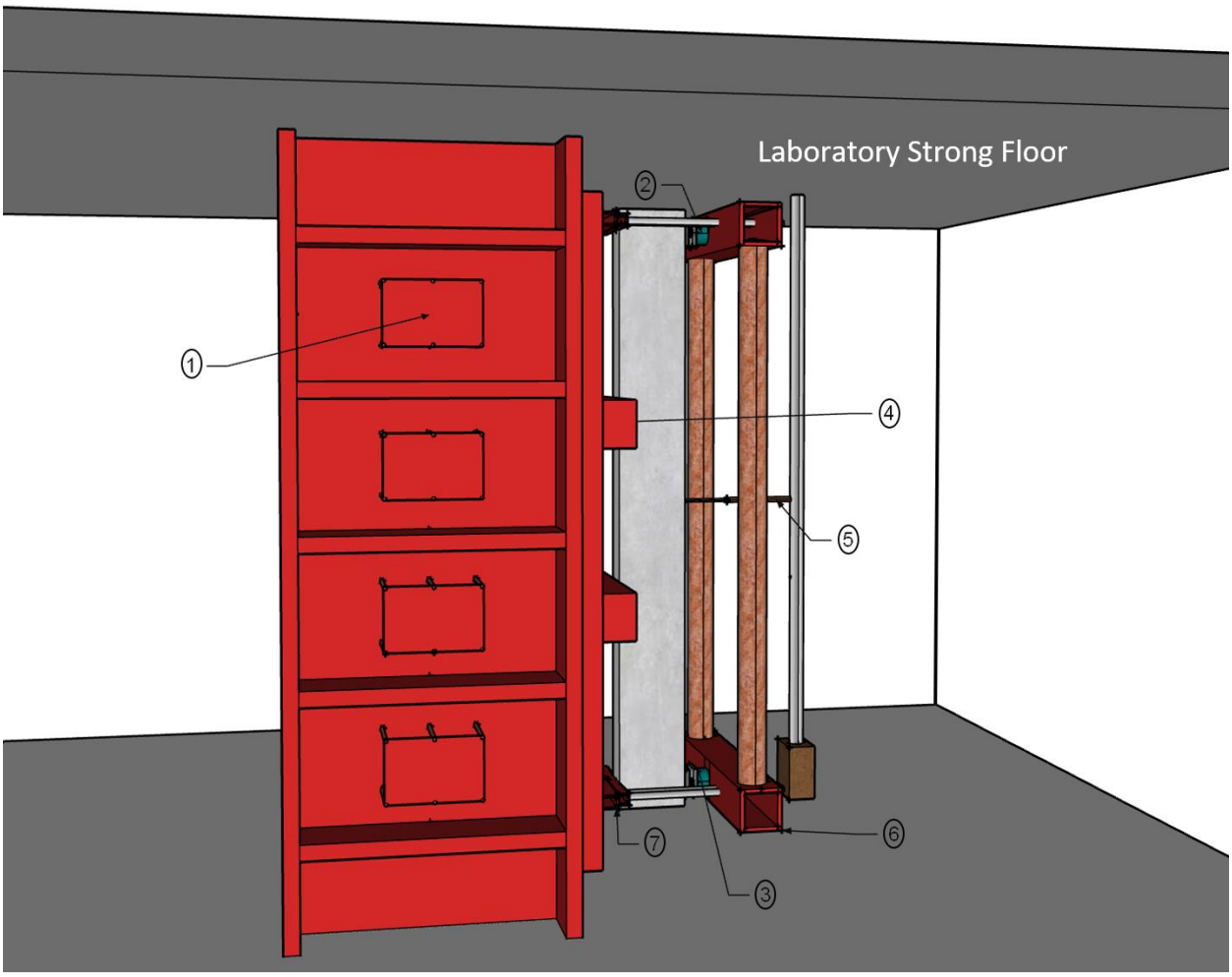

(1) Pressure relief vents	(2) Top load cell	(3) Bottom load cell	(4) Load transfer beam
(5) Mid-span LVDT	(6) Front Support	(7) Rear Support	

Figure 3-31 Side view of lateral load transfer device

3.5.2.3 Supports

To closely match the loading configuration used in the static testing, front and rear supports were used for both the top and bottom reactions. The front support consisted of a 1000 mm long 152 mm × 152 mm square HSS section welded to a circular load cell and tightened using four 19 mm diameter threaded steel rods. To simulate the roller condition, a 500-mm long 51 mm × 51 mm square HSS section and a smaller 440-mm long HSS section were used for the rear supports. **Figure 3-32** shows the support configuration in detail.

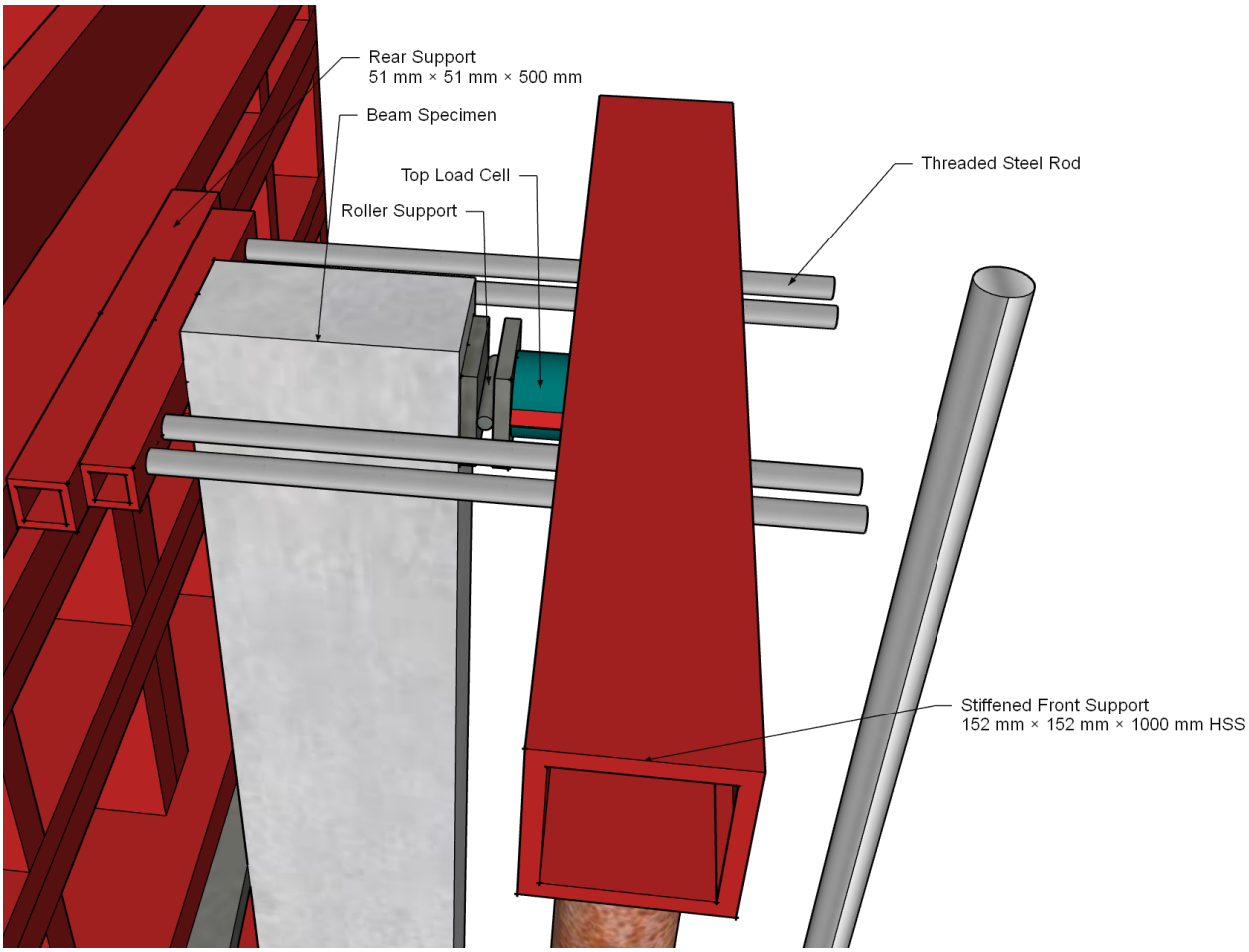

Figure 3-32 Support details

3.5.2.4 Pressure Sensors

To record data samples, two PCB Piezotronics Model #112A22 piezoelectric pressure sensors were connected to the data acquisition system (one attached at the bottom and one on the side of the end frame section of the shock-tube). A trigger is sent to the data acquisition system to record data samples once a blast wave is simulated.

3.5.2.5 Linear Variable Displacement Transducers (LVDT)

Complete displacement-time histories were recorded using a linear variable differential transducers (LVDT) placed at mid-height of the beam.

3.5.2.6 Data Acquisition System

A Yokogawa SL1000 High-Speed Data Acquisition Unit was used to collect data (strains, displacements, pressure readings, support reactions) during the test. The system has a capacity of recording 100,000 data samples per second.

3.5.2.7 High-Speed Video Camera

Two high-speed cameras (AOS Technology X-PRI) were used (one in front of the beam and the other at a 45° angle from the beam) during testing and recorded the response of the beams at a frame rate of 2000 frames per second.

3.5.2.8 Strain Gauges

For each specimen, a 350 Ω strain gauge with a length of 6 mm (FLA-6-350-11) was installed at the mid-span of each reinforcing bar to capture the strains experienced in these tensile bars and allow for further analysis.

3.5.2.9 Experimental Procedure

Testing of the beams was conducted under gradually increasing blast pressures until failure. The driver length was kept constant at 9 ft (2743 mm) for all tests, with the driver pressure (P_d) gradually increased from 30 psi (207 kPa) to 90 psi (621 kPa). It is noted that the sequence was selected to allow for comparison with previous research on plain HSC beams.

The following blast sequence was used for the 15M series: 30 psi, 50 psi, and 70 psi. The same sequence was used for the No.5 series with the addition of 90 psi which was meant to cause failure and allow for comparison with companion beam. A similar sequence was used for the 20M series except that two blasts were added: 60 psi (to cause failure in beam without stirrups) and 80 psi (to cause failure in beam with stirrups and beam with hybrid fibers). In general, Blast 1 (30 psi) was meant to test the beams within the elastic range or bring the steel reinforcement in the beams close to yielding. Blasts 2a to 3b (P_d = 50 to 90 psi) were applied to cause damage up to failure and allow for comparison with other specimens. Examples of the resulting shockwaves for Blast 1 to Blast 3b are shown in **Figure 3-33**. Shockwave properties in terms of peak reflected pressure (P_r), positive phase duration (t_d) and reflected impulse (I_r), representing the area under the positive phase of the pressure-time history, are also summarized in **Table 3-9**.

Table 3-9 Blast test properties

Name	**Driver Pressure** ***kPa (Psi)***	**Driver Length** ***mm (ft)***	**Average Reflected Pressure, P_r** ***kPa***	**Average Reflected Impulse, I_r** ***kPa·msec***	**Average Positive Phase Duration, t_p** ***msec***
Blast 1	207 (30)	2743 (9)	41.24	371.00	20.33
Blast 2a	345 (50)	2743 (9)	62.70	531.48	20.52
Blast 2b	414 (60)	2743 (9)	71.01	653.00	21.40
Blast 2c	483 (70)	2743 (9)	77.74	806.44	23.66
Blast 3a	552 (80)	2743 (9)	86.85	842.60	24.75
Blast 3b	621 (90)	2743 (9)	91.30	927.95	23.85

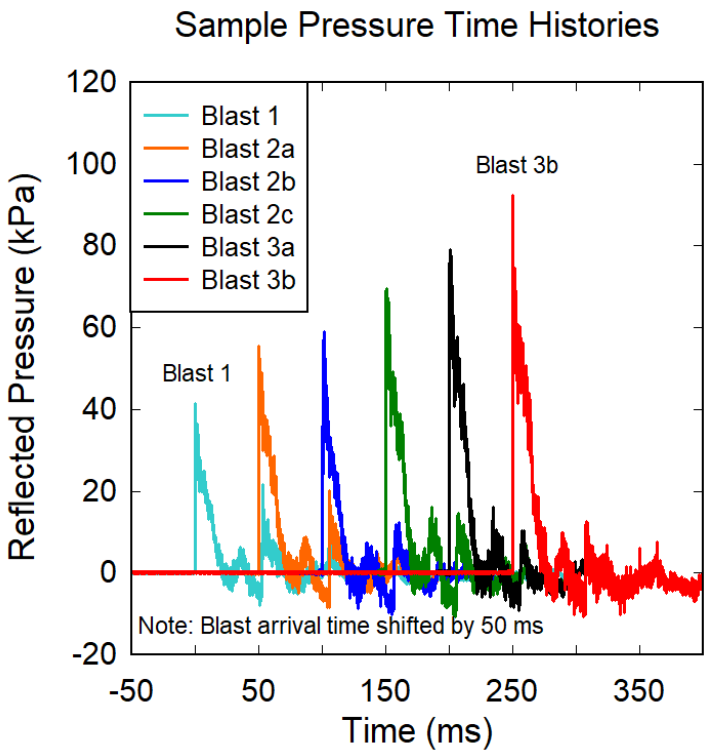

Figure 3-33 Sample shockwaves

Chapter 4: Experimental Results of the Static Tests

4.1 Chapter Overview

This chapter summarizes the individual experimental results for each of the nine beams tested under static four-point bending. The following results are presented for each beam: load vs. displacement curve, load vs. strain for longitudinal reinforcement, a plot of load vs. flexural and shear crack widths, a plot of flexural and shear crack widths vs. displacement and photographs of the beams at major events during testing along with a brief description of what happened.

A table summarizing key data extracted from the load-deflection curve is also provided for each beam, including yield load (P_y) and maximum load (P_{max}), yield displacement (Δ_y) displacement when load reached 85% of peak load (Δ_{85}) and maximum displacement (Δ_{max}), beam stiffness after cracking, ductility (Δ_{85}/Δ_y and Δ_{max}/Δ_y), toughness (area under the load-deflection curve until Δ_{85} and Δ_{max}) and the failure mechanism. The definitions of the different variables extracted from the load vs. mid-span deflection curve are shown in **Figure 4-1** and are summarized as follows:

A: load corresponding to yielding of specimen;
B: maximum load revisited by the specimen;
C: load corresponding to 85% of the peak load;
D: failure of specimen;
E: displacement at failure;
F: displacement corresponding to when load reached 85% of peak load;
G: displacement at yield;
A_{OABCDE}: toughness or area under the curve (shaded in grey).

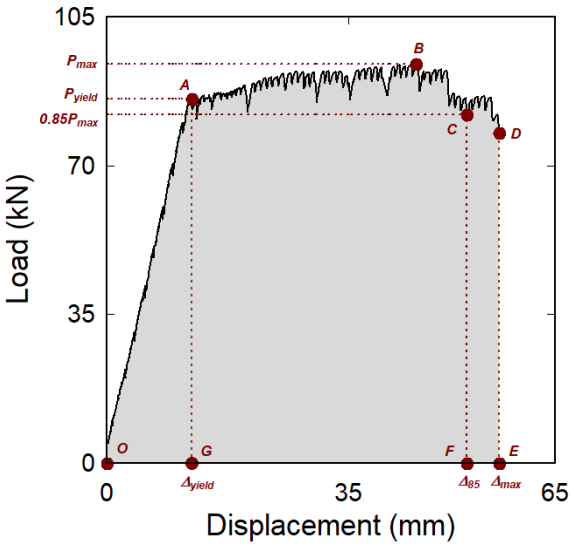

Figure 4-1 Illustration of the variables extracted from the load vs. mid-span deflection curve

4.2 Description of Experimental Results – Series 15M

4.2.1 SCC-0.75%S1-15M-0

The first specimen was designed with self-consolidating concrete and reinforced longitudinally with 15M normal-strength rebar without transverse reinforcement. Synthetic fibers were incorporated at a volumetric ratio of 0.75%. Results for this beam are summarized in **Table 4-1**. **Figure 4-2** shows the load-deflection curve. The growth of shear crack widths and tensile strain in longitudinal rebar are summarized in **Figure 4-3**. **Figure 4-4** shows detailed photos of major events during testing. The first hairline cracks were observed in the flexural region at an applied load of 20 kN. As the test progressed, hairline shear cracks appeared in the West shear span with a major shear crack forming when the applied load reached 79 kN. As the steel started to yield, the maximum load of 85.7 kN was reached at a corresponding displacement of 17.5 mm. As the beam went into the post-yield range, the fibers at the major shear crack began to pull-out, with the beam ultimately failing in shear, with the diagonal shear failure occurring on the West side (Δ_{max} = 36.4 mm).

Table 4-1 Summary of results for Beam SCC-0.75%S1-15M-0

Load (kN)		Displacement (mm)			Stiffness K (N/mm)	Ductility		Toughness (kN·mm)		Failure Mechanism
P_y	P_{max}	Δ_y	Δ_{85}	Δ_{max}		Δ_{85}/Δ_y	Δ_{max}/Δ_y	Au_{85}	Au_{max}	
-	85.7	-	18.1	36.4	6047	-	-	951	1529	Shear Failure

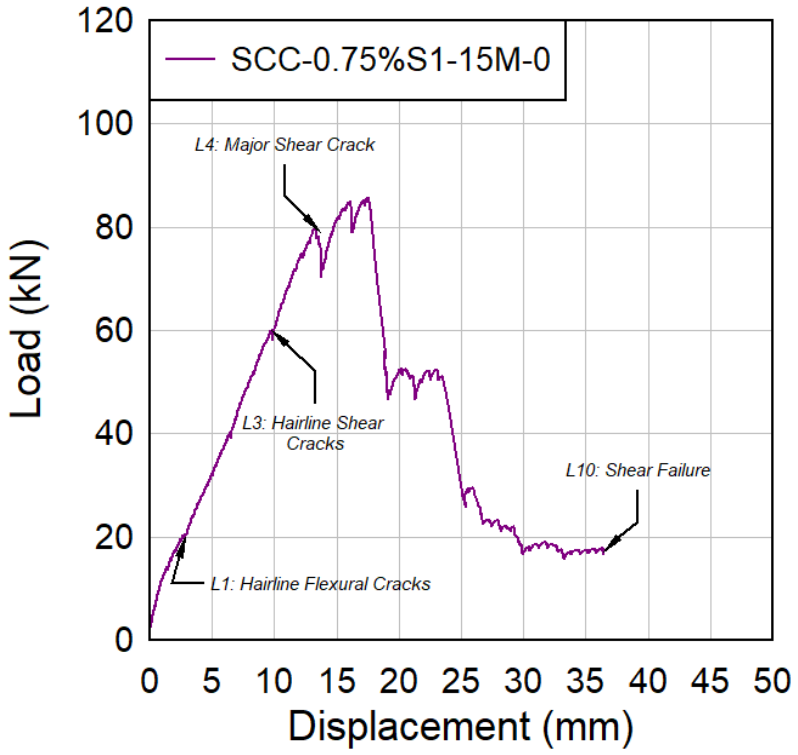

Figure 4-2 Load vs. mid-span deflection for Beam SCC-0.75%S1-15M-0

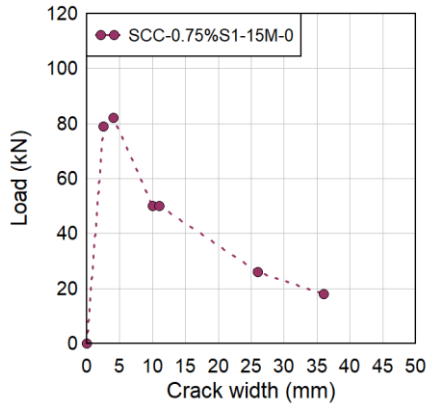

a) Maximum crack width (shear)

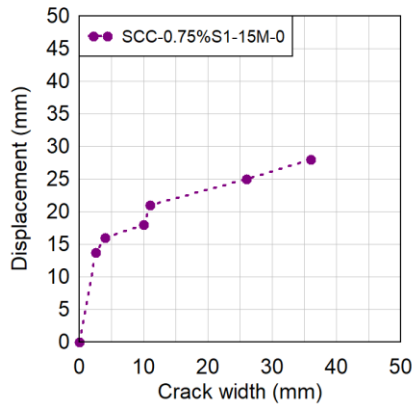

b) Maximum crack width (shear)

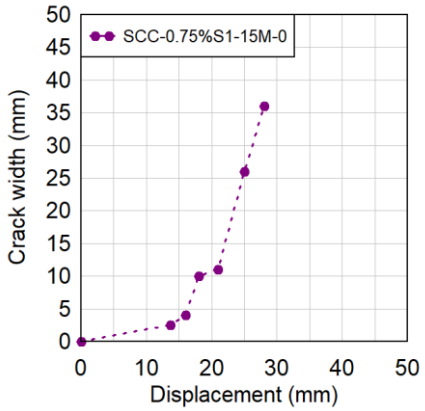

c) Maximum crack width (shear)

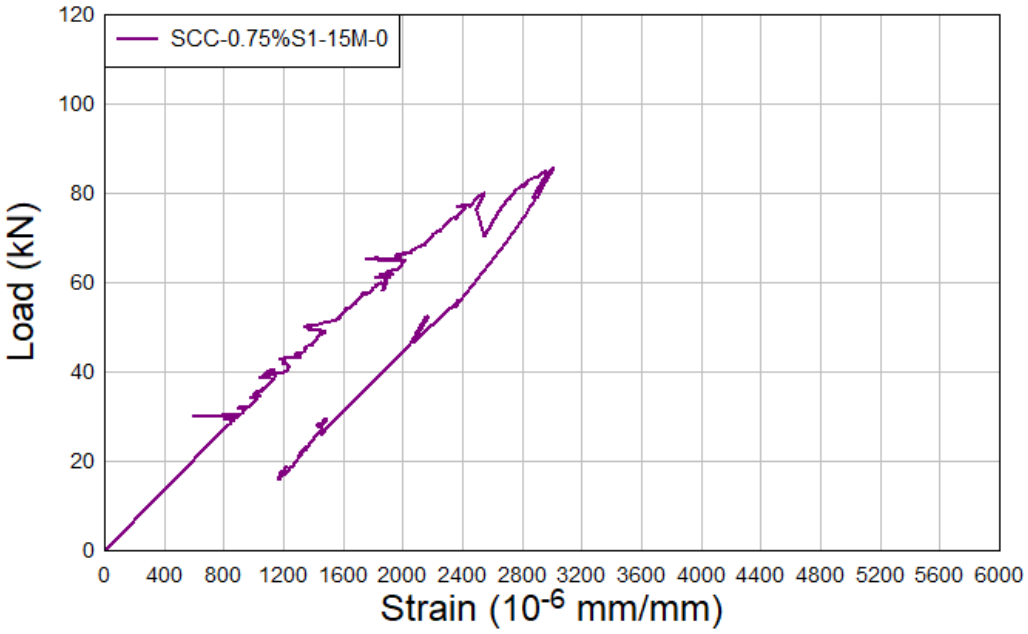

d) Tensile strain in longitudinal rebar

Figure 4-3 Experimental results for Beam SCC-0.75%S1-15M-0

<table>
<tr><th colspan="3">Experimental Parameters</th><th>Description</th></tr>
<tr><td>Load Stage</td><td>Load (kN)</td><td>Mid-Span Deflection (mm)</td><td rowspan="3">First hairline cracks appear in the flexural region</td></tr>
<tr><td>1</td><td>20</td><td>2.8</td></tr>
<tr><td colspan="3">  </td></tr>
<tr><td>Load Stage</td><td>Load (kN)</td><td>Mid-Span Deflection (mm)</td><td rowspan="3">Hairline shear cracks appear in the West shear span</td></tr>
<tr><td>3</td><td>60</td><td>9.8</td></tr>
<tr><td colspan="3">  </td></tr>
<tr><td>Load Stage</td><td>Load (kN)</td><td>Mid-Span Deflection (mm)</td><td rowspan="3">A major shear crack started to form</td></tr>
<tr><td>4</td><td>79</td><td>13.7</td></tr>
<tr><td colspan="3">  </td></tr>
<tr><td>Load Stage</td><td>Load (kN)</td><td>Mid-Span Deflection (mm)</td><td rowspan="3">Specimen fails with a shear failure on the West side</td></tr>
<tr><td>10</td><td>17</td><td>36.4</td></tr>
<tr><td colspan="3">  </td></tr>
</table>

Figure 4-4 Major events for Beam SCC-0.75%S1-15M-0

4.2.2 SCC-0.75%S1-15M-S

The second specimen was built with the same components as SCC-0.75%S1-15M-0, but had transverse reinforcement spaced at 100 mm in the shear spans. **Table 4-2** summarizes the results for this beam. **Figure 4-5** shows the load-deflection curve. **Figure 4-6** summarizes the growth of flexural crack widths and tensile strain in rebar. **Figure 4-7** demonstrates detailed photos of major events during testing. The first hairline flexural cracks were observed at an applied load of 23 kN. Yielding of the bottom longitudinal reinforcement occurred at 10.6 mm with a long deflection plateau, as shown in **Figure 4-5** (yield strains can also be seen in **Figure 4-6d**). Concrete started crushing at the top flexural zone when the displacement reached 36 mm. The maximum load recorded was 99 kN at a corresponding displacement of 39.3 mm. As the test progressed, the beam experienced a flexural failure at a maximum displacement of 70 mm with gradual concrete crushing in the compression zone.

Table 4-2 Summary of results for Beam SCC-0.75%S1-15M-S

Load (kN)		Displacement (mm)			Stiffness K (N/mm)	Ductility		Toughness (kN·mm)		Failure Mechanism
P_y	P_{max}	Δ_y	Δ_{85}	Δ_{max}		Δ_{85}/Δ_y	Δ_{max}/Δ_y	Au_{85}	Au_{max}	
80	99	10.6	44.4	70	7423	4.19	6.60	3624	5683	Concrete Crushing

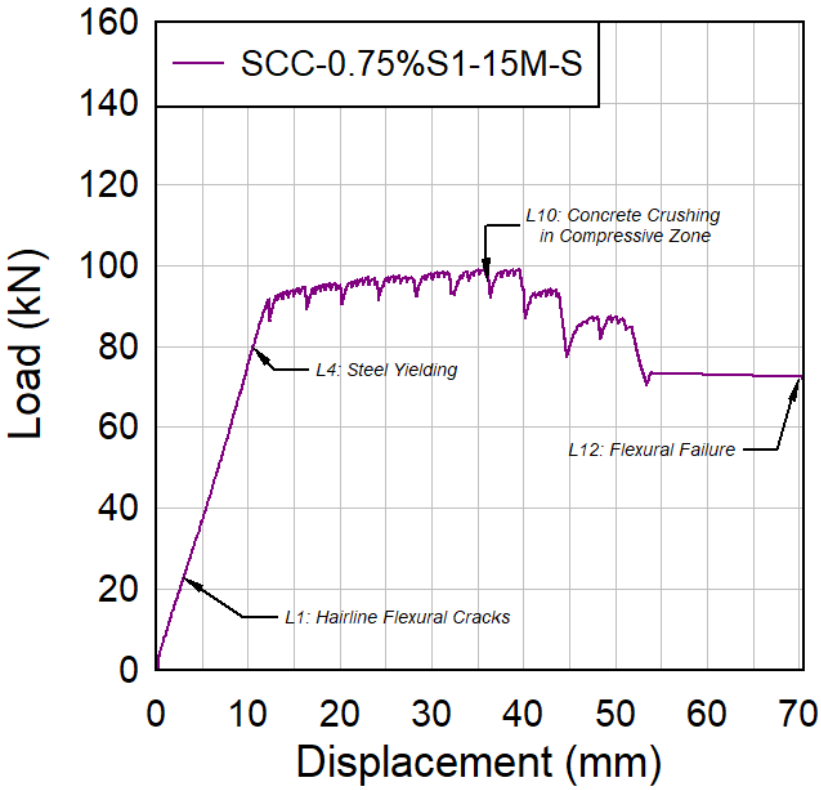

Figure 4-5 Load vs. mid-span deflection for Beam SCC-0.75%S1-15M-S

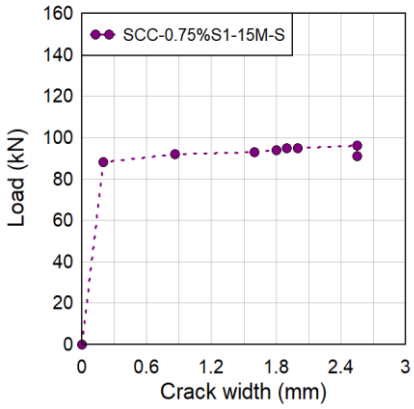

a) Maximum crack width (flexure)

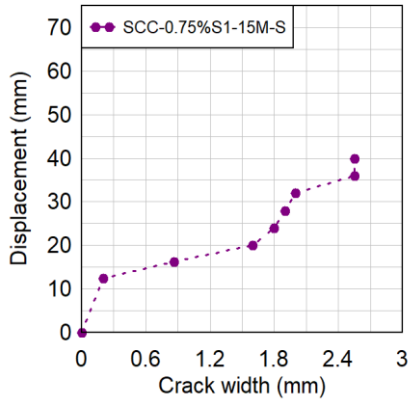

b) Maximum crack width (flexure)

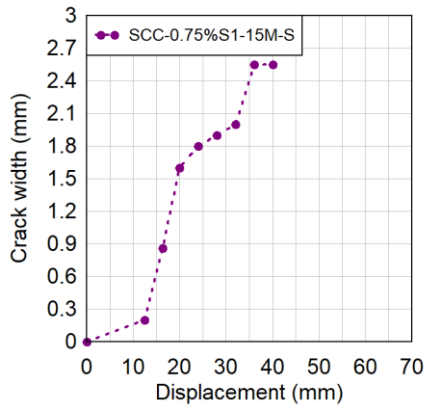

c) Maximum crack width (flexure)

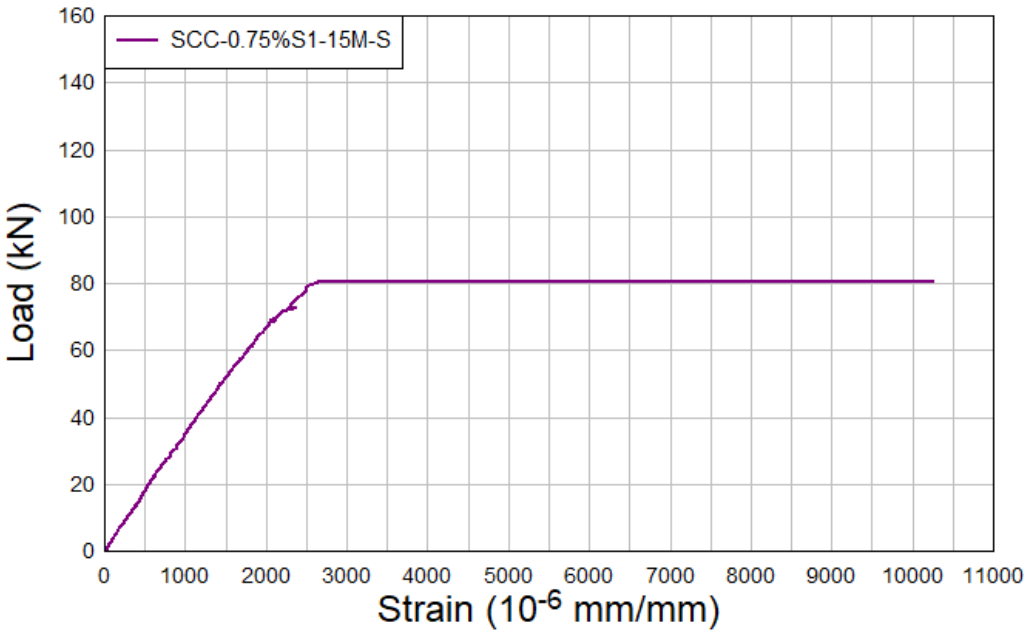

d) Tensile strain in longitudinal rebar

Figure 4-6 Experimental results for Beam SCC-0.75%S1-15M-S

<table>
<tr><th colspan="3">Experimental Parameters</th><th>Description</th></tr>
<tr><td>Load Stage</td><td>Load (kN)</td><td>Mid-Span Deflection (mm)</td><td rowspan="3">First hairline cracks appear in the flexural region</td></tr>
<tr><td>1</td><td>23</td><td>1.8</td></tr>
<tr><td colspan="3">  </td></tr>
<tr><td>Load Stage</td><td>Load (kN)</td><td>Mid-Span Deflection (mm)</td><td rowspan="3">Steel reinforcement yielding</td></tr>
<tr><td>4</td><td>80</td><td>10.6</td></tr>
<tr><td colspan="3">  </td></tr>
<tr><td>Load Stage</td><td>Load (kN)</td><td>Mid-Span Deflection (mm)</td><td rowspan="3">Concrete in compressive zone started crushing</td></tr>
<tr><td>10</td><td>96</td><td>36</td></tr>
<tr><td colspan="3">  </td></tr>
<tr><td>Load Stage</td><td>Load (kN)</td><td>Mid-Span Deflection (mm)</td><td rowspan="3">Specimen fails with gradual concrete crushing in compression zone</td></tr>
<tr><td>12</td><td>72</td><td>70</td></tr>
<tr><td colspan="3">  </td></tr>
</table>

Figure 4-7 Major events for Beam SCC-0.75%S1-15M-S

4.2.3 HSC-0%-15M-0

This beam was the first specimen in the 15M HSC series. It was designed with 15M longitudinal bars without stirrups and was built with plain high-strength concrete. Results for this beam test are summarized in **Table 4-3**. **Figure 4-8** shows the load-deflection curve. The growth of flexural crack widths and tensile strain in longitudinal reinforcement are displayed in **Figure 4-9**. **Figure 4-10** shows detailed photos of major events during testing. The first hairline cracks were observed in the flexural region at an applied load of 20 kN. As the applied load was increased, the specimen experienced a sudden shear failure on the East side without warning, although the strain gauge recorded a maximum of 0.0024 mm/mm indicating that the beam was close to yielding (ε_y = 0.0027 mm/mm). The maximum load recorded was 90 kN with a corresponding maximum deflection of 15.3 mm.

Table 4-3 Summary of results for Beam HSC-0%-15M-0

Load (kN)		Displacement (mm)			Stiffness K (N/mm)	Ductility		Toughness (kN·mm)		Failure Mechanism
P_y	P_{max}	Δ_y	Δ_{85}	Δ_{max}		Δ_{85}/Δ_y	Δ_{max}/Δ_y	Au_{85}	Au_{max}	
-	90	-	-	15.3	5882	-	-	-	922	Shear Failure

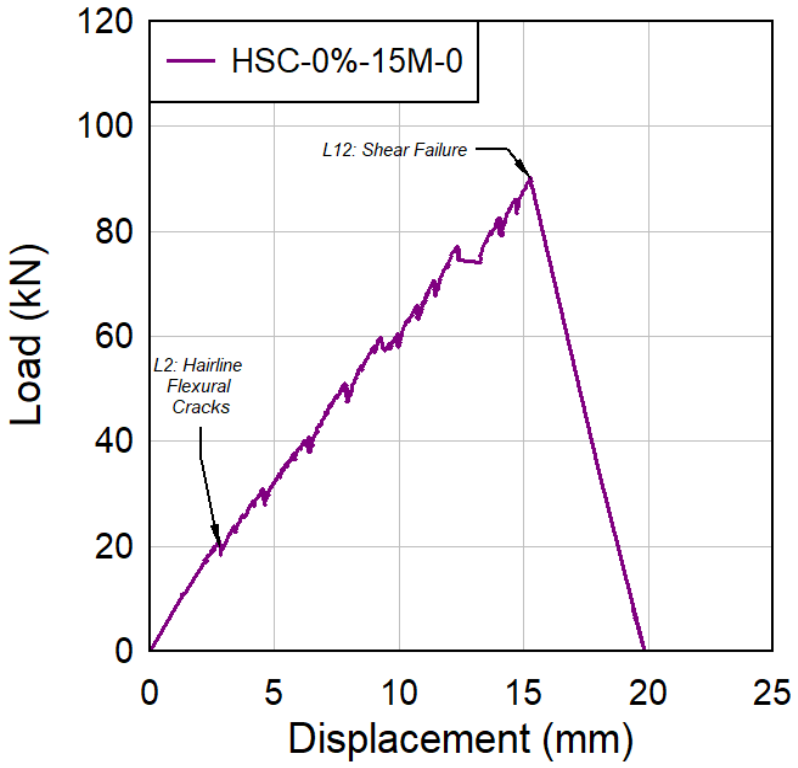

Figure 4-8 Load vs. mid-span deflection for Beam HSC-0%-15M-0

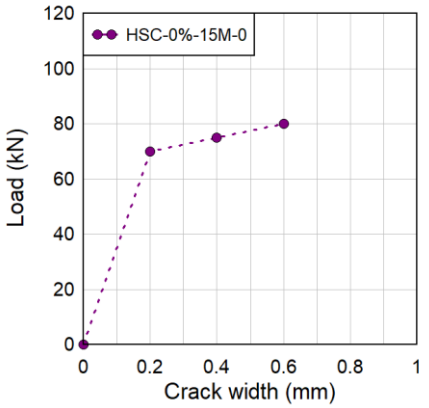

a) Maximum crack width (flexure)

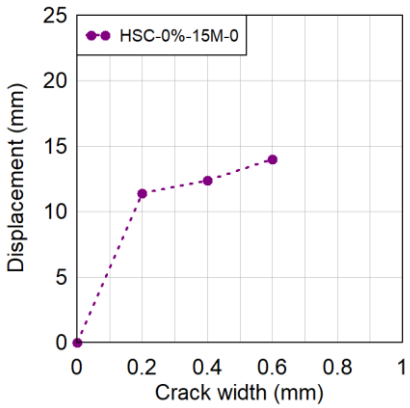

b) Maximum crack width (flexure)

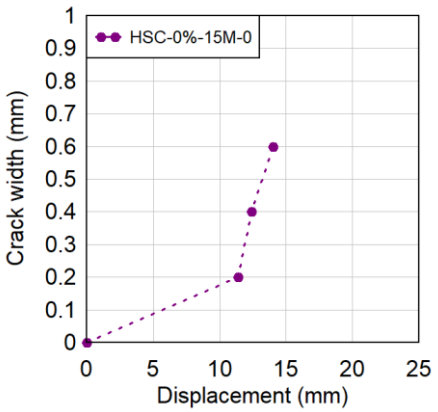

c) Maximum crack width (flexure)

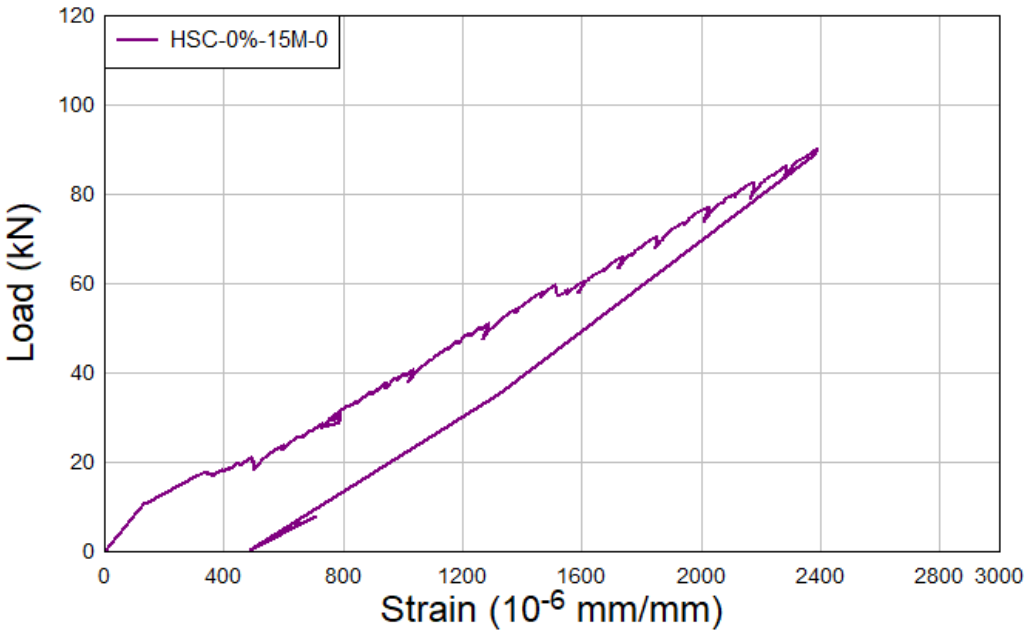

d) Tensile strain in longitudinal rebar

Figure 4-9 Experimental results for Beam HSC-0%-15M-0

<table>
<tr><th colspan="3">Experimental Parameters</th><th>Description</th></tr>
<tr><td>Load Stage</td><td>Load (kN)</td><td>Mid-Span Deflection (mm)</td><td rowspan="3">First hairline cracks appear in the flexural region</td></tr>
<tr><td>2</td><td>20</td><td>2.8</td></tr>
<tr><td colspan="3">  </td></tr>
<tr><td>Load Stage</td><td>Load (kN)</td><td>Mid-Span Deflection (mm)</td><td rowspan="3">Specimen fails suddenly with a shear failure on the East side</td></tr>
<tr><td>12</td><td>90</td><td>15.3</td></tr>
<tr><td colspan="3">  </td></tr>
</table>

Figure 4-10 Major events for Beam HSC-0%-15M-0

4.2.4 HSC-0.75%S1-15M-0

This beam was identical to HSC-0%-15M-0, but with the addition of 0.75% synthetic fibers. **Table 4-4** presents the results obtained for this beam. **Figure 4-11** shows the load-deflection curve. The growth of shear and flexural crack widths and tensile strain in rebar are presented in **Figure 4-12**. **Figure 4-13** shows detailed photos of major events during testing. The first hairline cracks were observed in the flexural zone at an applied load of 20 kN. As the applied load was increased, further cracks were observed along the beam length. The first shear crack was recorded in the West side of the beam when the applied load reached 40 kN. As the load was further increased, it was noted that the longitudinal reinforcement yielded at a displacement of 13.4 mm. Upon yielding, loading continued under displacement-control. The long yielding plateau illustrated in **Figure 4-12g** indicates how fibers were effective in bridging the widening of the flexural and shear cracks. However, a more major shear crack was observed in the East side of the beam at 30 mm displacement. The maximum load resisted by the beam was 112.2 kN after which the beam suffered a major increase in crack width at the previously formed shear crack, leading to fiber pullout and shear failure at a deflection of 67.3 mm.

Table 4-4 Summary of results for Beam HSC-0.75%S1-15M-0

Load (kN)		Displacement (mm)			Stiffness K (N/mm)	Ductility		Toughness (kN·mm)		Failure Mechanism
P_y	P_{max}	Δ_y	Δ_{85}	Δ_{max}		Δ_{85}/Δ_y	Δ_{max}/Δ_y	Au_{85}	Au_{max}	
99	112.2	13.4	-	67.3	7388	-	5.02	-	6574	Shear Failure

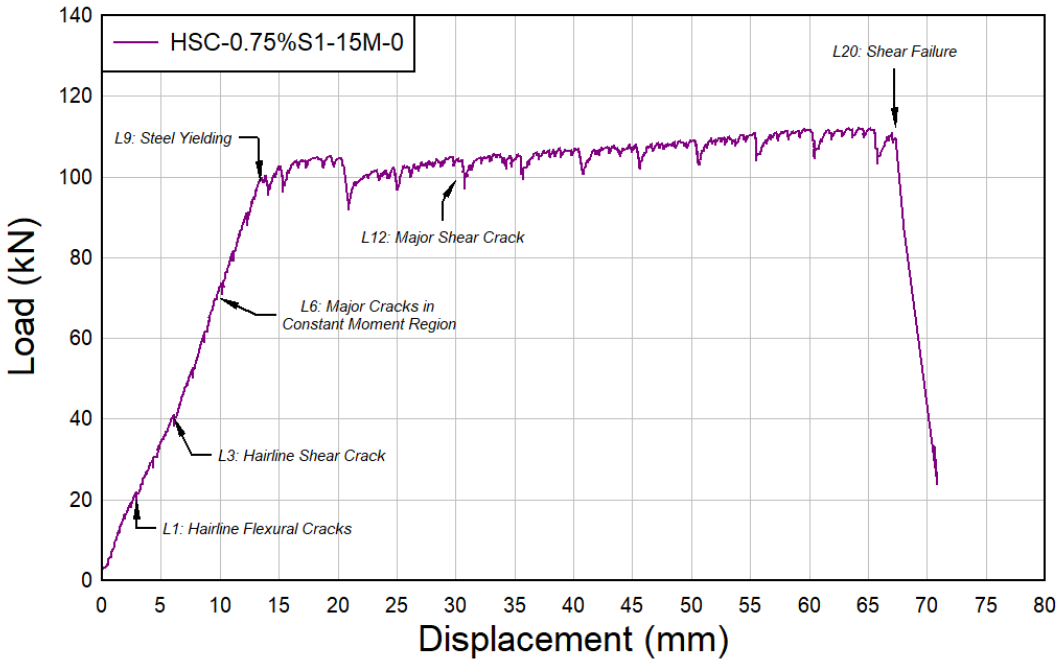

Figure 4-11 Load vs. mid-span deflection for Beam HSC-0.75%S1-15M-0

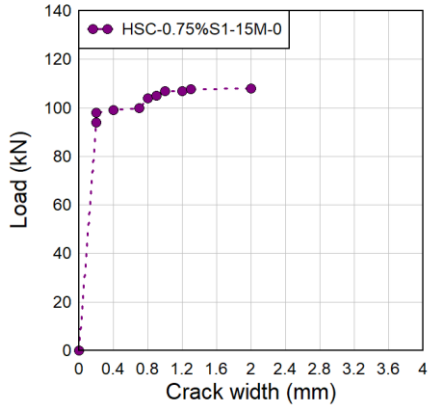

a) Maximum crack width (shear)

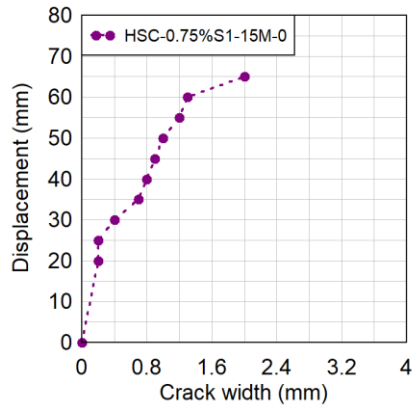

b) Maximum crack width (shear)

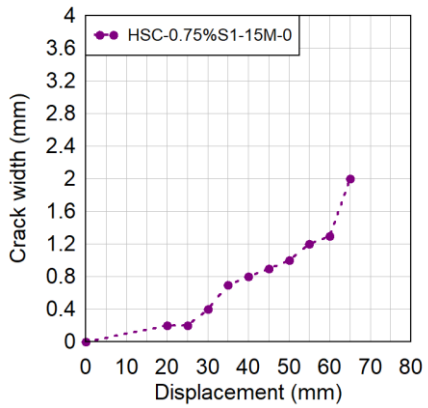

c) Maximum crack width (shear)

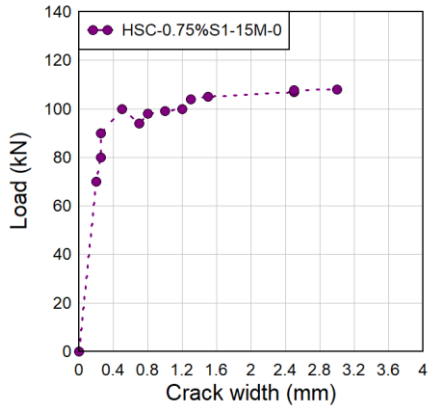

d) Maximum crack width (flexure)

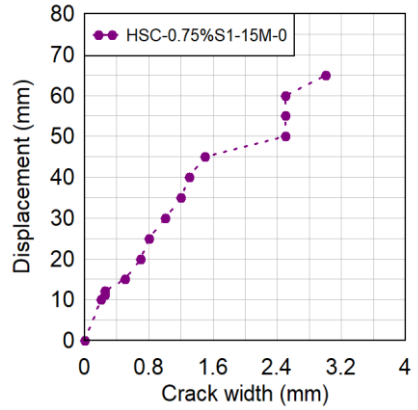

e) Maximum crack width (flexure)

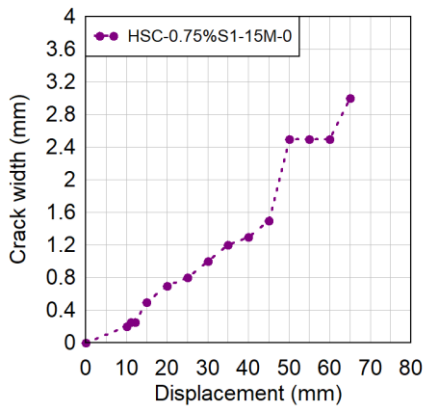

f) Maximum crack width (flexure)

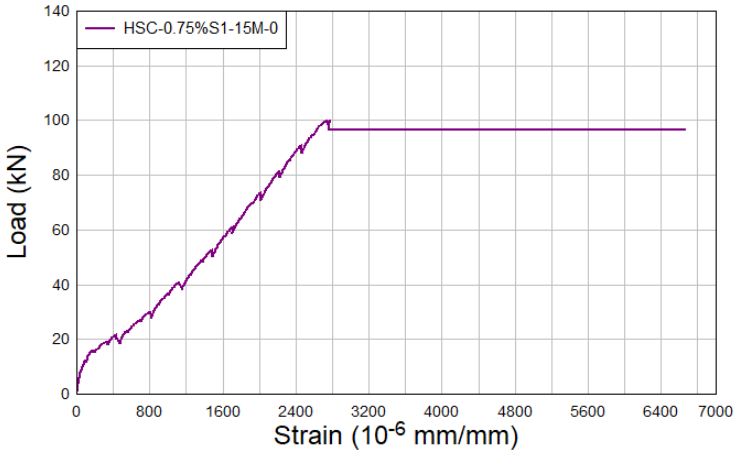

g) Tensile strain in longitudinal rebar

Figure 4-12 Experimental results for Beam HSC-0.75%S1-15M-0

<table>
<tr><th colspan="3">Experimental Parameters</th><th>Description</th></tr>
<tr><td>Load Stage</td><td>Load (kN)</td><td>Mid-Span Deflection (mm)</td><td rowspan="3">First hairline cracks appear in the flexural region</td></tr>
<tr><td>1</td><td>20</td><td>2.9</td></tr>
<tr><td colspan="3">  </td></tr>
<tr><td>Load Stage</td><td>Load (kN)</td><td>Mid-Span Deflection (mm)</td><td rowspan="3">First hairline flexural-shear crack appears in the West shear span</td></tr>
<tr><td>3</td><td>40</td><td>6.1</td></tr>
<tr><td colspan="3">  </td></tr>
<tr><td>Load Stage</td><td>Load (kN)</td><td>Mid-Span Deflection (mm)</td><td rowspan="3">Major cracks started to form in the constant moment region</td></tr>
<tr><td>6</td><td>70</td><td>10</td></tr>
<tr><td colspan="3"> 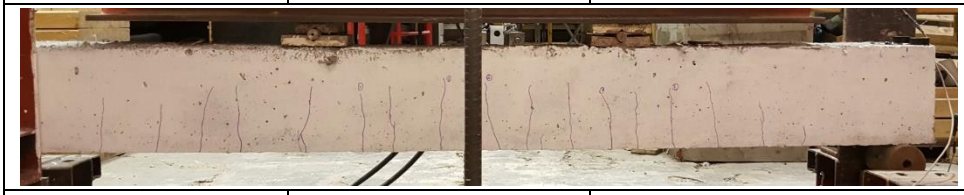 </td></tr>
<tr><td>Load Stage</td><td>Load (kN)</td><td>Mid-Span Deflection (mm)</td><td rowspan="3">Steel reinforcement yielding</td></tr>
<tr><td>9</td><td>99</td><td>13.4</td></tr>
<tr><td colspan="3">  </td></tr>
<tr><td>Load Stage</td><td>Load (kN)</td><td>Mid-Span Deflection (mm)</td><td rowspan="3">A major shear crack is observed in the East side</td></tr>
<tr><td>12</td><td>99</td><td>30</td></tr>
<tr><td colspan="3">  </td></tr>
<tr><td>Load Stage</td><td>Load (kN)</td><td>Mid-Span Deflection (mm)</td><td rowspan="3">Specimen fails with a shear failure on the East side</td></tr>
<tr><td>20</td><td>109.6</td><td>67.3</td></tr>
<tr><td colspan="3">  </td></tr>
</table>

Figure 4-13 Major events for Beam HSC-0.75%S1-15M-0

4.2.5 HSC-0.75%S1-15M-S

The third specimen of the 15M high-strength concrete series was built with the same components as the HSC-0.75%S1-15M-0, but had transverse reinforcement spaced at 100 mm in the shear spans. **Table 4-5** lists the main results for this test. **Figure 4-14** shows the load-deflection curve. **Figure 4-15** illustrates the growth of flexural crack widths and tensile strain in longitudinal reinforcement. **Figure 4-16** shows detailed photos of major events during testing. The first hairline flexural cracks were observed at an applied load of 20 kN. As the applied load was increased, hairline flexural-shear cracks appeared in the East region. Yielding of the bottom longitudinal reinforcement occurred when the load reached 90 kN (Δ_y = 12.3 mm). The maximum load recorded was 103.7 kN at a corresponding displacement of 53.8 mm. As the test progressed and when the displacement reached 80 mm, concrete started crushing around the loading plate. Soon after, concrete started to crush in the middle compression zone and a few seconds later, the crushing increased significantly, with the beam experiencing a flexural failure at a maximum displacement of 85 mm.

Table 4-5 Summary of results for Beam HSC-0.75%S1-15M-S

Load (kN)		Displacement (mm)			Stiffness K (N/mm)	Ductility		Toughness (kN·mm)		Failure Mechanism
P_y	P_{max}	Δ_y	Δ_{85}	Δ_{max}		Δ_{85}/Δ_y	Δ_{max}/Δ_y	Au_{85}	Au_{max}	
90	103.7	12.3	-	85	7317	4.60	6.91	4862	7823	Concrete Crushing

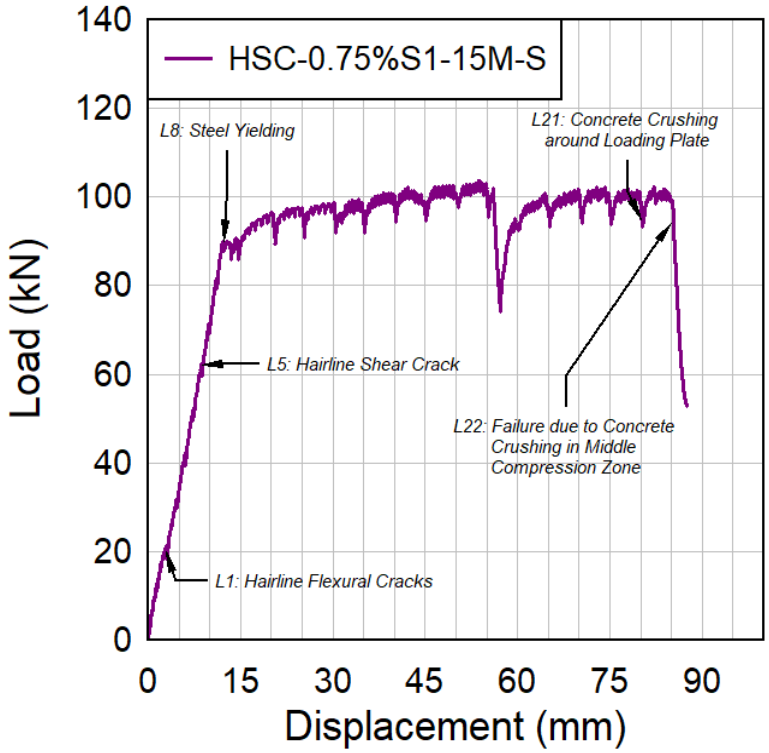

Figure 4-14 Load vs. mid-span deflection for Beam HSC-0.75%S1-15M-S

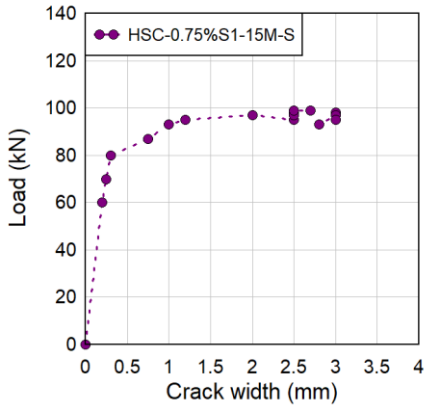

a) Maximum crack width (flexure)

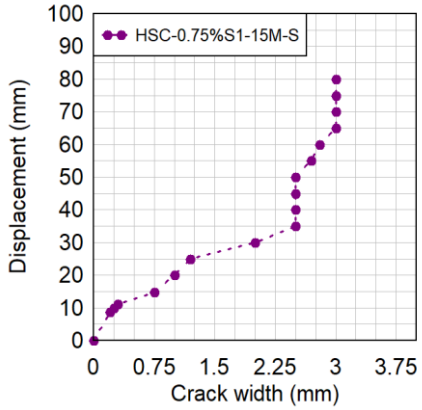

b) Maximum crack width (flexure)

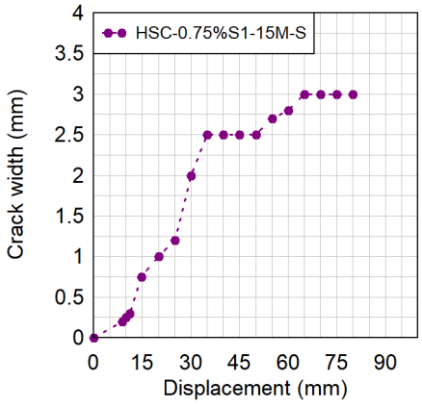

c) Maximum crack width (flexure)

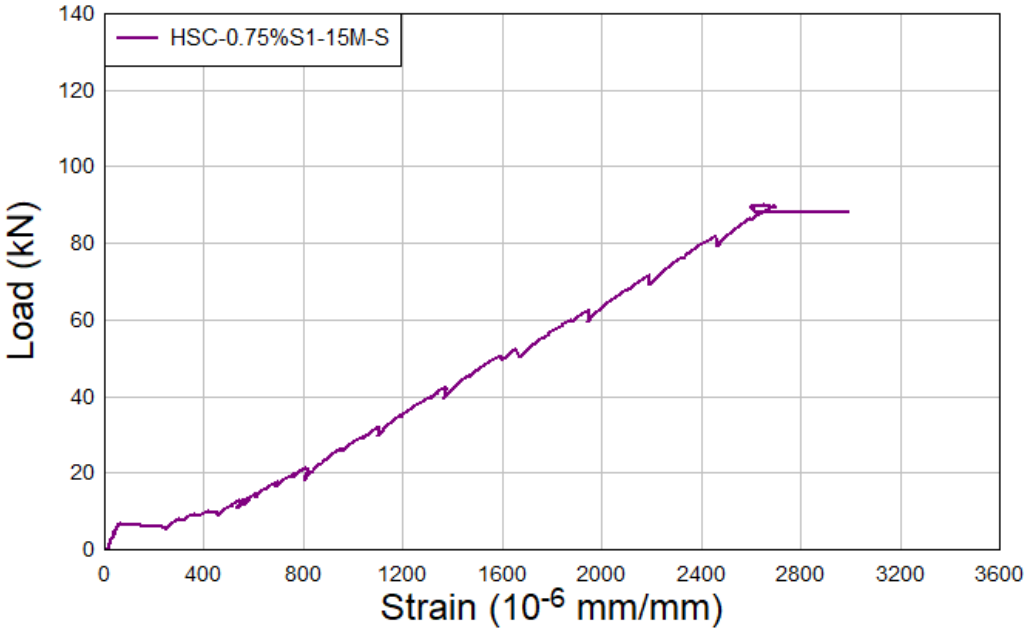

d) Tensile strain in longitudinal rebar

Figure 4-15 Experimental results for Beam HSC-0.75%S1-15M-S

<table>
<tr><th colspan="3">Experimental Parameters</th><th>Description</th></tr>
<tr><td>Load Stage</td><td>Load (kN)</td><td>Mid-Span Deflection (mm)</td><td rowspan="3">First hairline cracks appear in the flexural region</td></tr>
<tr><td>1</td><td>20</td><td>3</td></tr>
<tr><td colspan="3">  </td></tr>
<tr><td>Load Stage</td><td>Load (kN)</td><td>Mid-Span Deflection (mm)</td><td rowspan="3">First flexural-shear crack appears in the East region</td></tr>
<tr><td>5</td><td>62</td><td>8.7</td></tr>
<tr><td colspan="3">  </td></tr>
<tr><td>Load Stage</td><td>Load (kN)</td><td>Mid-Span Deflection (mm)</td><td rowspan="3">Steel reinforcement yielding</td></tr>
<tr><td>8</td><td>90</td><td>12.3</td></tr>
<tr><td colspan="3"> 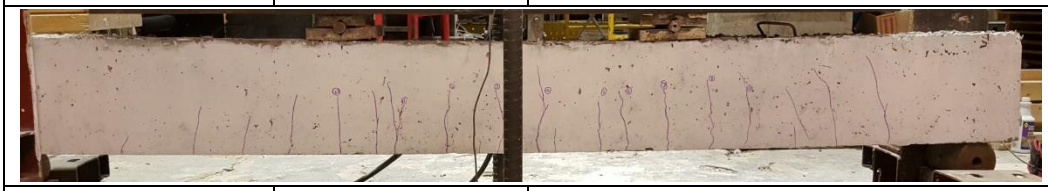 </td></tr>
<tr><td>Load Stage</td><td>Load (kN)</td><td>Mid-Span Deflection (mm)</td><td rowspan="3">Concrete crushing around loading plate</td></tr>
<tr><td>21</td><td>95</td><td>80</td></tr>
<tr><td colspan="3"> 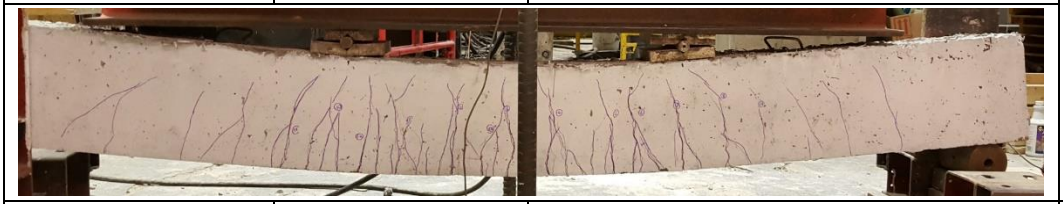 </td></tr>
<tr><td>Load Stage</td><td>Load (kN)</td><td>Mid-Span Deflection (mm)</td><td rowspan="3">Concrete starts crushing in the middle compression zone and after 10 s the crushing increases and the specimen fails</td></tr>
<tr><td>22</td><td>94</td><td>85</td></tr>
<tr><td colspan="3">  </td></tr>
</table>

Figure 4-16 Major events for Beam HSC-0.75%S1-15M-S

4.3 Description of Experimental Results – Series 20M

4.3.1 HSC-0.75%S1-20M-0

This beam was constructed with high-strength concrete and reinforced with 20M bars without transverse reinforcement. Synthetic fibers were incorporated at a volumetric ratio of 0.75%. **Table 4-6** summarizes the test results for this specimen. **Figure 4-17** shows the load-deflection curve and **Figure 4-18** demonstrates the growth of shear and flexural crack widths and tensile strain in rebar. **Figure 4-19** shows detailed photos of major events during testing. The first hairline cracks were observed in the flexural zone at an applied load of 20 kN. As the applied load was increased, further cracks were observed along the beam length with the formation of shear cracks in both shear spans at an applied load of 100 kN. Yielding of the longitudinal reinforcement occurred at 19.7 mm displacement. As the test progressed in the post-yield range, the specimen experienced a shear failure on the East side. The maximum load recorded was 170 kN with a corresponding maximum deflection of 30 mm.

Table 4-6 Summary of results for Beam HSC-0.75%S1-20M-0

Load (kN)		Displacement (mm)			Stiffness K (N/mm)	Ductility		Toughness (kN·mm)		Failure Mechanism
P_y	P_{max}	Δ_y	Δ_{85}	Δ_{max}		Δ_{85}/Δ_y	Δ_{max}/Δ_y	Au_{85}	Au_{max}	
160	170	19.7	-	30	8122	-	1.52	-	3983	Shear Failure

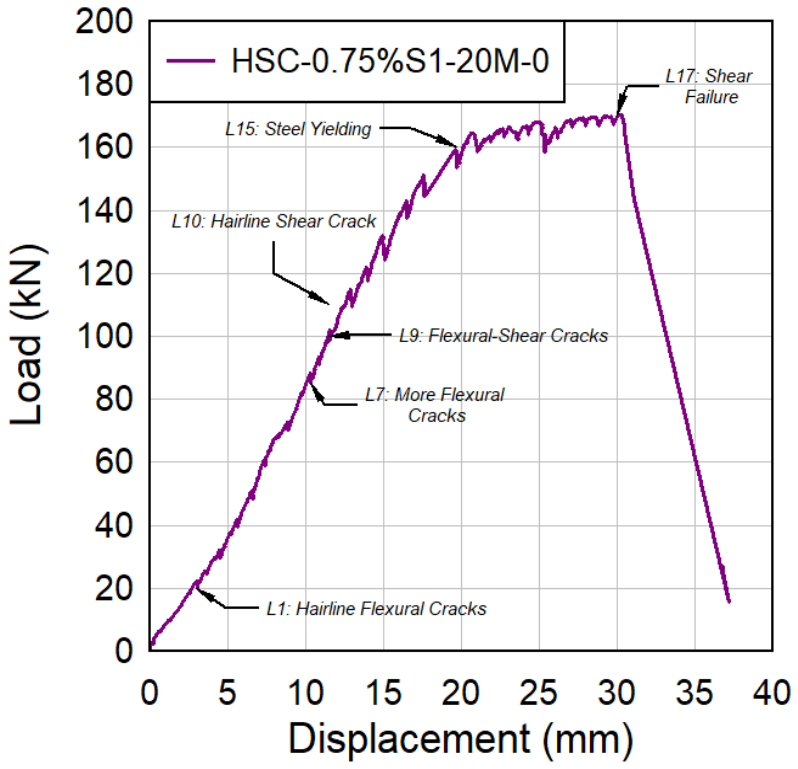

Figure 4-17 Load vs. mid-span deflection for Beam HSC-0.75%S1-20M-0

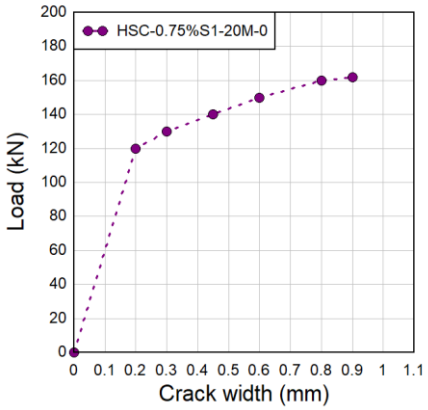

a) Maximum crack width (shear)

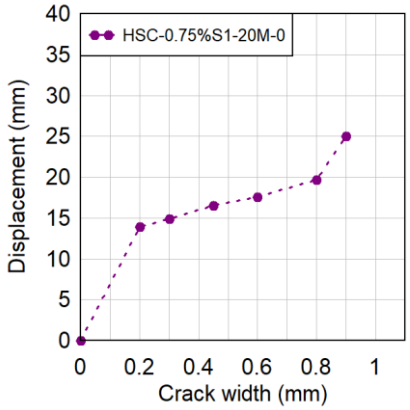

b) Maximum crack width (shear)

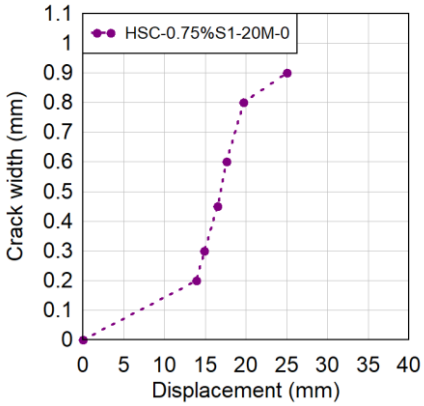

c) Maximum crack width (shear)

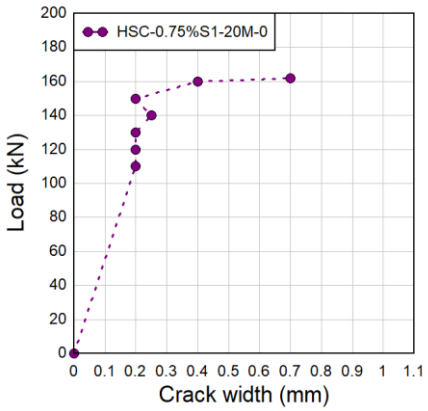

d) Maximum crack width (flexure)

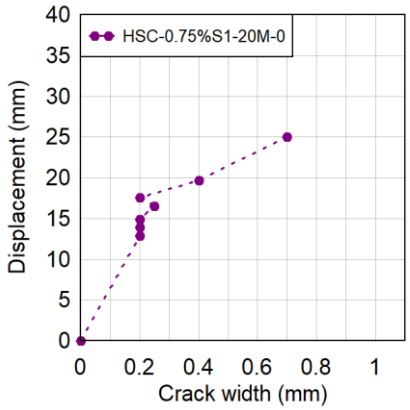

e) Maximum crack width (flexure)

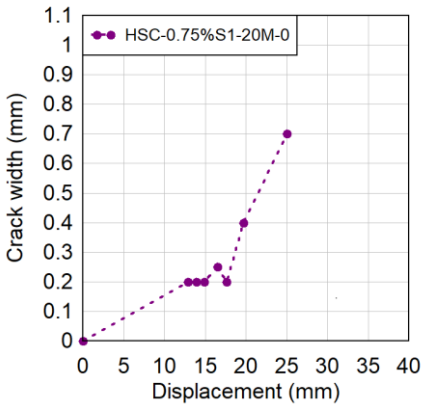

f) Maximum crack width (flexure)

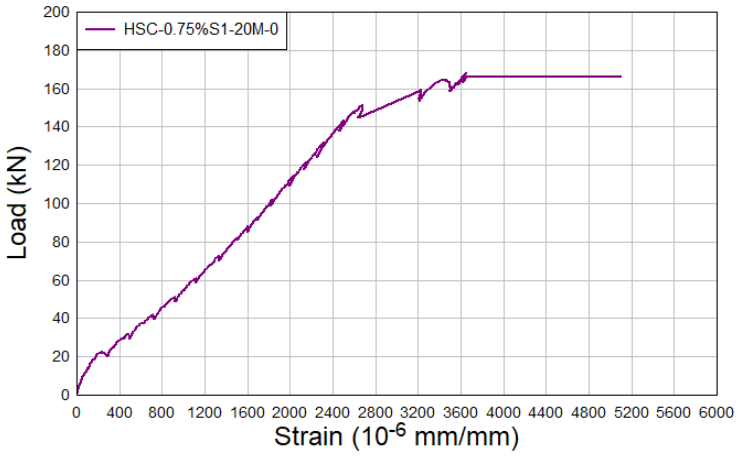

g) Tensile strain in longitudinal rebar

Figure 4-18 Experimental results for Beam HSC-0.75%S1-20M-0

Experimental Parameters			Description
Load Stage	Load (kN)	Mid-Span Deflection (mm)	First hairline cracks appear in the flexural region
1	20	3	
			
Load Stage	Load (kN)	Mid-Span Deflection (mm)	Further cracks appear in the constant moment region
7	85	10.3	
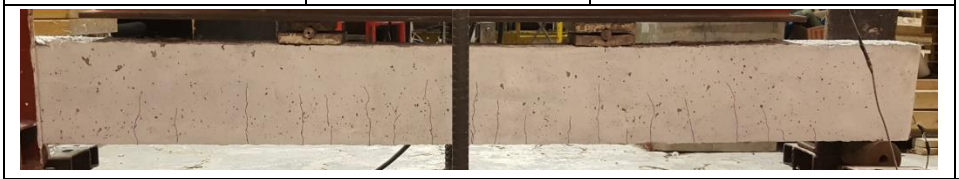			
Load Stage	Load (kN)	Mid-Span Deflection (mm)	Flexural-shear cracks started to form in the shear spans
9	100	11.5	
			
Load Stage	Load (kN)	Mid-Span Deflection (mm)	First hairline shear crack appears in the West shear span
10	110	11.5	
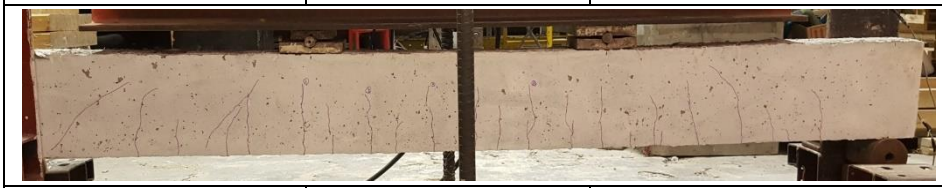			
Load Stage	Load (kN)	Mid-Span Deflection (mm)	Steel reinforcement yielding, shear cracks becoming more prominent
15	160	19.7	
			
Load Stage	Load (kN)	Mid-Span Deflection (mm)	Specimen fails with a shear failure on the East side
17	170	30	
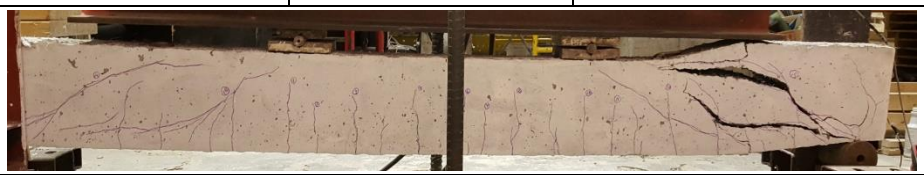			

Figure 4-19 Major events for Beam HSC-0.75%S1-20M-0

4.3.2 HSC-0.75%S1-20M-S

This specimen was built with the same components as the HSC-0.75%S1-20M-0, but had stirrups spaced at 100 mm in the shear spans. The results for this test are summarized in **Table 4-7**. **Figure 4-20** shows the load-deflection curve. The growth of shear and flexural crack widths and tensile strain in rebar are presented in **Figure 4-21**. **Figure 4-22** shows detailed photos of major events during testing. The first hairline flexural cracks were observed at an applied load of 20 kN. As the test progressed, hairline shear cracks appeared in the West region first, then in the East region at an applied load of 80 and 100 kN respectively. Yielding and concrete crushing at loading plate occurred simultaneously at 19.8 mm displacement when the load reached 150 kN. A noticeable yielding plateau is observed in **Figure 4-21g** indicating that fibers controlled the widening of cracks. The maximum load recorded was 156 kN at a corresponding displacement of 21.2 mm. Shortly after, concrete started crushing at the top middle region when the displacement reached 25 mm. The specimen experienced severe concrete crushing with the formation of a diagonal crack in the central beam region causing failure at Δ_{max} = 60 mm.

Table 4-7 Summary of results for Beam HSC-0.75%S1-20M-S

Load (kN)		Displacement (mm)			Stiffness K (N/mm)	Ductility		Toughness (kN·mm)		Failure Mechanism
P_y	P_{max}	Δ_y	Δ_{85}	Δ_{max}		Δ_{85}/Δ_y	Δ_{max}/Δ_y	Au_{85}	Au_{max}	
150	156	19.8	30.4	60	7576	1.54	3.03	3105	6123	Concrete Crushing with a Diagonal Crack

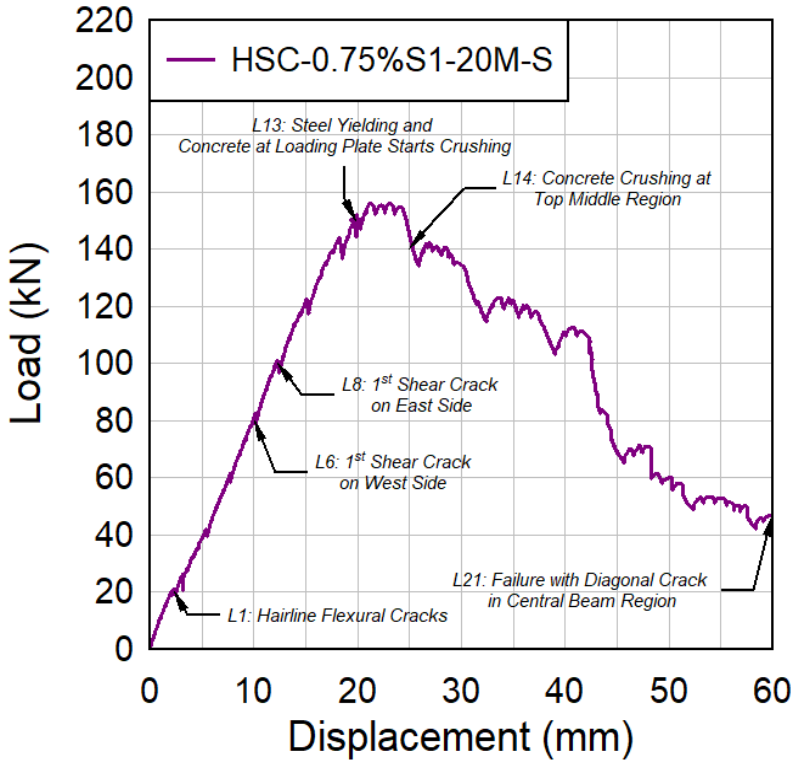

Figure 4-20 Load vs. mid-span deflection for Beam HSC-0.75%S1-20M-S

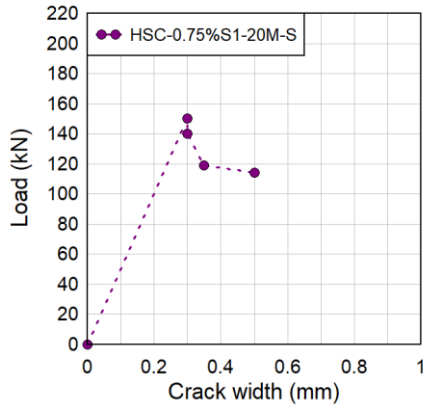

a) Maximum crack width (shear)

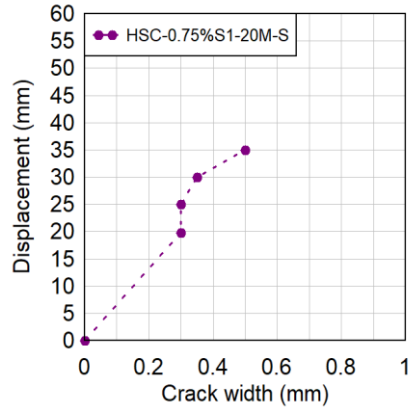

b) Maximum crack width (shear)

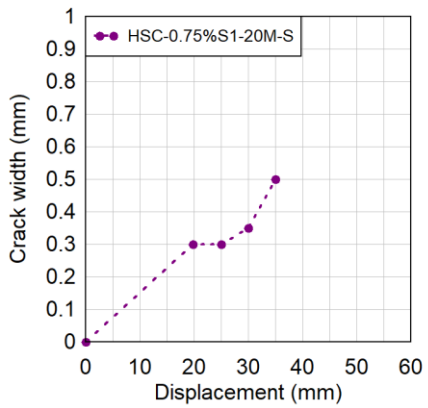

c) Maximum crack width (shear)

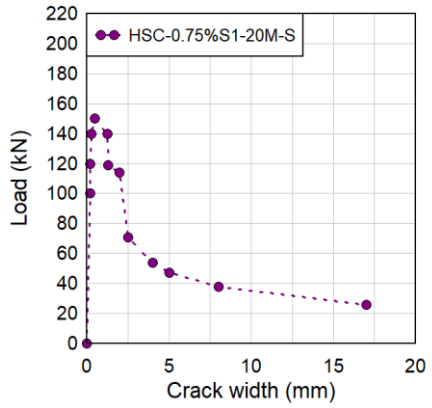

d) Maximum crack width (flexure)

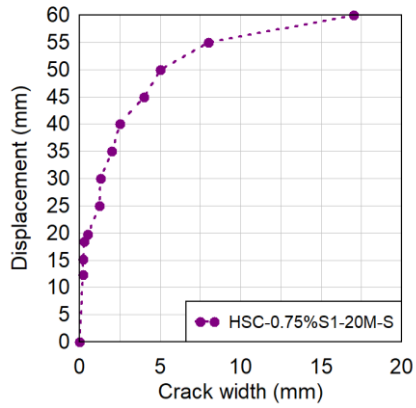

e) Maximum crack width (flexure)

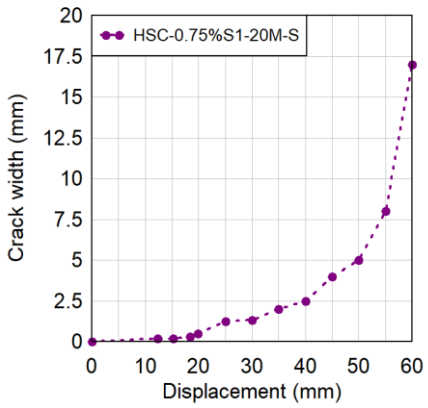

f) Maximum crack width (flexure)

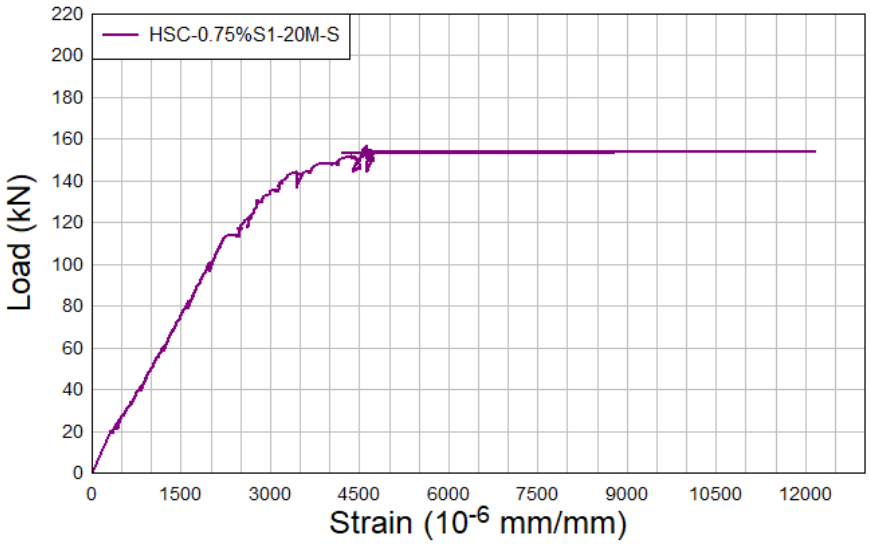

g) Tensile strain in longitudinal rebar

Figure 4-21 Experimental results for Beam HSC-0.75%S1-20M-S

Experimental Parameters			Description
Load Stage	Load (kN)	Mid-Span Deflection (mm)	First hairline cracks appear in the flexural region
1	20	2.4	
			
Load Stage	Load (kN)	Mid-Span Deflection (mm)	First shear crack appears on the West side
6	80	10.1	
			
Load Stage	Load (kN)	Mid-Span Deflection (mm)	First shear crack appears on the East side
8	100	12.3	
			
Load Stage	Load (kN)	Mid-Span Deflection (mm)	Steel reinforcement yielding and concrete at loading plate starts crushing
13	150	19.8	
			
Load Stage	Load (kN)	Mid-Span Deflection (mm)	Concrete starts crushing at the top middle region
14	140	25	
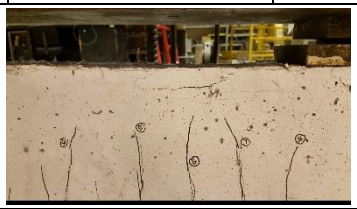			
Load Stage	Load (kN)	Mid-Span Deflection (mm)	Specimen fails with concrete crushing and a diagonal crack in the central beam region
21	46.7	60	
			

Figure 4-22 Major events for Beam HSC-0.75%S1-20M-S

4.3.3 HSC-HYB-20M-0

The last specimen in the 20M series had the same properties as HSC-0.75%S1-20M-0, except for the addition of smooth straight steel fibers at a volumetric ratio of 0.25%. No stirrups were used in this specimen. Results for this beam are summarized in **Table 4-8**. **Figure 4-23** shows the load-deflection curve. The growth of shear and flexural crack widths and tensile strain in rebar are presented in **Figure 4-24**. **Figure 4-25** shows detailed photos of major events during testing. The first hairline cracks were observed in the flexural region at an applied load of 40 kN. As the load was increased, further cracks appeared in the flexural region along with the formation of a shear crack on the West side at an applied load of 140 kN. Yielding of the bottom longitudinal reinforcement then occurred at 16 mm displacement when the load reached 160 kN. **Figure 4-24g** illustrates the significant yielding plateau recorded during the test, which can be explained by the bridging effect of fibers and the synergistic effects of the micro and macro fibers. This is further demonstrated in **Figure 4-24a – c**, where it can be seen that the width of the major shear crack did not expand beyond 2 mm. The use of hybrid fibers delayed concrete crushing at the top middle region, with the first signs of crushing noted at 45 mm displacement. The specimen experienced concrete crushing with the formation of a diagonal crack in the central beam region causing failure (Δ_{max} = 80 mm), similar to what was observed in the HSC-0.75%S1-20M-S specimen.

Table 4-8 Summary of results for Beam HSC-HYB-20M-0

Load (kN)		Displacement (mm)			Stiffness K (N/mm)	Ductility		Toughness (kN·mm)		Failure Mechanism
P_y	P_{max}	Δ_y	Δ_{85}	Δ_{max}		Δ_{85}/Δ_y	Δ_{max}/Δ_y	Au_{85}	Au_{max}	
160	170.8	16.0	43.3	80.0	10000	2.71	5.00	5822	10135	Concrete Crushing with a Diagonal Crack

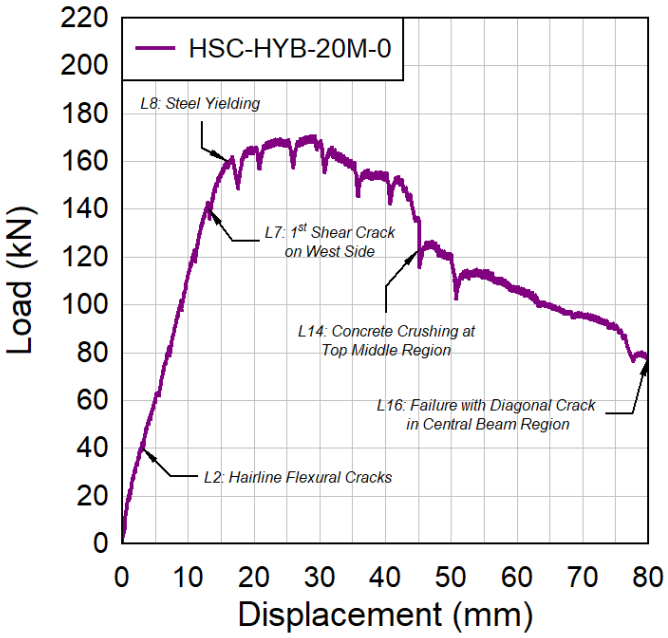

Figure 4-23 Load vs. mid-span deflection for Beam HSC-HYB-20M-0

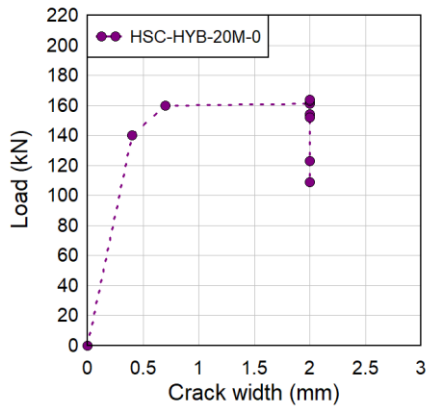

a) Maximum crack width (shear)

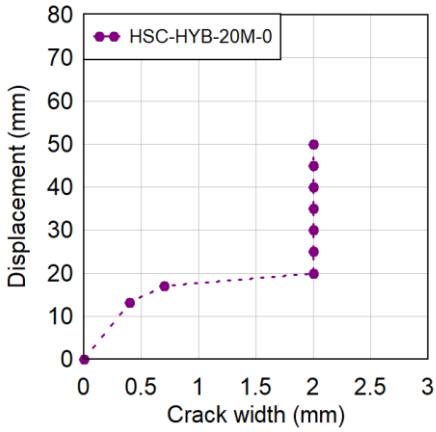

b) Maximum crack width (shear)

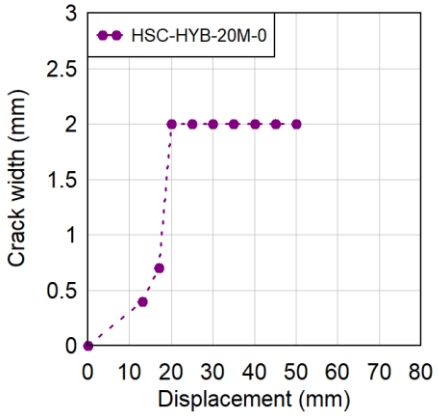

c) Maximum crack width (shear)

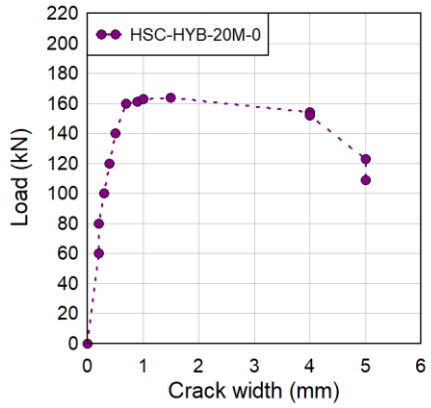

d) Maximum crack width (flexure)

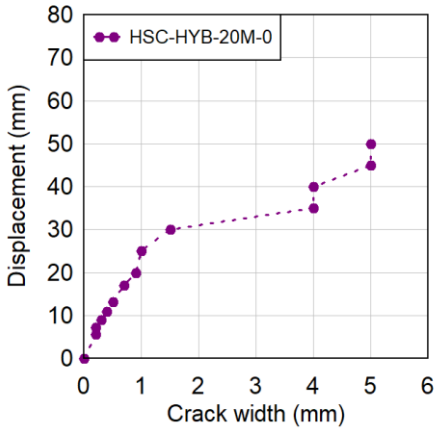

e) Maximum crack width (flexure)

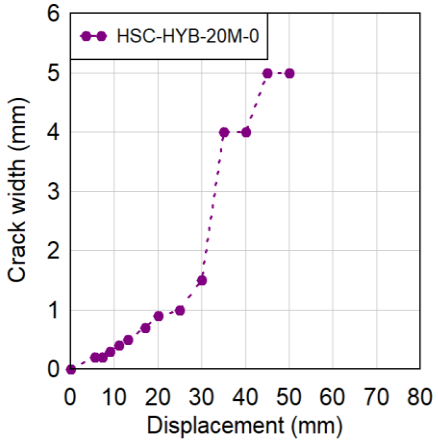

f) Maximum crack width (flexure)

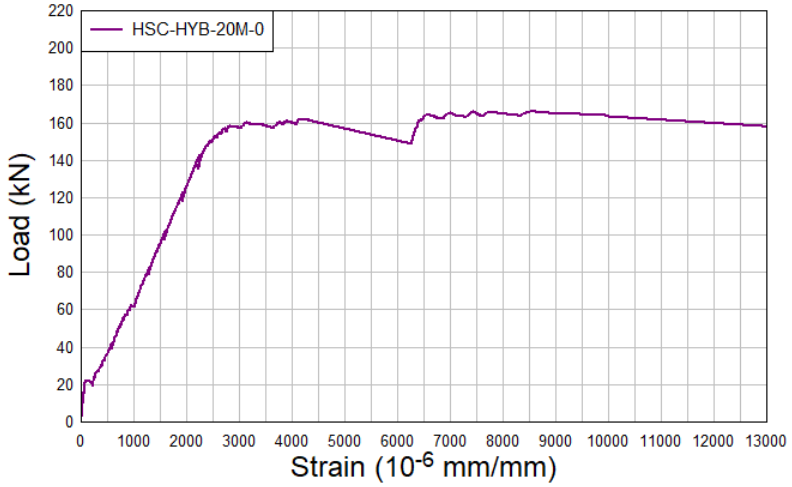

g) Tensile strain in longitudinal rebar

Figure 4-24 Experimental results for Beam HSC-HYB-20M-0

<table>
<tr><th colspan="3">Experimental Parameters</th><th>Description</th></tr>
<tr><td>Load Stage</td><td>Load (kN)</td><td>Mid-Span Deflection (mm)</td><td rowspan="3">First hairline cracks appear in the flexural region</td></tr>
<tr><td>2</td><td>40</td><td>3.1</td></tr>
<tr><td colspan="3">  </td></tr>
<tr><td>Load Stage</td><td>Load (kN)</td><td>Mid-Span Deflection (mm)</td><td rowspan="3">First shear crack appears on the West side</td></tr>
<tr><td>7</td><td>140</td><td>13.1</td></tr>
<tr><td colspan="3"> 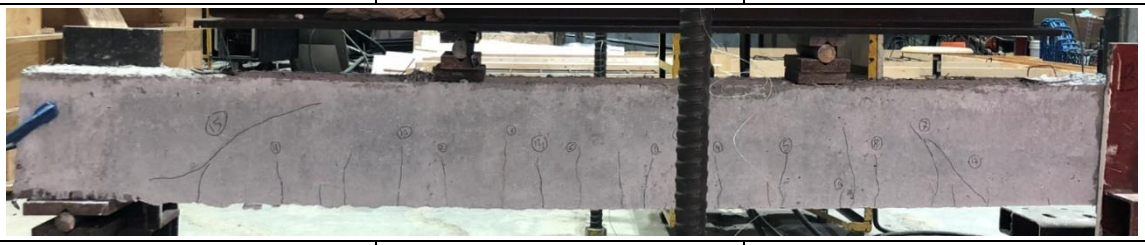 </td></tr>
<tr><td>Load Stage</td><td>Load (kN)</td><td>Mid-Span Deflection (mm)</td><td rowspan="3">Steel reinforcement yielding</td></tr>
<tr><td>8</td><td>160</td><td>16.0</td></tr>
<tr><td colspan="3"> 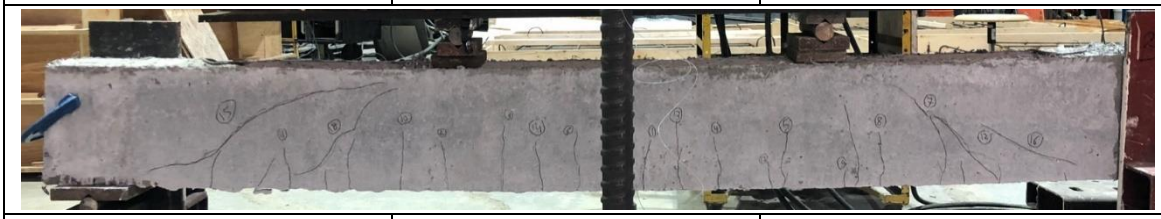 </td></tr>
<tr><td>Load Stage</td><td>Load (kN)</td><td>Mid-Span Deflection (mm)</td><td rowspan="3">Concrete starts crushing at the top middle region</td></tr>
<tr><td>14</td><td>123</td><td>45</td></tr>
<tr><td colspan="3"> 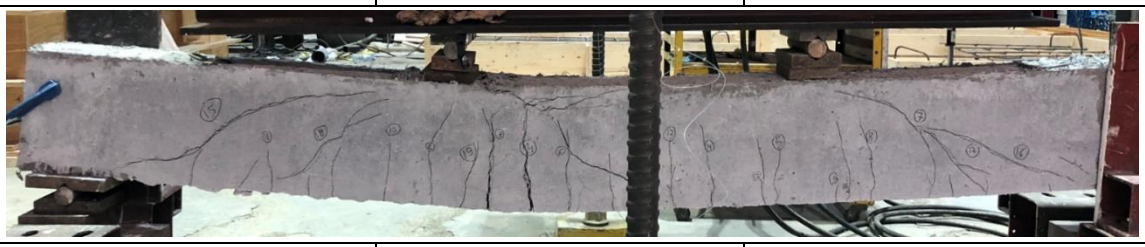 </td></tr>
<tr><td>Load Stage</td><td>Load (kN)</td><td>Mid-Span Deflection (mm)</td><td rowspan="3">Specimen fails with a diagonal crack in the central beam region</td></tr>
<tr><td>16</td><td>78</td><td>80</td></tr>
<tr><td colspan="3">  </td></tr>
</table>

Figure 4-25 Major events for Beam HSC-HYB-20M-0

4.4 Description of Experimental Results – Series No.5

4.4.1 HSC-0.75%S1-No.5(HS)-S

This specimen was constructed with high-strength concrete and reinforced with No.5 Grade 690 MPa bars and transverse reinforcement. Synthetic fibers were incorporated at a volumetric ratio of 0.75%. **Table 4-9** presents the results for this beam test. **Figure 4-26** shows the load-deflection curve and **Figure 4-27** reveals the growth of shear and flexural crack widths along with tensile strain in rebar. **Figure 4-28** shows detailed photos of major events during testing. The first hairline cracks were observed in the flexural zone at an applied load of 23.5 kN. As the applied load was increased, further cracks were observed along the beam length. Flexural-shear cracks started to form in the East shear span at an applied load of 80 kN and a shear crack was recorded when the applied load reached 100 kN. Signs of yielding were recorded at 28.1 mm displacement. Later during the test, concrete started crushing at the top flexural zone when the load reached a maximum of 213 kN leading to the sudden failure of the beam at Δ_{max} = 40.7 mm.

Table 4-9 Summary of results for Beam HSC-0.75%S1-No.5(HS)-S

Load (kN)		Displacement (mm)			Stiffness K (N/mm)	Ductility		Toughness (kN·mm)		Failure Mechanism
P_y	P_{max}	Δ_y	Δ_{85}	Δ_{max}		Δ_{85}/Δ_y	Δ_{max}/Δ_y	Au_{85}	Au_{max}	
185.5	213.1	28.1	-	40.7	6601	-	1.45	-	5622	Concrete Crushing

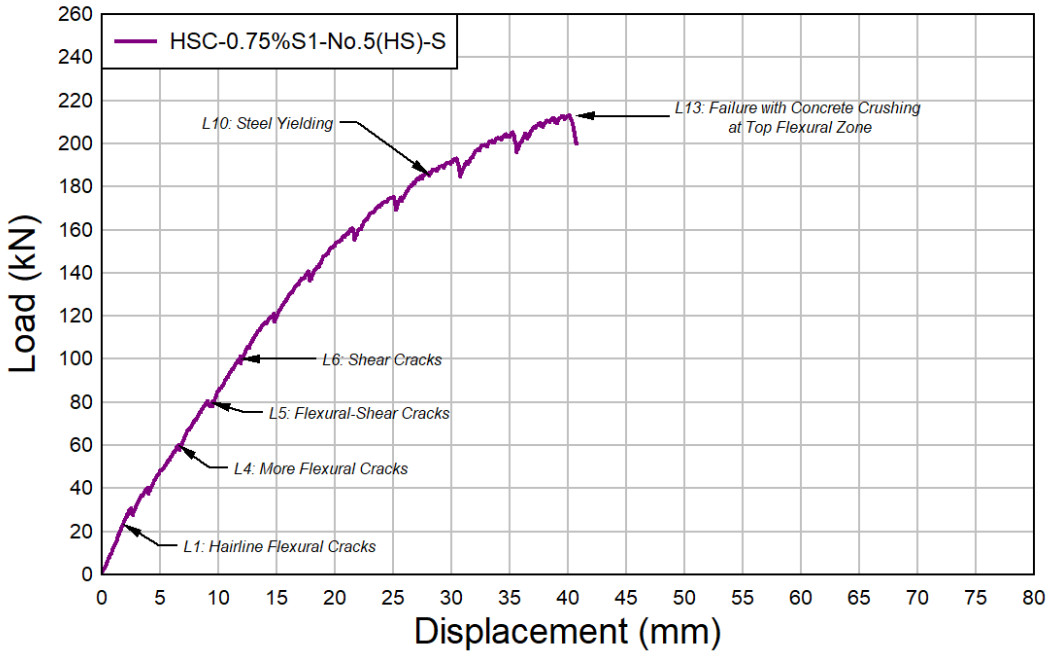

Figure 4-26 Load vs. mid-span deflection for Beam HSC-0.75%S1-No.5(HS)-S

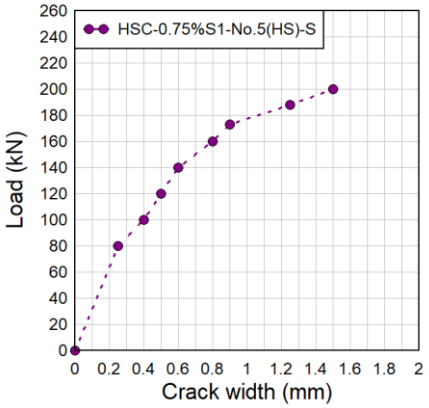

a) Maximum crack width (shear)

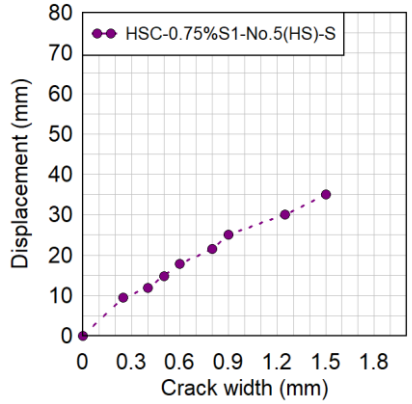

b) Maximum crack width (shear)

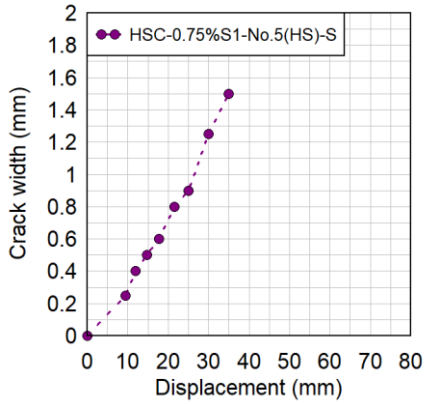

c) Maximum crack width (shear)

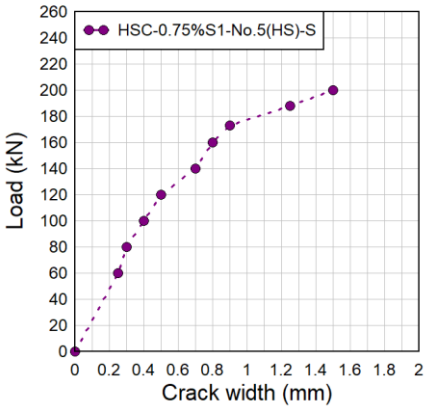

d) Maximum crack width (flexure)

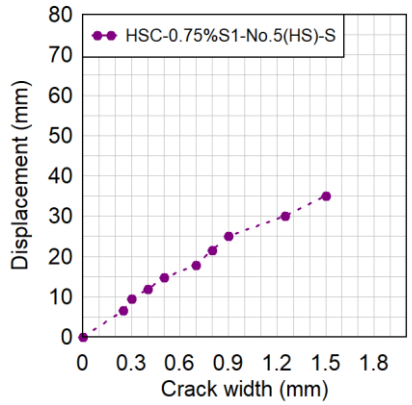

e) Maximum crack width (flexure)

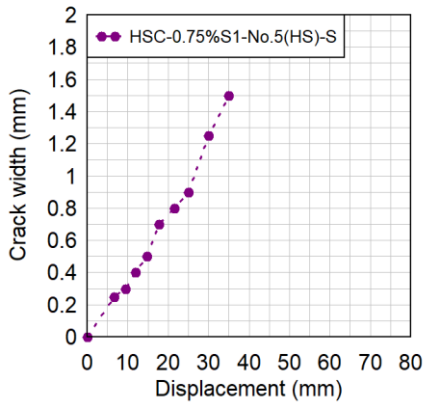

f) Maximum crack width (flexure)

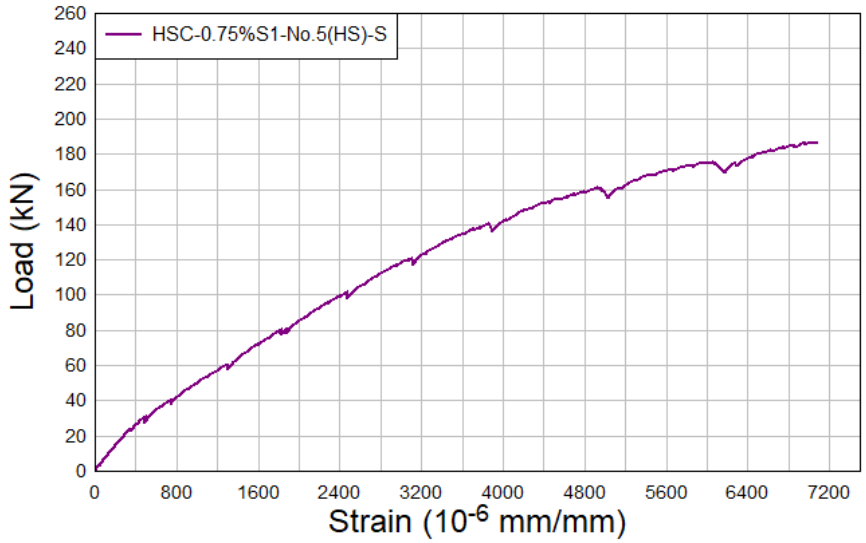

g) Tensile strain in longitudinal rebar

Figure 4-27 Experimental results for Beam HSC-0.75%S1-No.5(HS)-S

<table>
<tr><th colspan="3">Experimental Parameters</th><th>Description</th></tr>
<tr><td>Load Stage</td><td>Load (kN)</td><td>Mid-Span Deflection (mm)</td><td rowspan="3">First hairline cracks appear in the flexural region</td></tr>
<tr><td>1</td><td>23.5</td><td>1.84</td></tr>
<tr><td colspan="3"> 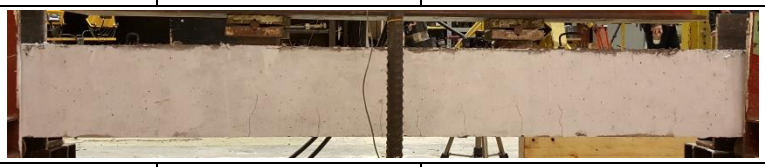 </td></tr>
<tr><td>Load Stage</td><td>Load (kN)</td><td>Mid-Span Deflection (mm)</td><td rowspan="3">Further cracks appear in the constant moment region</td></tr>
<tr><td>4</td><td>60</td><td>6.6</td></tr>
<tr><td colspan="3">  </td></tr>
<tr><td>Load Stage</td><td>Load (kN)</td><td>Mid-Span Deflection (mm)</td><td rowspan="3">Flexural-shear cracks started to form in the East shear span</td></tr>
<tr><td>5</td><td>80</td><td>9.4</td></tr>
<tr><td colspan="3"> 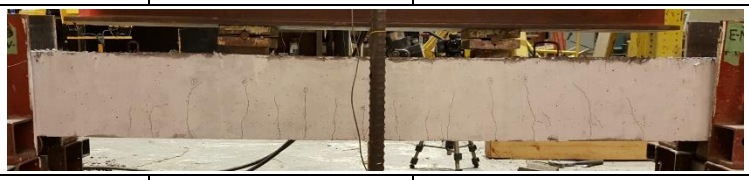 </td></tr>
<tr><td>Load Stage</td><td>Load (kN)</td><td>Mid-Span Deflection (mm)</td><td rowspan="3">Shear cracks appear in the shear spans</td></tr>
<tr><td>6</td><td>100</td><td>11.9</td></tr>
<tr><td colspan="3">  </td></tr>
<tr><td>Load Stage</td><td>Load (kN)</td><td>Mid-Span Deflection (mm)</td><td rowspan="3">Steel reinforcement yielding</td></tr>
<tr><td>10</td><td>185.5</td><td>28.1</td></tr>
<tr><td colspan="3">  </td></tr>
<tr><td>Load Stage</td><td>Load (kN)</td><td>Mid-Span Deflection (mm)</td><td rowspan="3">Specimen fails suddenly with concrete crushing at the top flexural zone</td></tr>
<tr><td>13</td><td>213.1</td><td>40.7</td></tr>
<tr><td colspan="3">  </td></tr>
</table>

Figure 4-28 Major events for Beam HSC-0.75%S1-No.5(HS)-S

Chapter 5: Experimental Results of the Shock-Tube Tests

5.1 Chapter Overview

This chapter summarizes the individual experimental results for each of the eight beams tested under simulated blast loading. The presented results include: reflected pressure and impulse time histories, displacement time histories with maximum and residual mid-span displacements, and photographs of the beams after each blast along with a brief description of the major damage observed and the failure mode where applicable.

A table summarizing key data is also provided for each beam, including reflected pressure (P_r) and reflected impulse (I_r), positive phase duration (t_d), maximum mid-span displacement (Δ_{max}) and residual mid-span displacement (Δ_{res}), support rotations (θ_{max}), dynamic peak load (P_{max}), observed damage after each blast, and the damage state (response limit) according to the CSA S850 standard. It is noted that the support rotations were approximately measured by dividing the maximum displacement by the beam's half-span due to the relatively small rotations. The definitions of the different variables extracted from the tests are shown in **Figure 5-1** and are summarized as follows:

P_r: reflected pressure which represents the pressure recorded at the shock-tube end frame;
t_d: positive phase duration or period of time taken for the maximum pressure to decay to zero pressure;
I_r: reflected impulse or area under the positive phase of the pressure-time history curve (hatched region);
Δ_{max}: maximum displacement;
Δ_{res}: residual displacement.

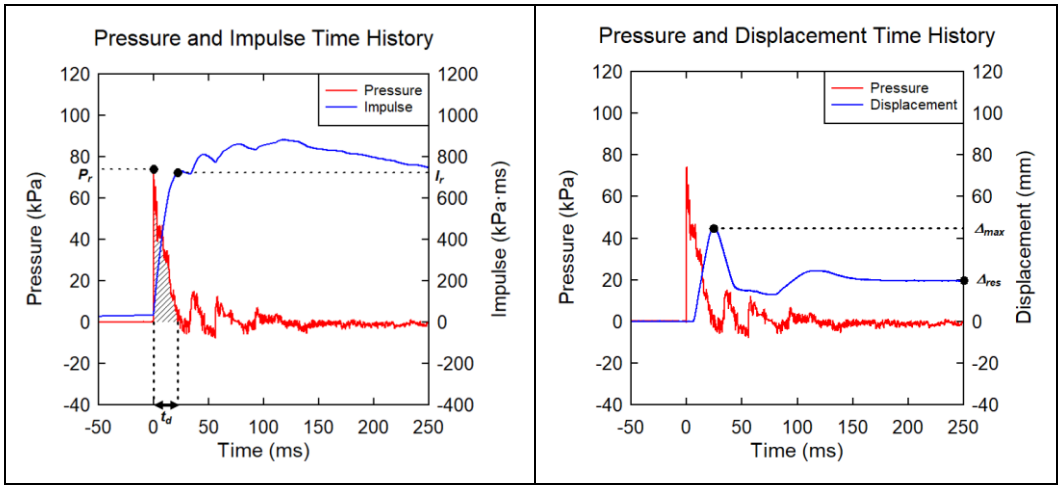

Figure 5-1 Illustration of the variables extracted from the curves

The experimental support rotations are compared with the response limits and component damage levels in the CSA S850 standard. **Table 5-1** summarizes the different response limits and their corresponding component damage for single and double-reinforced beams.

Table 5-1 CSA S850 response limits and damage levels (Adapted from Table 4.3 in the CSA S850 Standard)

Angle		Response Limit	Expected Damage Level
Single-reinforced beam	Double-reinforced beam		
$\theta < 1°$	$\theta < 1°$	<B1	Superficial
$1° \leq \theta < 2°$	$1° \leq \theta < 4°$	B2-B1	Moderate
$2° \leq \theta < 5°$	$4° \leq \theta < 6°$	B3-B2	Heavy
$5° \leq \theta < 10°$	$6° \leq \theta < 10°$	B4-B3	Hazardous
$\theta \geq 10°$	$\theta \geq 10°$	≥B4	Blowout

5.2 Description of Experimental Results – Series 15M

5.2.1 Specimen HSC-0%-15M-0

The HSC-0%-15M-0 beam was a control specimen designed with plain high-strength concrete (HSC) and reinforced longitudinally with 15M normal-strength rebar without transverse reinforcement. Results for this beam are summarized in **Table 5-2**. **Figure 5-2** shows reflected pressure, impulse, and displacement time histories along with dynamic resistance curves and strains in longitudinal rebar. Photographs of major events after each blast are shown in **Figure 5-3**. Blast 1 (30 psi) was enough to cause the specimen to fail in shear with a 2 mm wide diagonal shear crack on the bottom shear span as illustrated in **Figure 5-3b**. Failure occurred close to yielding, like what was observed under static testing. The maximum and residual mid-span displacements reached were 16.1 mm and 5.5 mm respectively.

Table 5-2 Summary of results for Beam HSC-0%-15M-0

Blast #	Shockwave Properties			Displacement		θ_{max} (°)	P_{max} (kN)	Observed Damage	CSA S850 Response Limits and Component Damage[1]	
	P_r (kPa)	I_r (kPa-ms)	t_d (ms)	Δ_{max} (mm)	Δ_{res} (mm)				Response Limit	Expected Damage Level
1	35.9	323.6	19.4	16.08	5.49	0.83	78.4	Shear Failure	<B1	Superficial

[1]: Blowout: $\theta \geq 10°$, Hazardous: $5° \leq \theta < 10°$; Heavy: $2° \leq \theta < 5°$; Moderate: $1° \leq \theta < 2°$; Superficial: $\theta < 1°$

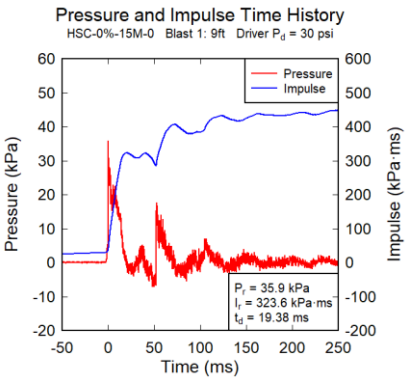

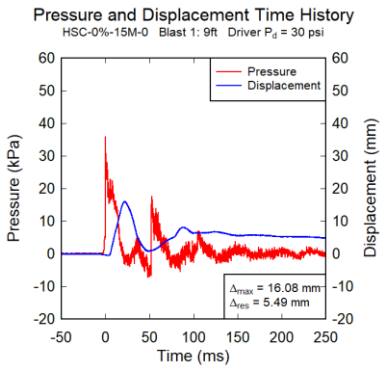

a) Blast 1: Reflected pressure, impulse, and displacement time histories.

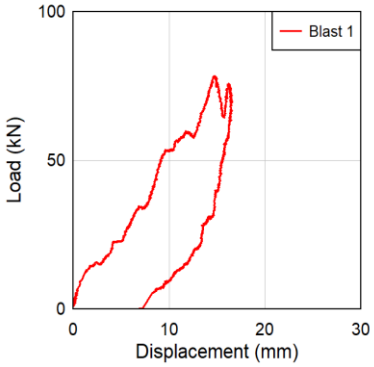

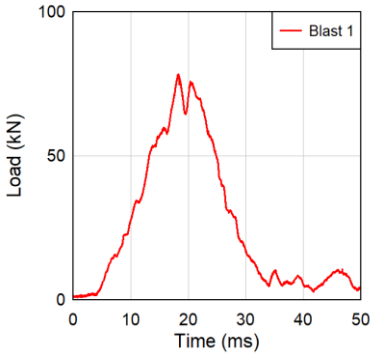

b) Dynamic resistance curves at Blast 1

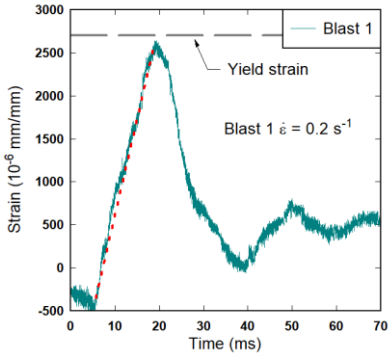

c) Tensile strain in rebar

Figure 5-2 Experimental results for Beam HSC-0%-15M-0

a) Blast 1

b) Close-up of shear failure (Blast 1)

Figure 5-3 HSC-0%-15M-0; photographs at the end of Blast 1

5.2.2 Specimen HSC-0.75%S1-15M-0

The HSC-0.75%S1-15M-0 beam was identical to the previous beam, but with the addition of 0.75% synthetic fibers. Results for this beam are summarized in **Table 5-3**. **Figure 5-4** shows reflected pressure, impulse, and displacement time histories along with dynamic resistance curves, crack width and strain in longitudinal rebar. Photographs of major events after each blast are displayed in **Figure 5-5**. The addition of fibers enhanced the behaviour of the beam allowing it to survive Blast 1 (30 psi), which only resulted in the formation of hairline flexural cracks along the span of the beam. Since Blast 1 was within the elastic range, a low residual displacement was measured. Blast 2a (50 psi) allowed the steel reinforcement to reach yielding and caused shear failure of the beam due to fiber pullout at the bottom shear span as shown in **Figure 5-5b** and **Figure 5-5e**. The maximum and residual mid-span displacements for this blast were recorded at 35.6 mm and 29.9 mm respectively. Buckling of the 6.35 mm top holding bar in the shear span was also observed after Blast 2a as shown in **Figure 5-5d**.

Table 5-3 Summary of results for Beam HSC-0.75%S1-15M-0

Blast #	Shockwave Properties			Displacement		θ_{max} (°)	P_{max} (kN)	Observed Damage	CSA S850 Response Limits and Component Damage[1]	
	P_r (kPa)	I_r (kPa-ms)	t_d (ms)	Δ_{max} (mm)	Δ_{res} (mm)				Response Limit	Expected Damage Level
1	44.4	377.7	20.6	18.84	3.43	0.97	94.2	Hairline F Cracks	<B1	Superficial
2a	65.6	553.5	20.6	35.55	29.94	1.82	144.9	Shear Failure	B2-B1	Moderate

[1]: Blowout: $\theta \geq 10°$, Hazardous: $5° \leq \theta < 10°$; Heavy: $2° \leq \theta < 5°$; Moderate: $1° \leq \theta < 2°$; Superficial: $\theta < 1°$

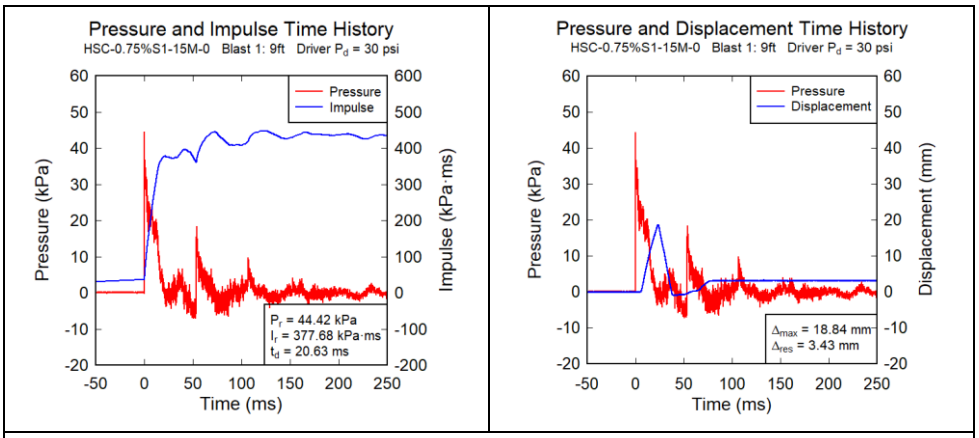

a) Blast 1: Reflected pressure, impulse, and displacement time histories.

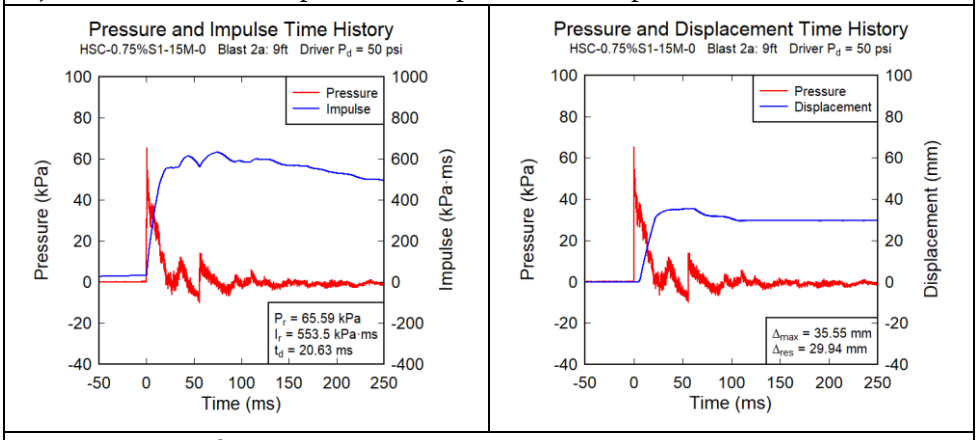

b) Blast 2a: Reflected pressure, impulse, and displacement time histories.

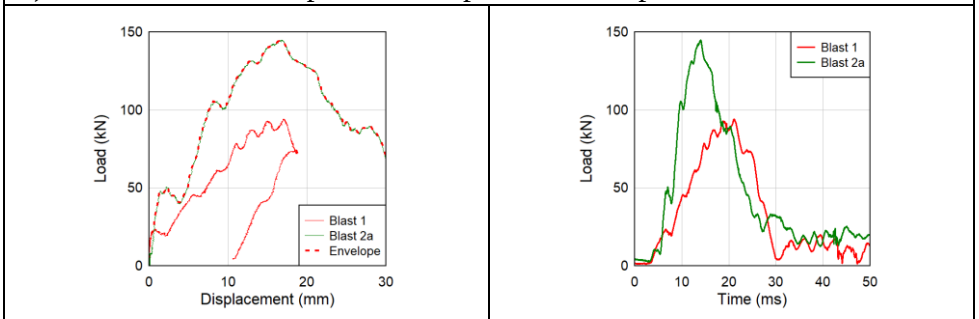

c) Dynamic resistance curves at varying blast intensities

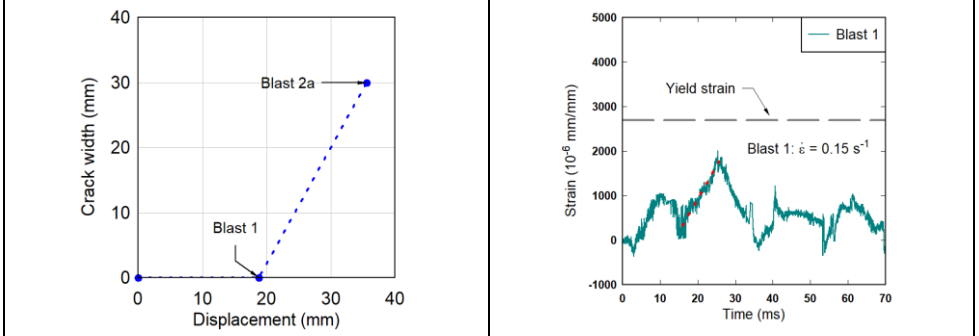

d) Maximum crack width (shear)

e) Tensile strain in rebar

Figure 5-4 Experimental results for Beam HSC-0.75%S1-15M-0

a) Blast 1

b) Blast 2a

c) Shear failure (Blast 2a)

d) Failure close-up (Blast 2a)

e) Principal shear crack (Blast 2a)

Figure 5-5 HSC-0.75%S1-15M-0; photographs at the end of Blast 1-2a

5.2.3 Specimen HSC-0.75%S1-15M-S

The HSC-0.75%S1-15M-S beam was built in a similar manner as the HSC-0.75%S1-15M-0 specimen, but had transverse reinforcement spaced at 100 mm in the shear spans. Results for this beam are summarized in **Table 5-4**. **Figure 5-6** shows reflected pressure, impulse, and displacement time histories along with dynamic resistance curves, crack width and strain in longitudinal rebar. Photographs of major events after each blast are provided in **Figure 5-7**. Blast 1 (30 psi) generated several hairline flexural cracks with a 0.4 mm critical crack just below the top point load application location. According to the strain gauge reading, the beam was tested within the elastic range for Blast 1, after which readings were considered unreliable. At Blast 2a (50 psi), the beam reached a maximum displacement of 29.6 mm causing the principal flexural crack to further widen to 4 mm. Blast 2c (70 psi) led to the failure of the specimen due to concrete crushing and fiber pullout. As can be seen in **Figure 5-7e** and **Figure 5-7f**, the same principal crack generated from the previous blasts expanded to a width of 13 mm with fibers pulling-out at this location. The maximum and residual mid-span displacements for this blast were recorded at 86.7 mm and 41.1 mm respectively. The CSA S850 standard predicts heavy damage based on the maximum rotation recorded (θ_{max} = 4.44°); however, the actual damage is less significant due to the provision of fibers.

Table 5-4 Summary of results for Beam HSC-0.75%S1-15M-S

Blast #	Shockwave Properties			Displacement		θ_{max} (°)	P_{max} (kN)	Observed Damage	CSA S850 Response Limits and Component Damage[1]	
	P_r (kPa)	I_r (kPa-ms)	t_d (ms)	Δ_{max} (mm)	Δ_{res} (mm)				Response Limit	Expected Damage Level
1	35.9	375.5	20.6	16.74	4.96	0.86	105.6	Hairline F Cracks	<B1	Superficial
2a	65.0	484.1	19.4	29.57	7.14	1.52	144.0	Further Crack Opening	B2-B1	Moderate
2c	72.0	711.7	20.6	86.70	41.1	4.44	161.9	Concrete Crushing & Fiber Pullout	B3-B2	Heavy

[1]: Blowout: $\theta \geq 10°$, Hazardous: $5° \leq \theta < 10°$; Heavy: $2° \leq \theta < 5°$; Moderate: $1° \leq \theta < 2°$; Superficial: $\theta < 1°$

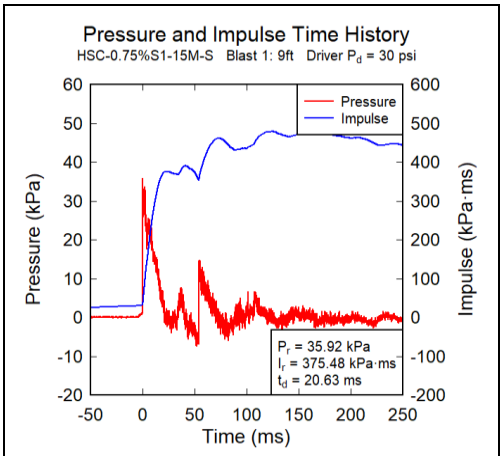

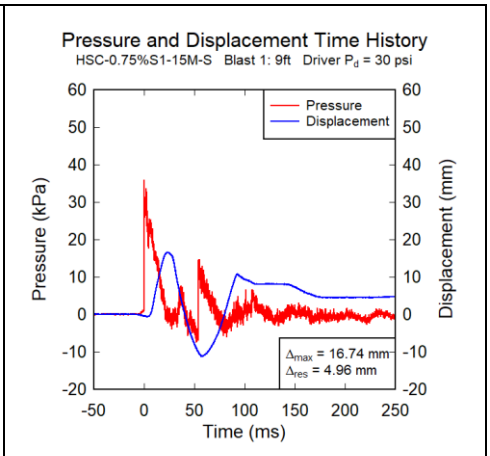

a) Blast 1: Reflected pressure, impulse, and displacement time histories.

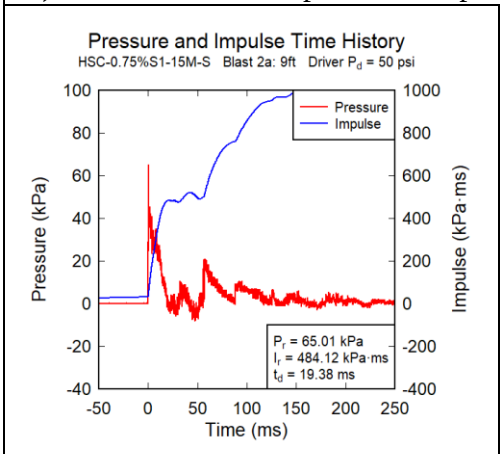

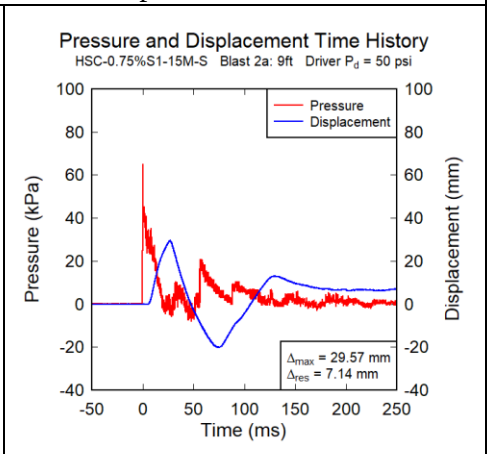

b) Blast 2a: Reflected pressure, impulse, and displacement time histories.

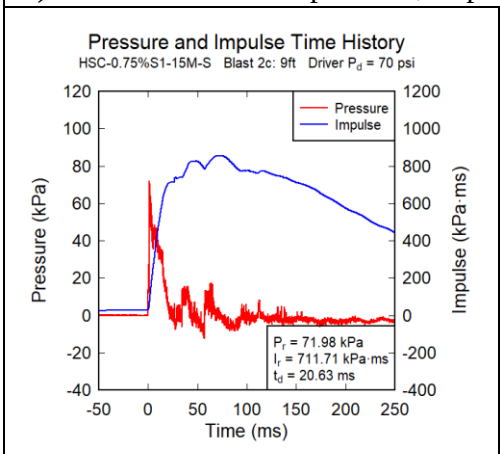

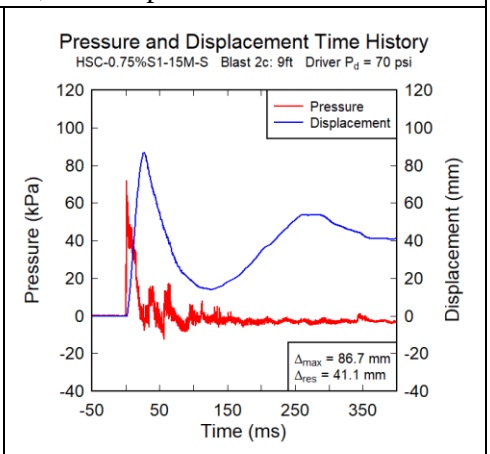

c) Blast 2c: Reflected pressure, impulse, and displacement time histories.

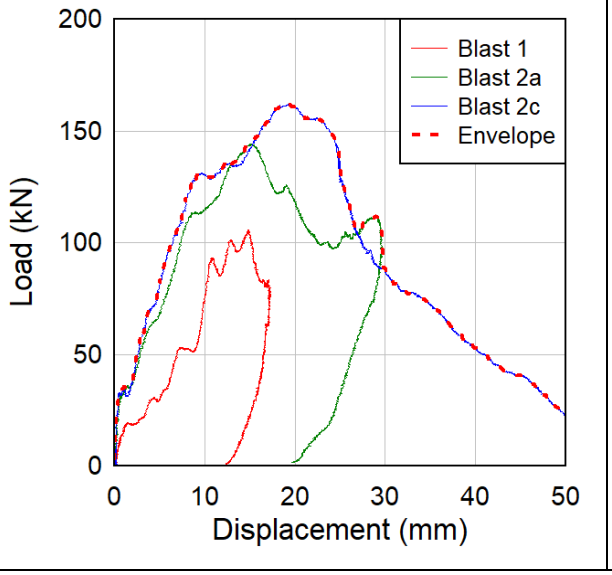

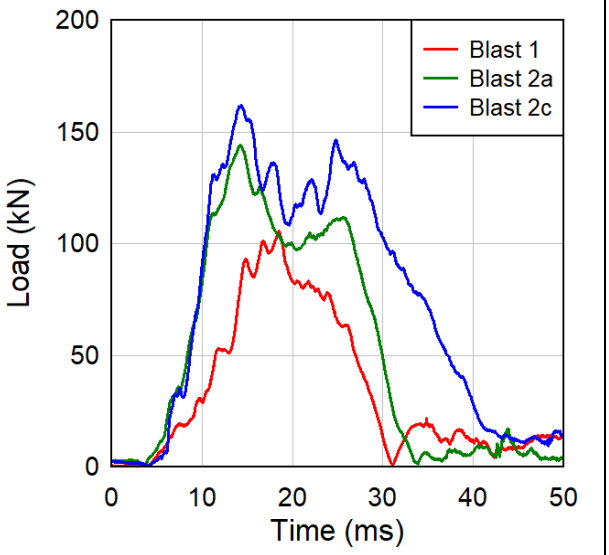

d) Dynamic resistance curves at varying blast intensities

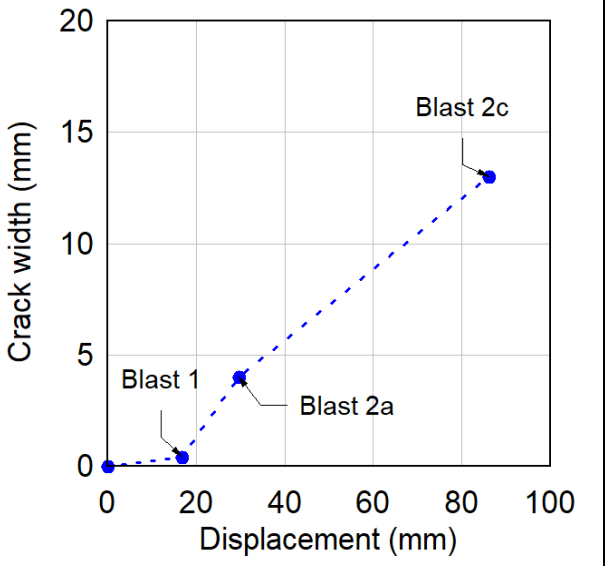

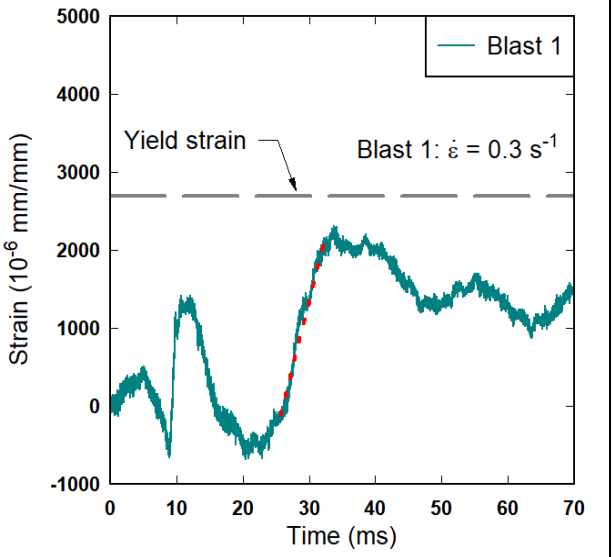

e) Maximum crack width (flexure)

f) Tensile strain in rebar

Figure 5-6 Experimental results for Beam HSC-0.75%S1-15M-S

a) Blast 1

b) Blast 2a

c) Blast 2c

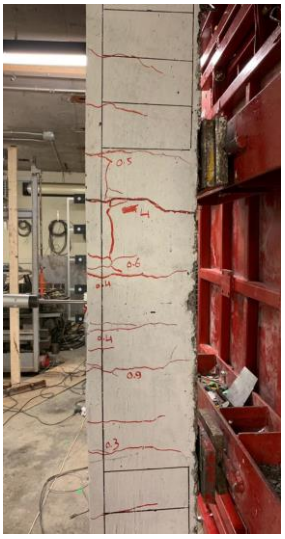

d) Mid-span cracking (Blast 2a)

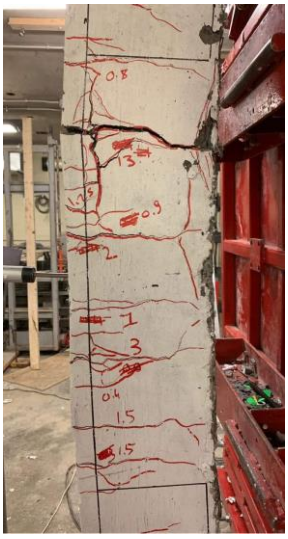

e) Mid-span concrete crushing (Blast 2c)

f) Mid-span fiber pullout (Blast 2c)

Figure 5-7 HSC-0.75%S1-15M-S; photographs at the end of Blast 1-2c

5.3 Description of Experimental Results – Series 20M

5.3.1 Specimen HSC-0.75%S1-20M-0

This beam was constructed with high-strength concrete and reinforced with 20M bars, without transverse reinforcement. Synthetic fibers were incorporated at a volumetric ratio of 0.75%. Results for this beam are provided in **Table 5-5**. **Figure 5-8** shows reflected pressure, impulse, and displacement time histories along with dynamic resistance curves, crack width and tensile strain in longitudinal reinforcement. Photographs of major events after each blast are illustrated in **Figure 5-9**. Blast 1 (30 psi) resulted in the appearance of hairline cracks over the span of the beam. The low residual displacement recorded after Blast 1 indicates that the rebar did not reach yielding. Existing cracks further propagated after Blast 2a (50 psi), with the development of diagonal shear cracks at both the top and bottom shear spans of the beam. The maximum shear crack width recorded was 1.5 mm. Unfortunately, the strain gauge reading was considered unreliable after Blast 1. Blast 2b (60 psi) caused a flexural-shear failure of the beam between the bottom support and lower point load location, with complete fiber pullout at the shear crack as shown in **Figure 5-9f**. The beam suffered a maximum and residual mid-span displacement of 84.1 mm and 60.6 mm respectively.

Table 5-5 Summary of results for Beam HSC-0.75%S1-20M-0

Blast #	Shockwave Properties			Displacement		θ_{max} (°)	P_{max} (kN)	Observed Damage	CSA S850 Response Limits and Component Damage[1]	
	P_r (kPa)	I_r (kPa-ms)	t_d (ms)	Δ_{max} (mm)	Δ_{res} (mm)				Response Limit	Expected Damage Level
1	44.6	378.7	20.6	12.50	1.54	0.64	102.3	Hairline F Cracks	<B1	Superficial
2a	61.0	521.0	20.6	18.49	3.18	0.95	161.7	Shear Cracks & Further Crack Opening	<B1	Superficial
2b	71.0	653.0	21.4	84.08	60.59	4.31	181.8	Shear Failure	B3-B2	Heavy

[1]: Blowout: $\theta \geq 10°$, Hazardous: $5° \leq \theta < 10°$; Heavy: $2° \leq \theta < 5°$; Moderate: $1° \leq \theta < 2°$; Superficial: $\theta < 1°$

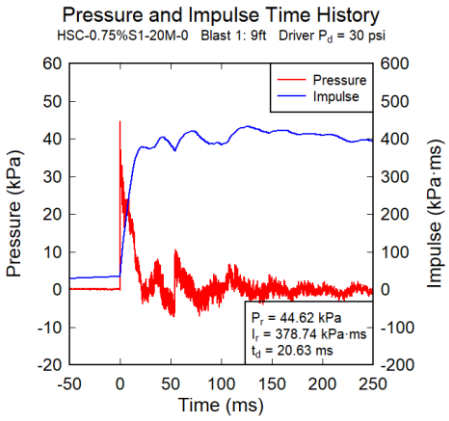

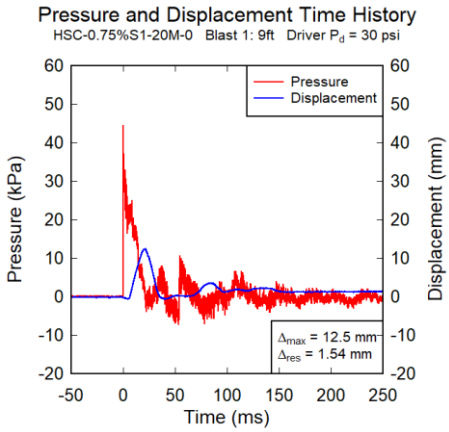

a) Blast 1: Reflected pressure, impulse, and displacement time histories.

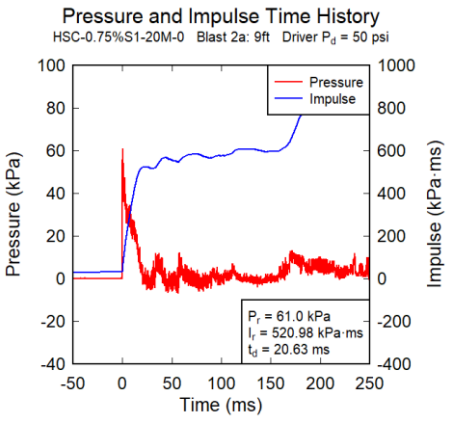

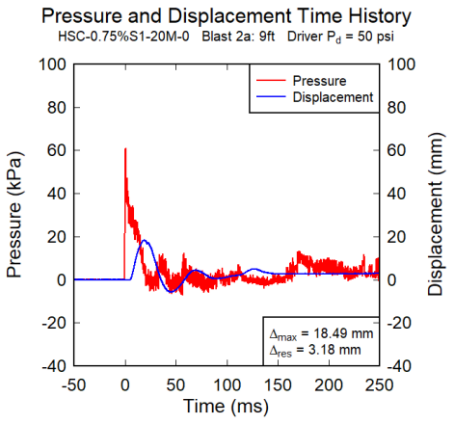

b) Blast 2a: Reflected pressure, impulse, and displacement time histories.

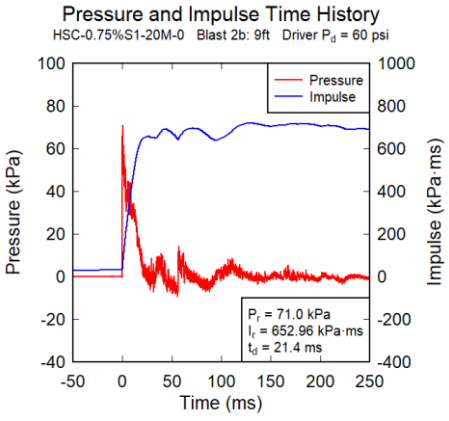

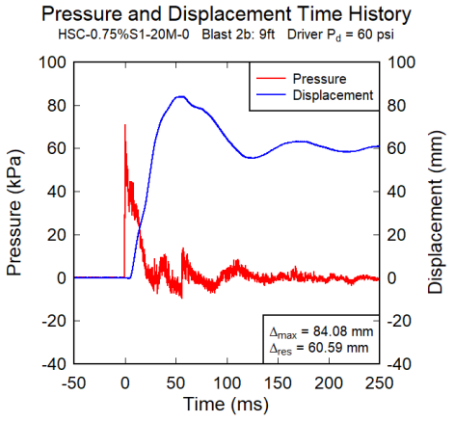

c) Blast 2b: Reflected pressure, impulse, and displacement time histories.

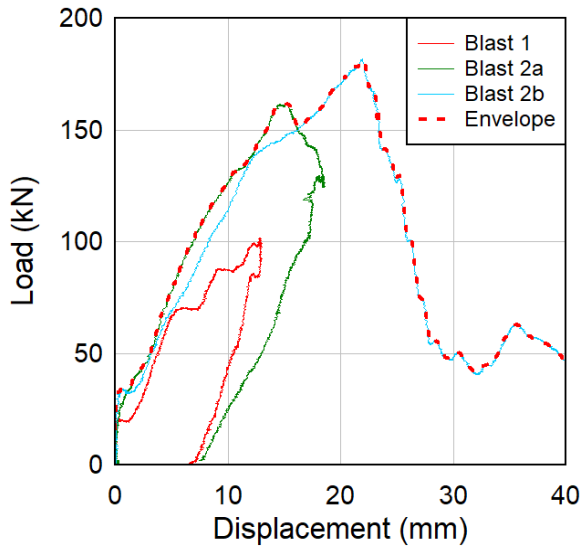

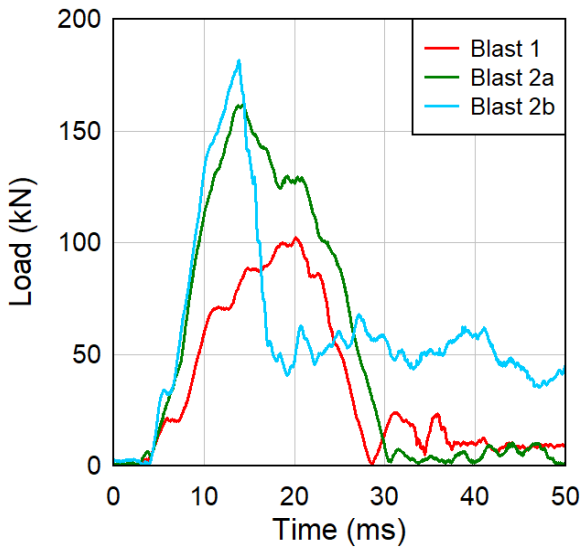

d) Dynamic resistance curves at varying blast intensities

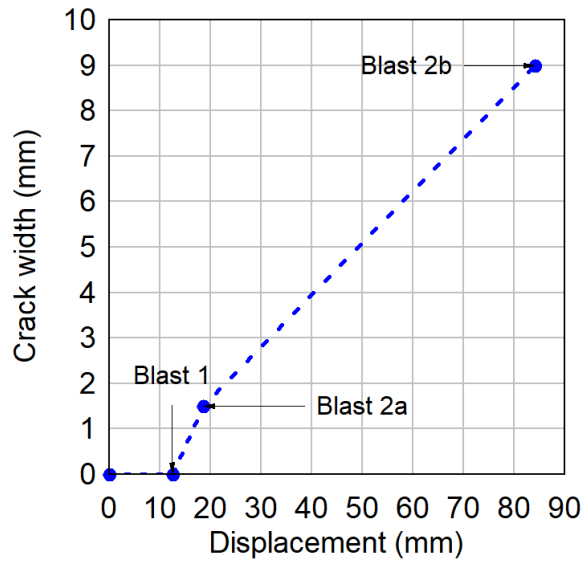

e) Maximum crack width (shear) [not considering shear failure]

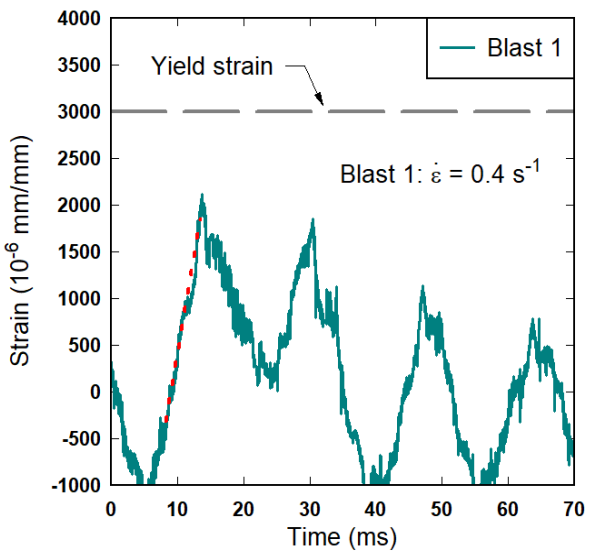

f) Tensile strain in rebar

Figure 5-8 Experimental results for Beam HSC-0.75%S1-20M-0

a) Blast 1

b) Blast 2a

c) Blast 2b

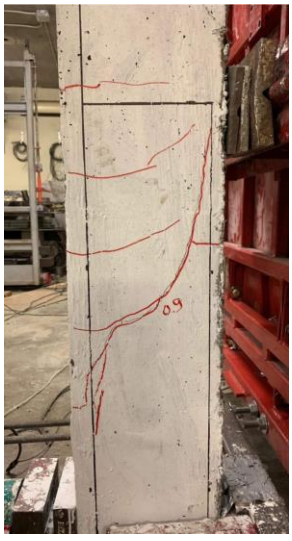

d) Shear crack (Blast 2a)

e) Shear failure (Blast 2b)

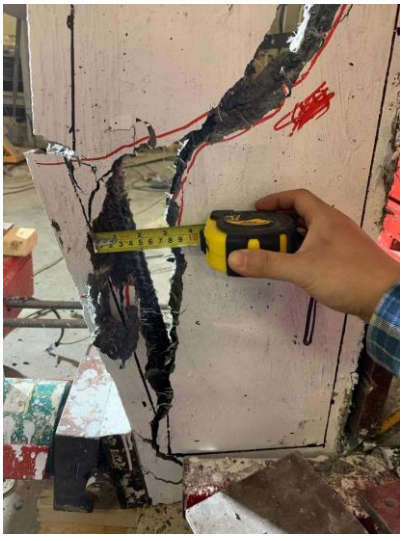

f) Principal shear crack (Blast 2b)

Figure 5-9 HSC-0.75%S1-20M-0; photographs at the end of Blast 1-2b

5.3.2 Specimen HSC-0.75%S1-20M-S

This specimen had the same components as the previous specimen, except for the addition of stirrups spaced at 100 mm in the shear spans. Results for this beam are summarized in **Table 5-6**. **Figure 5-10** shows reflected pressure, impulse, and displacement time histories along with dynamic resistance curves, crack width and strain in longitudinal rebar. Photographs of major events after each blast are shown in **Figure 5-11**. Blast 1 (30 psi) resulted in the formation of around 12 minor hairline cracks in the mid-span region. Blast 2a (50 psi) brought the beam to yielding and led to further hairline cracks over the span of the beam with the development of a major crack, having a width of 0.8 mm, at mid-span region of the beam. Blast 2c (70 psi) was sufficient to initiate concrete crushing and fiber pullout at the location of the major crack which increased in width to 4 mm as illustrated in **Figure 5-11c** and **Figure 5-11f**. Further propagation of existing cracks can also be observed. As demonstrated in **Figure 5-11d** and **Figure 5-11g**, Blast 3a (80 psi) resulted in the failure of the specimen due to concrete crushing and fiber pullout where a large block of concrete at mid-span compression zone is broken off. The maximum and residual mid-span displacements recorded for this blast were 186.6 mm and 143 mm respectively.

Table 5-6 Summary of results for Beam HSC-0.75%S1-20M-S

Blast #	Shockwave Properties			Displacement		θ_{max} (°)	P_{max} (kN)	Observed Damage	CSA S850 Response Limits and Component Damage[1]	
	P_r (kPa)	I_r (kPa-ms)	t_d (ms)	Δ_{max} (mm)	Δ_{res} (mm)				Response Limit	Expected Damage Level
1	44.0	334.5	18.9	12.17	1.06	0.62	70.4	Minor Hairline F Cracks	<B1	Superficial
2a	55.9	523.4	21.3	23.21	4.00	1.19	168.0	Further Crack Opening	B2-B1	Moderate
2c	83.9	723.8	21.9	44.70	19.89	2.29	210.2	Onset of Crushing & Fiber Pullout	B3-B2	Heavy
3a	90.9	832.0	23.8	186.57	143.00	9.49	170.1	Concrete Crushing & Fiber Pullout	B4-B3	Hazardous

[1]: Blowout: $\theta \geq 10°$, Hazardous: $5° \leq \theta < 10°$; Heavy: $2° \leq \theta < 5°$; Moderate: $1° \leq \theta < 2°$; Superficial: $\theta < 1°$

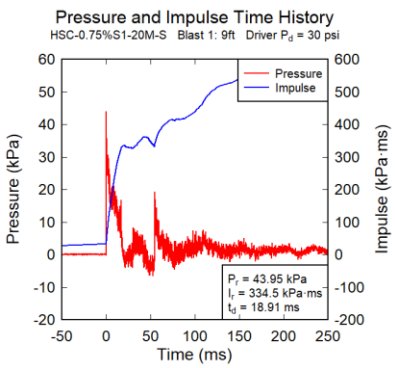

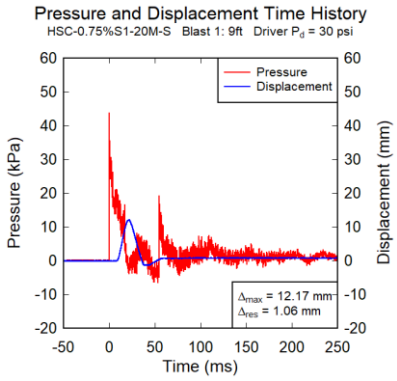

a) Blast 1: Reflected pressure, impulse, and displacement time histories.

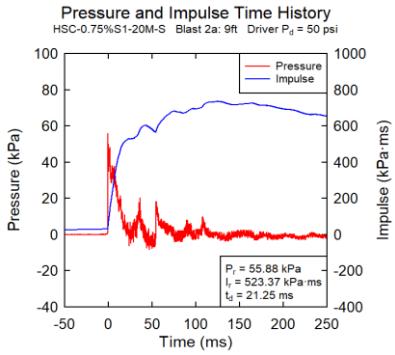

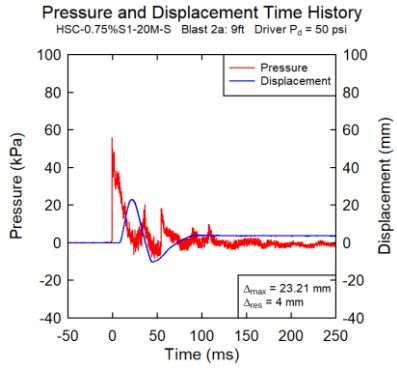

b) Blast 2a: Reflected pressure, impulse, and displacement time histories.

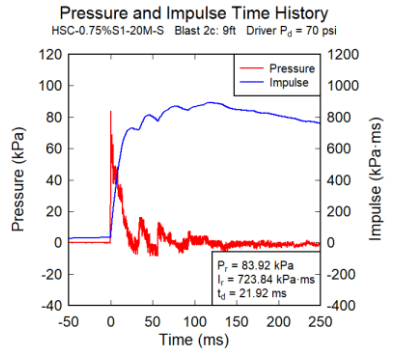

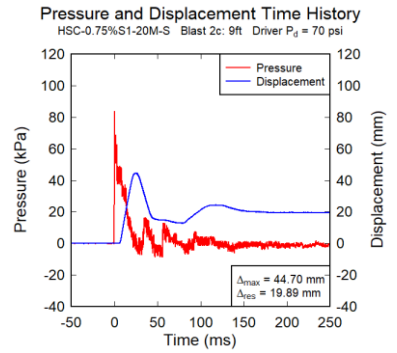

c) Blast 2c: Reflected pressure, impulse, and displacement time histories.

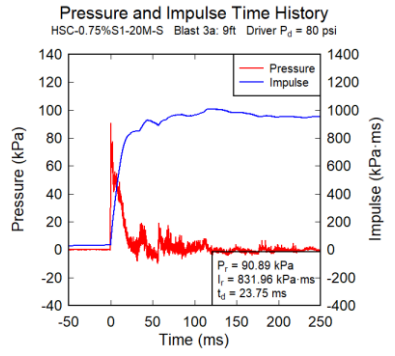

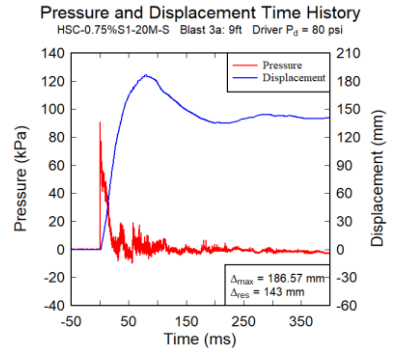

d) Blast 3a: Reflected pressure, impulse, and displacement time histories.

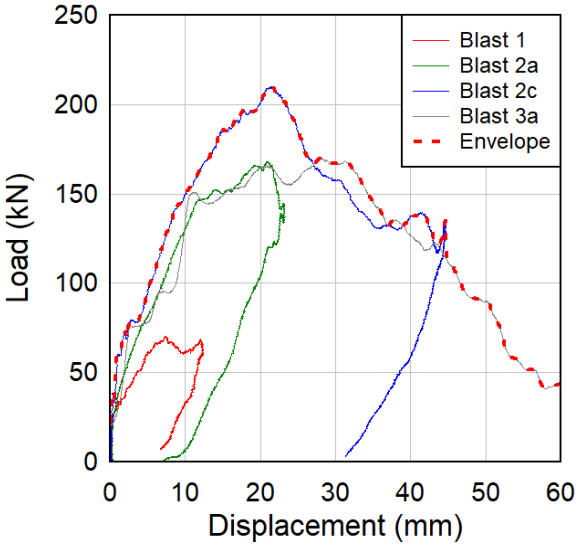

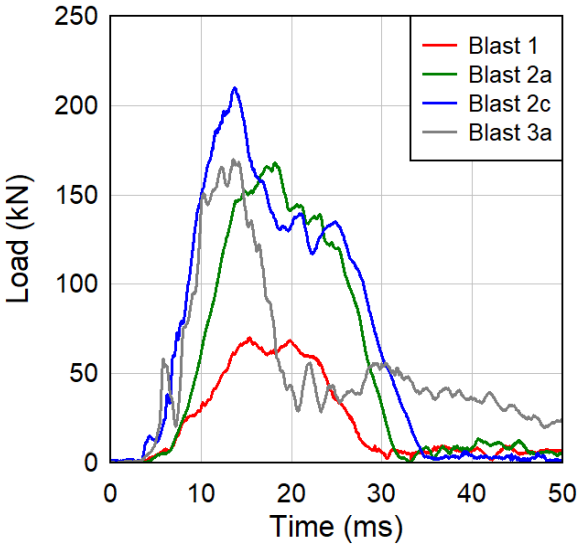

e) Dynamic resistance curves at varying blast intensities

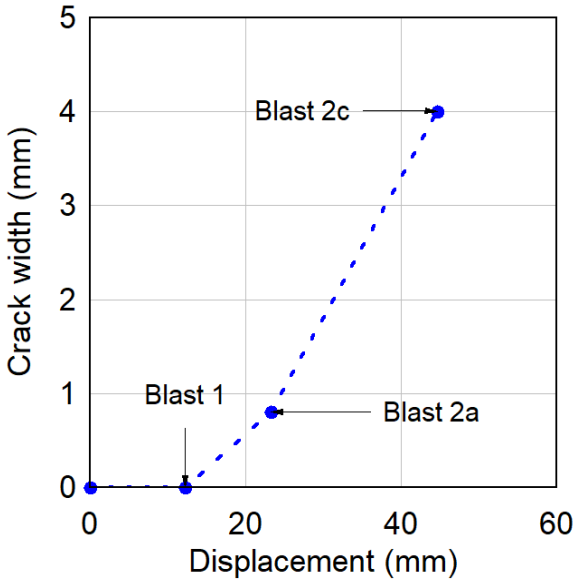

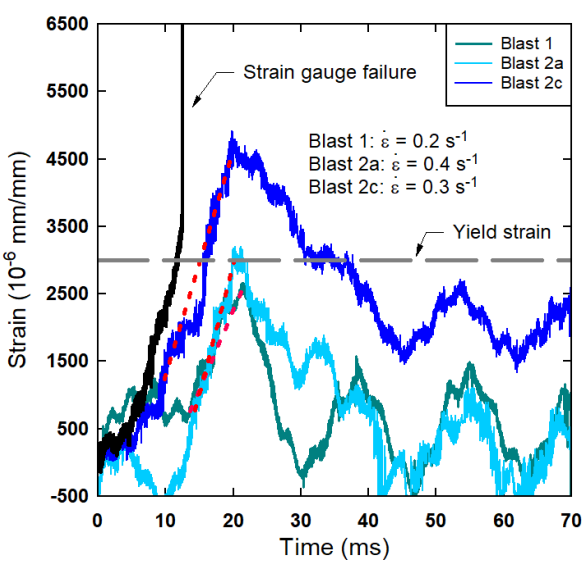

f) Maximum crack width (flexure)

g) Tensile strain in rebar

Figure 5-10 Experimental results for Beam HSC-0.75%S1-20M-S

a) Blast 1

b) Blast 2a

c) Blast 2c

d) Blast 3a

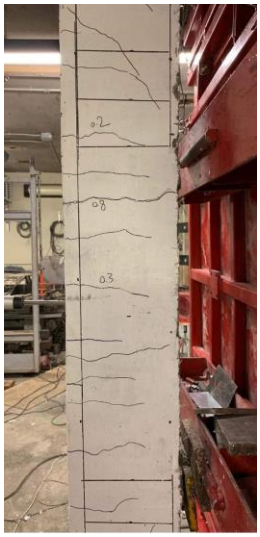

e) Mid-span cracking (Blast 2a)

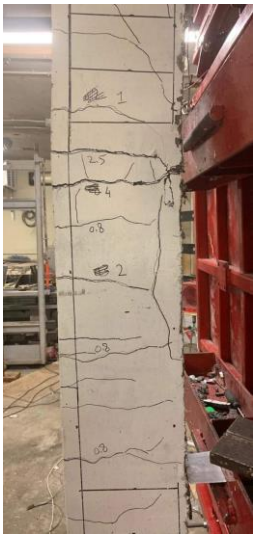

f) Concrete crushing at mid-span (Blast 2c)

g) Concrete crushing & fiber pullout (Blast 3a)

Figure 5-11 HSC-0.75%S1-20M-S; photographs at the end of Blast 1-3a

5.3.3 Specimen HSC-HYB-20M-0

The HSC-HYB-20M-0 beam had the same material composition as HSC-0.75%S1-20M-0, except for the addition of smooth straight steel fibers at a volumetric ratio of 0.25%. This allowed to investigate the effects of using hybrid fibers. Results for this beam are summarized in **Table 5-7**. **Figure 5-12** shows reflected pressure, impulse, and displacement time histories along with dynamic resistance curves, crack width and tensile strain in longitudinal rebar. Photographs of major events after each blast are provided in **Figure 5-13**. Unfortunately, the strain gauge did not show any reading when examined before starting the test. Blast 1 (30 psi) resulted in the development of hairline flexural cracks with a 0.3 mm major crack near mid-span region. Blast 2a (50 psi) resulted in further hairline cracks with the development of shear cracks in the shear spans. The width of the major crack increased to 2 mm. Blast 2c (70 psi) caused the existing cracks to further propagate deep into the section with the major crack reaching a width of 4 mm as shown in **Figure 5-13c** and **Figure 5-13f**. Blast 3a (80 psi) imposed the failure of the beam due to fiber pullout around mid-span region of the beam, where the major crack is located, resulting in a crack opening of 9 mm. As can be seen in **Figure 5-13d** and **Figure 5-13g**, fibers were able to hold the concrete together controlling concrete crushing and limiting the generation of any debris at failure. Unlike the companion beam with synthetic fibers only, shear failure was also prevented. The maximum and residual mid-span displacements for this blast were 60 mm and 25.2 mm respectively. Due to the use of hybrid fibers, the damage is less critical than what is predicted by the standard.

Table 5-7 Summary of results for Beam HSC-HYB-20M-0

Blast #	Shockwave Properties			Displacement		θ_{max} (°)	P_{max} (kN)	Observed Damage	CSA S850 Response Limits and Component Damage[1]	
	P_r (kPa)	I_r (kPa-ms)	t_d (ms)	Δ_{max} (mm)	Δ_{res} (mm)				Response Limit	Expected Damage Level
1	41.3	377.0	20.6	16.39	1.63	0.84	119.2	Hairline F Cracks	<B1	Superficial
2a	66.9	586.5	20.6	22.90	5.40	1.18	189.0	Shear Cracks & Further Crack Opening	B2-B1	Moderate
2c	76.7	961.8	26.3	41.14	15.43	2.11	209.1	Further Crack Opening	B3-B2	Heavy
3a	82.8	853.2	25.7	60.01	25.20	3.08	225.7	Fiber Pullout	B3-B2	Heavy

[1]: Blowout: $\theta \geq 10°$, Hazardous: $5° \leq \theta < 10°$; Heavy: $2° \leq \theta < 5°$; Moderate: $1° \leq \theta < 2°$; Superficial: $\theta < 1°$

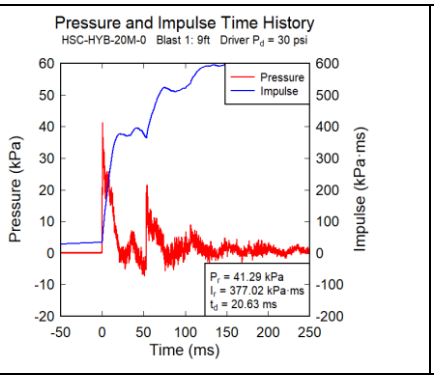

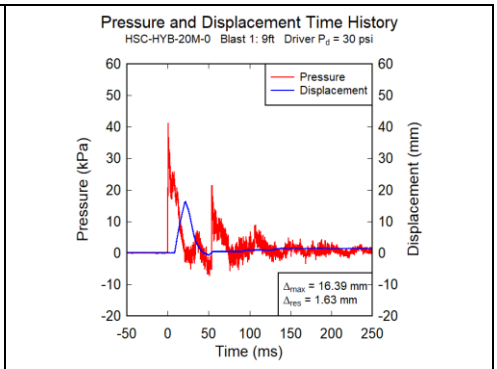

a) Blast 1: Reflected pressure, impulse, and displacement time histories.

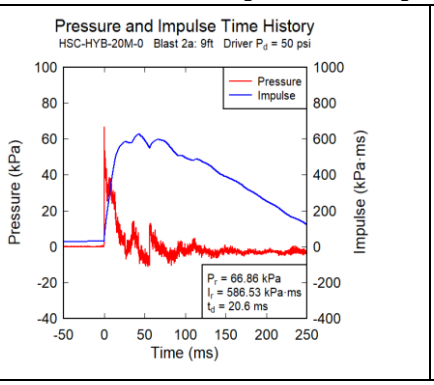

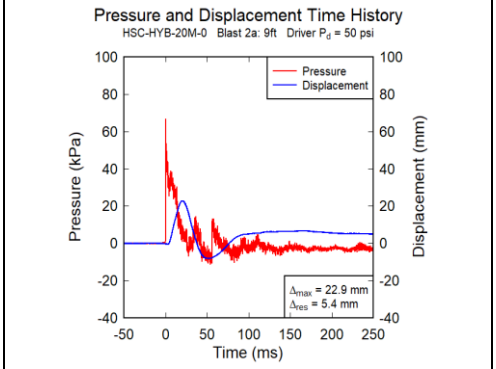

b) Blast 2a: Reflected pressure, impulse, and displacement time histories.

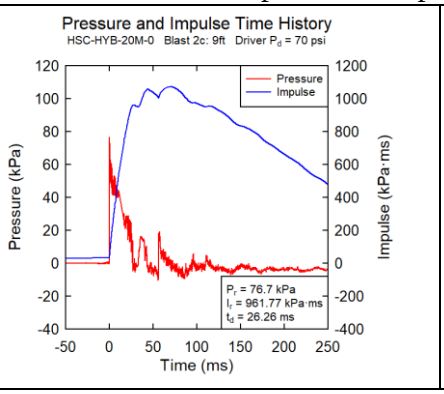

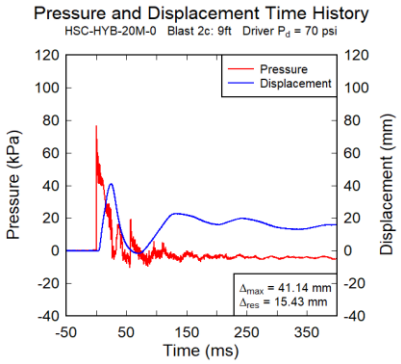

c) Blast 2c: Reflected pressure, impulse, and displacement time histories.

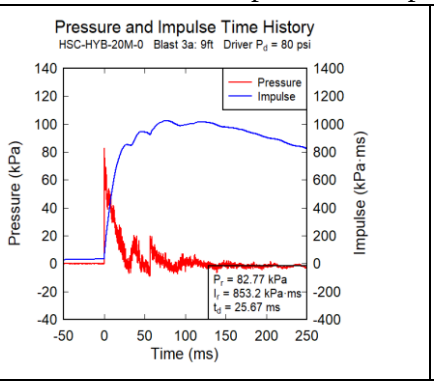

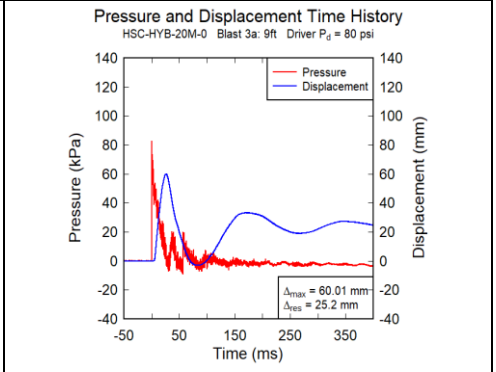

d) Blast 3a: Reflected pressure, impulse, and displacement time histories.

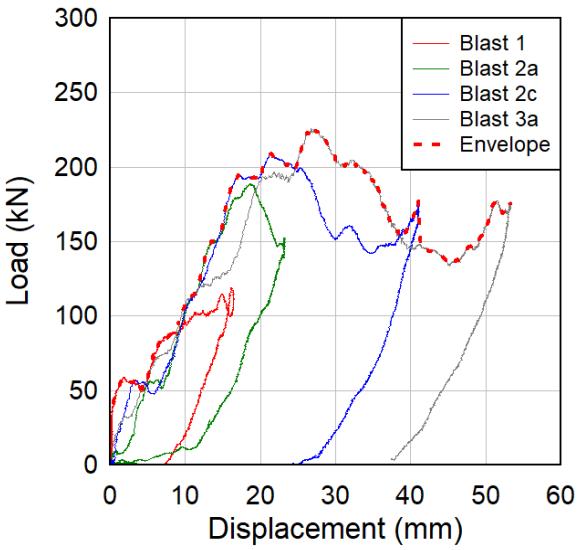

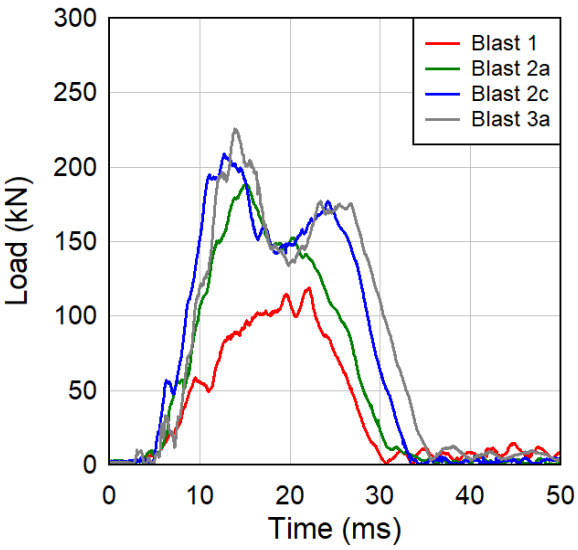

e) Dynamic resistance curves at varying blast intensities

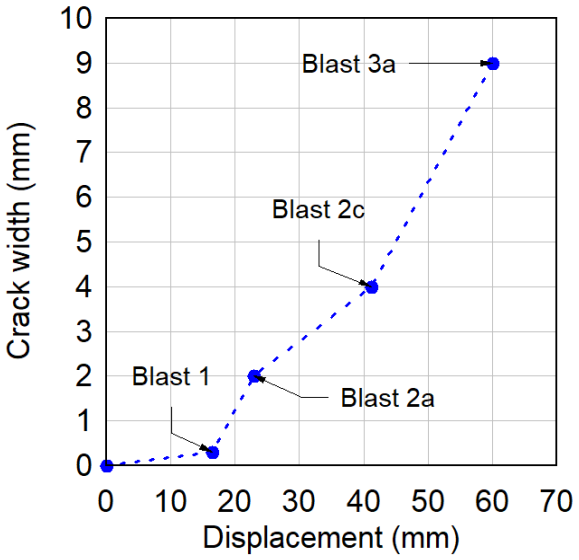

f) Maximum crack width (flexure)

N/A

g) Tensile strain in rebar

Figure 5-12 Experimental results for Beam HSC-HYB-20M-0

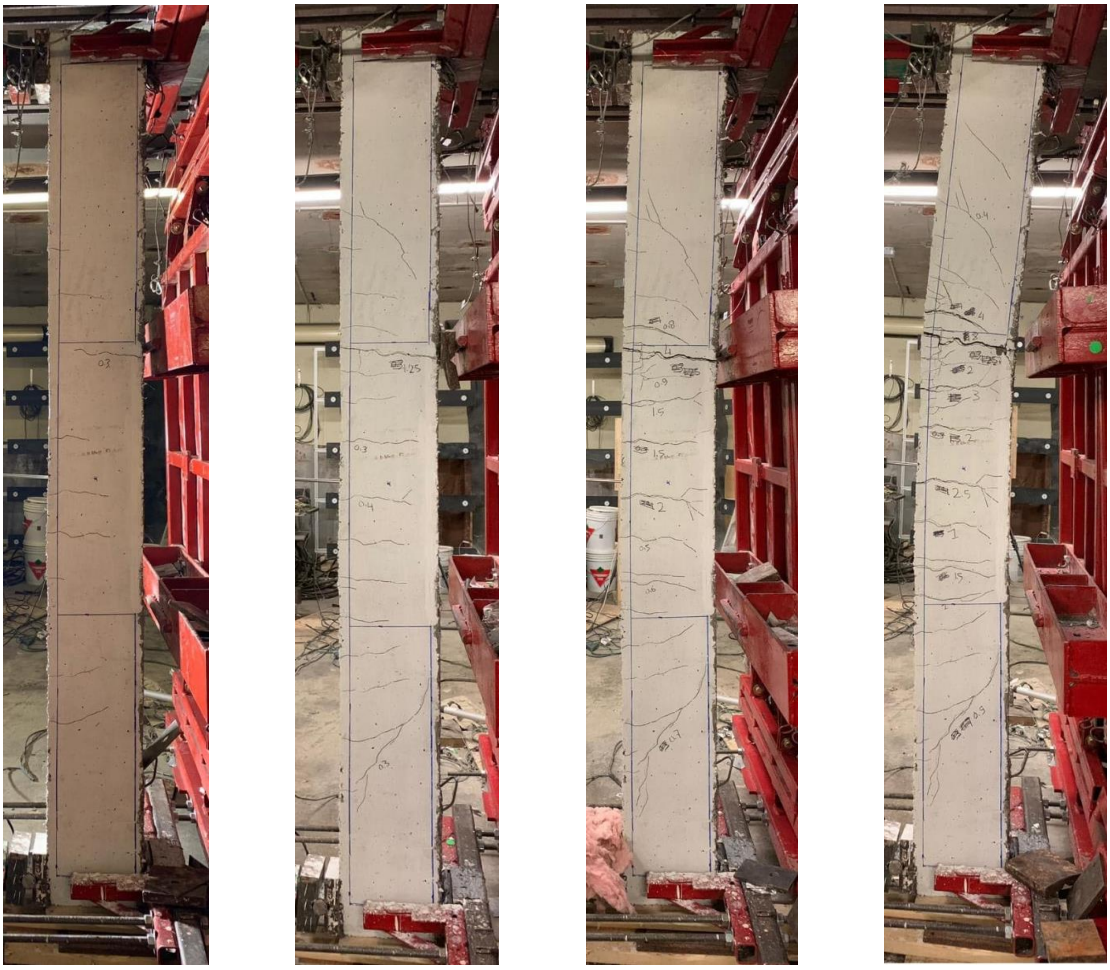

a) Blast 1 b) Blast 2a c) Blast 2c d) Blast 3a

e) Mid-span cracking (Blast 2a) f) Crack propagation (Blast 2c) g) Mid-span fiber pullout (Blast 3a)

Figure 5-13 HSC-HYB-20M-0; photographs at the end of Blast 1-3a

5.3.4 Specimen HSC-0.75%S1-20M-10M-d/2

The HSC-0.75%S1-20M-10M-d/2 beam had the same components as the HSC-0.75%S1-20M-S specimen, except for the addition of 10M bars at the top of the beam section and the use of closed hoops spaced at 100 mm all the way. Results for this beam are summarized in **Table 5-8**. **Figure 5-14** shows reflected pressure, impulse, and displacement time histories along with dynamic resistance curves, crack width and strain in compression rebar. Photographs of major events after each blast are provided in **Figure 5-15**. Unfortunately, the tensile strain gauge did not show any reading when examined before starting the test. Blast 1 (30 psi) resulted in the appearance of several flexural hairline cracks. Blast 2c (70 psi) resulted in a 3 mm wide major crack at the beam mid-span, with the formation of further cracks in the flexural and shear regions as illustrated in **Figure 5-15b** and **Figure 5-15d**. Blast 3b (90 psi) brought the compression rebar to yielding and led to the failure of the beam due to concrete crushing and fiber pullout near the upper point load location. As can be seen in **Figure 5-15e** and **Figure 5-15f**, the principal crack generated from Blast 2c (70 psi) expanded to a width of 10 mm with fibers pulling-out at this location. The maximum and residual mid-span displacements for this blast were recorded at 64.7 mm and 4.4 mm respectively. Compared to CSA response limit, the damage is less prominent due to the improved detailing and provision of synthetic fibers.

Table 5-8 Summary of results for Beam HSC-0.75%S1-20M-10M-d/2

Blast #	Shockwave Properties			Displacement		θ_{max} (°)	P_{max} (kN)	Observed Damage	CSA S850 Response Limits and Component Damage[1]	
	P_r (kPa)	I_r (kPa-ms)	t_d (ms)	Δ_{max} (mm)	Δ_{res} (mm)				Response Limit	Expected Damage Level
1	45.1	405.6	20.6	10.80	0.33	0.55	133.6	Hairline F Cracks	<B1	Superficial
2c	79.8	723.6	20.7	44.16	21.06	2.27	244.9	Shear Cracks & Further Crack Opening	B2-B1	Moderate
3b	90.1	979.8	26.3	86.23	64.65	4.42	221.7	Concrete Crushing & Fiber Pullout	B3-B2	Heavy

[1]: Blowout: $\theta \geq 10°$, Hazardous: $6° \leq \theta < 10°$; Heavy: $4° \leq \theta < 6°$; Moderate: $1° \leq \theta < 4°$; Superficial: $\theta < 1°$

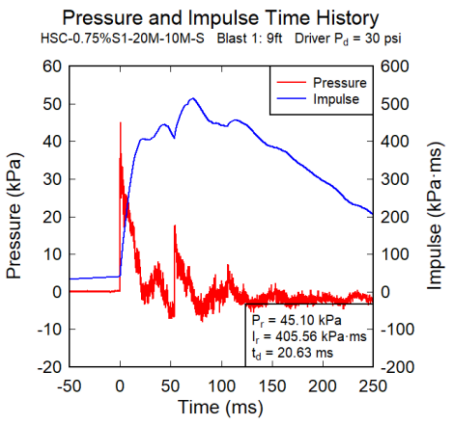

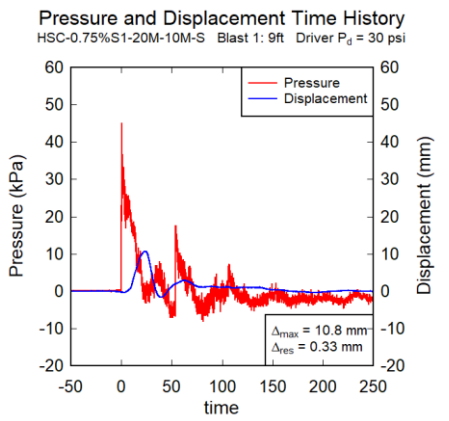

a) Blast 1: Reflected pressure, impulse, and displacement time histories.

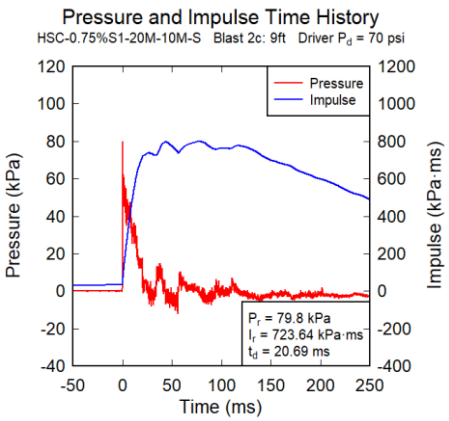

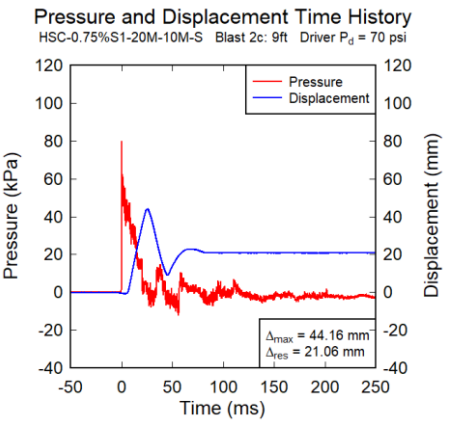

b) Blast 2c: Reflected pressure, impulse, and displacement time histories.

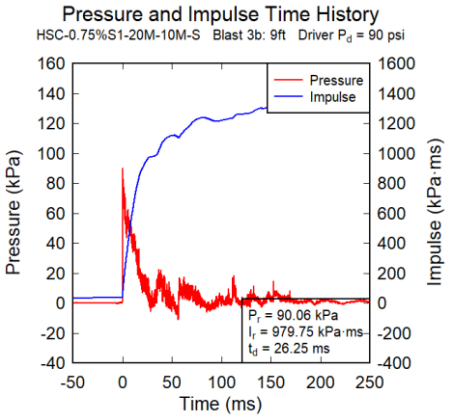

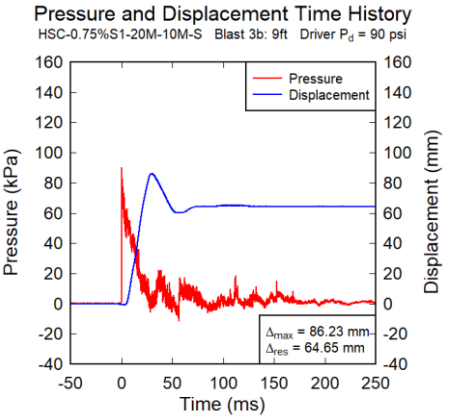

c) Blast 3b: Reflected pressure, impulse, and displacement time histories.

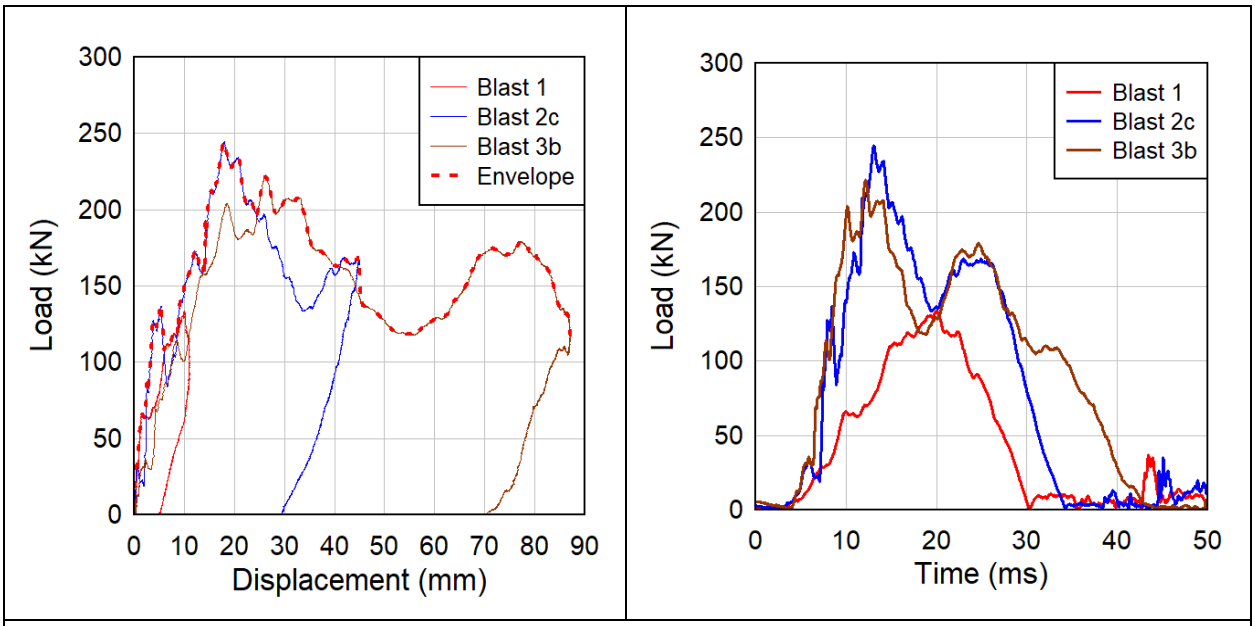

d) Dynamic resistance curves at varying blast intensities

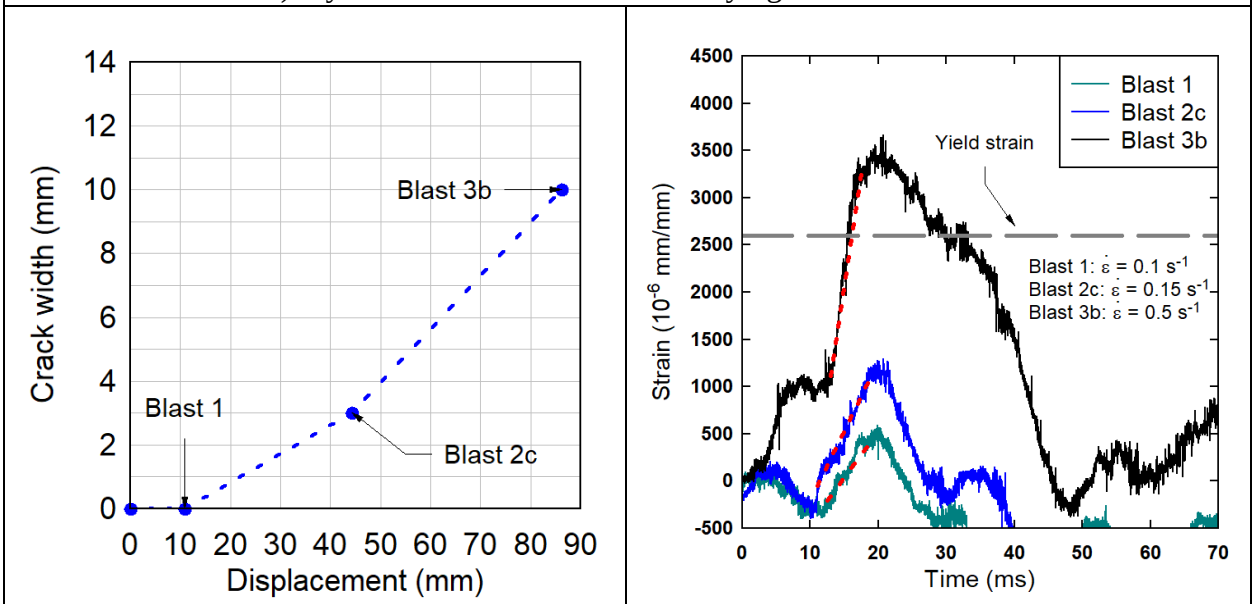

e) Maximum crack width (flexure)

f) Compressive strain in rebar

Figure 5-14 Experimental results for Beam HSC-0.75%S1-20M-10M-d/2

a) Blast 1

b) Blast 2c

c) Blast 3b

d) Mid-span cracking (Blast 2c)

e) Concrete crushing (Blast 3b)

f) Fiber pullout (Blast 3b)

Figure 5-15 HSC-0.75%S1-20M-10M-d/2; photographs at the end of Blast 1-3b

5.4 Description of Experimental Results – Series No.5

5.4.1 Specimen HSC-0.75%S1-No.5(HS)-S

The HSC-0.75%S1-No.5(HS)-S beam was constructed with high-strength concrete and reinforced with No.5 high-strength (Grade 690 MPa) bars and transverse reinforcement. Synthetic fibers were incorporated at a volumetric ratio of 0.75%. Results for this beam are summarized in **Table 5-9**. **Figure 5-16** shows reflected pressure, impulse, and displacement time histories along with dynamic resistance curves, crack width and strain in longitudinal rebar. Photographs of major events after each blast are presented in **Figure 5-17**. Blast 1 (30 psi) tested the beam within the elastic range and caused the formation of hairline flexural cracks. Blast 2a (50 psi) led to further cracks with the formation of a 0.5 mm major flexural crack just below the upper loading point. Several cracks were also observed in the shear spans. The strain gauge recorded a maximum of 0.005 mm/mm indicating that the high-strength steel bars were still in the pre-yield range (ε_y = 0.0065 mm/mm). As shown in **Figure 5-17c** and **Figure 5-17f**, crack widening was prominent after Blast 2c (70 psi), which tested the beam in the post-yield range, with the major crack expanding to a width of 1.25 mm. Blast 3b (90 psi) can be considered as the last blast since the beam experienced severe concrete crushing where large chunks of concrete were disintegrated and broken off at mid-span. The beam suffered maximum and residual mid-span displacements of 174 mm and 109 mm respectively.

Table 5-9 Summary of results for Beam HSC-0.75%S1-No.5(HS)-S

Blast #	Shockwave Properties			Displacement		θ_{max} (°)	P_{max} (kN)	Observed Damage	CSA S850 Response Limits and Component Damage[1]	
	P_r (kPa)	I_r (kPa-ms)	t_d (ms)	Δ_{max} (mm)	Δ_{res} (mm)				Response Limit	Expected Damage Level
1	45.4	395.4	21.3	16.53	4.03	0.85	101.9	Hairline F Cracks	<B1	Superficial
2a	61.8	520.4	20.6	22.25	1.32	1.14	161.2	Shear Cracks & Further Crack Opening	B2-B1	Moderate
2c	76.3	911.3	28.8	37.84	8.99	1.94	212.6	Further Crack Opening	B2-B1	Moderate
3b	92.5	876.1	21.4	173.96	109.06	8.86	254.1	Severe Concrete Crushing	B4-B3	Hazardous

[1]: Blowout: $\theta \geq 10°$, Hazardous: $5° \leq \theta < 10°$; Heavy: $2° \leq \theta < 5°$; Moderate: $1° \leq \theta < 2°$; Superficial: $\theta < 1°$

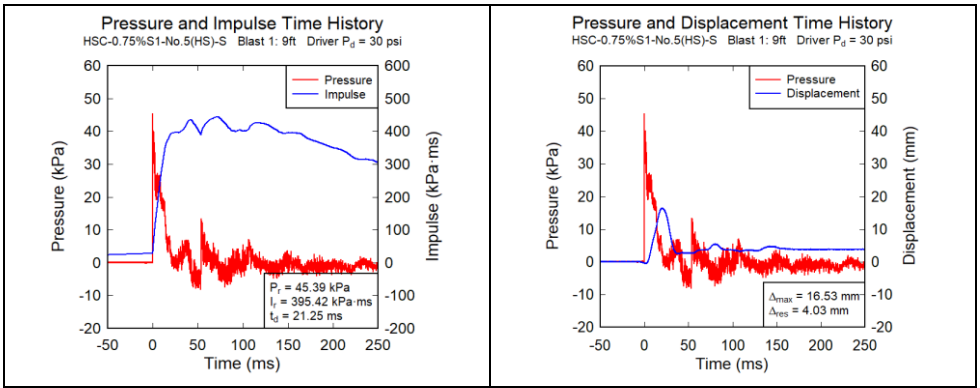

a) Blast 1: Reflected pressure, impulse, and displacement time histories.

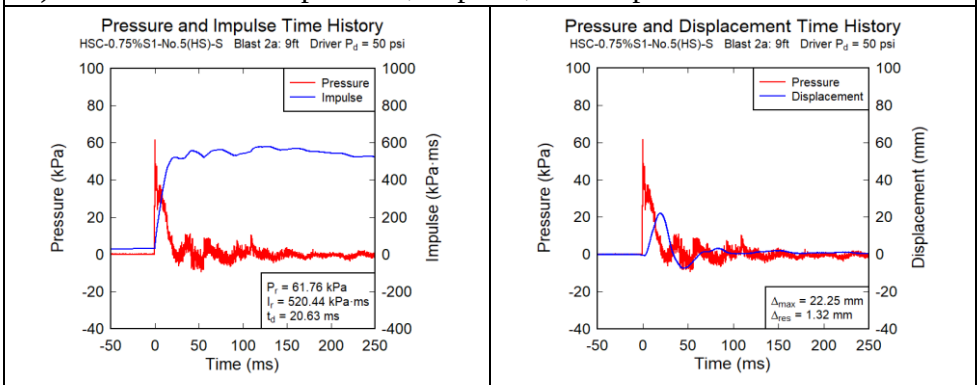

b) Blast 2a: Reflected pressure, impulse, and displacement time histories.

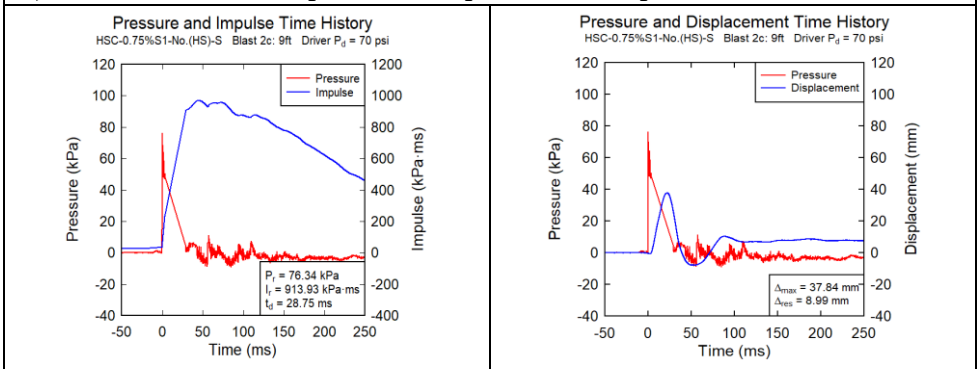

c) Blast 2c: Reflected pressure, impulse, and displacement time histories.

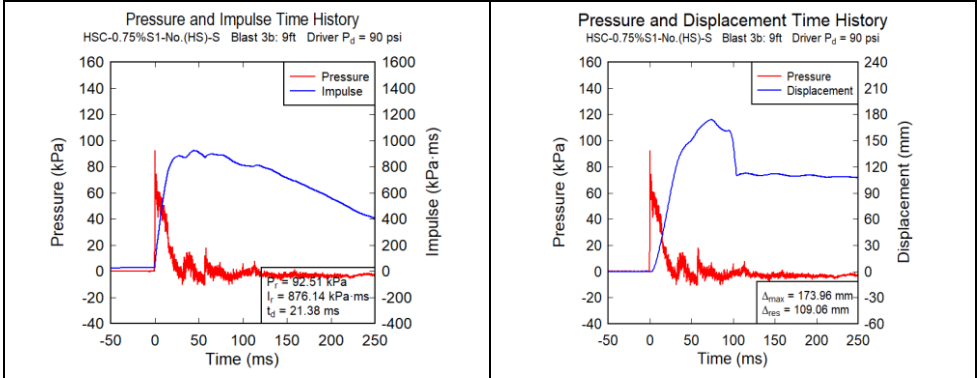

d) Blast 3b: Reflected pressure, impulse, and displacement time histories.

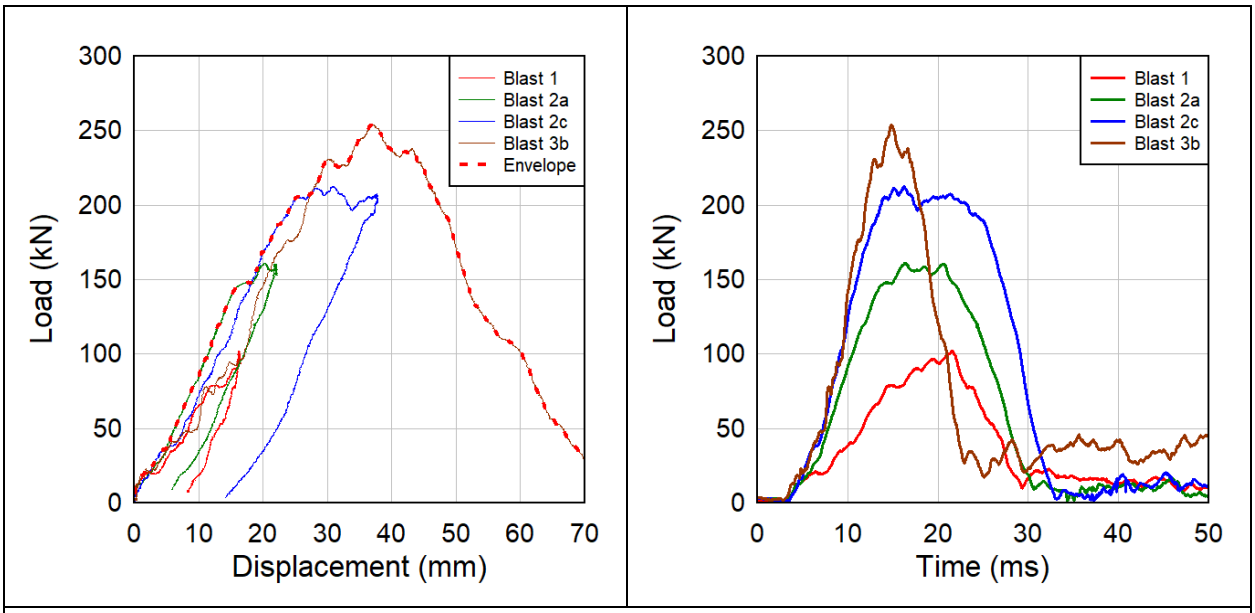

e) Dynamic resistance curves at varying blast intensities

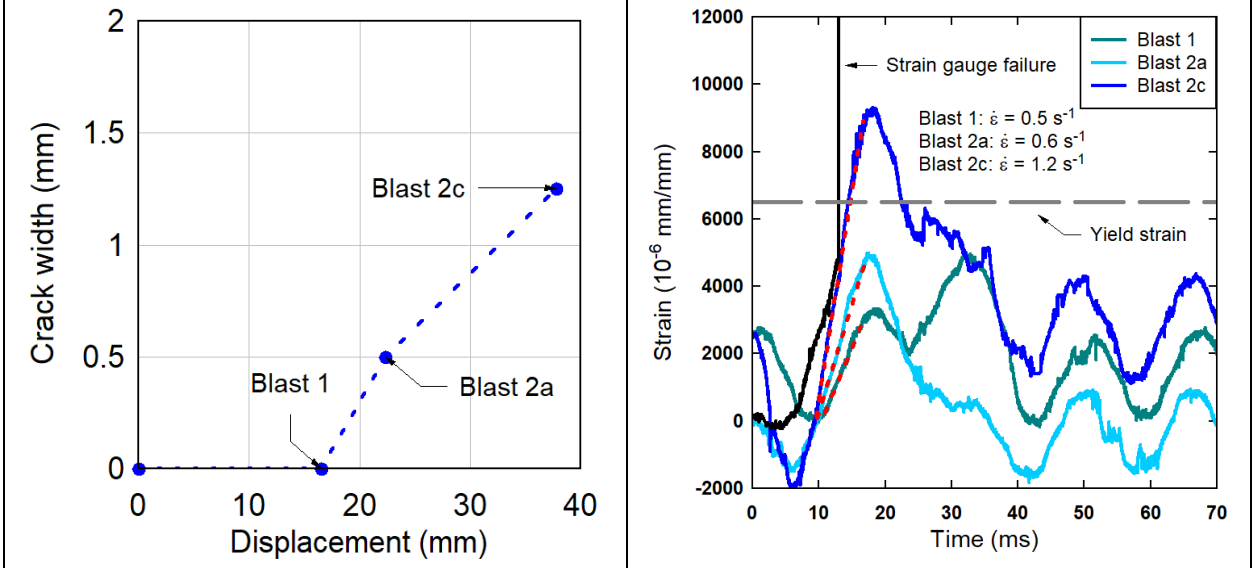

f) Maximum crack width (flexure)

g) Tensile strain in rebar

Figure 5-16 Experimental results for Beam HSC-0.75%S1-No.5(HS)-S

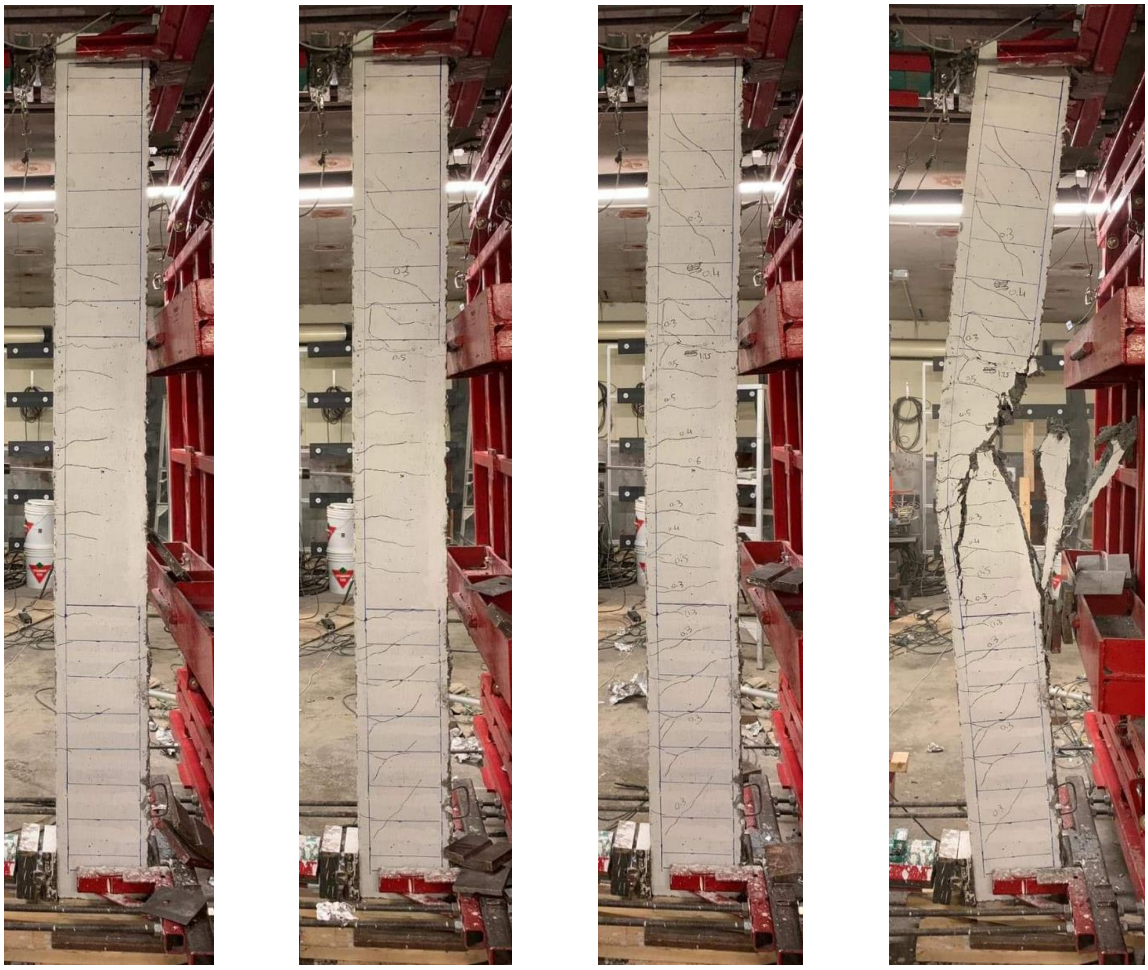

a) Blast 1 b) Blast 2a c) Blast 2c d) Blast 3b

e) Mid-span cracking (Blast 2a) f) Crack widening (Blast 2c) g) Mid-span concrete crushing (Blast 3b)

Figure 5-17 HSC-0.75%S1-No.5(HS)-S; photographs at the end of Blast 1-3b

Chapter 6: Discussion of Static Experimental Results

6.1 Chapter Overview

This chapter discusses the effects of test parameters on the quasi-static response of the fiber-reinforced concrete beams tested in this study. The effects of the variables are examined by comparing the maximum load-carrying capacity, maximum displacement, beam stiffness, ductility, toughness, and failure mode of the specimens.

The following aspects are discussed in the sections that follow:

The effects of synthetic fibers in SCC beams:

- In shear: SCC-0%-15M-0* vs. SCC-0.75%S1-15M-0
- In flexure: SCC-0%-15M-S* vs. SCC-0.75%S1-15M-S

The effects of synthetic fibers in HSC beams:

- In shear:
  - HSC-0%-15M-0 vs. HSC-0.75%S1-15M-0
  - HSC-0%-20M-0† vs. HSC-0.75%S1-20M-0
- In flexure:
  - HSC-0%-15M-S† vs. HSC-0.75%S1-15M-0 & HSC-0.75%S1-15M-S
  - HSC-0%-20M-S† vs. HSC-0.75%S1-20M-0 & HSC-0.75%S1-20M-S

The effects of hybrid fibers:

- HSC-HYB-20M-0 vs. HSC-0.75%S1-20M-0 & HSC-0.75%S1-20M-S

The effects of synthetic fibers in HSC beams with high-strength (690 MPa) bars:

- HSC-0%-No.5(HS)-S‡ vs. HSC-0.75%S1-No.5(HS)-S

The effects of steel reinforcement type in HSFRC beams:

- HSC-0.75%S1-15M-S vs. HSC-0.75%S1-No.5(HS)-S

Table 6-1 and **Table 6-2** summarize the results for the nine beams included in this study in terms of maximum load, maximum displacement, stiffness, ductility, toughness and failure mode (refer to **Chapter 4** for the definition of the parameters).

To allow for better comparison of the results, a set of other beams tested by other researchers are also discussed. These beams are marked with *, † and ‡ in **Table 6-2**:

- Beams SCC-0%-15M-0* and SCC-0%-15M-S* were tested by Castonguay (2017) and were built with plain SCC, 15M bars, without and with stirrups respectively.

- Beams HSC-0%-15M-S†, HSC-0%-20M-0† and HSC-0%-20M-S† were built with plain HSC and were tested by Algassem (2016), and were designed with 15M bars and stirrups, and 20M bars without and with stirrups, respectively.
- Finally, beam HSC-0%-No.5(HS)-S‡ was tested by Li (2016) and was built with plain HSC and Grade 690 MPa No.5 high-strength bars.

Table 6-1 Summary of test results from current study

Beam ID	Load (kN)		Displacement (mm)			Stiffness K (N/mm)	Ductility		Toughness (kN·mm)		Failure Mechanism
	P_y	P_{max}	Δ_y	Δ_{85}	Δ_{max}		Δ_{85}/Δ_y	Δ_{max}/Δ_y	Au_{85}	Au_{max}	
SCC-0.75%S1-15M-0	-	85.7	-	18.1	36.4	6047	-	-	951	1529	Shear Failure
SCC-0.75%S1-15M-S	80.0	99.0	10.6	44.4	70.0	7423	4.19	6.60	3624	5683	Concrete Crushing
HSC-0%-15M-0	-	90.0	-	-	15.3	5882	-	-	-	922	Shear Failure
HSC-0.75%S1-15M-0	99.0	112.2	13.4	-	67.3	7388	-	5.02	-	6574	Shear Failure
HSC-0.75%S1-15M-S	90.0	103.7	12.3	-	85.0	7317	4.60	6.91	4862	7823	Concrete Crushing
HSC-0.75%S1-20M-0	160.0	170.0	19.7	-	30.0	8122	-	1.52	-	3983	Shear Failure
HSC-0.75%S1-20M-S	150.0	156.0	19.8	30.4	60.0	7576	1.54	3.03	3105	6123	Concrete Crushing with a Diagonal Crack
HSC-HYB-20M-0	160.0	170.8	16.0	43.3	80.0	10000	2.71	5.00	5822	10135	Concrete Crushing with a Diagonal Crack
HSC-0.75%S1-No.5(HS)-S	185.5	213.1	28.1	-	40.7	6601	-	1.45	-	5622	Concrete Crushing

Table 6-2 Summary of test results for companion beams tested by other researchers

Beam ID	Load (kN)		Displacement (mm)			Stiffness K (N/mm)	Ductility		Toughness (kN·mm)		Failure Mechanism
	P_y	P_{max}	Δ_y	Δ_{85}	Δ_{max}		Δ_{85}/Δ_y	Δ_{max}/Δ_y	Au_{85}	Au_{max}	
SCC-0%-15M-0*	-	88.1	-	-	15.1	6870	-	-	-	758	Shear Failure
SCC-0%-15M-S*	90.4	101.3	13.2	40.0	60.0	6873	3.03	4.56	3227	4716	Concrete Crushing
HSC-0%-15M-S†	94.5	104.6	14.6	-	40.7	5573	-	2.74	-	3272	Concrete Crushing
HSC-0%-20M-0†	-	83.8	-	-	10.7	7274	-	-	-	470	Shear Failure
HSC-0%-20M-S†	118.2	137.5	15.0	-	31.0	7911	-	2.07	-	2998	Concrete Crushing
HSC-0%-No.5(HS)-S‡	185.4	194.7	31.4	-	34.0	5904	-	1.09	-	3686	Concrete Crushing with Diagonal Cracks

*: Tested by Castonguay, S. (2017)
†: Tested by Algassem, O. (2016)
‡: Tested by Li, Yang (2016)

6.2 Effects of Synthetic Fibers on Shear and Flexural Response of SCC Beams

Beams SCC-0%-15M-0* and SCC-0.75%S1-15M-0 can be used to study the effect of macro-synthetic fibers on the shear resistance of normal-strength SCC concrete beams under static loading. Both beams were designed without transverse reinforcement, but contained plain SCC and fiber-reinforced SCC having 0.75%S1 fibers, respectively.

As seen in **Figure 6-2** both beams failed in shear under static loading. Moreover, as shown in **Figure 6-1a**, the use of synthetic fibers did not lead to a noticeable increase in shear resistance. This can be explained by the fact that the use of fibers allowed the longitudinal steel in beam SCC-0.75%S1-15M-0 to reach yielding, though the beam eventually fails in shear. In the control beam, the failure is brittle and occurs suddenly after the formation of the first diagonal shear crack, which leads to beam collapse. In the case of the FRC beam, the failure is relatively more ductile as the fibers gradually pulled-out across the critical shear crack. This phenomenon delayed the propagation and widening of the diagonal shear crack. **Figure 6-3** shows the sequence of failure. For example, the major shear crack in beam SCC-0.75%S1-15M-0 was first observed at a mid-span displacement (Δ) of 16 mm, with the beam finally failing at Δ = 36 mm as the fibers gradually pulled-out at the critical shear crack. As a result, beam SCC-0.75%S1-15M-0 shows improved ductility and larger toughness when compared to beam SCC-0%-15M-0* as demonstrated in **Figure 6-4**.

The effect of synthetic fibers on flexural response can be examined by comparing the behaviour of beams SCC-0%-15M-S* and SCC-0.75%S1-15M-S. The beams in this set were also designed with plain SCC and fiber-reinforced SCC (with 0.75%S1 fibers), respectively, but were detailed with sufficient stirrups in the shear spans (s = 100 mm) to prevent shear failure.

The static load-deflection response of the beams is shown in **Figure 6-1b**, where it can be seen that the provision of minimum stirrups in both beams allowed the specimens to fail in flexure. It can be observed that the use of synthetic fibers does not lead to a significant effect on maximum strength and stiffness. However, the use of fibers delays crushing of concrete in compression and enhances tensile cracking resistance which leads to an improvement in beam ductility (Δ_{max}/Δ_y = 6.60 vs. 4.56) and overall toughness (5683 vs. 4716 kN·mm) as summarized in **Figure 6-4**. Crack widths were also better controlled in the FRC specimen, which shows a more diffused cracking pattern, with a greater number of cracks in the mid-span region, when compared to the control specimen as illustrated in **Figure 6-2**. Crushing is also noticeably better controlled.

In summary, the results show that the use of macro-synthetic fibers improved shear response in beams built without stirrups by allowing for a more ductile failure, however the use of 0.75% fibers was not sufficient to prevent shear failure. In beams detailed with stirrups, the use of fibers improved post-peak ductility, toughness and cracking behaviour due to the improved response of FRC in compression and tension.

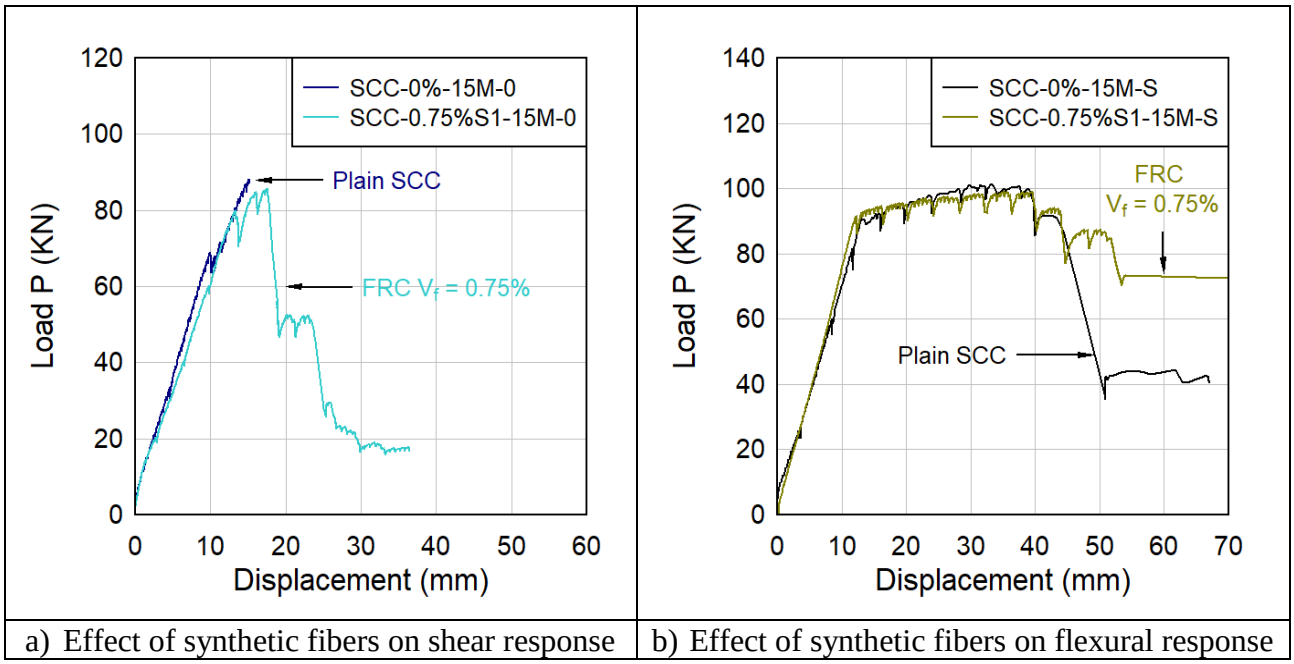

a) Effect of synthetic fibers on shear response | b) Effect of synthetic fibers on flexural response

Figure 6-1 Load vs. mid-span deflection curves; effects of fibers in SCC beams

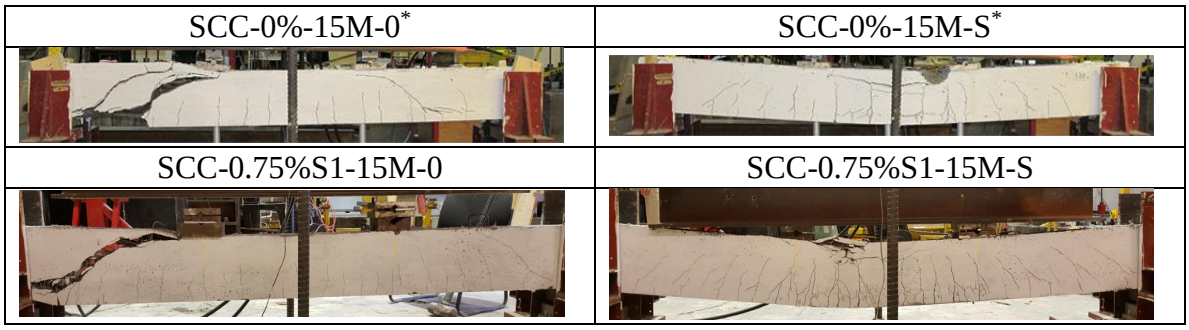

Figure 6-2 Photos of beams at end of testing; effects of fibers in SCC beams

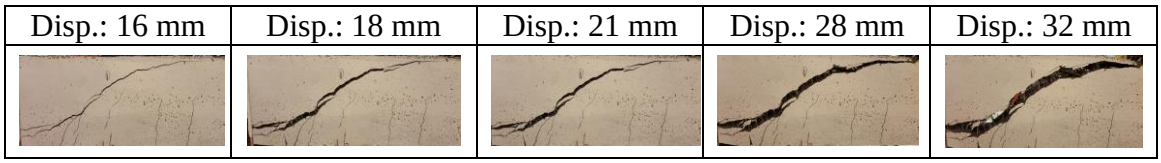

Figure 6-3 Sequence of shear failure in Beam SCC-0.75%S1-15M-0 with gradual fiber pullout

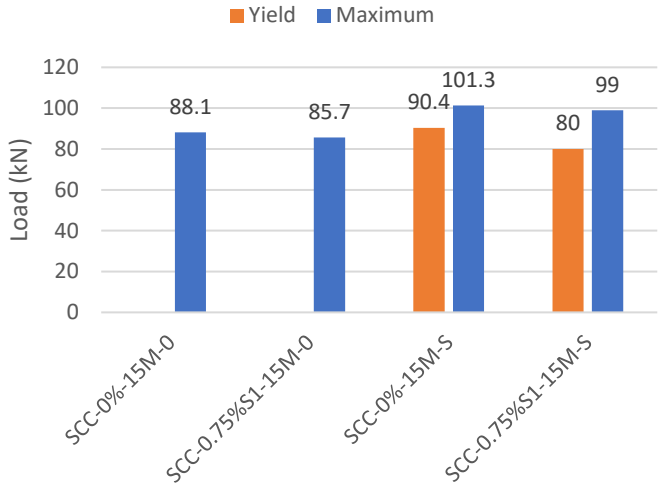

a) Load resistance

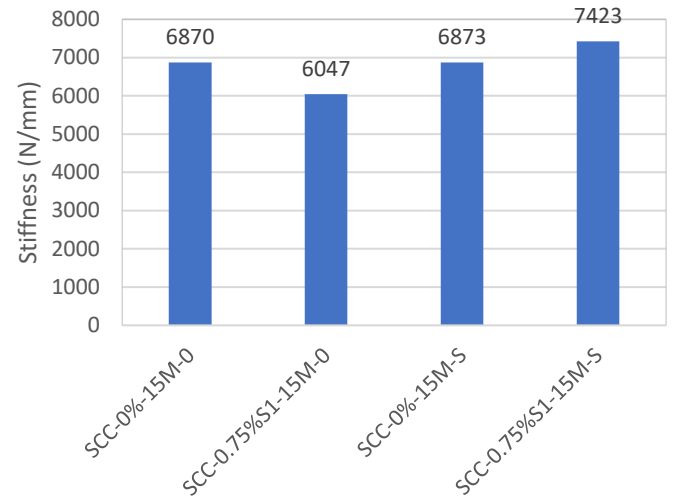

b) Stiffness

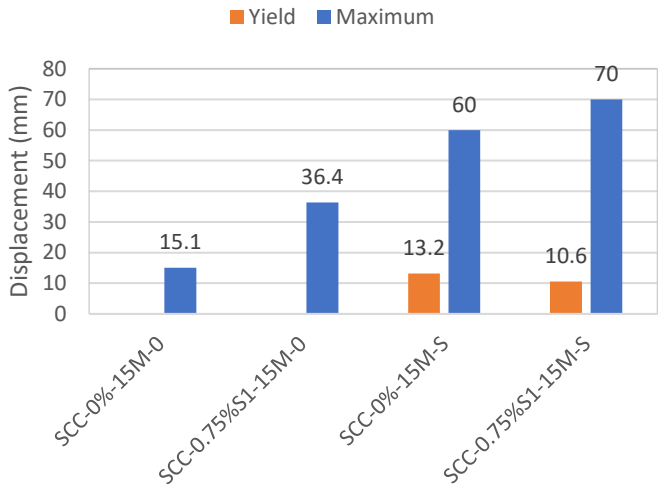

c) Displacement

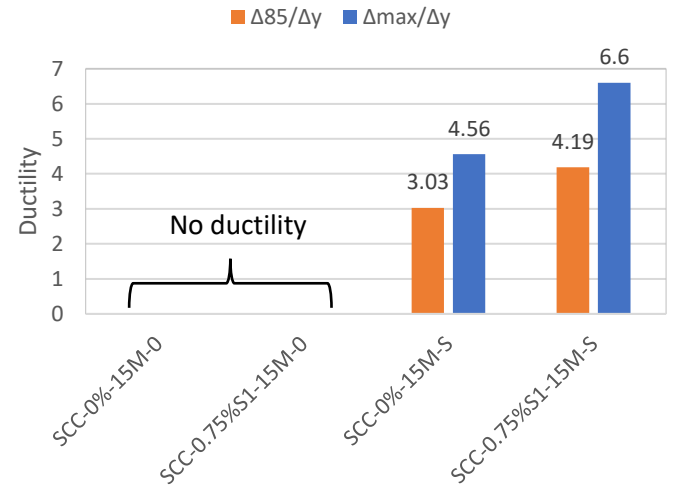

d) Ductility

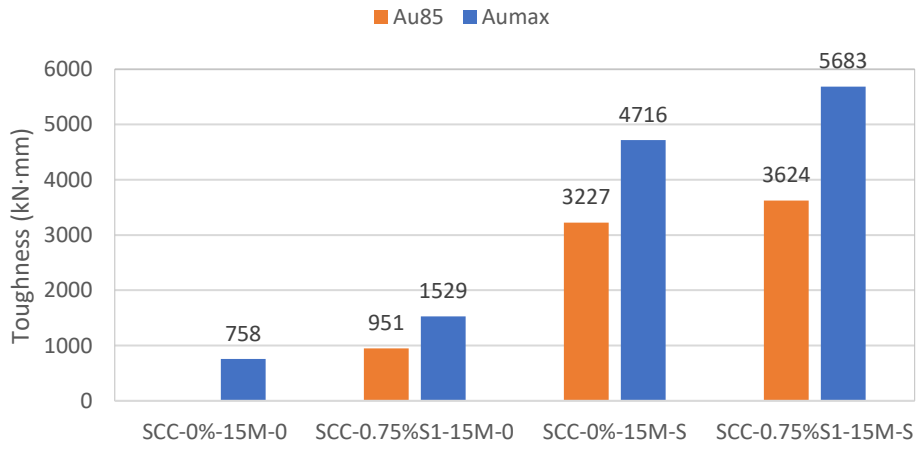

e) Toughness

Figure 6-4 Load vs. mid-span deflection parameters; effects of fibers in SCC beams

6.3 Effects of Synthetic Fibers on Shear Response of HSC Beams

This section examines the effects of synthetic fibers on the static load-deflection responses of the high-strength concrete beams built without stirrups. The following specimens are included in the analysis: 1) HSC-0%-15M-0 vs. HSC-0.75%S1-15M-0 and 2) HSC-0%-20M-0† vs. HSC-0.75%S1-20M-0, which were designed with plain HSC and fiber-reinforced HSC containing 0.75%S1 fibers, respectively.

The results for the beams in the 15M set are shown in **Figure 6-5a**, where it can be seen that the fibers significantly improved beam response by increasing shear resistance. Beam HSC-0%-15M-0 failed in a brittle manner soon after the formation of the first diagonal shear crack as shown in **Figure 6-7a**. In comparison, the response of beam HSC-0.75%S1-15M-0 shows a clear deflection plateau after yielding, which allowed the beam to experience a dominant flexural behaviour up to Δ_{max} = 67.3 mm. Comparing the results in **Figure 6-8**, it can be seen that the fibers led to significant increases in maximum capacity (25%), ductility and overall toughness (613%). However, the beam eventually failed in shear as the low-modulus synthetic fibers failed at the critical shear crack under the effects of sustained loading. The failure was associated with widening of the shear crack, until the pullout capacity of the fibers was exhausted (see **Figure 6-7a**). This same failure mode was previously observed by Yoo et al. (2019) in FRC beams reinforced with 0.75% steel fibers. The results indicate that while the use of 0.75%S1 fibers leads to a remarkable increase in ductility (Δ_{max}/Δ_y = 5.02), it was insufficient to completely substitute for stirrups.

Examining **Figure 6-5b**, it can be observed that similar results were obtained in the 20M specimens, where the addition of fibers increased shear capacity and overall strength (103% enhancement), with a significant improvement in ductility (Δ_{max}/Δ_y=1.52) and toughness (3983 vs. 470 kN·mm). Once again, the fibers allowed the beam to reach its full flexural capacity, with yielding of the longitudinal bars and sustained post-peak response, before the fiber shear capacity was exceeded leading to eventual shear collapse.

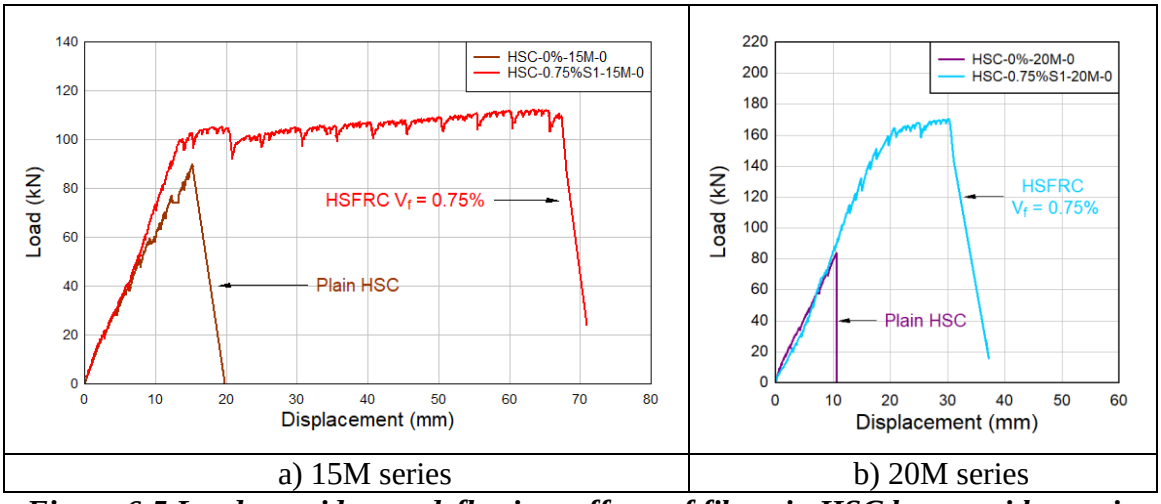

a) 15M series | b) 20M series

Figure 6-5 Load vs. mid-span deflection; effects of fibers in HSC beams without stirrups

6.4 Effects of Synthetic Fibers on Flexural Response of HSC Beams

This section examines the effects of synthetic fibers on the flexural behaviour of the high-strength concrete beams built with stirrups by comparing the responses of: 1) HSC-0%-15M-S† vs. HSC-0.75%S1-15M-S and 2) HSC-0%-20M-S† vs. HSC-0.75%S1-20M-S, which were designed with plain HSC and HSFRC containing 0.75%S1 fibers, respectively. Since beams HSC-0.75%S1-15M-0 and HSC-0.75%S1-20M-0 showed sustained flexural response, they are also included in the comparisons.

The results of the beams in the 15M set are shown in **Figure 6-6a**. It can be observed that all beams reach flexural yielding. Examining the beams with stirrups, it can be observed that both beams show similar peak loads, however the use of 0.75% synthetic fibers in beam HSC-0.75%S1-15M-S improved flexural response by increasing stiffness, ductility and toughness (see **Figure 6-8**). The use of fibers in this beam delayed concrete crushing and allowed the HSFRC beam to reach larger displacement before failure (Δ_{max} = 85 mm). Similar enhancements are also observed in the FRC specimen designed without stirrups (HSC-0.75%S1-15M-0), though this beam eventually fails in shear. Despite the difference in failure mode, the HSFRC beam failed at a large displacement of Δ_{max} = 67.3 mm which exceeded that of the plain HSC beam. Both FRC beams show enhanced ductility ratios (Δ_{max}/Δ_y = 6.91 and 5.02) when compared to the control specimen (Δ_{max}/Δ_y =2.74). Similarly, the fiber-reinforced specimens show superior toughness (A_u), with 139% and 101% improvements in energy absorption capacity for the beams with and without stirrups when compared to the plain HSC beam.

Similar observations can be made when examining the results of the 20M series in **Figure 6-6b**. In this series, the beam with fibers but without stirrups (HSC-0.75%S1-20M-0) shows higher load capacity and similar stiffness, maximum displacements (Δ_{max} = 30 mm and 31 mm) and ductility when compared to the HSC control beam built with stirrups (HSC-0%-20M-S†). However, as in the previous series, the use of fibers was not sufficient to prevent eventual shear failure and completely substitute for stirrups as shown in **Figure 6-7a**. Comparing the beams with transverse reinforcement, it can be seen that the combined use of 0.75% fibers and stirrups in beam HSC-0.75%S1-20M-S led to a more gradual failure due to the improved control of crushing in HSFRC in compression. However, it can be noted that the rate of strength decay is more important when compared to the companion beam with 15M bars (HSC-0.75%S1-15M-S) due to the increase in longitudinal steel ratio which imposed greater demands on the mid-span compression zone.

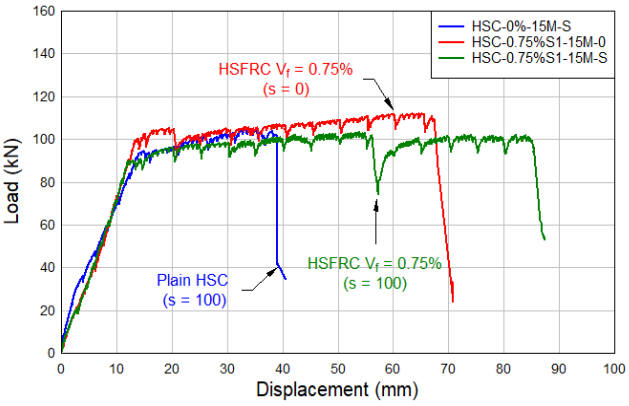

a) 15M series

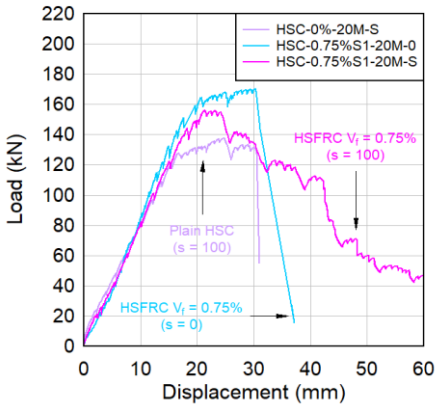

b) 20M series

Figure 6-6 Load vs. mid-span deflection; effects of fibers in HSC beams with stirrups

HSC-0%-15M-0

HSC-0%-20M-0†

HSC-0.75%S1-15M-0

HSC-0.75%S1-20M-0

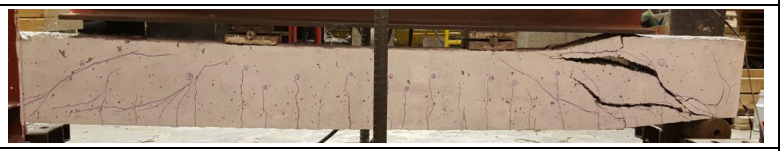

a) Effect of synthetic fibers on shear (15M & 20M)

HSC-0%-15M-S†

HSC-0%-20M-S†

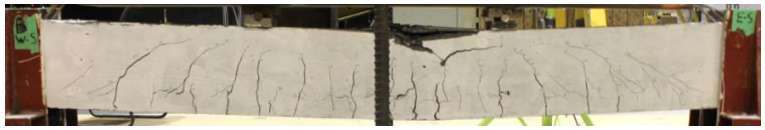

HSC-0.75%S1-15M-0

HSC-0.75%S1-20M-0

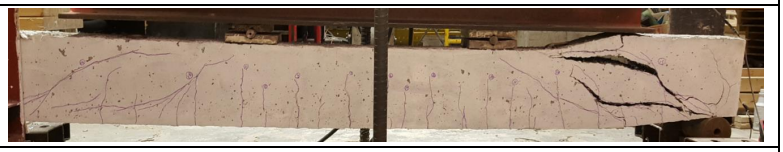

HSC-0.75%S1-15M-S

HSC-0.75%S1-20M-S

b) Effect of synthetic fibers on flexure (15M & 20M)

Figure 6-7 Photos of beams at end of testing; effects of fibers in HSC beams

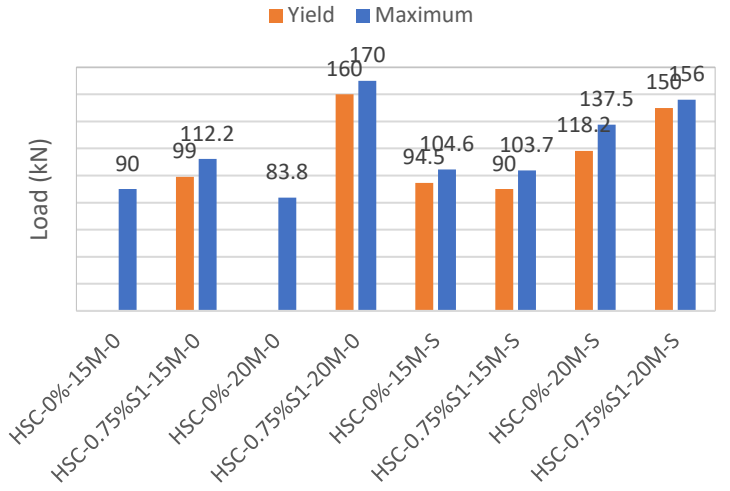

a) Load resistance

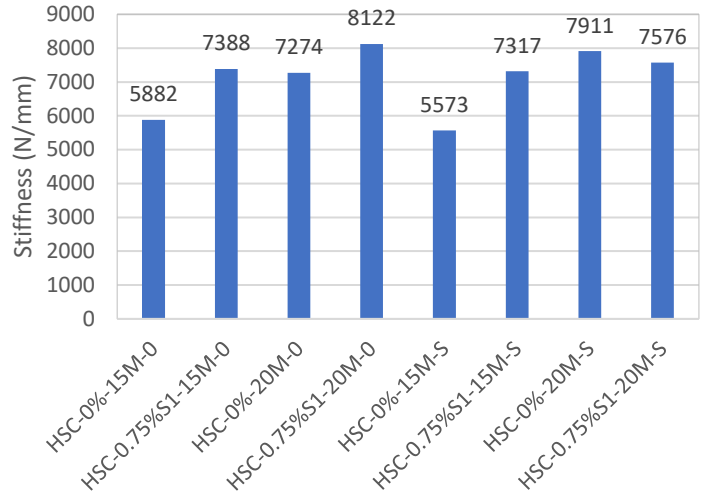

b) Stiffness

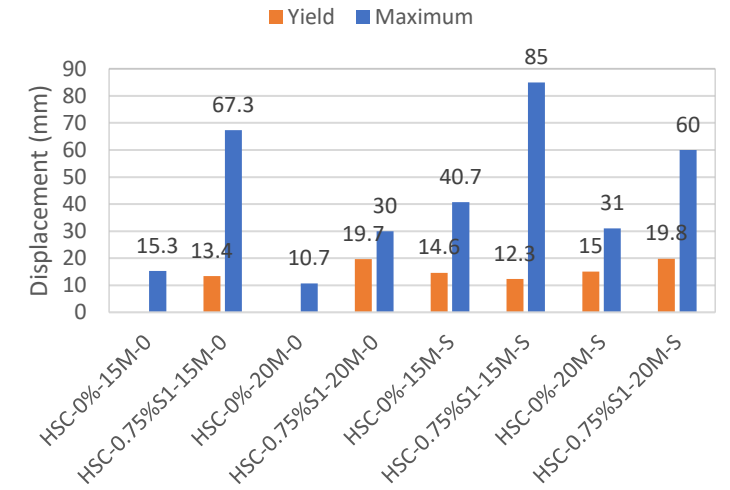

c) Displacement

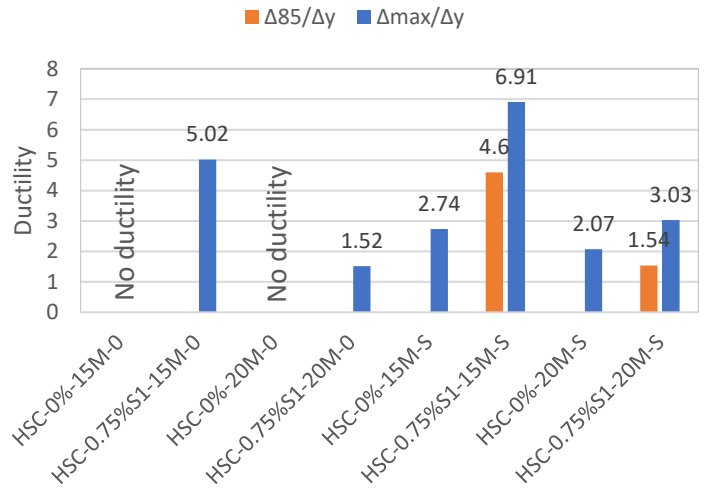

d) Ductility

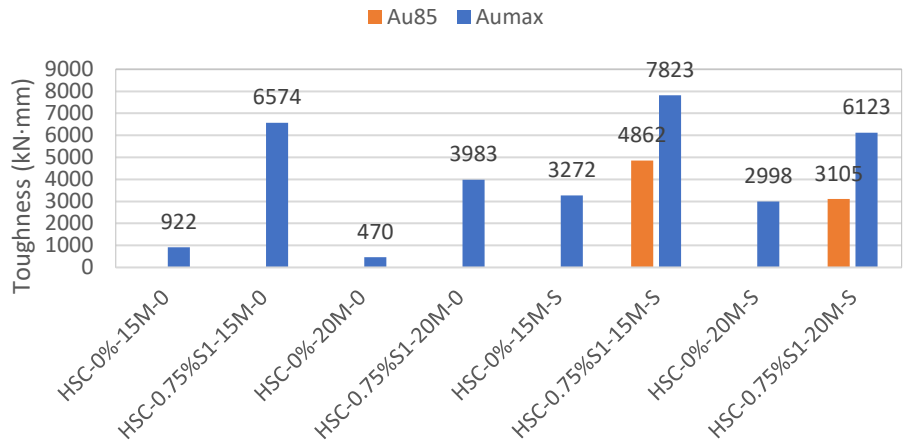

e) Toughness

Figure 6-8 Load vs. mid-span deflection parameters; effects of fibers in HSC beams

6.5 Effects of Hybrid Fibers

As noted in the previous sections, the use of 0.75%S1 fibers significantly enhanced the load-deflection response of the HSC beams, but was not sufficient to prevent shear failure. In this section, the effect of increased fiber content and hybrid fibers are studied by comparing the results of beam HSC-HYB-20M-0 (1% hybrid fibers) and HSC-0.75%S1-20M-0 (0.75%S1 fibers). It is noted that both beams had identical properties with the exception of the addition of 0.25% steel micro fibers in the hybrid specimen. To allow for further discussion, the results are also compared to the companion HSFRC beam built with stirrups (HSC-0.75%S1-20M-S).

Figure 6-9 compares the response of the specimens in this series, where it can be seen that the use of hybrid fibers substitutes for transverse reinforcement, and improves the overall flexural response by increasing stiffness, ductility and toughness. It can be observed that the load-deflection response of beams HSC-0.75%S1-20M-S and HSC-HYB-20M-0 follow similar trends, however the response of the hybrid beam significantly outperformed that of its companion, with enhancements in peak strength (9%), stiffness (32%), ductility (Δ_{max}/Δ_y = 5.00 vs. 3.03) and overall toughness (10135 vs. 6123 kN·mm) (see **Figure 6-11**). Lin & Ostertag (2017) previously reported the synergistic effect of hybrid fibers in arresting cracks by enhancing the fiber/matrix bond. The results are even more impressive when compared to beam HSC-0.75%S1-20M-0, where the hybrid fibers prevented shear failure and led to a more ductile failure response, despite the lack of stirrups. Banthia et al. (2014) previously noted that the use of hybrid fiber-reinforced concrete is effective in improving the mechanical properties of FRC in flexure and direct shear. The enhancement can be linked to the ability of the micro-steel fibers to bridge micro cracks formed around macro fibers, which in turn results in a synergy effect and an ability to delay fiber pullout failure.

As shown in **Figure 6-10**, despite the diagonal shear crack which formed on the West side of beam HSC-HYB-20M-0, the width of this crack did not expand beyond 2 mm, which allowed the beam with hybrid fibers to experience a ductile flexural failure. As a result, beam HSC-HYB-20M-0 shows a flexural dominant response, with failure concentrated in the mid-span region, similar to what was observed in the HSC-0.75%S1-20M-S beam which contained stirrups.

In summary, the results show that the use of 1% hybrid fibers was effective in increasing HSC beam shear resistance, with an ability to substitute for transverse reinforcement and prevent shear failure. The ability of the hybrid fibers to improve the compressive and tensile response of HSC also led to significant enhancements in overall flexural performance.

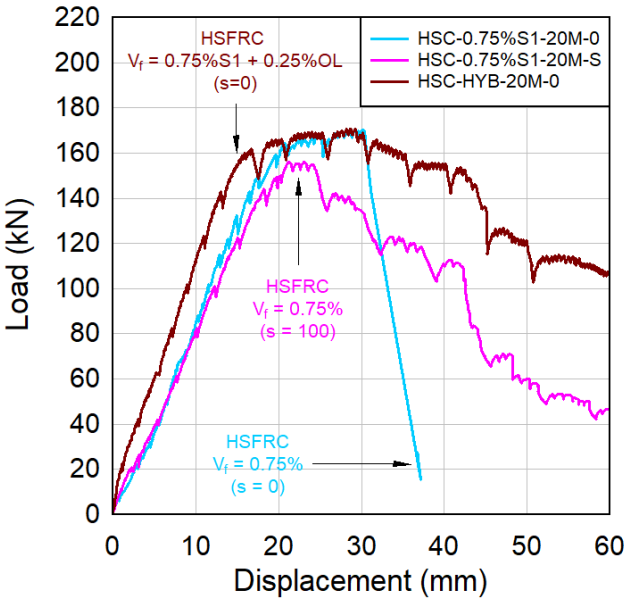

Figure 6-9 Load vs. mid-span deflection curve; effects of hybrid fibers

HSC-0.75%S1-20M-0

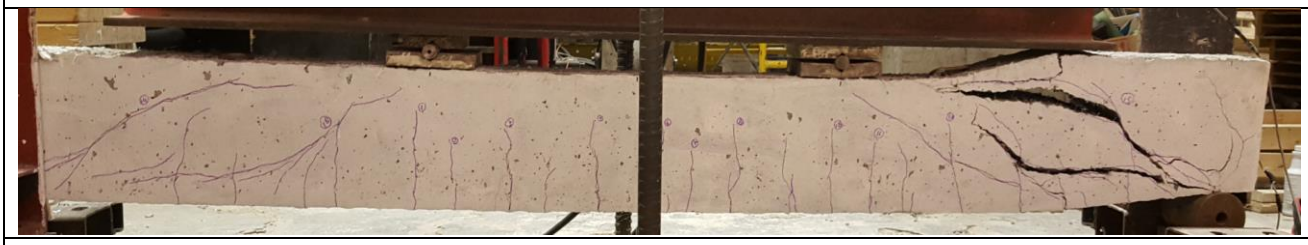

HSC-0.75%S1-20M-S

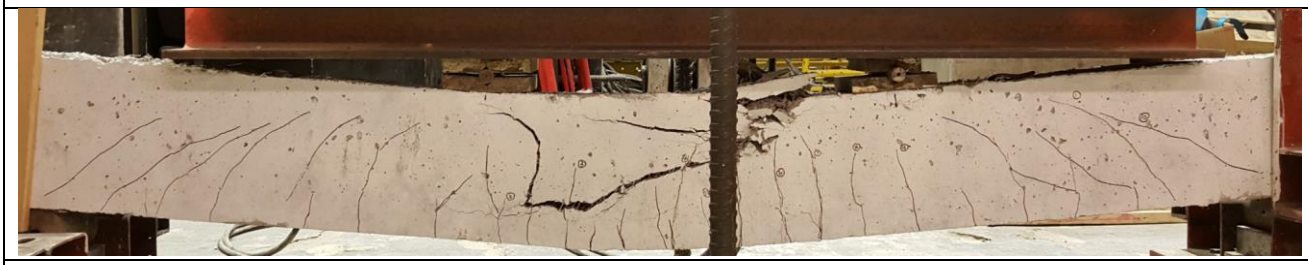

HSC-HYB-20M-0

Figure 6-10 Photos of beams at end of testing; effects of hybrid fibers

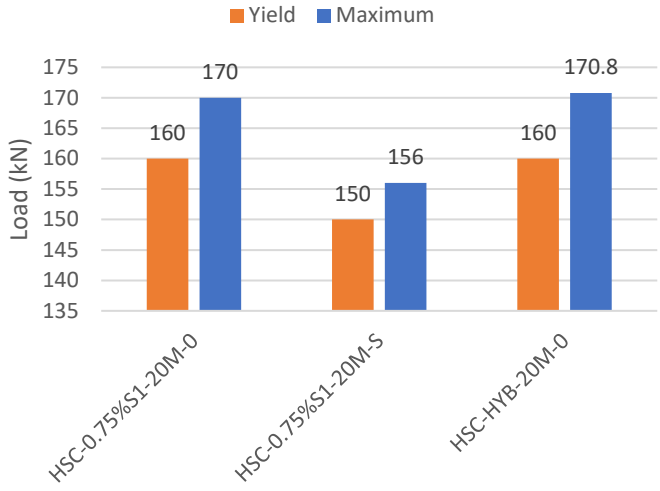

a) Load resistance

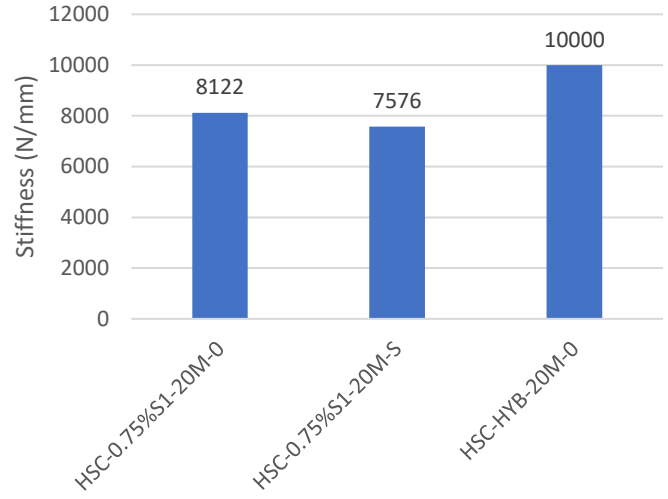

b) Stiffness

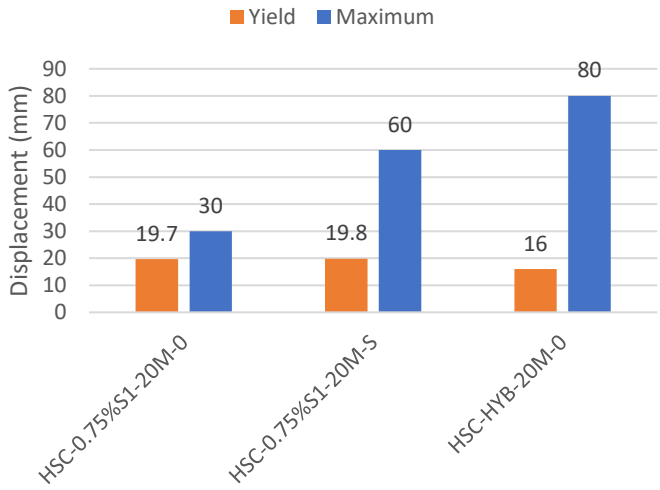

c) Displacement

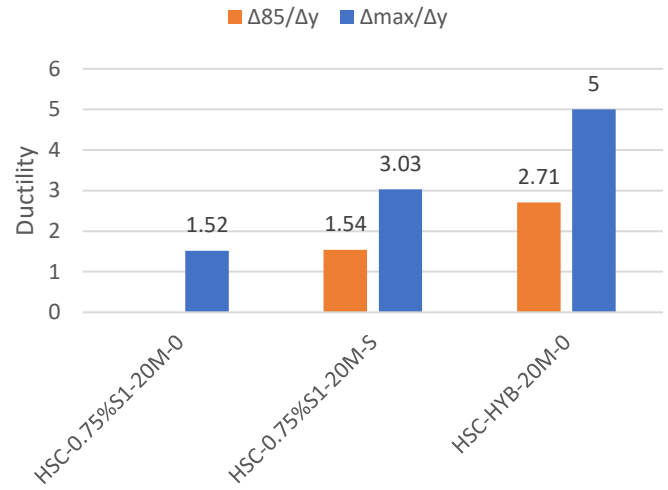

d) Ductility

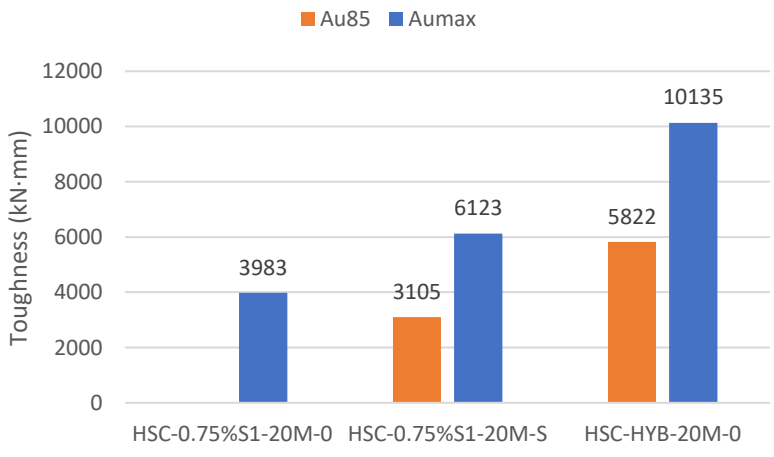

e) Toughness

Figure 6-11 Load vs. mid-span deflection parameters; effects of hybrid fibers

6.6 Effects of Synthetic Fibers in HSC Beams with High-Strength (690 MPa) Bars

This comparison examines the effect of synthetic fibers on the response of HSC beams detailed with high-strength (Grade 690 MPa) reinforcement. Included in the comparison are beams HSC-0%-No.5(HS)-S‡ and HSC-0.75%S1-No.5(HS)-S which were built with plain HSC and HSFRC containing 0.75% synthetic fibers, respectively. Both beams were built with No.5 high-strength bars and contained stirrups which were spaced at 100 mm in the shear spans.

The comparison of the load-deflection response of the beams is shown in **Figure 6-12**, where it can be seen that the use of synthetic fibers led to increases of 9% and 12% in strength and stiffness. While both beams show rounding of the load-deflection curve due to the nature of the high-strength steel response, the plain HSC beam fails more suddenly by crushing of concrete due to the strain demands imposed by the high-strength bars on the HSC compression zone. The provision of synthetic fibers allows a delay in this failure and results in enhancements of 20%, 33% and 53% in maximum displacement, ductility and overall toughness (see **Figure 6-14**). Nonetheless, failure in the synthetic fiber-reinforced concrete beam can still be considered brittle due to the relatively sudden compression failure (as shown in **Figure 6-13**), although the beam shows a considerably high ultimate load resistance of 213 kN and deflection of ~ 40 mm. Similarly, as shown in **Figure 6-13**, the use of fibers resulted in a more diffused cracking pattern, with reduced crack widths and better control of damage. It is noted that the use of No.5 high-strength bars in this beam led to near "balanced conditions" (where $\rho \approx \rho_b$), despite the use of HSC. Previous research by Aldabagh et al. (2019) on more lightly reinforced beams has shown that the use of synthetic fibers can enhance curvature ductility and cracking behavior of HSC beams reinforced with Grade 690 MPa ASTM A1035 bars. The enhanced behavior can be explained by the ability of fibers to delay crushing of concrete, which can allow for better use of the high-strength bars, and the ability of fibers to better control cracking; further research is recommended.

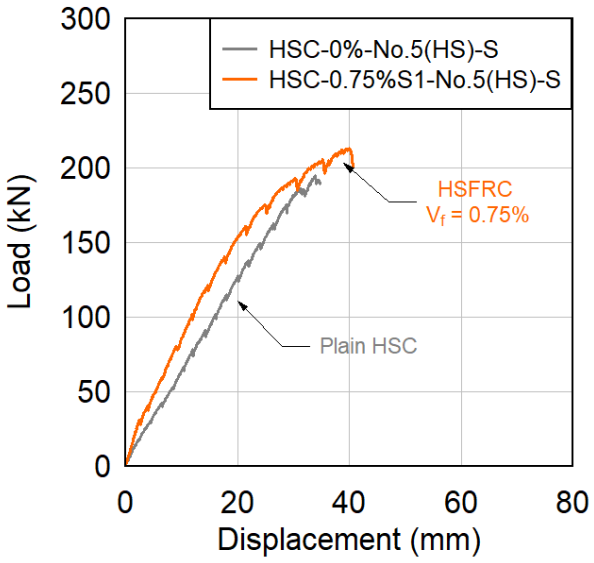

Figure 6-12 Load vs. mid-span deflection curve; effects of fibers in beams with HSR

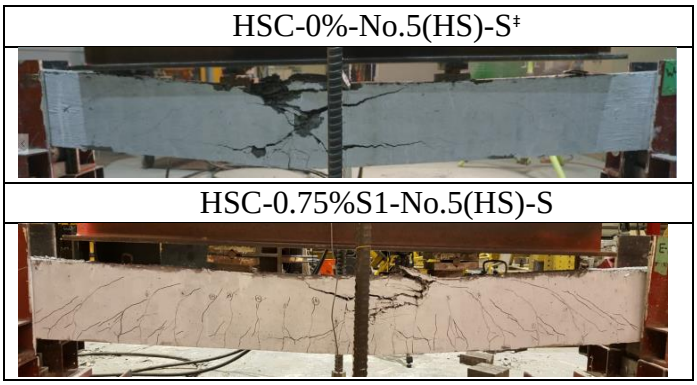

Figure 6-13 Photos of beams at end of testing; effects of fibers in beams with HSR

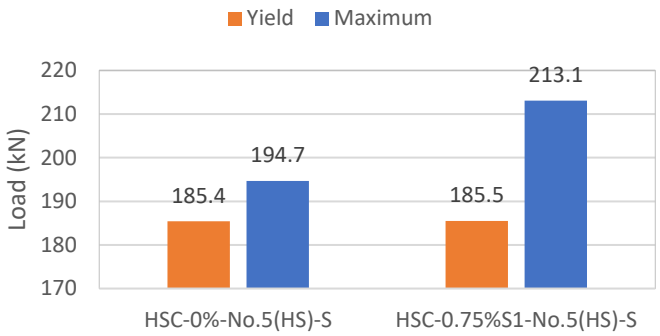

a) Load resistance

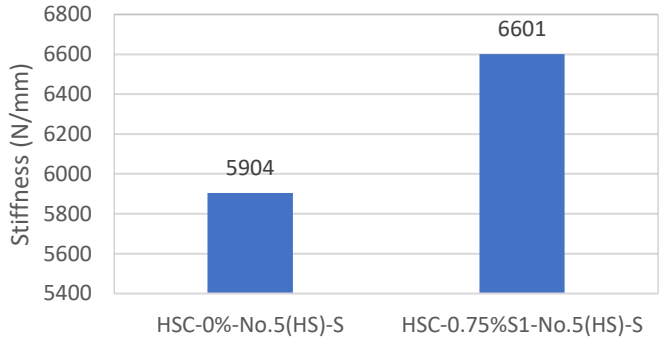

b) Stiffness

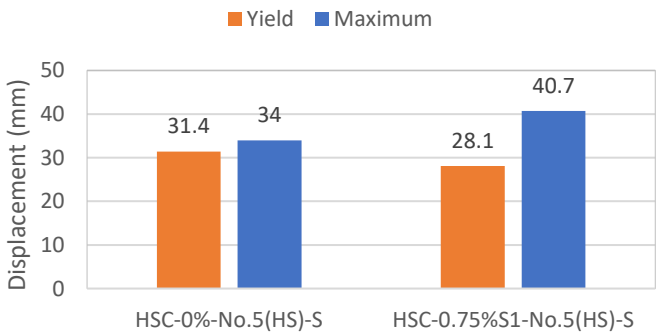

c) Displacement

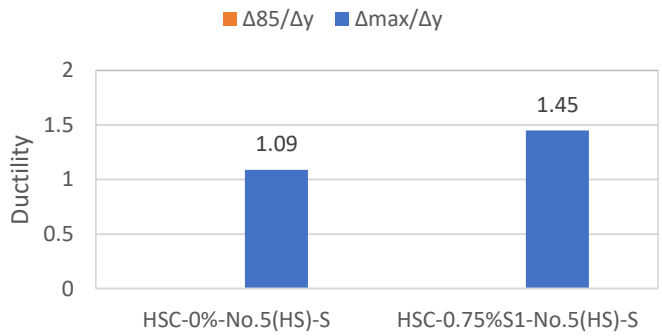

d) Ductility

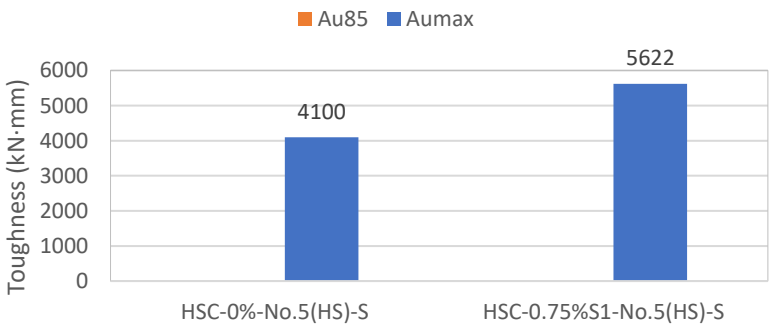

e) Toughness

Figure 6-14 Load vs. mid-span deflection parameters; effects of fibers in beams with HSR

6.7 Effects of Steel Reinforcement Type in HSFRC

This final section examines the effect of reinforcement type on the response of HSFRC beams by comparing the responses of beams HSC-0.75%S1-15M-S and HSC-0.75%S1-No.5(HS). Both beams were built with HSFRC containing 0.75%S1 fibers and stirrups, but were designed with Grade 400 MPa 15M bars and Grade 690 MPa high-strength bars, respectively.

Figure 6-15 shows that the use of No.5 high-strength bars resulted in a 105% increase in load-carrying capacity when compared to the use of 15M normal-strength bars. As noted previously, beam HSC-0.75%S1-15M-S showed a large deflection plateau (Δ_{max} = 85 mm) before eventually failing due to concrete crushing as illustrated in **Figure 6-16**. In comparison, failure occurs more suddenly in the beam with high-strength reinforcement due to the increased demands on the HSFRC compression zone. As a result, the beam containing synthetic fibers and high-strength steel shows a significant reduction in ductility ratio (Δ_{max}/Δ_y = 1.45 vs. 6.91) with a 28% reduction in overall toughness (A_u), despite the increase in capacity. **Figure 6-17** provides a comparison of the results obtained for the 15M and No.5 specimens.

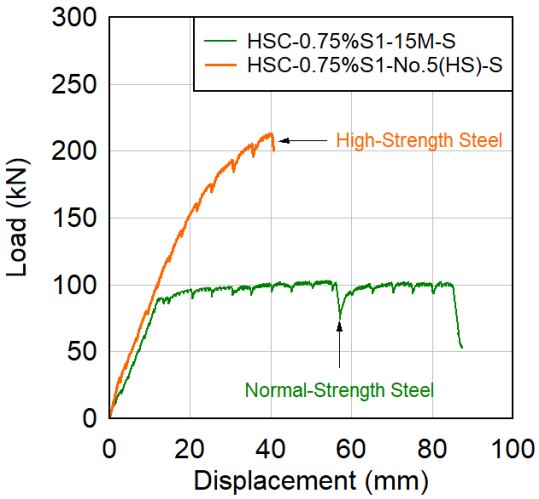

Figure 6-15 Load vs. mid-span deflection curves; effects of steel type in HSFRC beams

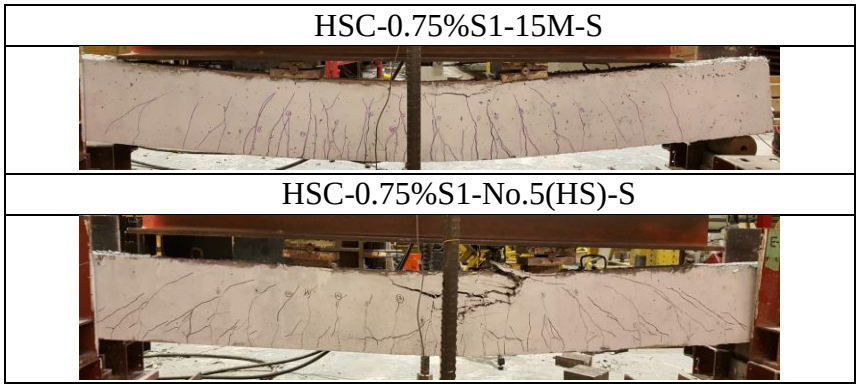

Figure 6-16 Photos of beams at end of testing; effects of steel type in HSFRC beams

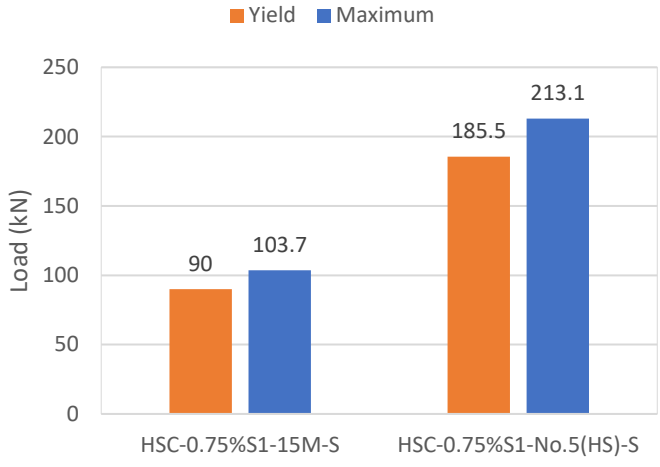

a) Load resistance

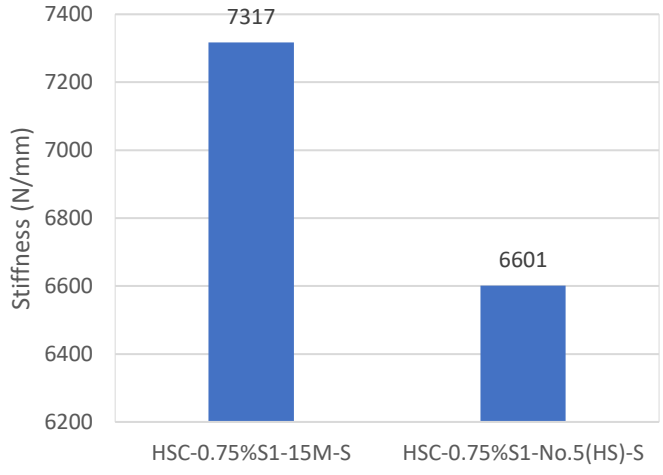

b) Stiffness

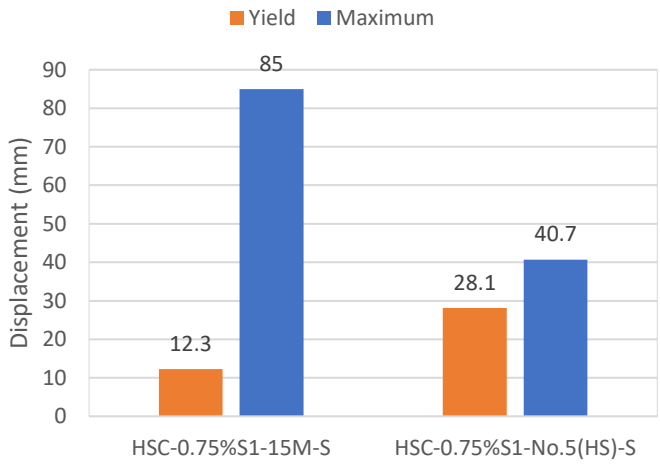

c) Displacement

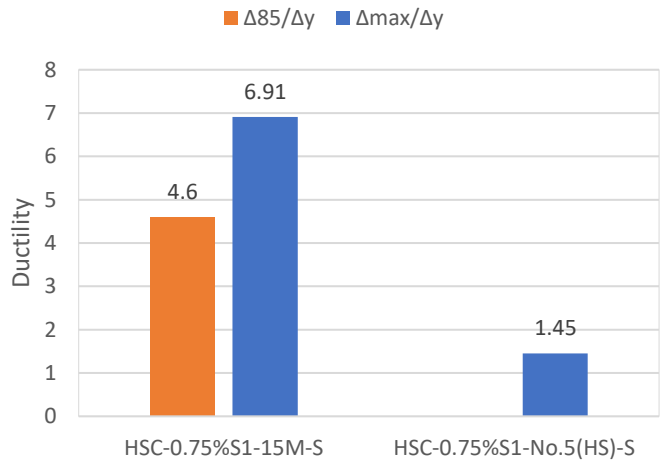

d) Ductility

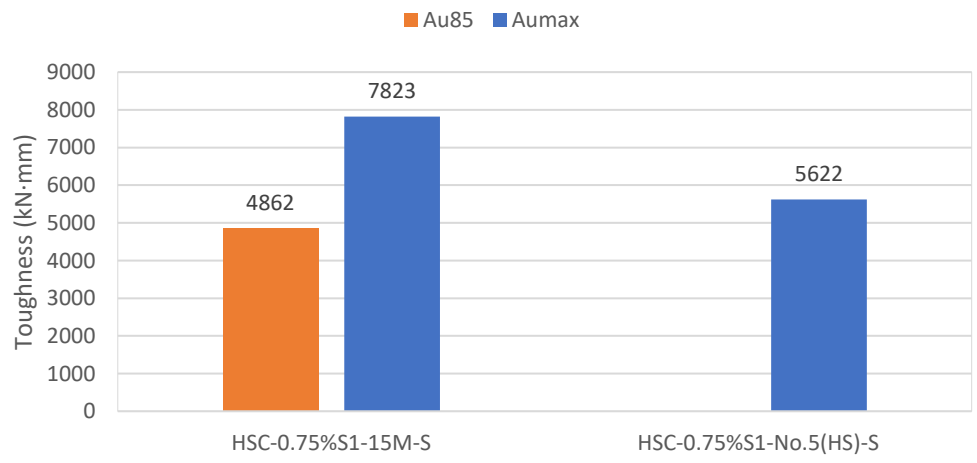

e) Toughness

Figure 6-17 Load vs. mid-span deflection parameters; effects of steel type in HSFRC beams

Chapter 7: Discussion of Dynamic Experimental Results

7.1 Chapter Overview

This chapter discusses the effects of the test variables on the performance of the beams tested under blast loads. The performance criteria used to discuss the results includes: maximum and residual mid-span displacements, magnitude of blast pressure at failure, failure mode and damage tolerance, including crack control and secondary fragmentation. The following aspects are discussed in the sections that follow:

The effects of synthetic fibers on the shear performance of HSC beams without stirrups:

- In Series 15M: HSC-0.75%S1-15M-0 vs. HSC-0%-15M-0
- In Series 20M: HSC-0.75%S1-20M-0 vs. HSC-0%-20M-0*

The effects of synthetic fibers on the flexural performance of HSC beams with stirrups:

- In Series 15M: HSC-0.75%S1-15M-S vs. HSC-0%-15M-S*
- In Series 20M: HSC-0.75%S1-20M-S vs. HSC-0%-20M-S*

The effects of hybrid fibers:

- In Series 20M, comparing beams with 1% hybrid fibers and 0.75%S1 fibers:
  - HSC-HYB-20M-0 vs. HSC-0.75%S1-20M-0 & HSC-0.75%S1-20M-S

The effects of reinforcement ratio:

- In beams with fibers, but without stirrups:
  - HSC-0.75%S1-15M-0 vs. HSC-0.75%S1-20M-0
- In beams with fibers and stirrups:
  - HSC-0.75%S1-15M-S vs. HSC-0.75%S1-20M-S

The effects of reinforcement type:

- In beams with Grade 690 and 400 MPa bars, and fibers:
  - HSC-0.75%S1- No.5(HS)-S vs. HSC-0.75%S1-15M-S

The effects of synthetic fibers in beams with high-strength steel reinforcement:

- In beams with Grade 690 MPa bars, with and without fibers:
  - HSC-0.75%S1-No.5(HS)-S vs. HSC-0%-No.5(HS)-S†

The effects of fibers and detailing:

  - HSC-0.75%S1-20M-10M-d/2 vs. HSC-0.75%S1-20M-S & HSC-0%-20M-10M-d/4‡

7.2 General Observations

Figure 7-2 through **Figure 7-7** summarize the response of the beams in terms of maximum and residual mid-span displacements, along with notes regarding the blasts which caused failure.

Similar to the previous section, the results are compared to a series of control beams tested by other researchers. These beams, marked with *, † and ‡, were tested by Algassem (2016), Li (2016) and Charles (2019) respectively and allowed for an investigation into the effects of fibers when compared to beams built with plain HSC, normal-strength bars, high-strength bars and blast detailing, respectively. **Table 7-1** and **Table 7-2** summarize the results obtained for beams tested in this study and in these previous studies, while **Figure 7-1** demonstrates the design details for beams tested by other researchers. A detailed discussion on the effects of the test parameters on beam response is provided in the sections that follow.

Table 7-1 Summary of test results

Beam ID	Shockwave Properties				Displacement		θ_{max} (°)	Failure Mode
	Shot (psi)	P_r (kPa)	I_r (kPa-ms)	t_d (ms)	Δ_{max} (mm)	Δ_{res} (mm)		
HSC-0%-15M-0	30	35.9	323.6	19.4	16.08	5.49	0.83	Shear
HSC-0.75%S1-15M-0	30	44.4	377.7	20.6	18.84	3.43	0.97	Shear
	50	65.6	553.5	20.6	35.55	29.94	1.82	
HSC-0.75%S1-15M-S	30	35.9	375.5	20.6	16.74	4.96	0.86	Concrete Crushing / Fiber Pullout
	50	65.0	484.1	19.4	29.57	7.14	1.52	
	70	72.0	711.7	20.6	86.70	41.10	4.44	
HSC-0.75%S1-20M-0	30	44.6	378.7	20.6	12.50	1.54	0.64	Shear
	50	61.0	521.0	20.6	18.49	3.18	0.95	
	60	71.0	653.0	21.4	84.08	60.59	4.31	
HSC-0.75%S1-20M-S	30	44.0	334.5	18.9	12.17	1.06	0.62	Concrete Crushing / Fiber Pullout
	50	55.9	523.4	21.3	23.21	4.00	1.19	
	70	83.9	723.8	21.9	44.70	19.89	2.29	
	80	90.9	832.0	23.8	186.57	143.00	9.49	
HSC-HYB-20M-0	30	41.3	377.0	20.6	16.39	1.63	0.84	Fiber Pullout
	50	66.9	586.5	20.6	22.90	5.40	1.18	
	70	76.7	961.8	26.3	41.14	15.43	2.11	
	80	82.8	853.2	25.7	60.01	25.20	3.08	
HSC-0.75%S1-20M-10M-d/2	30	38.4	405.6	20.6	10.80	0.33	0.55	Concrete Crushing / Fiber Pullout
	70	79.8	723.6	20.7	44.16	21.06	2.27	
	90	90.1	979.8	26.3	86.23	64.65	4.42	
HSC-0.75%S1-No.5(HS)-S	30	45.4	395.4	21.3	16.53	4.03	0.85	Concrete Crushing
	50	61.8	520.4	20.6	22.25	1.32	1.14	
	70	76.3	911.3	28.8	37.84	8.99	1.94	
	90	92.5	876.1	21.4	173.96	109.06	8.86	

Table 7-2 Summary of test results from previous researchers

Beam ID	Shockwave Properties				Displacement		θ_{max} (°)	Failure Mode
	Shot (psi)	P_r (kPa)	I_r (kPa-ms)	t_d (ms)	Δ_{max} (mm)	Δ_{res} (mm)		
HSC-0%-20M-0*	30	38.7	370.8	19.2	19.31	9.21	0.99	Shear
HSC-0%-15M-S*	30	42.9	340.7	15.9	21.40	4.71	1.10	Concrete Crushing
	50	58.64	516.0	17.6	124.00	22.04	6.41	
HSC-0%-20M-S*	30	39.2	360.0	18.4	15.12	0.15	0.78	Concrete Crushing
	50	57.4	538.2	18.8	32.91	12.43	1.69	
	70	68.8	702.6	20.4	118.06	71.69	6.06	
HSC-0%-No.5(HS)-S†	30	43.8	207	21.8	17.72	3.13	0.81	Concrete Crushing / Spalling
	50	59.1	345	21.2	26.77	1.16	1.22	
	70	77.6	483	24.4	64.71	19.96	2.96	
HSC-0%-20M-10M-d/4‡	30	45.1	370.4	19.1	11.47	1.67	0.55	Concrete Crushing
	70	74.9	703.9	21.1	34.59	17.33	1.65	
	90	88.7	837.2	20.2	71.57	48.19	3.4	

*: Tested by Algassem, O. (2016): Plain HSC beams with normal-strength bars
†: Tested by Li, Y. (2016): Plain HSC beams with high-strength bars
‡: Tested by Charles, C. (2019): Plain HSC beams with blast detailing

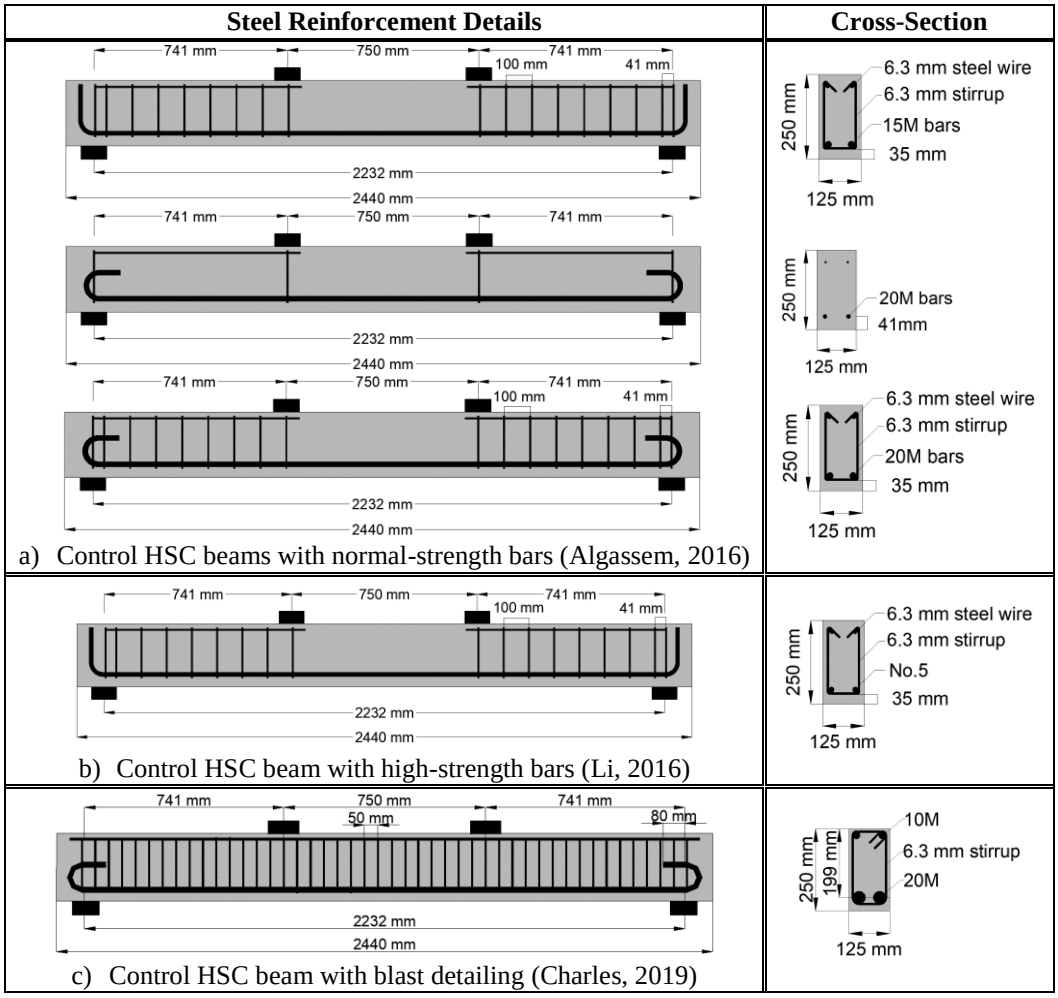

a) Control HSC beams with normal-strength bars (Algassem, 2016)

b) Control HSC beam with high-strength bars (Li, 2016)

c) Control HSC beam with blast detailing (Charles, 2019)

Figure 7-1 Beam design details from previous researchers

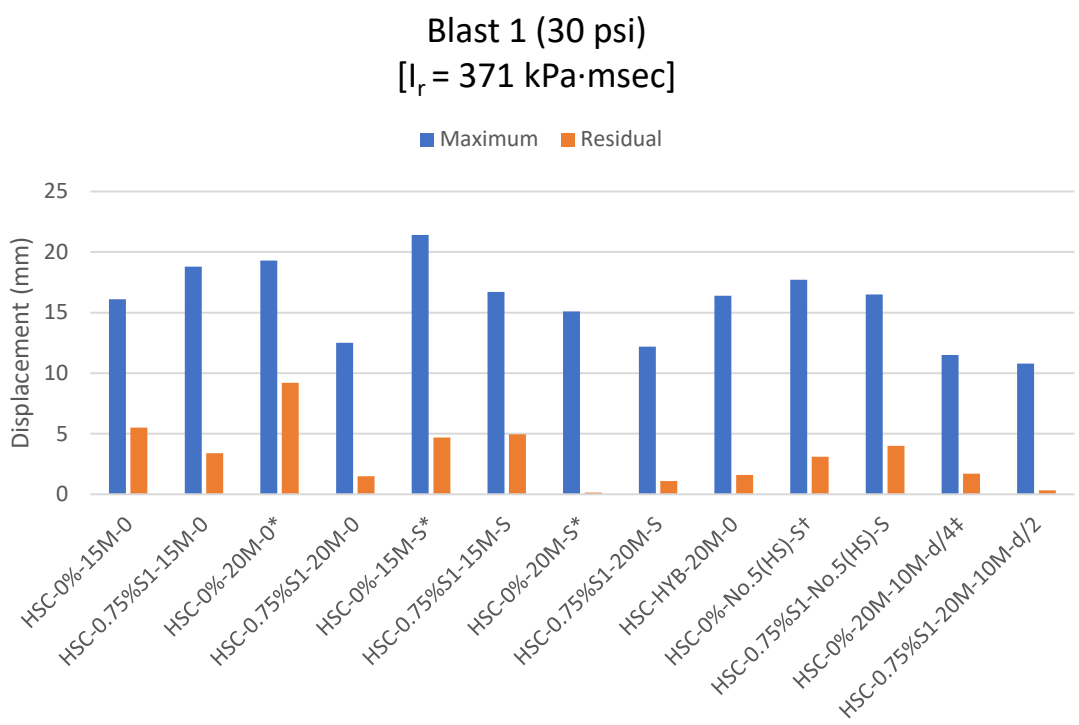

Figure 7-2 Maximum and residual displacements for Blast 1

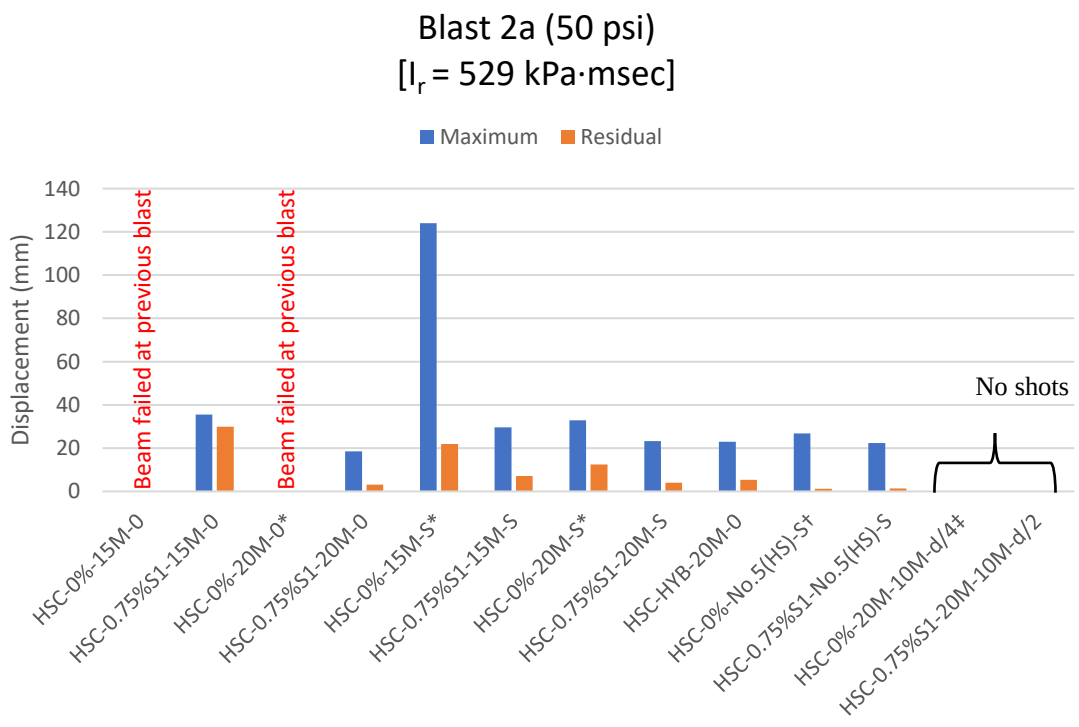

Figure 7-3 Maximum and residual displacements for Blast 2a

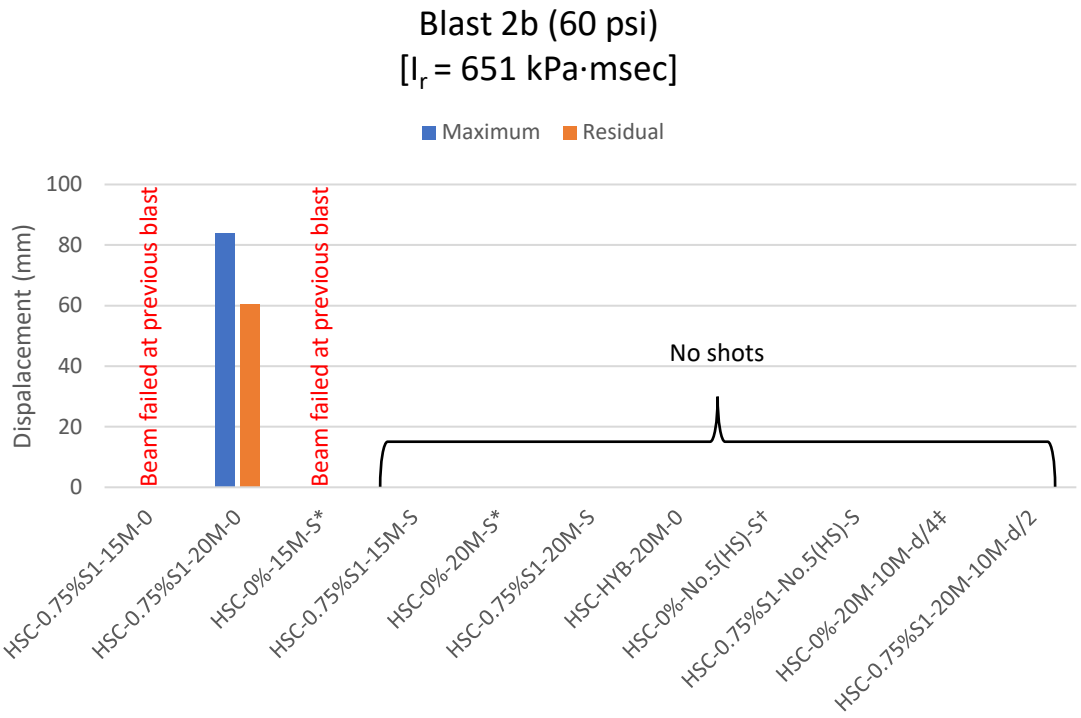

Figure 7-4 Maximum and residual displacements for Blast 2b

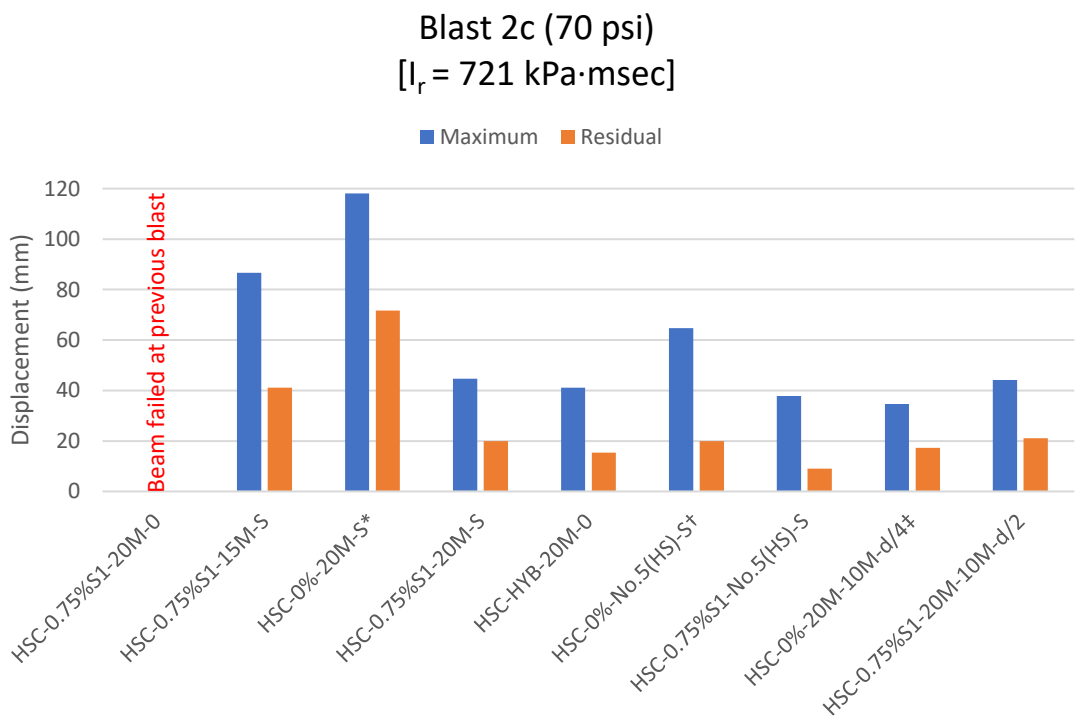

Figure 7-5 Maximum and residual displacements for Blast 2c

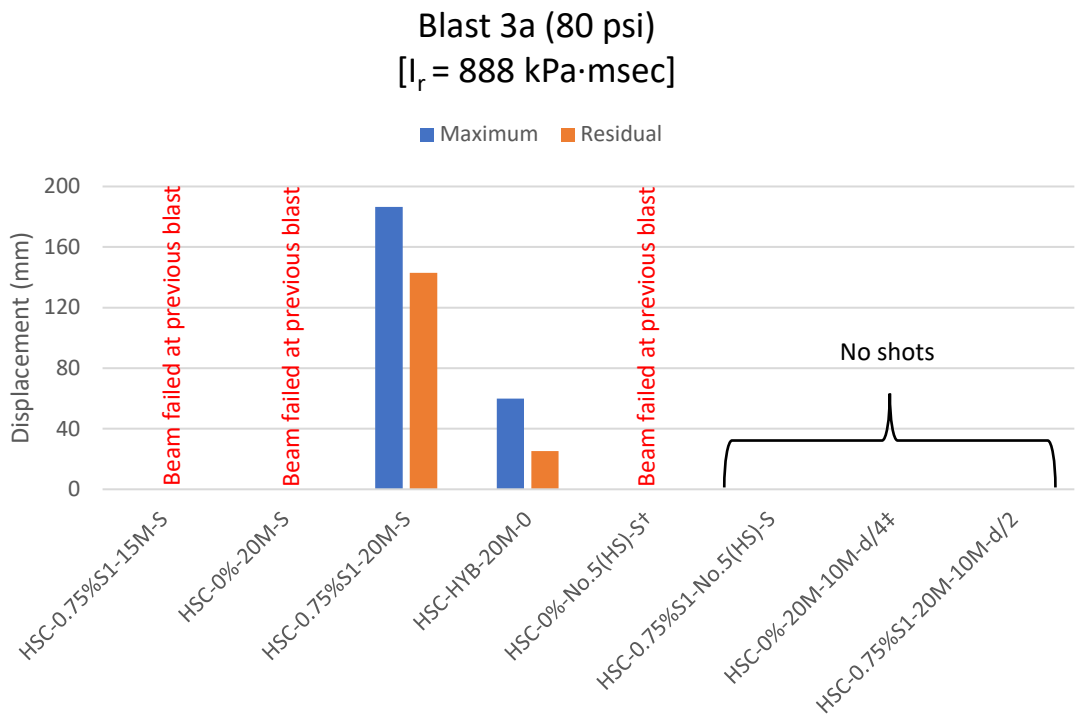

Figure 7-6 Maximum and residual displacements for Blast 3a

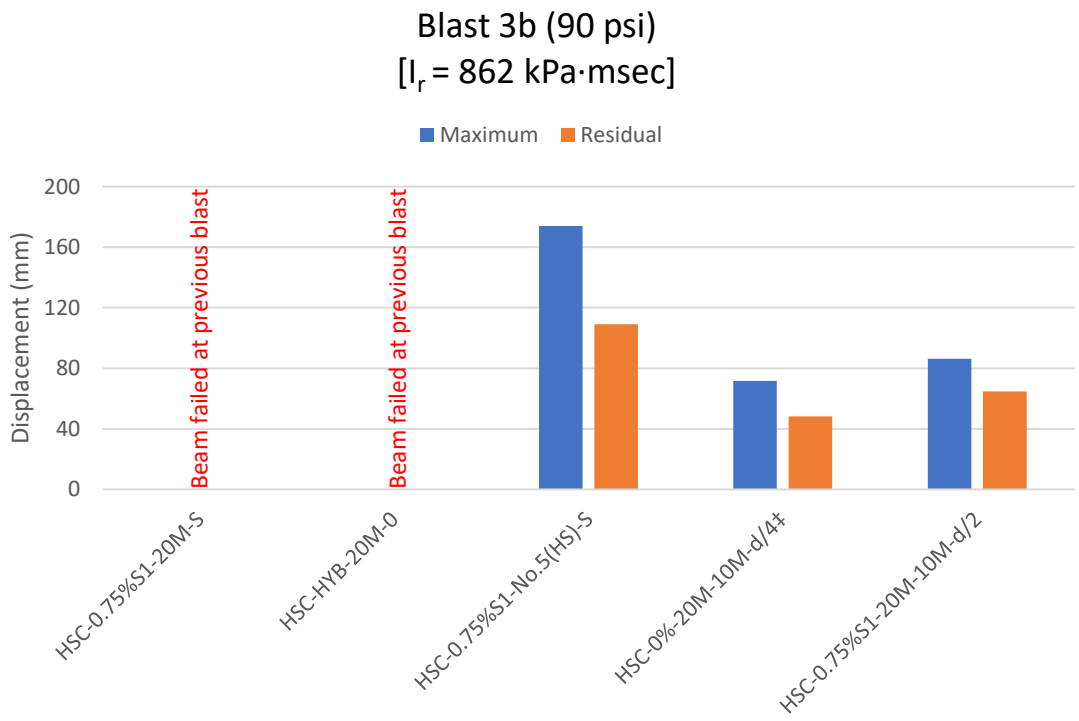

Figure 7-7 Maximum and residual displacements for Blast 3b

7.3 Effects of Synthetic Fibers on Shear Performance (Series 15M & 20M)

The effect of synthetic fibers on shear resistance can be investigated by comparing the following two sets of specimens: 1) HSC-0%-15M-0 vs. HSC-0.75%S1-15M-0 and 2) HSC-0%-20M-0* vs. HSC-0.75%S1-20M-0. The beams in each individual set had the same steel ratio (ρ =1.5% for the first set and ρ =2.4% for the second set) but were cast with plain HSC and HSFRC containing 0.75% synthetic fibers, respectively. In all cases, the beams were designed without stirrups. Comparative displacement histories and bar charts are shown in **Figure 7-8** and **Figure 7-9**, respectively. Photographs showing damage and failure are provided in **Figure 7-10** and **Figure 7-11**.

Keeping in mind the differences in failure mode, the displacement data shows that the companion HSC/HSFRC beams in the 15M series had similar maximum displacements at Blast 1 – 30 psi, however the specimen with fibers shows a 38% reduction in residual displacement. Similarly, in the 20M set, the beam with synthetic fibers shows reductions of 35% and 84% in maximum and residual displacements, respectively.

The effect of the fibers is better evaluated by comparing the blast capacities of the beams. Companion beams in each set failed in shear, but at different blast intensities as shown in **Figure 7-10** and **Figure 7-11**. The control beam in the 15M set failed at Blast 1 – 30 psi (I_r = 324 kPa·ms), while the 15M beam with 0.75%S1 survived this shot with fibers restraining the shear crack as shown in **Figure 7-10e**. Failure in the HSFRC beam occurred at Blast 2a – 50 psi (I_r = 554 kPa·ms) after initiation of yielding of the longitudinal reinforcement, similar to what was observed under static testing. The final failure occurred due to the fiber pullout across the shear crack in the bottom shear span. In a similar way, the plain HSC beam in the 20M set experienced a major diagonal crack in the top shear span at Blast 1 – 30 psi (I_r = 371 kPa·ms) leading to shear failure, while shear cracks were observed one blast later (Blast 2a – 50 psi) in the companion HSFRC specimen owing to the fiber bridging effect. Shear failure in the HSFRC specimen occurred at Blast 2b – 60 psi (I_r = 653 kPa·ms) with complete fiber pullout at the same diagonal crack which formed during the previous blast.

In summary, the results confirm that synthetic fibers increase the shear resistance of HSC beams under blast loading, which results in a delay in failure. However, while the use of 0.75% fibers allowed for the development of yield stresses in the longitudinal reinforcement, it was not sufficient to completely replace stirrups and prevent eventual shear failure. The same effect was observed in the static tests; however, the results indicate that brittle shear failure was initiated earlier under blast loading. For example, in the 15M and 20M series, the fibers were able to bridge the critical shear crack up to maximum mid-span displacements of 30 and 19 mm, respectively, compared to 67 and 30 mm, under static loading. The result points to a loss in fiber efficiency under dynamic loads. Banthia et al. (1996) previously reported that fibers improve the fracture energy under dynamic loads, but the enhancements are not as pronounced as under static

conditions. Similar observations have been reported by Zhang (2008) and Xu et al. (2004), where the toughness of FRC under impact decreased with increased drop height.

Comparing to previous research on steel FRC beams, Min et al. (2014) found that 0.75% steel fibers was sufficient to substitute for stirrups in beams under static loads, but not under impact loads. Likewise, Lee et al. (2018) noted that 1% fibers increased impact resistance, but did not prevent shear failure. Conversely, Ulzurrun and Zanuy (2017) and Algassem et al. (2019) found that 1% steel fibers were sufficient to ensure ductile flexural failure and substitute for stirrups under impact and blast, respectively. Kishi and Mikami et al. (2012) previously noted that a static shear-to-flexure ratio ≥ 1.5 is needed to ensure ductile flexural failure in conventional reinforced concrete beams tested under impact. To better study this effect, the flexural (M_{fl}) and shear (V_{rf}) capacities of the tested beams were determined using the Imam et al. (1995) and Yazdanbakhsh et al. (2015) models, respectively (see **Chapter 8**). Using these models, the static peak loads corresponding to flexure ($P_{fl} = 2 \cdot M_{fl}/a$, where a = shear span) and shear ($P_v = V_{rf} \cdot 2$) were found to be 97.3 kN & 116.5 kN (for beam HSC-0.75%S1-15M-0) and 136.8 kN & 131.0 kN (for beam HSC-0.75%S1-20M-0). It can be observed that the shear-to-flexure capacity ratios ($\alpha = \frac{P_v}{P_{fl}}$) are lower than 1.5 ($\alpha$ =1.20 and 0.96, respectively), which can explain why the use 0.75% synthetic fibers was not sufficient to prevent shear failure under blast loads.

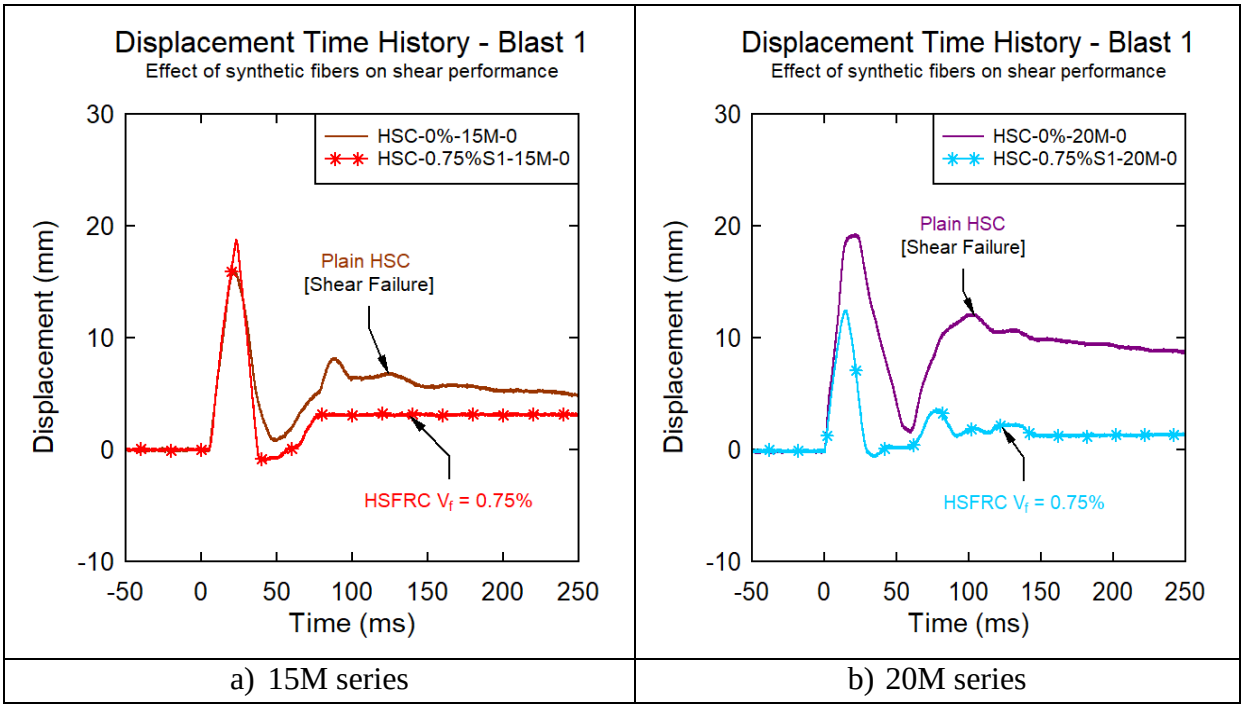

a) 15M series | b) 20M series

Figure 7-8 Displacement time histories; effects of synthetic fibers on shear performance (Series 15M & 20M)

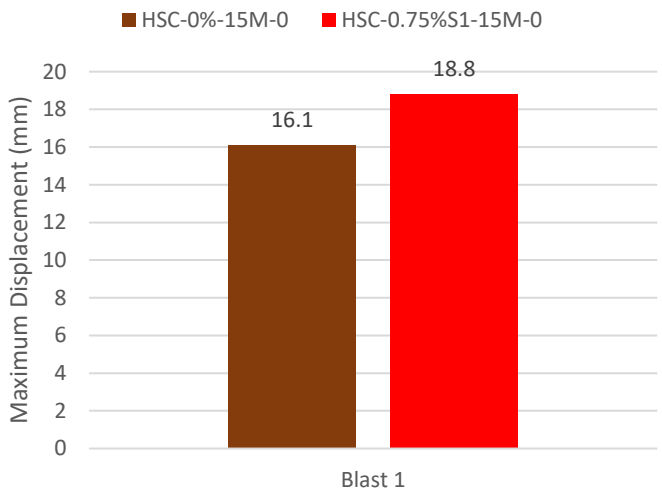

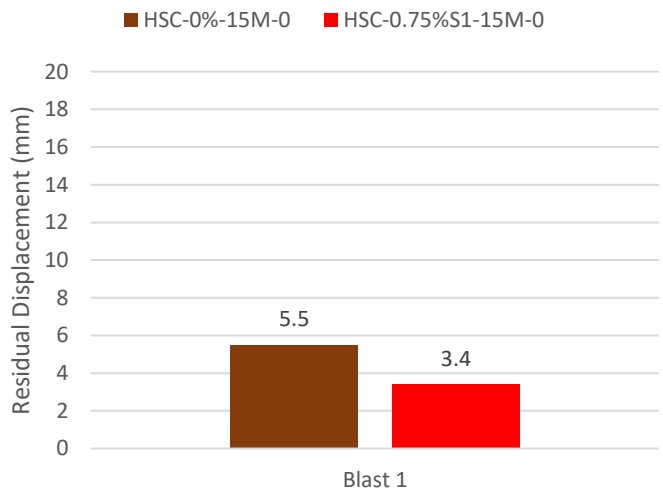

a) 15M series (Maximum & residual displacements)

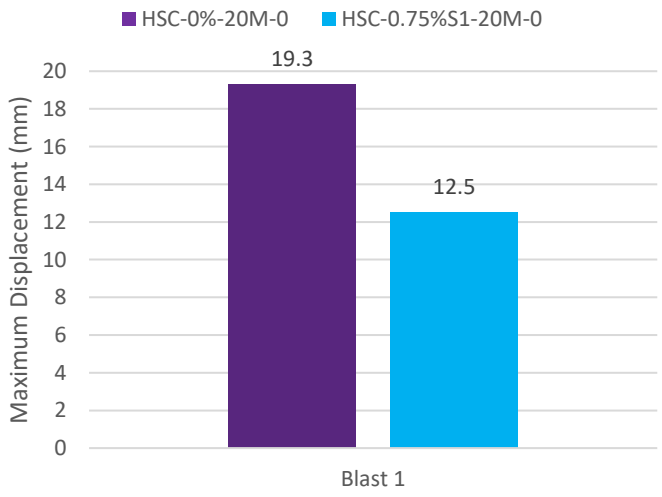

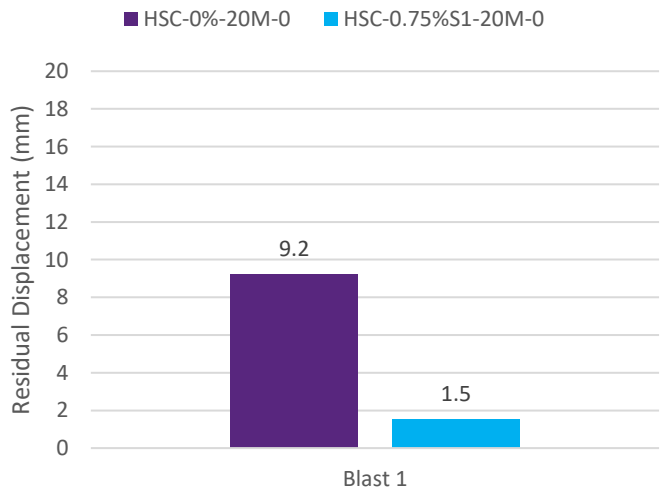

b) 20M series (Maximum & residual displacements)

Figure 7-9 Maximum and residual displacements; effects of synthetic fibers on shear performance (Series 15M & 20M)

a) HSC-0%-15M-0
Blast 1 (30 psi)

b) HSC-0.75%S1-15M-0
Blast 1 (30 psi)

Blast 2a (50 psi)

c) HSC-0%-15M-0
Shear failure
Blast 1 (30 psi)

d) HSC-0.75%S1-15M-0
Hairline flexural-shear crack
Blast 1 (30 psi)

Shear failure
Blast 2a (50 psi)

Figure 7-10 Photographs; effects of synthetic fibers on shear performance (Series 15M)

a) HSC-0%-20M-0*
Blast 1 (30 psi)

b) HSC-0.75%S1-20M-0
Blast 1 (30 psi)

Blast 2b (60 psi)

c) HSC-0%-20M-0*
Shear failure
Blast 1 (30 psi)

d) HSC-0.75%S1-20M-0
Shear crack
Blast 2a (50 psi)

Shear failure
Blast 2b (60 psi)

Figure 7-11 Photographs; effects of synthetic fibers on shear performance (Series 20M)

7.4 Effects of Synthetic Fibers on Flexural Performance (Series 15M & 20M)

The effect of synthetic fibers on flexural response can be examined by comparing the behaviour of beams 1) HSC-0%-15M-S* vs. HSC-0.75%S1-15M-S and 2) HSC-0%-20M-S* vs. HSC-0.75%S1-20M-S. Unlike the previous section, all beams in this comparison were reinforced with stirrups spaced at 100 mm in the shear spans, with steel ratios of ρ = 1.5% and 2.4%, respectively. It is noted that the first beam in each set was built with plain HSC and the second beam built with HSFRC containing 0.75% of S1 fibers. Comparative displacement time histories and bar charts are shown in **Figure 7-12** and **Figure 7-13**, respectively. Relevant photographs are provided in **Figure 7-14** and **Figure 7-16**.

The effect of fibers on blast performance can first be examined by comparing the beam displacements at equivalent blasts. Beginning with the 15M set, it can be observed that the use of synthetic fibers reduced maximum displacement by 22% at Blast 1 – 30 psi. While both beams show similar residual displacements, the fibers significantly reduced the rebound displacement by 41%. The same effect is observed in the 20M set, where the fiber-reinforced concrete specimen shows reductions of 19% and 89% in maximum inbound and rebound deformations. Blast 2a – 50 psi tested all four beams in the inelastic (post-yield) range. As a result, the synthetic fibers reduced maximum and residual displacements, by 76% & 68% in the 15M set, and by 29% & 68% in the 20M set. Likewise, beam HSC-0.75%S1-20M-S shows reductions of 62% and 72% in maximum and residual deformations at Blast 2c – 70 psi. As shown in **Figure 7-12**, beam HSC-0.75%S1-20M-S also shows a noticeable reduction in rebound displacement at Blast 2a – 50 psi.

Compared to the plain HSC beams, the HSFRC beams in both sets were able to resist a greater blast load prior to failure. Failures in the control HSC beams with 15M and 20M bars occurred at Blast 2a – 50 psi (I_r = 516 kPa·ms) and Blast 2c – 70 psi (I_r = 703 kPa·ms), respectively. In both cases, failure was associated with severe crushing and disintegration of concrete in the mid-span compression zone, leading to significant flying debris. The severe failures can be explained by the poor toughness of HSC in compression, as well as the significant rebound during blast testing, which further weakened the unreinforced "compression" zone. In comparison, significantly improved damage tolerance is observed in the FRC companions as illustrated in **Figure 7-14** and **Figure 7-16**. As a result, failure was delayed to Blast 2c – 70 psi (I_r = 712 kPa·ms) and Blast 3a – 80 psi (I_r = 832 kPa·ms) for the FRC beams with 15M and 20M bars, respectively.

Coughlin et al. (2010) and Richardson et al. (2016) previously reported that the improved toughness and fragmentation resistance of synthetic fiber-reinforced concrete make it suitable to increase the damage tolerance of reinforced concrete members subjected to extreme loads. The ability of fibers to delay crushing/spalling and prevent the formation of blast fragments is clear in the high-speed video stills of the 15M series beams shown in **Figure 7-15**.

In the 20M series, the fibers also controlled crushing at Blast 2c (70 psi), although beam HSC-0.75%S1-20M-S suffered more noticeable damage in the mid-span region at the next blast (Blast 3a – 80 psi). The increased damage can partly be attributed to the repeated testing, combined

with the extreme blast pressure applied on this specimen. Nonetheless, no spalling of cover concrete occurred despite the large residual deformation experienced by this specimen.

In summary, the results show that the provision of synthetic fibers leads to flexural strength enhancements in HSC beams, which results in improved control of displacements at equivalent blasts and an ability to resists higher blast loads before failure. The enhancements can be attributed to the ability of fibers to increase toughness of HSC in compression and increase post-cracking resistance in tension. The use of fibers was also very effective in increasing damage tolerance by controlling severe concrete crushing and eliminating spalling in the mid-span beam region.

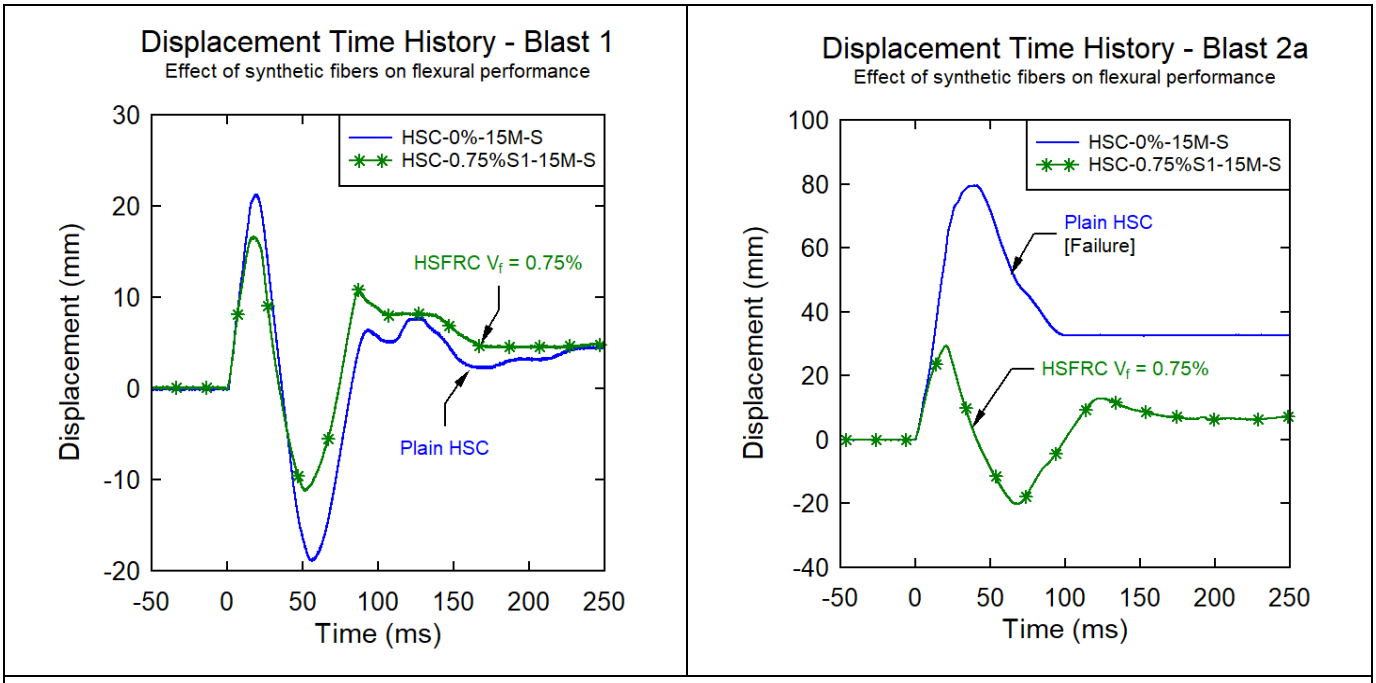

a) 15M series (Blast 1 – 2a)

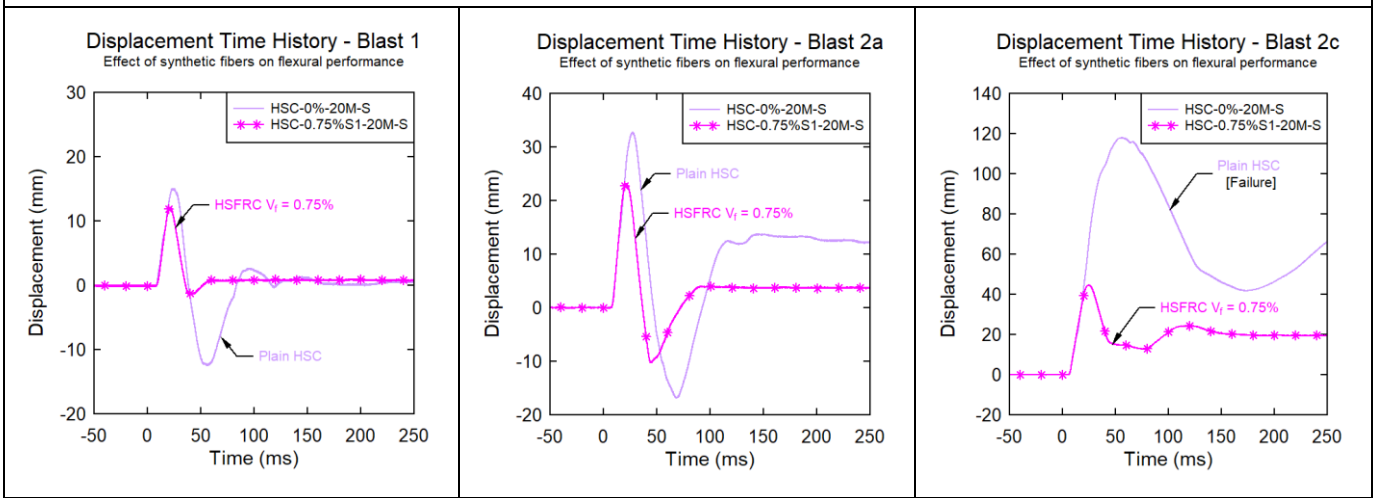

b) 20M series (Blast 1 – 2c)

Figure 7-12 Displacement time histories; effects of synthetic fibers on flexural performance (Series 15M & 20M)

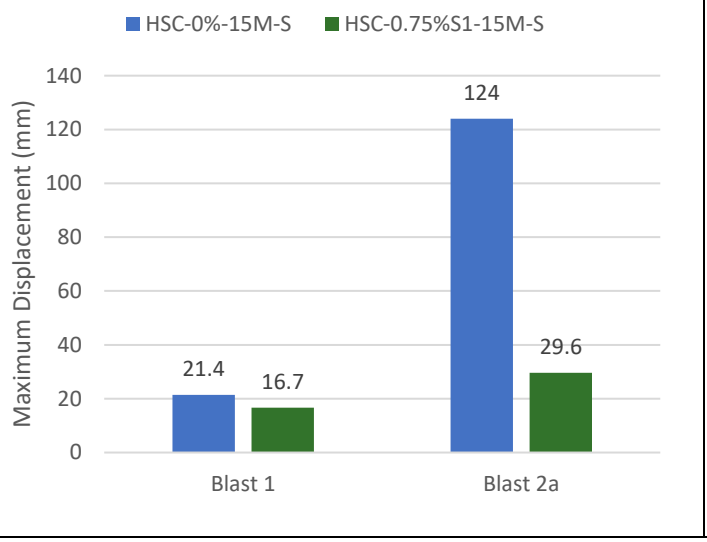

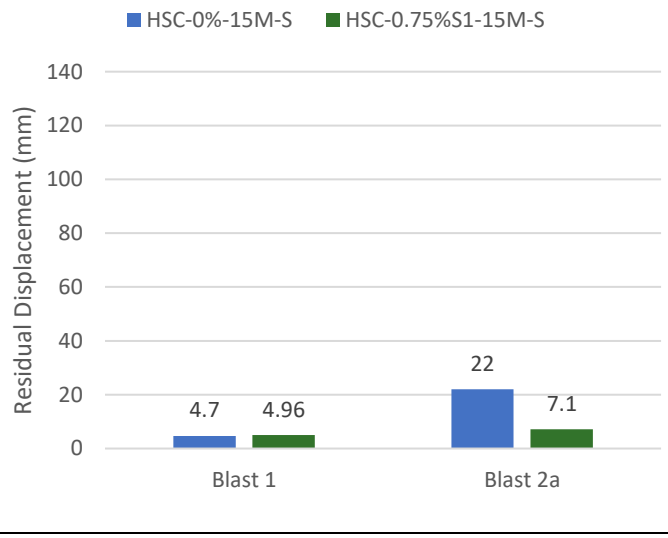

a) 15M series (Maximum & residual displacements – all blasts)

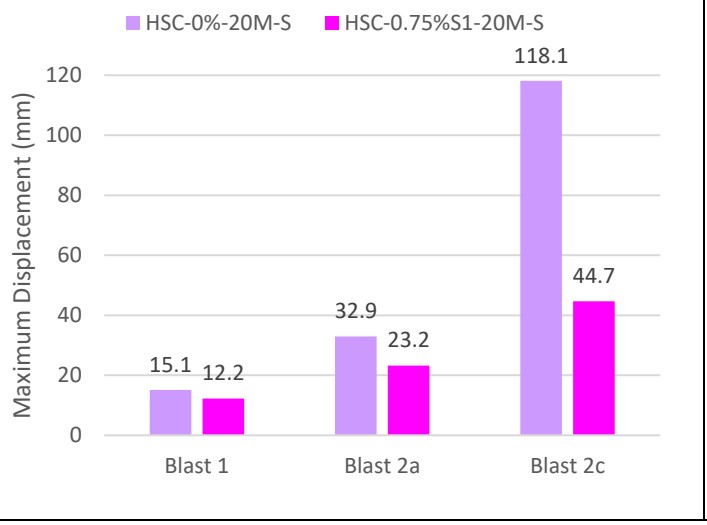

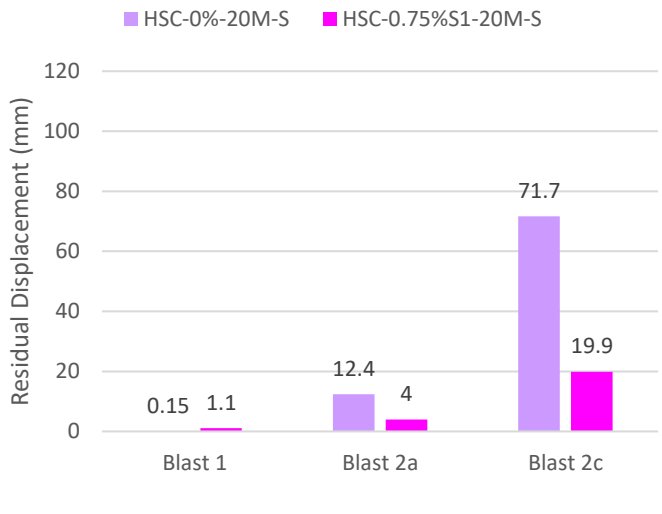

b) 20M series (Maximum & residual displacements – all blasts)

Figure 7-13 Maximum and residual displacements; effects of synthetic fibers on flexural performance (Series 15M & 20M)

a) HSC-0%-15M-S*

Blast 2a (50 psi)

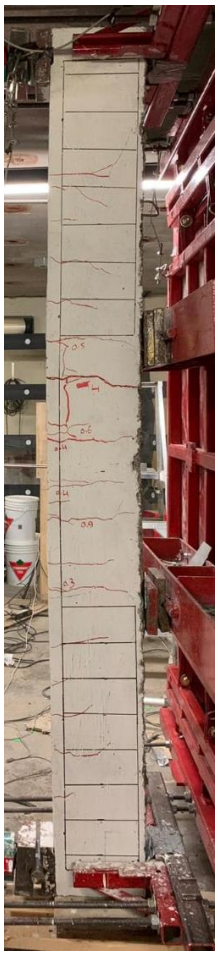

b) HSC-0.75%S1-15M-S

Blast 2a (50 psi)

Blast 2c (70 psi)

c) HSC-0%-15M-S*

Mid-span crushing

Blast 2a (50 psi)

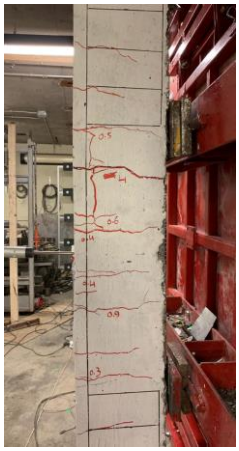

d) HSC-0.75%S1-15M-S

Mid-span cracking

Blast 2a (50 psi)

Mid-span fiber pullout

Blast 2c (70 psi)

Figure 7-14 Photographs; effects of synthetic fibers on flexural performance (Series 15M)

a) HSC-0%-15M-S*
Blast 2a (50 psi)

b) HSC-0.75%S1-15M-S
Blast 2c (70 psi)

Figure 7-15 High-speed videos showing secondary blast fragments (Series 15M)

a) HSC-0%-20M-S*	b) HSC-0.75%S1-20M-S	
Blast 2c (70 psi)	Blast 2c (70 psi)	Blast 3a (80 psi)

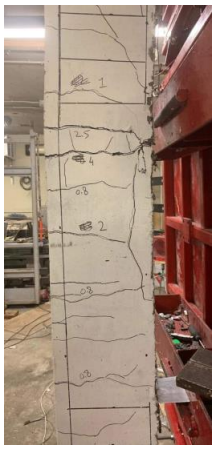

c) HSC-0%-20M-S* Mid-span crushing Blast 2c (70 psi)	d) HSC-0.75%S1-20M-S	
	Mid-span crushing Blast 2c (70 psi)	Mid-span crushing & fiber pullout Blast 3a (80 psi)

Figure 7-16 Photographs; effects of synthetic fibers on flexural performance (Series 20M)

7.5 Effects of Hybrid Fibers

As noted in the previous sections, the use of 0.75% synthetic fibers was not sufficient to prevent shear failure under blast loads. Similarly, under static loads, the use of 0.75% fibers allowed for sustained post-yield deformations, however the low-modulus synthetic fibers eventually pulled-out at the critical shear crack. Previous research indicates that 1% fibers is the minimum required to replace stirrups and ensure ductile response in HSC beams (Tahenni et al., 2016; Biolzi et al., 2017). Likewise, Conforti et al. (2015) reported that 1.45% polypropylene synthetic fibers were required to completely substitute the minimum shear reinforcement and ensure ductile flexural response in wide-shallow beams. Previous research also indicates that the use of hybrid fibers results in a synergy effect that improves the properties of concrete under both static and dynamic loads (Pakravan et al., 2017; Drdlova et al., 2018).

The effect of increased fiber content and hybrid fibers is investigated by comparing the results of beams HSC-HYB-20M-0 and HSC-0.75%S1-20M-0, which had similar properties (20M bars, no stirrups and 0.75%S1 fibers), except for the addition of smooth straight steel fibers at a ratio of 0.25% in the HSC-HYB-20M-0 specimen. For comparison, the response of the hybrid beam (no stirrups) is also compared to beams HSC-0%-20M-S* and HSC-0.75%S1-20M-S which were designed with stirrups, and plain HSC/0.75% HSFRC, respectively. Comparative displacement time histories and bar charts for these beams are shown in **Figure 7-17** and **Figure 7-18**, respectively. Relevant photographs are provided in **Figure 7-19**.

Comparing to beam HSC-0.75%S1-20M-0, it can be observed that the beam with hybrid fibers showed increased blast capacity, with failure occurring at Blast 3a – 80 psi (I_r = 853 kPa·ms) compared to Blast 2b – 60 psi (I_r = 653 kPa·ms). More importantly, adding 0.25% of steel fibers to the FRC mix transformed the failure mode from shear to flexure, resulting in a more ductile response and an ability to substitute for transverse reinforcement.

The hybrid FRC beam also outperformed the companion HSC and HSFRC beams designed with stirrups, both in terms of displacement control and overall blast performance. The advantage of hybrid fibers is pronounced at Blasts 2a (50 psi) and Blasts 2c (70 psi), with reductions of 30% & 65% and 57% & 78% in maximum and residual deformations when compared to beam HSC-0%-20M-S* (plain HSC and stirrups). Similarly, the hybrid fibers allowed the HSC-HYB-20M-0 beam to successfully survive one more blast before failure (failure at Blast 3a – 80 psi, I_r = 853 kPa·ms vs. failure at Blast 2c – 70 psi, I_r = 703 kPa·ms for the plain HSC companion).

A similar trend is observed when comparing the results to beam HSC-0.75%S1-20M-S, where the hybrid fibers allow for reductions of 8% & 22% in maximum and residual deformations at Blast 2c – 70 psi, and 68% & 82% at Blast 3a – 80 psi. Even though both beams failed at Blast 3a, the hybrid beam shows significant reduction in damage when compared to the HSFRC beam built with stirrups and mono fibers as shown in **Figure 7-20**. The high-speed video shows that concrete crushing in beam HSC-0.75%S1-20M-S results in significant crushing and flying debris at failure.

In conclusion, the combined use of macro-synthetic fibers and micro-steel fibers resulted in significant enhancements in performance which outperformed that of companion beams built with and without stirrups. In addition to reducing maximum and residual displacements at equivalent subsequent blasts, the hybrid fibers increased shear capacity and prevented shear failure, despite the lack of transverse reinforcement. The use of hybrid fibers was also very effective in controlling damage. The enhancements clearly demonstrate the synergy that can be gained when using hybrid fibers in HSC, where the micro and macro fibers work together to arrest the formation of cracks, delay fiber pullout, and increase the toughness of HSC in compression and flexure.

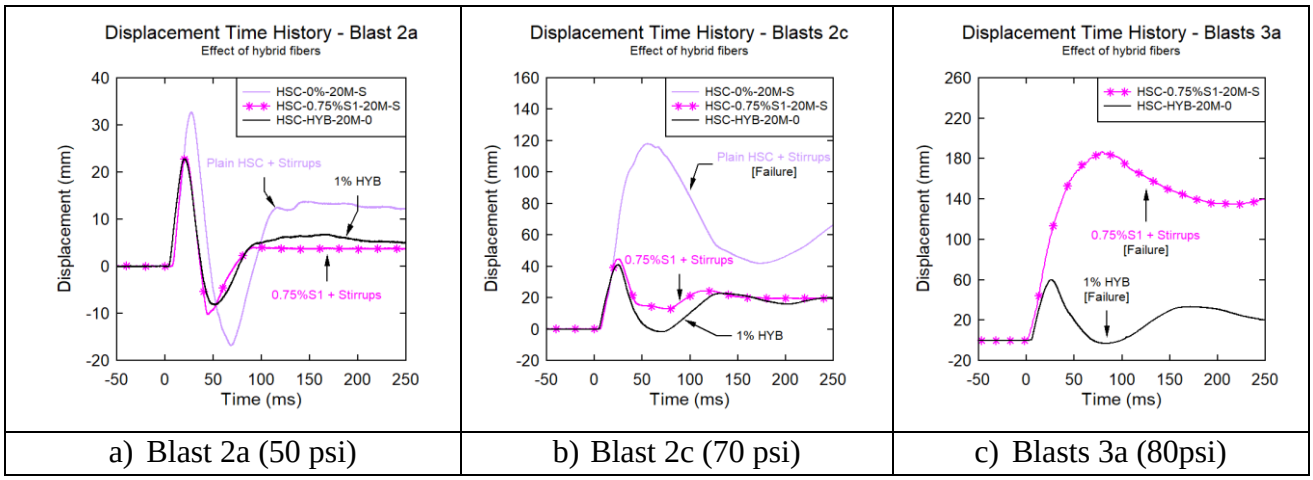

a) Blast 2a (50 psi) | b) Blast 2c (70 psi) | c) Blasts 3a (80psi)

Figure 7-17 Displacement time histories; effects of hybrid fibers

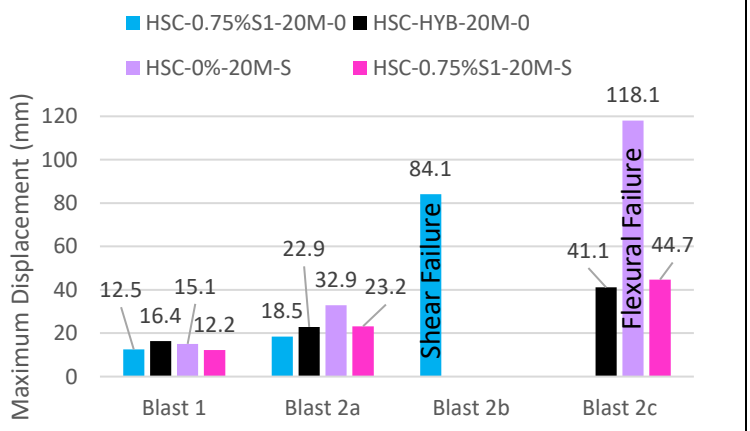

a) Maximum displacements (all blasts)

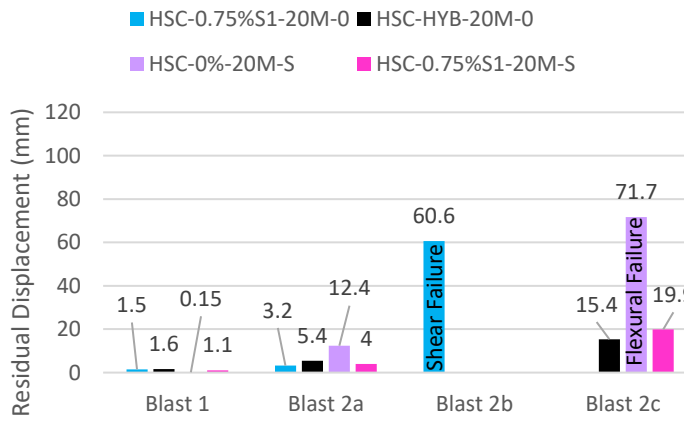

b) Residual displacements (all blasts)

Figure 7-18 Maximum and residual displacements; effects of hybrid fibers

				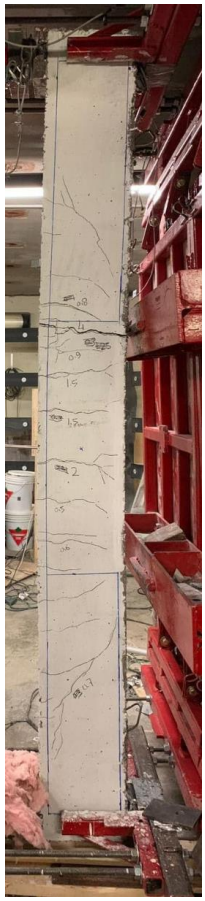	
a) HSC-0.75%S1-20M-0	b) HSC-0%-20M-S*	c) HSC-0.75%S1-20M-S		d) HSC-HYB-20M-0	
Blast 2b (60 psi)	Blast 2c (70 psi)	Blast 2c (70 psi)	Blast 3a (80 psi)	Blast 2c (70 psi)	Blast 3a (80 psi)

		
e) HSC-0.75%S1-20M-0 Shear failure Blast 2b (60 psi)	f) HSC-0.75%S1-20M-S Mid-span crushing & fiber pullout Blast 3a (80 psi)	g) HSC-HYB-20M-0 Mid-span fiber pullout Blast 3a (80 psi)

Figure 7-19 Photographs; effects of hybrid fibers

a) HSC-0.75%S1-20M-S
Blast 3a (80 psi)

b) HSC-HYB-20M-0
Blast 3a (80 psi)

Figure 7-20 High-speed videos showing secondary blast fragments

7.6 Effects of Reinforcement Ratio

Previous research indicates that the blast and impact resistance of conventional and steel fiber-reinforced HSC beams is affected by the longitudinal steel ratio (Algassem, 2016). The influence of this parameter in beams built with synthetic fibers can be investigated in the following two sets of specimens: 1) HSC-0.75%S1-15M-0 and HSC-0.75%S1-20M-0 and 2) HSC-0.75%S1-15M-S and HSC-0.75%S1-20M-S. The beams in both sets were built with HSFRC having 0.75%S1 fibers, but were reinforced with 2-15M (ρ = 1.5%) and 2-20M (ρ = 2.4%), respectively.

The results of beams HSC-0.75%S1-15M-0 and HSC-0.75%S1-20M-0 are first compared to study the influence of steel reinforcement ratio in HSFRC beams built without transverse reinforcement. Comparative displacement time histories and bar charts are shown in **Figure 7-21** and **Figure 7-22**, respectively. Relevant photographs are provided in **Figure 7-23**. It can be observed that the increase in steel ratio resulted in reductions of 34% and 56% in maximum and residual displacements at Blast 1 – 30 psi for the beam with 20M vs. 15M bars. The overall blast capacity was also affected by increasing the steel ratio. Failure of beam HSC-0.75%S1-15M-0 occurred at Blast 2a – 50 psi (I_r = 554 kPa·ms) while the use of 20M rebar delayed failure until Blast 2b – 60 psi (I_r = 653 kPa·ms). Both beams experienced similar shear failures due to complete fiber pullout at the bottom shear spans. The static tests showed that the use of synthetic fibers allowed both beams to reach their ultimate flexural capacity (with maximum loads of 99 and 160 kN at yielding) and this can explain the increased blast resistance of beam HSC-0.75%S1-20M-0.

The benefit of increased steel ratio is further studied by comparing the responses of beams HSC-0.75%S1-15M-S and HSC-0.75%S1-20M-S which showed flexural dominant blast behavior due to the combined use of fibers and stirrups. Comparative displacement time histories and bar charts are shown in **Figure 7-24** and **Figure 7-25**, respectively. Relevant photographs are provided in **Figure 7-26**. As expected, the use of larger reinforcement ratio significantly reduced the magnitude of mid-span displacements at equivalent blasts. For instance, the maximum and residual deformations of the 20M beam were reduced by 27% and 79% for Blast 1 – 30 psi, with reductions of 22% and 44% for Blast 2a – 50 psi, when compared to the beam with 15M bars. At Blast 2c – 70 psi, the reductions reach 48% for maximum displacement, with a 52% decrease in residual displacement. It can also be observed that increasing the reinforcement ratio significantly reduced the maximum rebound displacement at Blasts 1 – 30 psi and 2a – 50 psi.

As illustrated in **Figure 7-26**, the use of larger bars also reduced crack widths at equivalent blasts. In addition, the beam with 20M bars shows greater blast resistance, with failure in beams HSC-0.75%S1-15M-S and HSC-0.75%S1-20M-S occurring at Blast 2c – 70 psi (I_r = 712 kPa·ms) and Blast 3a – 80 psi (I_r = 832 kPa·ms), respectively. However, examining the photos in **Figure 7-26**, it can be seen that the beam reinforced with 20M bars shows more prominent damage at failure with concrete crushing in the mid-span region due to the increase in blast impulse. Algassem (2016) previously noted that increasing the steel ratio in conventional HSC beams improved control of displacements and overall blast capacity but increased the extent of damage

at failure, which corresponds to the observation in the current study. Similar conclusions have been reported by other researchers for beams tested under impact. Among them, Adhikary et al. (2012) reported that the use of larger bars improved impact response by reducing maximum deflections, but resulted in greater damage near the point of impact. Other researchers like Zhan et al. (2015), Yoo et al. (2015) and Louw et al. (1992) have reported similar conclusions.

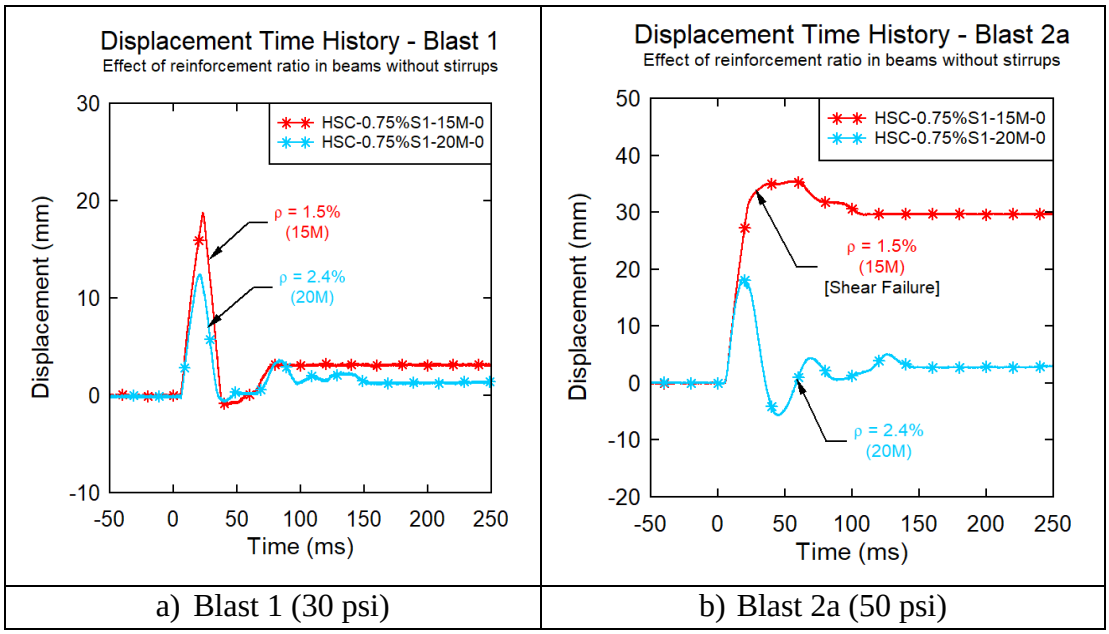

a) Blast 1 (30 psi) | b) Blast 2a (50 psi)

Figure 7-21 Displacement time histories; effects of reinforcement ratio (Without stirrups)

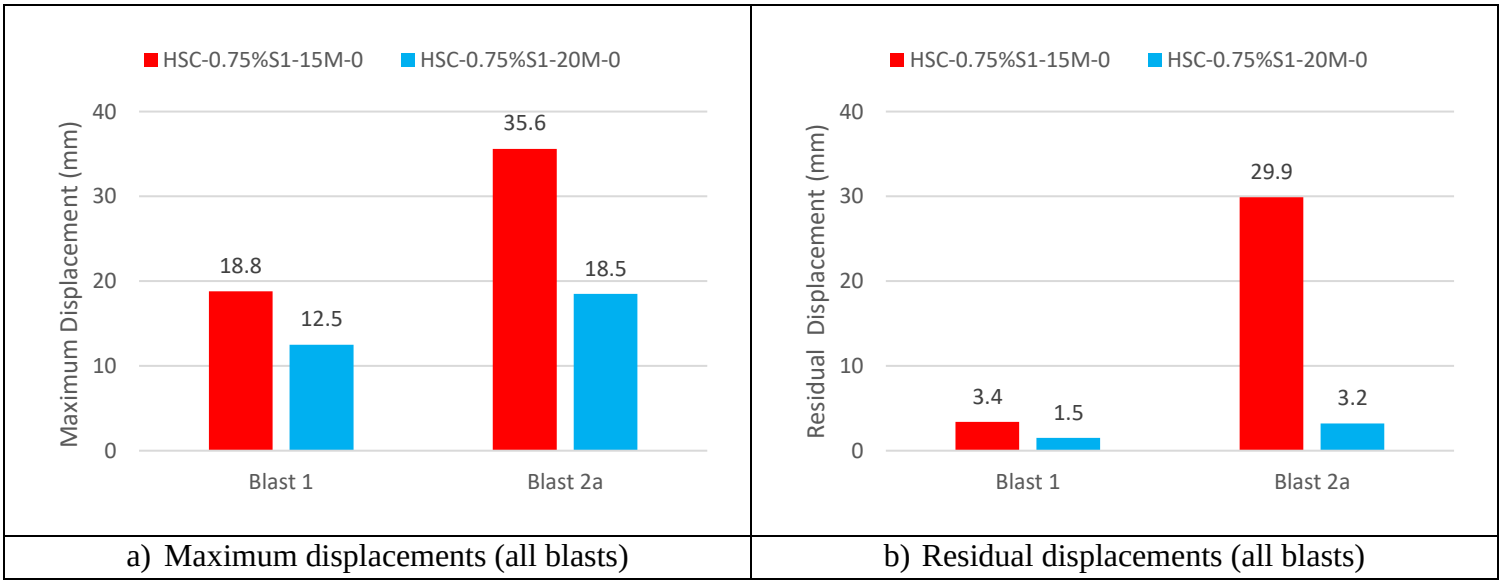

a) Maximum displacements (all blasts) | b) Residual displacements (all blasts)

Figure 7-22 Maximum and residual displacements; effects of reinforcement ratio (Without stirrups)

a) HSC-0.75%S1-15M-0
Blast 2a (50 psi)

b) HSC-0.75%S1-20M-0
Blast 2a (50 psi)

b) HSC-0.75%S1-20M-0
Blast 2b (60 psi)

c) HSC-0.75%S1-15M-0
Shear failure
Blast 2a (50 psi)

d) HSC-0.75%S1-20M-0
Shear crack
Blast 2a (50 psi)

d) HSC-0.75%S1-20M-0
Flexural-shear failure
Blast 2b (60 psi)

Figure 7-23 Photographs; effects of reinforcement ratio (Without stirrups)

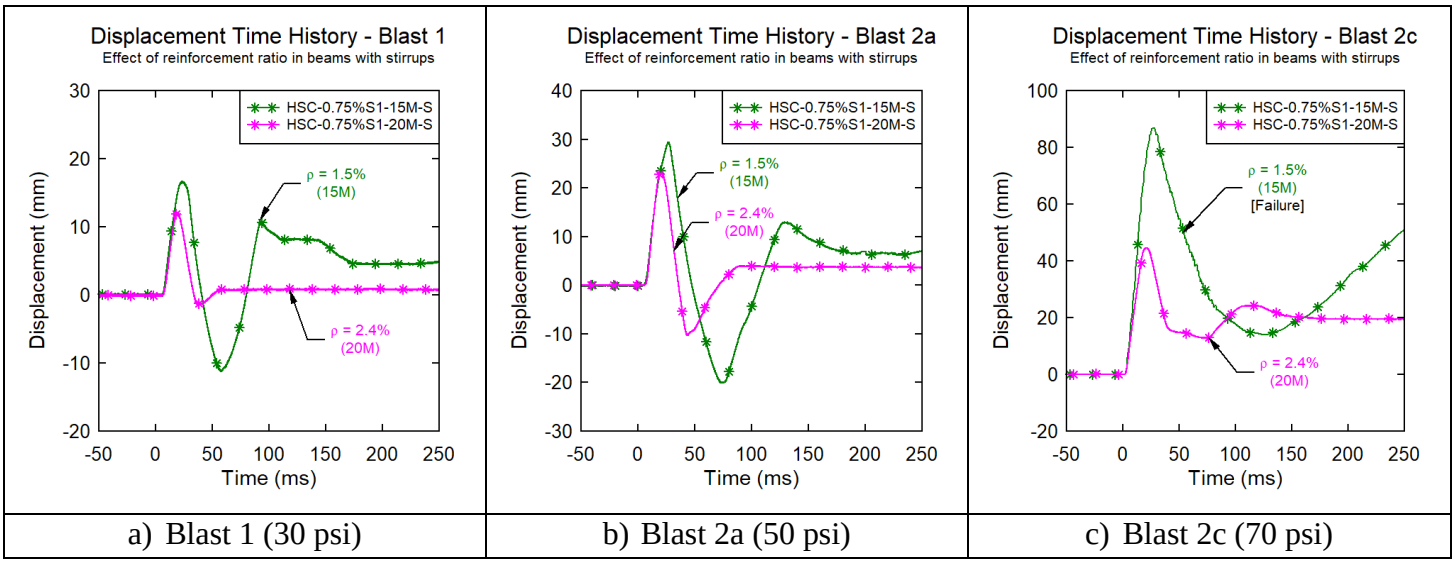

a) Blast 1 (30 psi) | b) Blast 2a (50 psi) | c) Blast 2c (70 psi)

Figure 7-24 Displacement time histories; effects of reinforcement ratio (With stirrups)

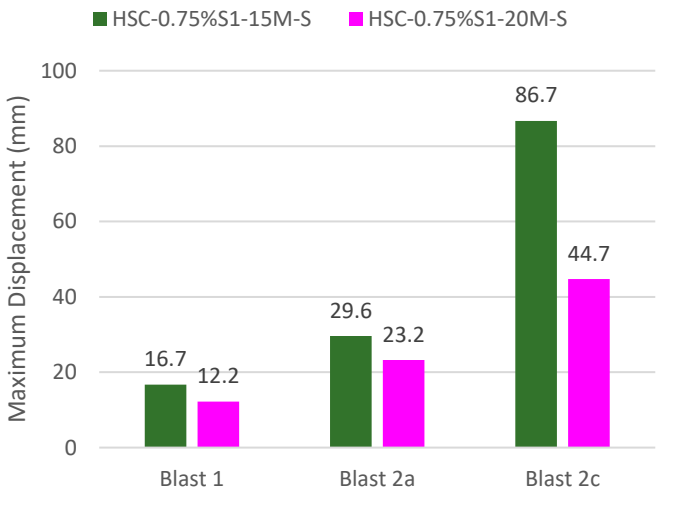

a) Maximum displacements (all blasts)

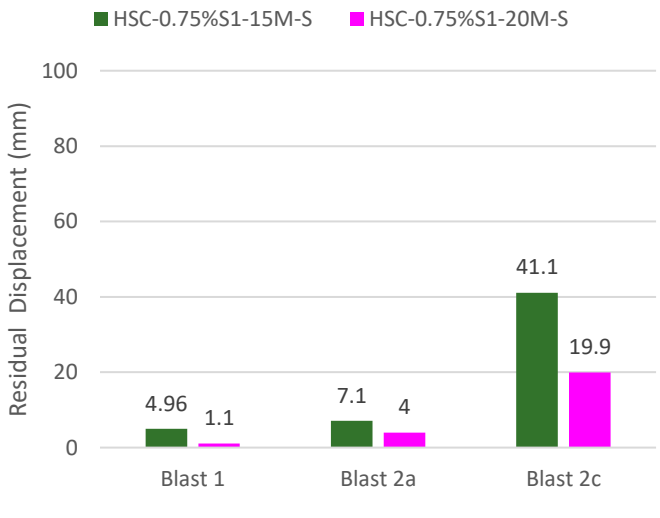

b) Residual displacements (all blasts)

Figure 7-25 Maximum and residual displacements; effects of reinforcement ratio (With stirrups)

a) HSC-0.75%S1-15M-S	b) HSC-0.75%S1-20M-S	
Blast 2c (70 psi)	Blast 2c (70 psi)	Blast 3a (80 psi)

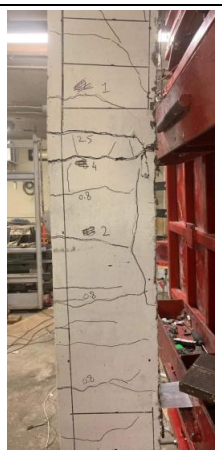

c) HSC-0.75%S1-15M-S Mid-span fiber pullout Blast 2c (70 psi)	d) HSC-0.75%S1-20M-S	
	Mid-span crushing Blast 2c (70 psi)	Mid-span crushing & fiber pullout Blast 3a (80 psi)

Figure 7-26 Photographs; effects of reinforcement ratio (With stirrups)

7.7 Effects of Steel Type in Beams with Synthetic Fibers

Previous research by Li and Aoude (2019a) has shown that the use of high-strength steel can significantly increase the blast resistance of high-strength concrete beams. Li and Aoude (2019b) have also shown that the use of such reinforcement improves the blast resistance of steel FRC beams. The effect of steel type in HSC beams built with synthetic fibers is examined by comparing the behaviour of beams HSC-0.75%S1-15M-S and HSC-0.75%S1-No.5(HS)-S, which were constructed with 15M conventional (Grade 400 MPa) and No.5 high-strength (Grade 690 MPa) reinforcement, respectively. Comparative displacement time histories and bar charts are shown in **Figure 7-27** and **Figure 7-28**. Relevant photographs are provided in **Figure 7-29**.

Both beams have similar displacements at Blast 1 – 30 psi, though the beam with high-strength bars shows a noticeable reduction in maximum rebound displacement. The next two shots brought the beam with normal-strength bars into the inelastic range. As a result, the specimen with HS reinforcement shows reductions of 25% & 56% in maximum deformations, and corresponding decreases of 82% & 78% in residual displacements, at Blasts 2a – 50 psi and 2c – 70 psi respectively. Similar to the observation at Blast 1, the high-strength bars also improved control of the rebound displacement at Blast 2a.

Reinforcement type also affected the blast capacity, with beam HSC-0.75%S1-No.5(HS) surviving one more blast prior to failure. Failure in the beams with NS and HS reinforcement occurred at Blasts 2c – 70 psi and 3b – 90 psi (I_r = 712 and 876 kPa·ms), respectively. Failure in both beams was associated with concrete crushing at mid-span compression zone. However, the failure photos and high-speed videos in **Figure 7-30** indicate that the HSC-0.75%S1-No.5(HS)-S beam suffered a more severe failure due to increased strain demands imposed by the high-strength reinforcement on the mid-span compression zone. Nonetheless, prior to failure, the use of HS reinforcement was able to better control major flexural crack widths at equivalent blasts. For example, the maximum crack width reached 13 and 1.25 mm at Blast 2c – 70 psi for the beams with NS and HS steel, respectively. The reduction in crack width can be explained by the reduced tensile strains in the high-strength reinforcement under equivalent applied loads. This same effect has previously been observed by Li (2016), where combining HS steel and 1% steel fibers resulted in significant improvements in blast performance when compared to NS reinforcement.

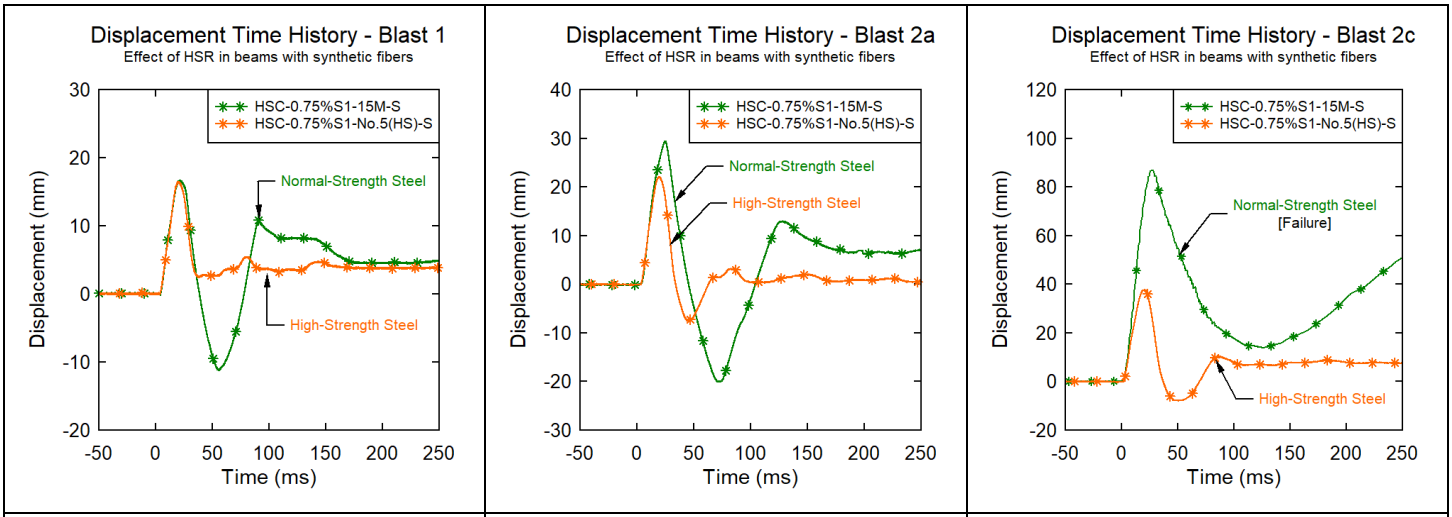

a) Blast 1 (30 psi) | b) Blast 2a (50 psi) | c) Blast 2c (70 psi)

Figure 7-27 Displacement time histories; effects of HSR in beams with synthetic fibers

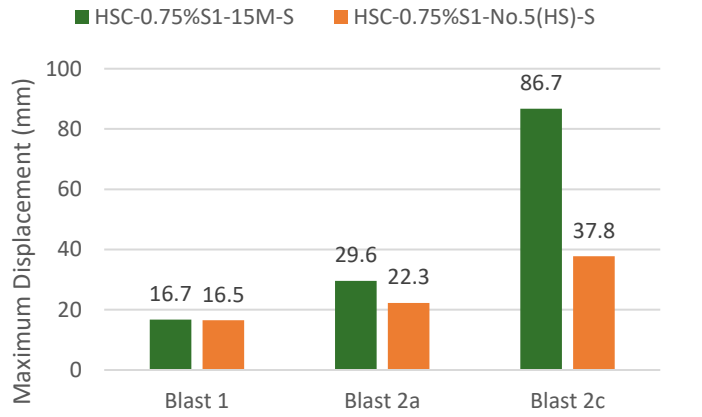

a) Maximum displacements – inbound (all blasts)

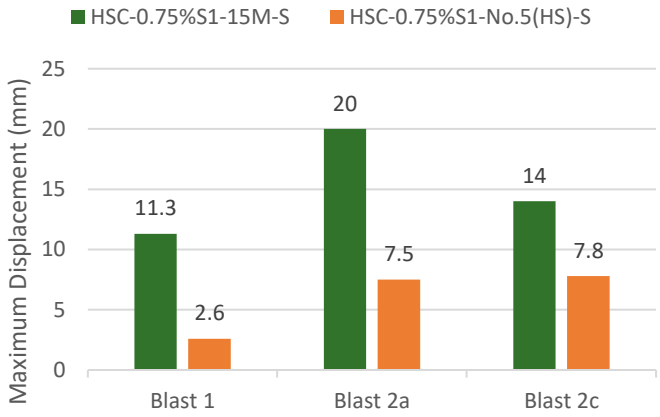

b) Maximum displacements – rebound (all blasts)

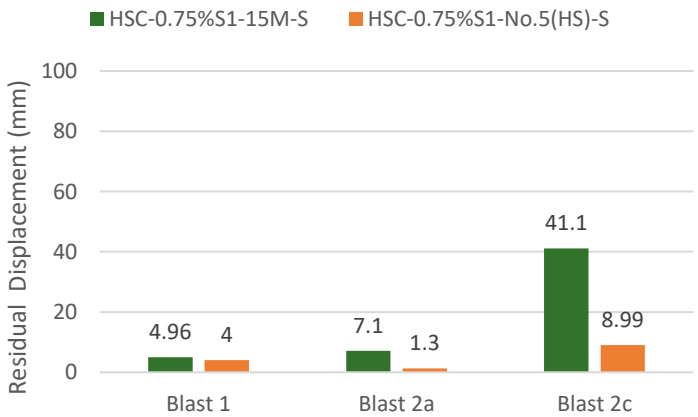

c) Residual displacements (all blasts)

Figure 7-28 Maximum and residual displacements; effects of HSR in beams with synthetic fibers

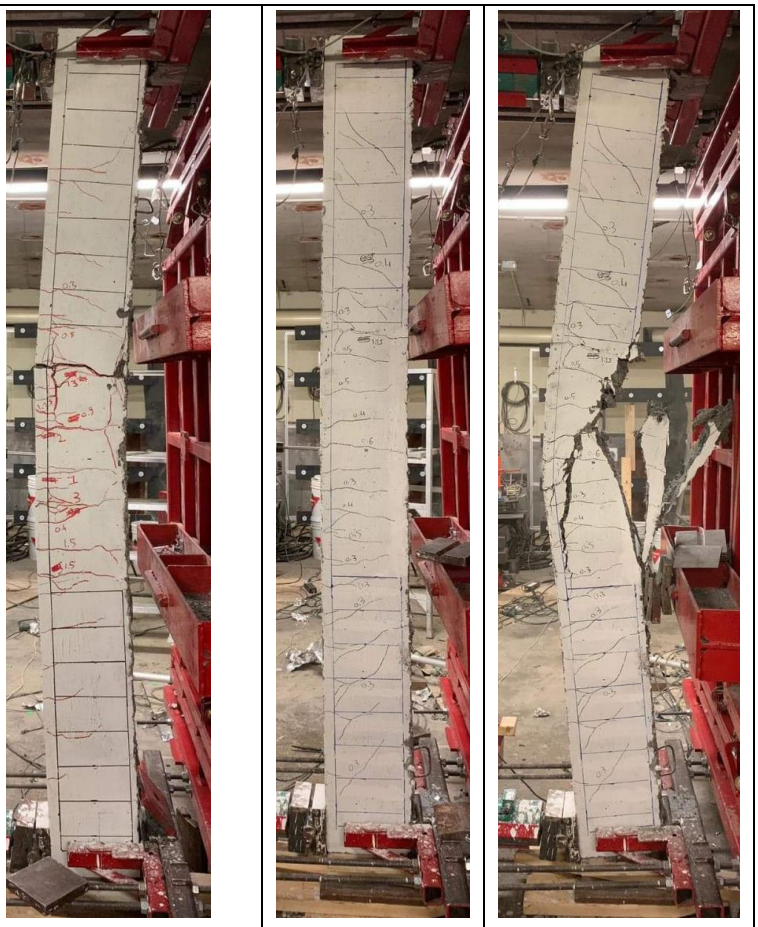

a) HSC-0.75%S1-15M-S	b) HSC-0.75%S1-No.5(HS)-S	
Blast 2c (70 psi)	Blast 2c (70 psi)	Blast 3b (90 psi)

Figure 7-29 Photographs; effects of HSR in beams with synthetic fibers

a) HSC-0.75%S1-15M-S Blast 2c (70 psi)	b) HSC-0.75%S1-No.5(HS)-S Blast 3b (90 psi)

Figure 7-30 High-speed videos showing secondary blast fragments

7.8 Effects of Synthetic Fibers in Beams with Grade 690 MPa Reinforcement

This comparison examines the effect of synthetic fibers on the response of HSC beams reinforced with Grade 690 MPa high-strength bars. Specimens HSC-0%-No.5(HS)-S[†], tested by Li and Aoude (2019), and HSC-0.75%S1-No.5(HS)-S, from the current study, are used for comparison. Both high-strength steel beams had similar properties, but were designed with plain HSC and HSFRC containing 0.75% synthetic fibers, respectively. Comparative displacement time histories and bar charts are shown in **Figure 7-31** and **Figure 7-32**, respectively (tension steel strain data is also presented in **Figure 7-33**). Relevant photographs are provided in **Figure 7-34**.

A review of the displacement results shows that the two beams had similar maximum and residual displacements at Blast 1 – 30 psi, since their response remained in the elastic range. At Blast 2a – 50 psi, the use of synthetic fibers reduced maximum displacement by 17% when compared to the control HSC beam, while the residual displacements remained similar. Examination of the strain gauge data in **Figure 7-33** shows that the reinforcement in both beams remained close, but just below yield levels during these blasts (as also confirmed by the low residual displacements; see **Figure 7-32b**). Nonetheless, the HSFRC beam shows important reductions in rebound displacement control at Blasts 1 – 30 psi and 2a – 50 psi due to the enhanced toughness and stiffness of HSFRC.

The next shot brought both beams closer to the inelastic range. As a result, the beam with synthetic fibers shows significant reductions of 42% and 55% in maximum and residual displacements when compared to the control beam at Blast 2c – 70 psi. It can also be observed that the use of synthetic fibers allowed the high-strength reinforcement to reach post-yield levels as shown in **Figure 7-33** (in comparison the beam with plain HSC fails prior to yielding).

The control HSC beam failed at Blast 2c – 70 psi (I_r = 750 kPa·ms) due to severe concrete crushing in the mid-span zone. Moreover, the beam shows important cover concrete spalling, leading to significant flying debris at failure, as shown in in **Figure 7-34**. In comparison, the HSFRC specimen withstood one more blast, successfully resisting crushing and spalling at Blast 2c. However, subsequent testing at Blast 3b resulted in beam failure (I_r = 876 kPa·ms). **Figure 7-35** compares high-speed video stills showing the failure process in the plain HSC and HSFRC beams. The stills show that despite the relatively severe failure in the HSFRC specimen during the final shot (Blast 3b), the cover concrete at mid-span did not spall. Blast fragments are also clearly reduced when compared to the plain HSC beam. The results further confirm the ability of fibers to enhance the toughness and tensile resistance of high-strength concrete, which results in improved fragmentation resistance and damage tolerance.

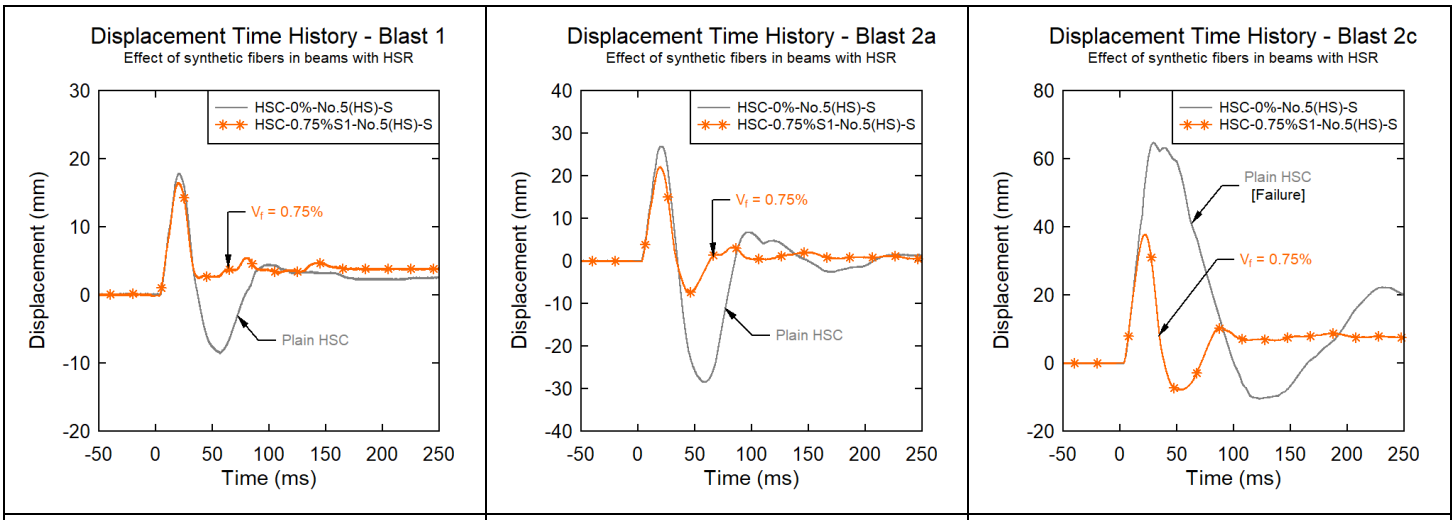

a) Blast 1 (30 psi) | b) Blast 2a (50 psi) | c) Blast 2c (70 psi)

Figure 7-31 Displacement time histories; effects of synthetic fibers in beams with HSR

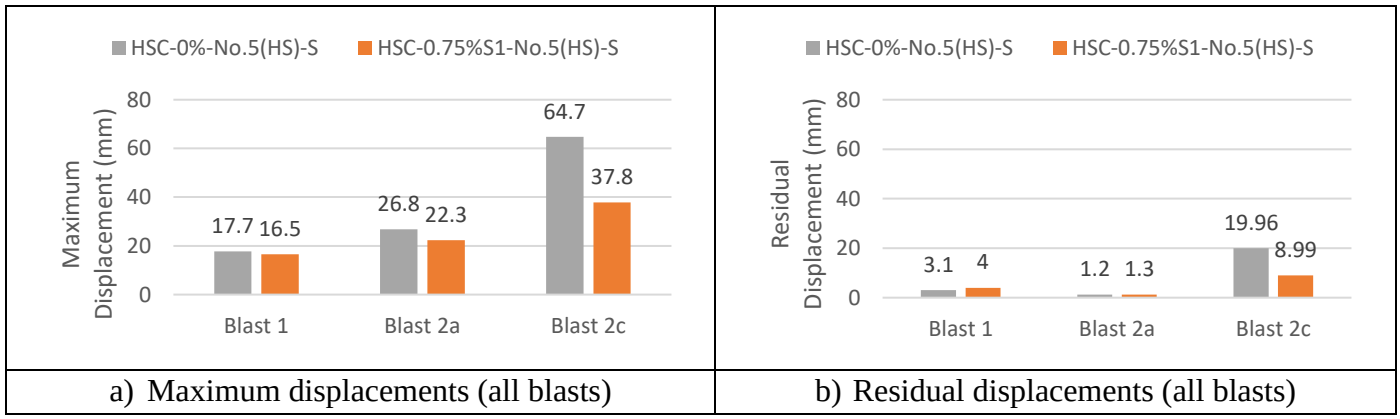

a) Maximum displacements (all blasts) | b) Residual displacements (all blasts)

Figure 7-32 Maximum and residual displacements; effects of synthetic fibers in beams with HSR

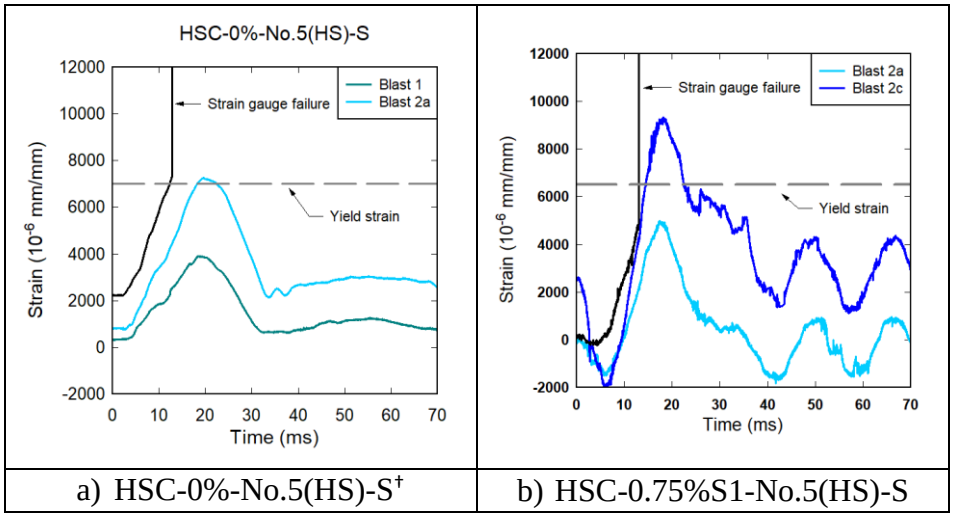

a) HSC-0%-No.5(HS)-S† | b) HSC-0.75%S1-No.5(HS)-S

Figure 7-33 Tensile strain in rebar

a) HSC-0%-No.5(HS)-S[†]
Blast 2c (70 psi)

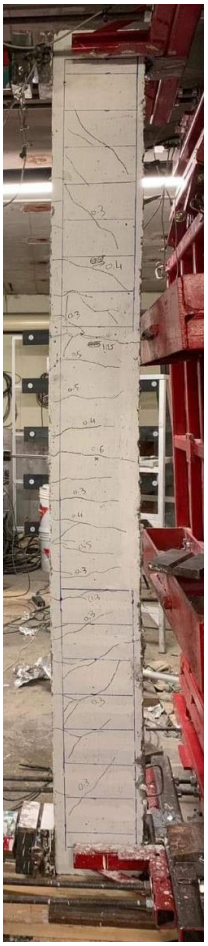

b) HSC-0.75%S1-No.5(HS)-S
Blast 2c (70 psi)

Blast 3b (90 psi)

c) HSC-0%-No.5(HS)-S[†]
Mid-span spalling
Blast 2c (70 psi)

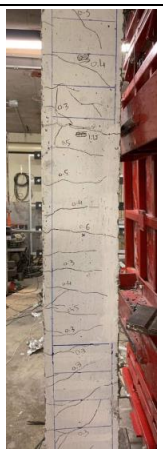

d) HSC-0.75%S1-No.5(HS)-S
Crack widening
Blast 2c (70 psi)

Mid-span crushing
Blast 3b (90 psi)

Figure 7-34 Photographs; effects of synthetic fibers in beams with HSR

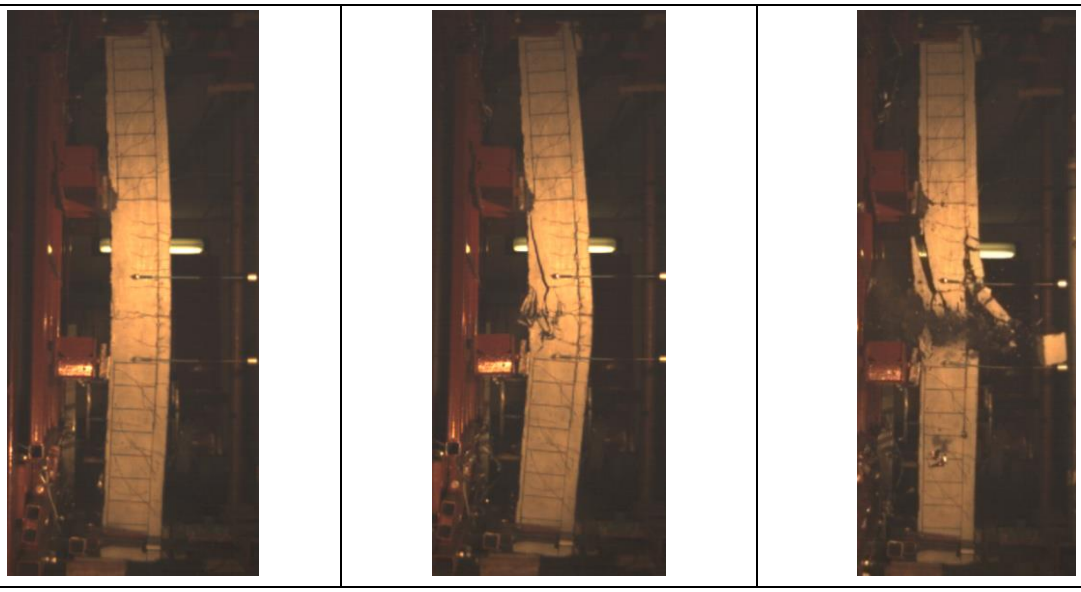

a) HSC-0%-No.5(HS)-S[†]
Blast 2c (70 psi)

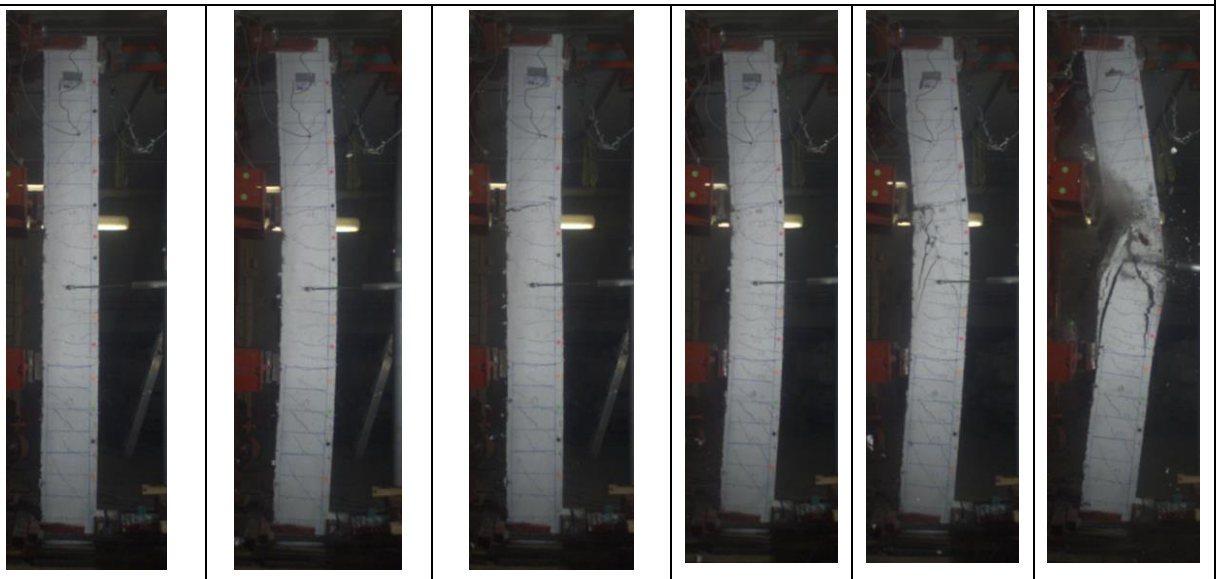

b) HSC-0.75%S1-No.5(HS)-S
Blast 2c (70 psi)

c) HSC-0.75%S1-No.5(HS)-S
Blast 3b (90 psi)

Figure 7-35 High-speed videos showing secondary blast fragments

7.9 Effects of Fibers and Detailing

7.9.1 Effects of Detailing in HSFRC Beams

To improve the blast resistance of reinforced concrete beams, modern blast codes such as the CSA S850 Blast Standard (CSA, 2012) impose stringent requirements for the detailing of the steel reinforcement. This section examines the effects of improved detailing on the blast behaviour of FRC beams by comparing the results of beams with nominal and intermediate blast detailing:

- **HSC-0.75%S1-20M-S:** Single reinforcement (20M bars in tension) with open-stirrups spaced at s = 100 mm (d/2) in the shear spans only; and
- **HSC-0.75%S1-20M-10M-d/2:** Double reinforcement (20M bars in tension and 10M bars in compression) with closed hoops spaced at s = 100 mm throughout the full beam span.

Comparative displacement time histories and bar charts are shown in **Figure 7-36** and **Figure 7-37**. Relevant photographs are provided in **Figure 7-38**. Examination of the displacement data shows that both beams have similar maximum and residual displacements at Blasts 1 – 30 psi and 2c – 70 psi. Nevertheless, the beam with improved detailing was able to resist a greater blast before failure. Failure in beam HSC-0.75%S1-20M-S occurred at Blast 3a – 80 psi (I_r = 832 kPa·ms) and was associated with relatively significant concrete crushing. The use of intermediate blast detailing in beam HSC-0.75%S1-20M-10M-d/2 delayed failure to Blast 3b – 90 psi (I_r = 980 kPa·ms). Despite the larger blast intensity, the doubly-reinforced FRC beam shows a reduction of 54% in maximum displacement (at 90 psi) when comparing to the nominally-detailed FRC beam (at 80 psi), with reduction in the amount of damage as shown in **Figure 7-38**.

7.9.2 Ability of Synthetic Fibers to Relax Blast Detailing

The ability of synthetic fibers to relax steel detailing is studied by comparing the responses of HSC-0%-20M-10M-d/4‡ and HSC-0.75%S1-20M-10M-d/2. It is noted that both beams had identical properties (double reinforcement with 20M/10M bars) but were designed with plain HSC and fiber-reinforced HSC, with closed hoops spaced at d/4 (50 mm) and d/2 (100 mm), respectively. Comparative displacement time histories and bar charts are shown in **Figure 7-36** and **Figure 7-37**. Relevant photographs are provided in **Figure 7-38**. The results show that the use of fibers allowed the HSFRC beam with relaxed detailing to closely match the performance of the more heavily detailed d/4 specimen, both in terms of mid-span displacements and blast capacity. Moreover, the response of beam HSC-0.7%S1-20M-10M-d/2 outperformed that of the plain HSC beam with heavy detailing in terms of damage tolerance. Both beams failed at Blast 3b – 90 psi (I_r = 837 kPa·ms and 980 kPa·ms for the plain and HSFRC beam, respectively); however, as shown in **Figure 7-38**, concrete crushing was better controlled in the beam with synthetic fibers which also shows greater fragmentation resistance. Indeed, failure in the plain doubly-reinforced HSC beam results in the ejection of cover concrete, while the use of fibers was found to eliminate such

spalling. Thus, the limited results indicate that synthetic fibers can be one solution to relax stringent blast detailing requirements in HSC beams; further research is recommended.

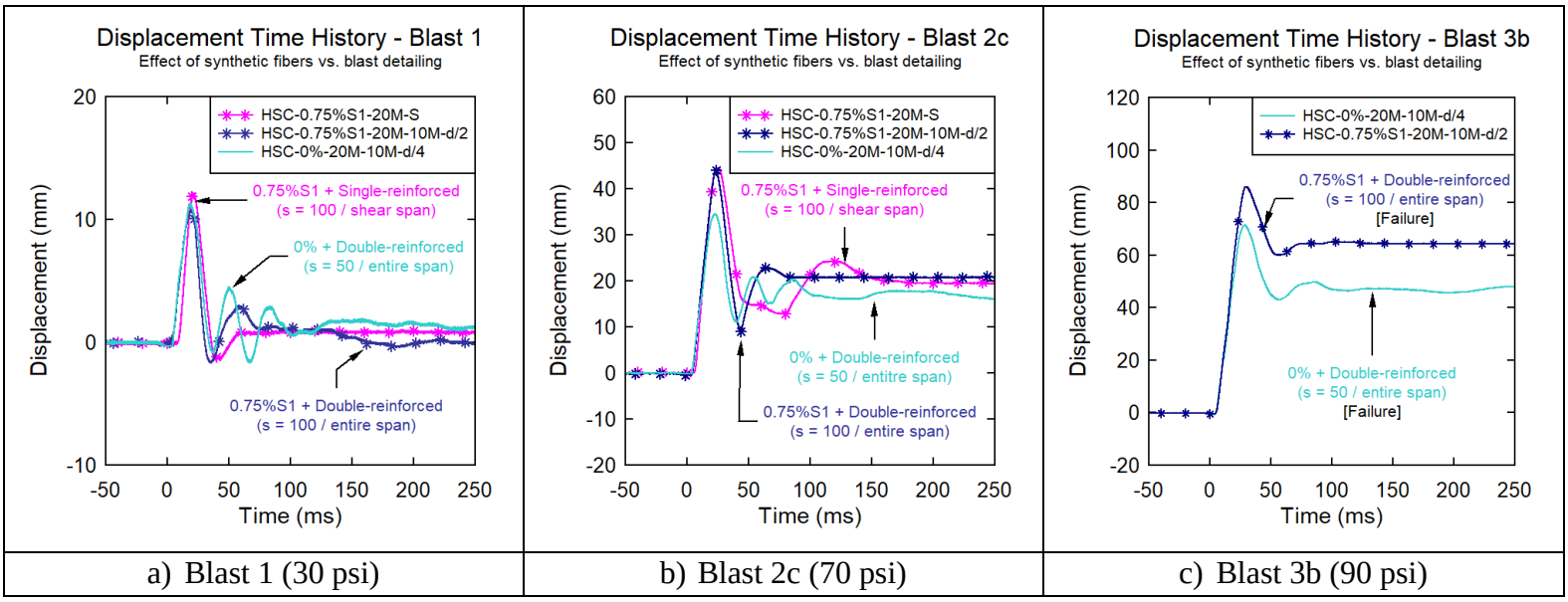

a) Blast 1 (30 psi) | b) Blast 2c (70 psi) | c) Blast 3b (90 psi)

Figure 7-36 Displacement time histories; effects of fibers and detailing

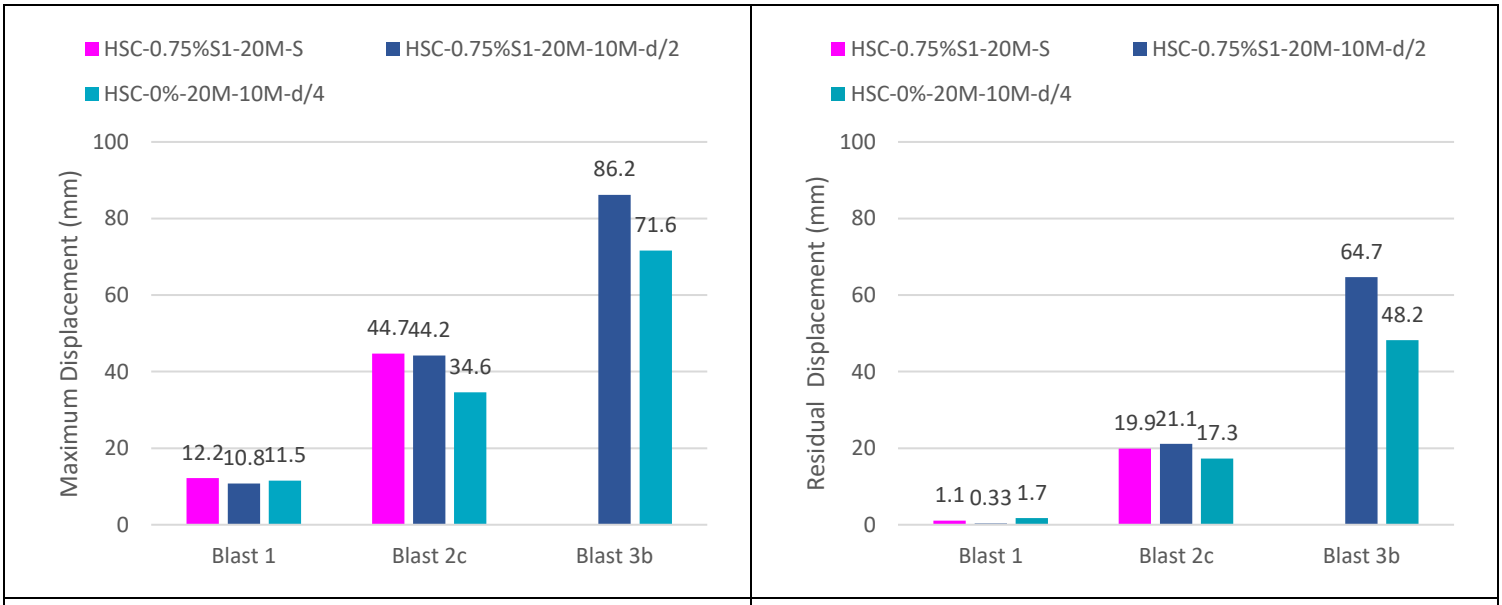

a) Maximum displacements (all blasts) | b) Residual displacements (all blasts)

Figure 7-37 Maximum and residual displacements; effects of fibers and detailing

		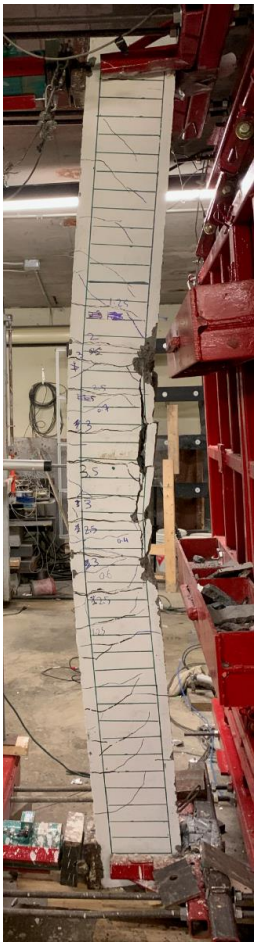
a) HSC-0.75%S1-20M-S	b) HSC-0.75%S1-20M-10M-d/2	c) HSC-0%-20M-10M-d/4‡
Blast 3a (80 psi)	Blast 3b (90 psi)	Blast (90 psi)

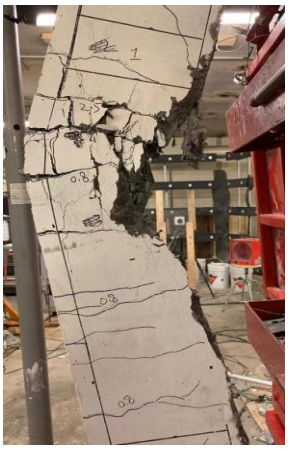	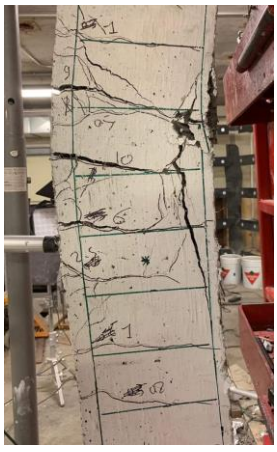	
d) HSC-0.75%S1-20M-S Blast 3a (80 psi)	e) HSC-0.75%S1-20M-10M-d/2 Fiber pullout Blast 3b (90 psi)	f) HSC-0%-20M-10M-d/4‡ Mid-span crushing Blast 3b (90 psi)

Figure 7-38 Photographs; effects of fibers and detailing

7.10 Dynamic Resistance Curves

This research program included replicate beams with similar designs which were tested under dynamic and static four-point bending. The use of load cells at the supports allowed for a measurement of the dynamic resistance of the beams during shock-tube testing.

7.10.1 Dynamic vs. Static Resistance

The static and dynamic resistance curves for all beams are compared in **Figure 7-39**. The maximum loads under dynamic and static loading, and their ratios (P_{max}^{D}/P_{max}^{S}) are also reported in the plots. Other parameters are summarized in **Table 7-3** and **Table 7-4** for beams tested in this study and in previous studies, respectively. It is noted that the resistance curves were obtained by combining the individual curves from all blast intensities (i.e. they represent envelopes of the dynamic reaction curves, see **Chapter 5**).

Considering all tested HSFRC beams, the average dynamic strength ratio is found to be 1.30, with higher loads recorded under blast loading when compared to static loading. The increase in strength under dynamic conditions can be explained by the increase in concrete and steel strength properties at high strain-rates. However, it is evident that beam ductility decreases under dynamic loads for most of the HSFRC beams. This is particularly clear in **Figure 7-39a** and **Figure 7-39b** which show reduced deformation capacity in beams HSC-0.75%S1-15M-0 and HSC-0.75%S1-15M-S as well as when comparing the toughness under dynamic and static conditions as further discussed in the next sub-section.

7.10.2 Effects of Fibers on Dynamic Resistance Curves

The effect of fibers on the dynamic resistance curves can examined by comparing the dynamic strength (P_{max}^{D}) and toughness (A_u^D) of companion HSFRC and plain HSC beams in **Figure 7-40** (comparative plots of the resistance curves are also shown in **Figure 7-41**). It can be observed that the HSFRC beams show increased loads and toughness when compared to their plain HSC companions. However, the HSFRC beams show lower dynamic-to-static toughness ratios (A_u^D/A_u^S) when compared to the companion plain HSC beams as is clear in the trend lines shown in **Figure 7-40**. As noted before, several researchers have reported that fibers are not as effective in improving concrete properties under dynamic loading when compared to static conditions, which can explain the observed trend (Banthia et al., 1987). No clear trend emerges for the strength ratios (P_{max}^{D}/P_{max}^{S}) with average ratios of 1.29 and 1.32 when considering all the HSFRC and plain HSC beams included in this comparison.

7.11 Effects of Other Parameters on Dynamic Resistance Curves

Figure 7-42 summarizes the effect of the other test parameters on the dynamic resistance curves, including the effects of hybrid fibers, longitudinal steel ratio and stirrups.

Comparing the results in **Figure 7-42a**, it can be observed the use of hybrid fibers leads to improvements of 7% and 24% in dynamic strength, and increases of 5% and 76% in dynamic toughness, when comparing to companion beams HSC-0.75%S1-20M-S and HSC-0.75%S1-20M-0, which were built with 0.75% macro fibers and designed with and without stirrups, respectively. The significant increase in toughness when compared to beam HSC-0.75%S1-20M-0 can be explained by the change in failure mode from shear to flexure in the beam with 1% hybrid fibers.

The effect of detailing can be examined in **Figure 7-42b**, where it can be seen that the provision of compression bars and closed hoops in HSC-0.75%S1-20M-10M-d/2 leads to improvements of 16% and 15% in peak resistance and dynamic toughness when comparing to beam HSC-0.75%S1-20M-S which had nominal detailing. Likewise, it can be observed that the doubly-reinforced HSFRC beam with d/2 ties shows similar resistance, with an increase in overall toughness (A_u^D = 11166 vs. 10185 kN·mm), when comparing with the more heavily detailed HSC beam with d/4 ties (HSC-0%-20M-10M-d/4‡). The result further shows that synthetic fibers can be used to relax blast detailing requirements in modern codes.

The effect of reinforcement ratio on the response of HSFRC beams can be investigated in **Figure 7-42c** and **Figure 7-42d**, where it can be seen that the HSFRC beams with 20M bars show similar stiffness but increased dynamic strength and toughness when compared to the companion beams with 15M bars (see **Figure 7-40**).

Finally, examining **Figure 7-42e**, it can be seen that the HS reinforcement had a significant effect on increasing dynamic strength in beams with synthetic fibers (P_{max}^D= 254.1 vs. 161.9 kN), similar to what was observed in the static tests. It can also be noticed that the beam with HS reinforcement shows significant increase in toughness (A_u^D= 11061 vs. 5513 kN·mm).

Table 7-3 Summary of test results

Beam ID	Static Results		Blast ID	Dynamic Results		Ratios	
	Peak Load	Toughness		Peak Load	Toughness[1]	Peak Load	Toughness
	P_{max}^{S} (kN)	A_u^S (J)		P_{max}^{D} (kN)	A_u^D (J)	P_{max}^{D}/P_{max}^{S}	A_u^D/A_u^S
HSC-0%-15M-0	90.2	922	1	78.4	690	0.87	0.75
HSC-0.75%S1-15M-0	112.2	6574	1	94.1	1136	1.29	0.48
			2a	144.9	3142		
			Envelope	144.9	3173 [4278]		
HSC-0.75%S1-15M-S	103.7	7823	1	105.6	1016	1.56	0.70
			2a	144.0	3021		
			2c	161.9	5410		
			Envelope	161.9	5513 [9447]		
HSC-0.75%S1-20M-0	170	3983	1	101.7	838	1.07	1.60
			2a	161.7	1999		
			2b	181.8	6196		
			Envelope	181.8	6374 [9033]		
HSC-0.75%S1-20M-S	156	6123	1	70.4	683	1.35	1.93
			2a	168.0	2843		
			2c	210.2	6618		
			3a	170.1	10976		
			Envelope	210.2	11791 [21120]		
HSC-HYB-20M-0	170.8	10135	1	119.2	1342	1.32	0.82
			2a	188.9	2529		
			2c	209.1	5719		
			3a	225.7	7830		
			Envelope	225.7	8290 [17420]		
HSC-0.75%S1-No.5(HS)-S	213.1	5622	1	101.9	844	1.19	1.97
			2a	161.1	2068		
			2c	212.6	5102		
			3b	254.1	10446		
			Envelope	254.1	11061 [18460]		

[1]: Toughness under the envelope curve considering all blasts

[] = Cumulative energy, obtained by summing the toughness results from individual blasts

Table 7-4 Dynamic resistance results – companion HSC beams tested by other researchers

Beam ID	Static Results		Blast ID	Dynamic Results		Ratios	
	Peak Load	Toughness		Peak Load	Toughness[1]	Peak Load	Toughness
	P_{max}^{S} (kN)	A_u^S (J)		P_{max}^{D} (kN)	A_u^D (J)	P_{max}^{D}/P_{max}^{S}	A_u^D/A_u^S
HSC-0%-20M-0*	83.8	470	1	142.3	1401	1.7	2.98
HSC-0%-15M-S*	104.6	3272	1	125.3	1762	1.32	1.36
			2a	138.5	4461		
			Envelope	138.5	4461 [6223]		
HSC-0%-20M-S*	137.6	2998	1	125.8	1017	1.49	2.32
			2a	190.2	3610		
			2c	205.2	6954		
			Envelope	205.2	6954 [11581]		
HSC-0%-No.5(HS)-S†	194.7	3686	1	125.2	1288	1.23	1.99
			2a	188.7	3145		
			2c	240.1	7323		
			Envelope	240.1	7323 [11756]		

*: Tested by Algassem, O. (2016)

†: Tested by Li, Y. (2016)

[1]: Toughness under the envelope curve considering all blasts

[] = Cumulative energy, obtained by summing the toughness results from individual blasts

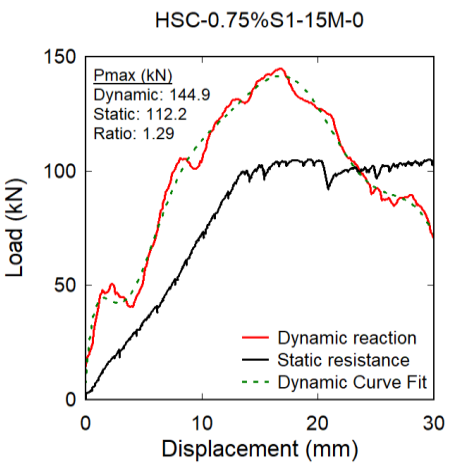

a) HSC-0.75%S1-15M-0

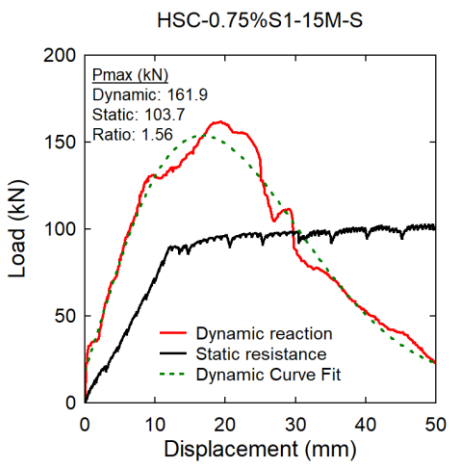

b) HSC-0.75%S1-15M-S

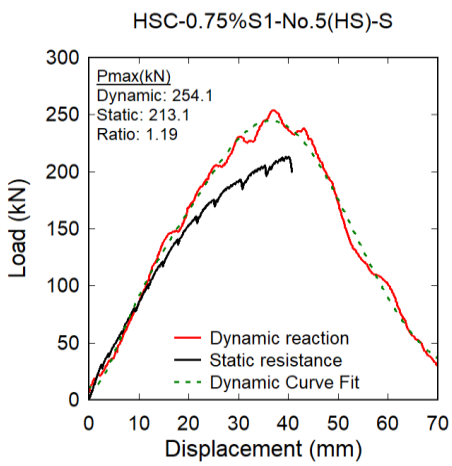

c) HSC-0.75%S1-No.5(HS)-S

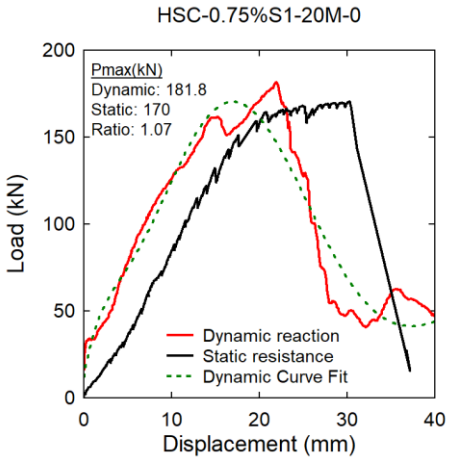

d) HSC-0.75%S1-20M-0

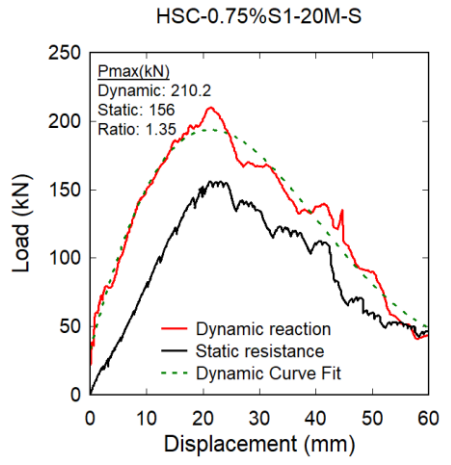

e) HSC-0.75%S1-20M-S

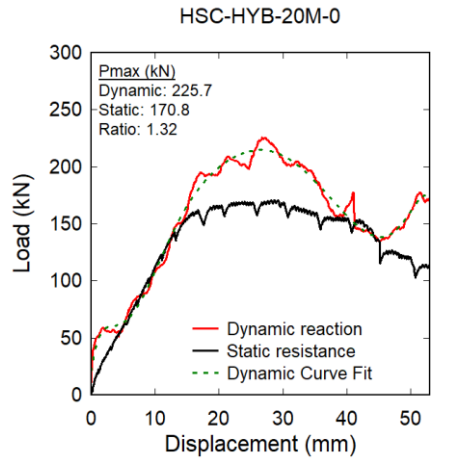

f) HSC-HYB-20M-0

Figure 7-39 Dynamic vs. static resistance curves

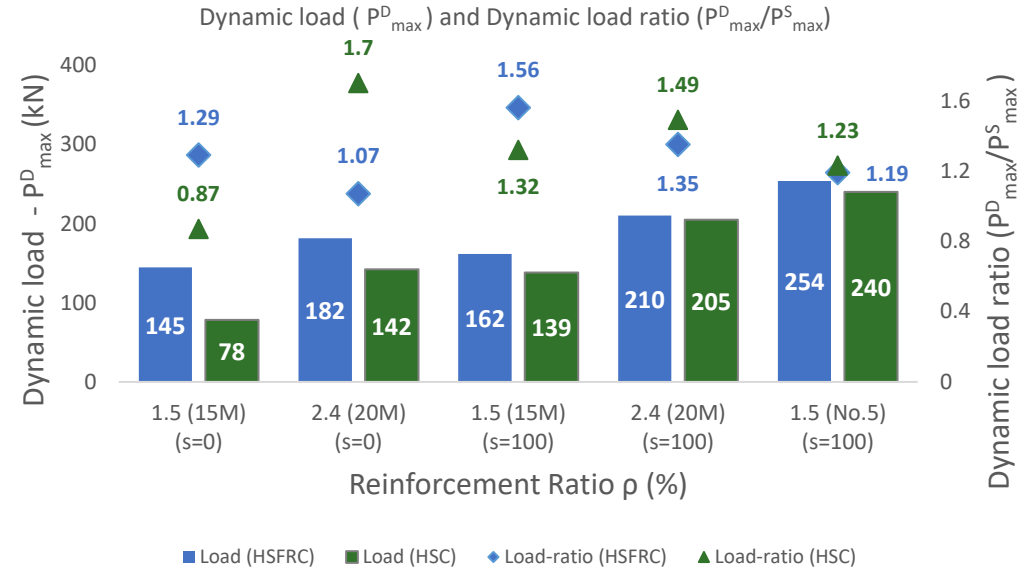

a) Effect of synthetic fibers on dynamic loads & load ratios

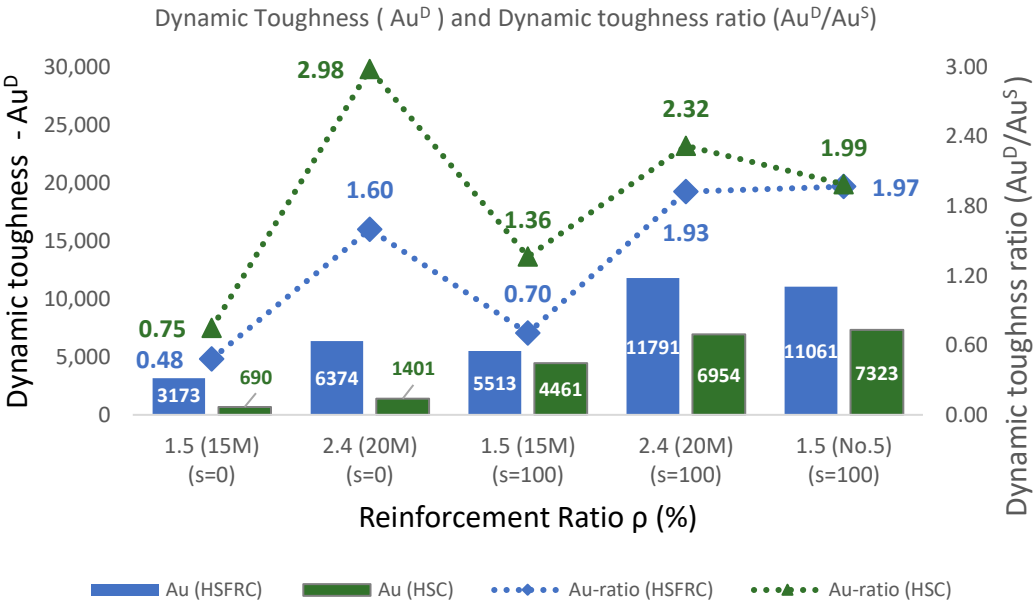

b) Effect of synthetic fibers on dynamic toughness & toughness ratios

(Note: s = 100 indicates beam contains stirrups, while s = 0 indicates beam is designed without stirrups)

Figure 7-40 Effect of synthetic fibers on dynamic loads and dynamic toughness

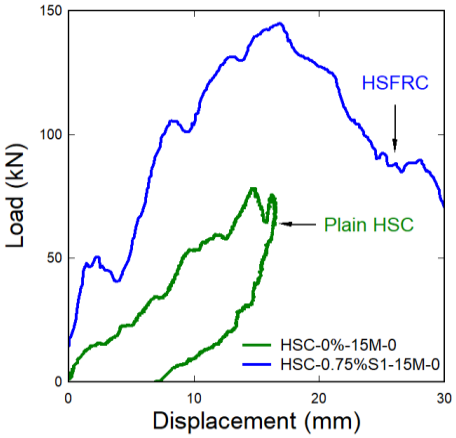

a) Effect of synthetic fibers on shear (15M)

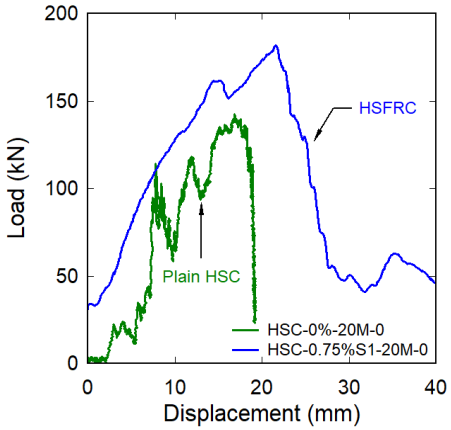

b) Effect of synthetic fibers on shear (20M)

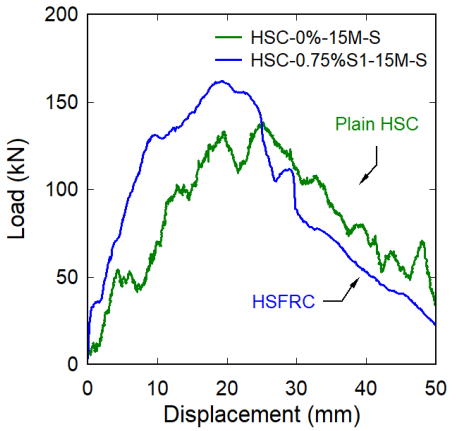

c) Effect of synthetic fibers on flexure (15M)

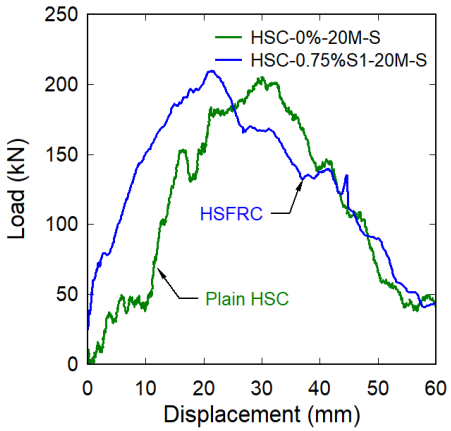

d) Effect of synthetic fibers on flexure (20M)

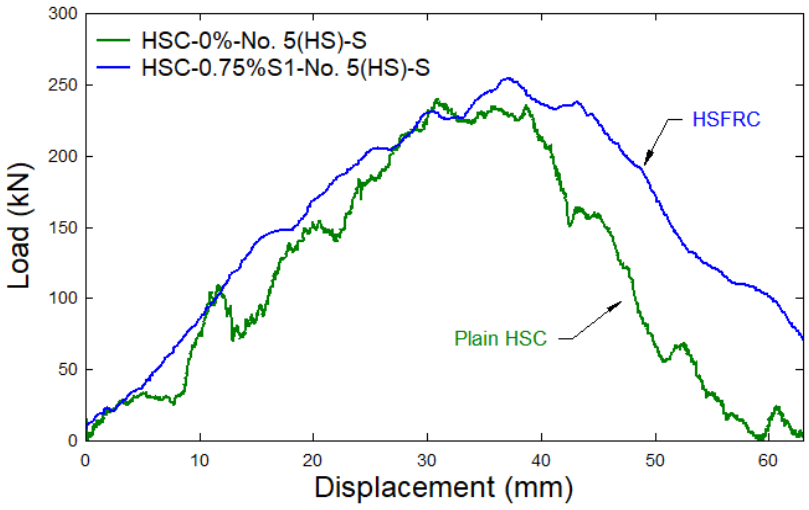

e) Effect of synthetic fibers in beams with HSR

Figure 7-41 Effect of synthetic fibers on dynamic resistance curves

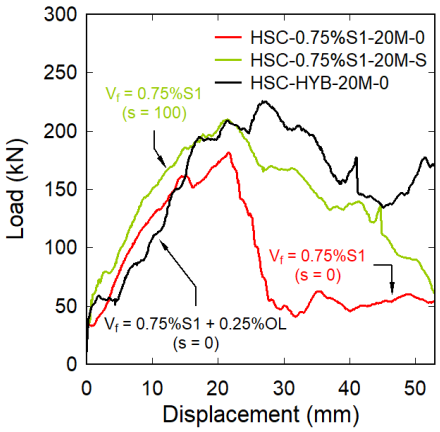

a) Effect of hybrid fibers

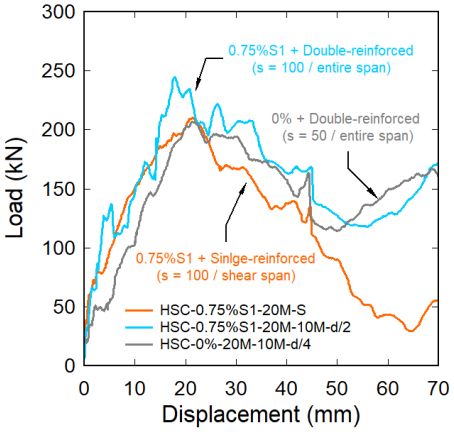

b) Effect of synthetic fibers vs. blast detailing

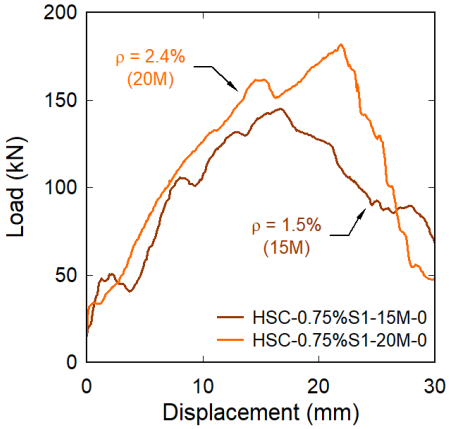

c) Effect of reinforcement ratio (without stirrups)

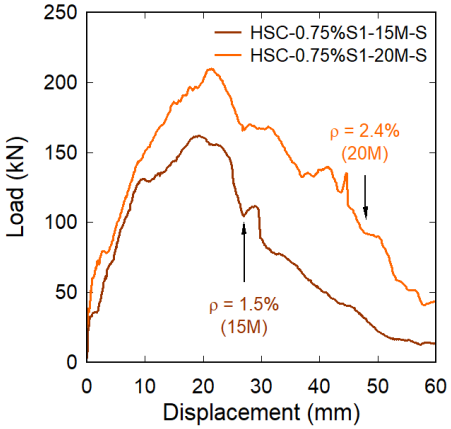

d) Effect of reinforcement ratio (with stirrups)

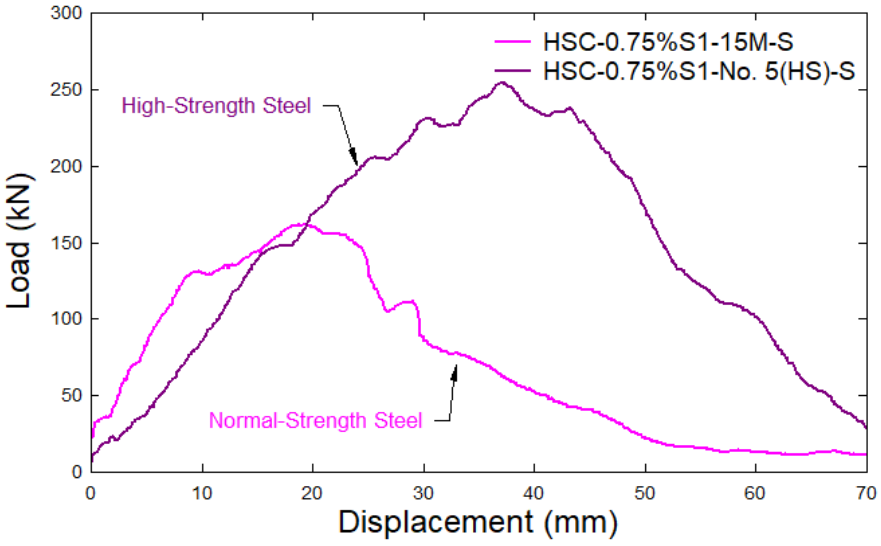

e) Effect of HSR in beams with synthetic fibers

Figure 7-42 Effect of other parameters on dynamic resistance curves

Chapter 8: Prediction of Static & Dynamic Response

8.1 Chapter Overview

This chapter presents an analytical/numerical study which aims at predicting the static and blast behaviour of the beams tested in this research. In the first section, various FRC models available in the literature are used to predict the flexural and shear strengths of the beams tested under static loading. Next, the load-deflection curves (resistance functions) under static and dynamic loading are predicted using sectional analysis and finite element (FE) modelling. Using the developed resistance functions, the dynamic responses of the beams are then predicted using single-degree of freedom (SDOF) analysis.

8.2 Flexural and Shear Strength Predictions

8.2.1 Flexural Strength Predictions

Several models have been proposed in the literature to predict the flexural strength of fiber-reinforced concrete (FRC) beams. In this research the following two models are considered:

ACI 544.4R (1998) model

This approach was developed by ACI Committee 544 (1988) for predicting the flexural capacity of normal-strength FRC beams. Based on the assumptions and equilibrium of forces shown in **Figure 8-1**, the moment resistance ($\boldsymbol{M_n}$) of an FRC beam is obtained as follows:

$$\boldsymbol{M_n = A_s f_y \left(d - \frac{a'}{2}\right) + \sigma_t b(h-e)\left(\frac{h}{2} + \frac{e}{2} - \frac{a'}{2}\right)} \quad \textbf{(8-1)}$$

where A_s and f_y are the tension steel area and yield strength; h, d, c, a' are the beam height, effective depth, neutral axis depth, and compressive stress block depth (taken as βc); and e is the distance from the extreme compression fiber to the top of the tensile stress block of FRC (taken as $e = \frac{(\varepsilon_{s,fiber}+0.003)}{0.003} c$). According to this model, the tensile stress of FRC is taken as $\sigma_t = 0.00772 \frac{l_f}{d_f} V_f F_{be}$ with $\varepsilon_{s,fiber} = \sigma_t / E_{cf}$; E_{cf} = modulus of elasticity of fiber-reinforced concrete; l_f , d_f and V_f = fiber length, diameter and fiber content (taken as 50 mm, 0.68 mm and 0.75%); and F_{be} = bond efficiency of the fiber which varies between 1.0 – 1.2. In this study, an F_{be} = 1.2 was used in the analysis of the FRC beams.

Imam et al. (1995) model

Since the ACI model was derived for normal-strength concrete, Imam et al. (1995) proposed a new equation to predict the flexural capacity of high-strength concrete beams containing fibers. The model adjusts the tensile stress of fibrous concrete (σ_t) and the depth of the concrete stress block (c), which may be different in high-strength FRC when compared to normal-strength FRC.

According to the model, $\sigma_t = 2F$ and $\beta = \frac{a'}{c} = 0.65$, with F defined as the fiber factor. By implementing these changes in the original ACI expression, the moment capacity is given as:

$$\boldsymbol{M_n = \frac{1}{2}\rho f_y b d^2 (2-\eta) + 0.83 F b d^2 (0.75-\eta)(2.15+\eta)} \quad \textbf{(8-2)}$$

where the factors η and F are calculated as: $\eta = \frac{\rho f_y + 2.32F}{0.85 f_c' + 3.08F}$ and $F = \frac{l_f}{d_f} V_f D_f$. In these equations, ρ = the longitudinal reinforcement ratio, f_c' = the compressive strength of concrete and l_f , d_f and V_f are as described previously. Finally, D_f is a bond efficiency factor which varies between 1.0 and 0.5 (1.0 for hooked fiber, 0.9 for deformed fiber and 0.5 for smooth fiber). Since macro-synthetic fibers are less efficient than hooked fibers yet more efficient than smooth fibers, a factor of 0.9 was used in the current study.

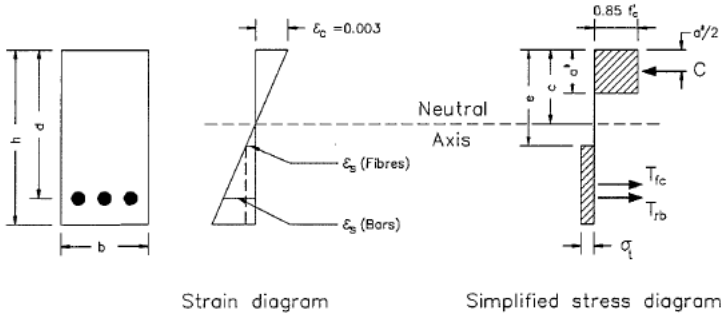

Figure 8-1 ACI 544.4R model for predicting FRC moment capacity (Imam et al., 1995)

8.2.2 Shear Strength Predictions

A review of the literature shows that a large number of models have been developed to predict the shear strength of fiber-reinforced concrete beams. However, the majority of these models have been calibrated based on tests on steel fiber-reinforced concrete (SFRC). **Table 8-1** summarizes some of these models. Yazdanbakhsh et al. (2015) assessed the applicability of 11 shear models originally developed for SFRC to predict the shear strength of 23 large-scale FRC beams made with macro-synthetic fibers. The results showed that the Mansur et al. (1986), Ashour et al. (1992) and RILEM (2003) analytical models predicted the shear strength of SNFRC beams with reasonable accuracy. On the other hand, other models (Sharma (1986), Li et al. (1992), etc.) showed poor predictions.

Using the results obtained from their experimental tests, the authors of this study also conducted regression analysis to refine the RILEM model for SNFRC as follows:

$$\boldsymbol{v_{fc,SNFRC} = 1.28 v_{C,RLM} + 0.69 v_{f,RLM}} \quad \textbf{(8-3)}$$

$$\boldsymbol{v_{C,RLM} = 0.15 \sqrt[3]{3(d/a)}\, k (100 \rho f_c')^{1/3}} \quad \textbf{(8-4)}$$

$$\boldsymbol{v_{f,RLM} = k_1 0.5 \frac{d}{a} f_{e,3}} \quad \textbf{(8-5)}$$

where $v_{C,RLM}$ and $v_{f,RLM}$ are the shear strength provided by concrete and the fiber reinforcement respectively according to the RILEM model; d is the effective depth of the cross section; a is the shear span; k and k_1 are factors related to size effect ($k = 1 + \sqrt{200/d} \leq 2$; $k_1 = \frac{1600-d}{1000} \geq 1$); ρ is the longitudinal reinforcement ratio; and $f_{e,3}$ is the equivalent flexural strength of FRC measured at a deflection of L/150 or 3 mm (for a 150×150 mm prism tested on a 450 mm span) in accordance with the ASTM C1609 standard.

Similarly, using the results obtained from another database of test results on steel fiber-reinforced concrete, the authors proposed the following equation for SFRC beams:

$$v_{fc,SFRC} = 1.39 v_{C,RLM} + 0.77 v_{f,RLM} \quad \textbf{(8-6)}$$

Table 8-1 Various models for predicting shear strength of SFRC (Yazdanbakhsh et al., 2015)

Investigator	Model
Sharma	$v_{fc} = \frac{2}{3} f_{sp} \cdot (d/a)^{0.25}$ f_{sp} = split-cylinder tensile strength of concrete d/a = effective depth-to-shear span ratio
Mansur et al.	$v_{fc} = \left(0.16\sqrt{f'_c} + 17.2\frac{\rho Vd}{M}\right) + v_b$ f'_c = cylinder compressive strength of plain concrete, MPa V and M are the expected ultimate shear and bending moment ρ = flexural reinforcement ratio $v_b = 0.41\tau F$ (accounts for the fiber pullout resistance) τ = average fiber matrix interfacial bond stress
Narayanan and Darwish	$v_{fc} = e\left[0.24 f_{spfc} + 80 \cdot \rho\frac{d}{a}\right] + v_b$ $e = 2.8d/a \quad a/d < 2.8$ $e = 1 \quad a/d \geq 2.8$ $f_{spfc} = f_{cuf}/(20 - \sqrt{F}) + 0.7 + \sqrt{F}$ f_{cuf} = cube compressive strength of fiber concrete
Ashour et al. based on ACI shear formula	$v_{fc} = (0.7\sqrt{f'_c} + 7F)\frac{d}{a} + 17.2\rho\frac{d}{a}$
Ashour et al. based on Zsutty's formula	$v_{fc} = \left(2.11\sqrt[3]{f'_c}\right) \cdot (\rho\frac{d}{a})^{0.333} \quad a/d > 2.5$ $v_{fc} = \left(2.11\sqrt[3]{f'_c}\right) \cdot (\rho\frac{d}{a})^{0.333} \times \frac{2.5}{a/d} + v_b(2.5 - a/d) \quad a/d \leq 2.5$
Li et al.	$v_{fc} = 1.25 + 4.68\left[(f_f f_{sp})^{3/4} (\rho\frac{d}{a})^{1/3} (d)^{-1/3}\right] \quad a/d > 2.5$ $v_{fc} = 9.16 \cdot [(f_f)^{2/3} \rho^{1/3} (\frac{d}{a})] \quad a/d \leq 2.5$ f_f = flexural strength of fiber concrete (modulus of rupture)
Swamy et al.	$v_{fc} = 0.9\sigma_{cu} + v_c$ $\sigma_{cu} = v_b$ = post-cracking tensile strength of FRC: $\sigma_{cu} = 0.41\tau \cdot F \quad L_f < L_c$ $\sigma_{cu} = 0.41(1 - \frac{\sigma_{fu}}{4\tau} \cdot \frac{D_f}{L_f}) \cdot \sigma_{fu} \cdot V_f \quad L_f \geq L_c$ L_f = fiber length, L_c = critical fiber length σ_{fu} = fiber fracture stress v_c = contribution of concrete to shear strength. In this study the ACI Building Code equation is used to calculate v_c
Imam et al.	$v_{fc} = 0.6\Psi \times \sqrt[3]{\omega} \times \left[\sqrt{f'_c} + 275\sqrt{\frac{\omega}{(a/d)^2}}\right]/(bd)$ $\Psi = \frac{1+\sqrt{5.08/d_a}}{\sqrt{1+d/(25d_a)}}$ d_a = maximum aggregate size (mm) $\omega = \rho(1 + 4F)$
Kwak et al.	$v_{fc} = 3.7e(f_{spfc})^{2/3} (\rho\frac{d}{a})^{1/3} + 0.8 v_b$
RILEM (Dupont and Vandewalle)	$v_{fc} = v_{c,RLM} + v_{f,RLM}$ $v_{c,RLM} = 0.15 \cdot \sqrt[3]{3(d/a)} \cdot k \cdot (100\rho \cdot f'_c)^{1/3}$ $k = 1 + \sqrt{200/d} \leq 2$ $v_{f,RLM} = k_1 \cdot 0.5\frac{d}{a} f_{e,3}$ $k_1 = \frac{1600-d}{1000} \geq 1$ f_{e3} = equivalent flexural strength
fib-MC2010	$v_{Rd} = v_{Rd,F} + v_{Rd,s}$ $v_{Rd,F} = \frac{0.18}{\gamma_c} k \cdot \left[100\rho \cdot \left(1 + 7.5\frac{f_{ftuk}}{f_{ctk}}\right) f_{ck}\right]^{1/3} + 0.15\sigma_{cp}$ $k = 1 + \sqrt{200/d} \leq 2$ f_{ctk} = characteristic concrete tensile strength, f_{ck} = characteristic concrete compressive strength $f_{Ftu}(w_u) = f_{Fts} - \frac{w_u}{2.5} \cdot (f_{Fts} - 0.5 f_{R3} + 0.2 f_{R1}) \geq 0$ f_{Ftu} = the ultimate residual tensile strength at 1.5 mm crack width $f_{Fts} = 0.45 f_{R,1}$ $f_{R,j} = \frac{3F_j L}{2bh_{sp}^2}$ F_j = the force corresponding to crack mouth opening at stage j

8.2.3 Discussion

Table 8-2 compares the experimental and predicted results for the FRC beams tested in this study. The moment capacities (M_{fl}) were predicted using the ACI 544.4R (1998) and Imam et al. (1995) models. The flexural load capacities were then calculated as: $P_{fl} = 2 \cdot M_{fl}/a$, where a is the shear span. In addition, the shear capacities of the beams were predicted using the model proposed by Yazdanbakhsh et al. (2015) as it is calibrated for SNFRC. In order to compare to the moment capacities, the shear load capacities were calculated as $P_v = 2 \cdot V_{rf}$. Finally, the shear-to-flexure capacity ratios (P_v/P_{fl}) were also calculated using the Imam and Yazdanbakhsh formulations. A ratio larger than 1.0 indicates that the models predict flexural failure, whereas a value below 1.0 predicts shear failure prior to development of flexural capacity.

Considering all SNFRC beams with stirrups, it can be observed that the ACI 544.4R and Imam models underestimate the experimental load capacities (P_{exp}) by 12% and 9%, respectively. Nonetheless, the model proposed by Imam et al. (1995) provided greater accuracy, which is expected since this model is adapted for high-strength FRC. Next, examining the shear capacities, it can be observed that $P_v \gg P_{exp}$ for all beams with stirrups, with shear-to-flexure ratios of 1.95 to 2.48. The results confirm that the combined use of macro-synthetic fibers and minimum stirrups allowed the beams to safely prevent shear failure under static loads. Kishi and Mikami (2012) previously noted that a static shear-to-flexure ratio ≥ 1.5 was sufficient to ensure ductile flexural failure in conventional reinforced concrete beams tested under impact. In the current study, all SNFRC beams with ratios ~ 2 or greater failed in flexure under both static and dynamic loads.

Comparing the experimental and predicted loads for SNFRC beams built without stirrups, it can be observed that the ACI 544.4R and Imam models underestimated the experimental loads by 17% and 13%, respectively. It can also be observed that the shear capacities predicted by the Yazdanbakhsh model were generally close to the experimental load capacities. Although the P_v/P_{fl} ratios are generally greater than 1.0, it can be observed that the ratios are much lower when compared to the beams with stirrups, ranging from $0.96 \leq P_v/P_{fl} \leq 1.2$. In the experiments, all beams with 0.75%S1 fibers reached flexural yielding; however, they eventually failed in shear under the effects of sustained loading. Thus, it can be concluded that ratios ≤ 1.2 are insufficient to prevent shear failure and substitute for stirrups in high-strength FRC beams reinforced with macro-synthetic fibers under static loads. Similarly, since the ratios are close to unity (and much lower than 1.5), it can explain the brittle failures observed under blast loading. It is important to note that, since the hybrid beam had both synthetic and steel fibers, the two refined equations (**Equation (8-3)** and **Equation (8-6)**) proposed by Yazdanbakhsh et al. (2015) were used to predict the shear-to-flexure ratio of the beam. Using this approach, ratios of 1.11 and 1.21 were obtained for the SNFRC and SFRC relationships, respectively. Hence, both models correctly predicted the flexural failure experienced by the hybrid beam.

Figure 8-2 and **Figure 8-3** show comparisons of shear and shear-to-flexure ratios when using other shear models proposed in the literature. It can be observed that most models predict

$P_v/P_{fl} < 1.2$ for the beams without stirrups, with several models having ratios < 1.0. On the other hand, most models predict ratios > 2.0 for the beams with combined stirrups and fibers, which corresponds to the above observations.

Table 8-2 Comparison of experimental vs. predicted moment and shear capacities

Beam ID	P_{exp} (kN)	ACI 544.4R (1988)		Imam et al. (1995)		Yazdanbakhsh et al. (2015)		P_v/P_{fl}
		M_{fl} (kNm)	P_{fl} (kN)	M_{fl} (kNm)	P_{fl} (kN)	V (kN)	P_v (kN)	
SCC-0.75%S1-15M-0	85.7	33.6	90.8	35.0	94.5	50.8	101.7	1.08
HSC-0.75%S1-15M-0	112.2	34.5	93.2	36.1	97.3	58.3	116.5	1.20
HSC-0.75%S1-20M-0	170	48.5	130.8	50.7	136.8	65.5	131.0	0.96
HSC-HYB-20M-0	170.8	49.6	134.0	51.5	138.9	84.1	168.1	1.21
SCC-0.75%S1-15M-S	99	33.6	90.9	35.0	94.5	117.0	233.9	2.48
HSC-0.75%S1-15M-S	103.7	33.9	91.6	35.4	95.5	121.3	242.5	2.54
HSC-0.75%S1-20M-S	156	49.0	132.2	50.5	136.3	133.2	266.4	1.95

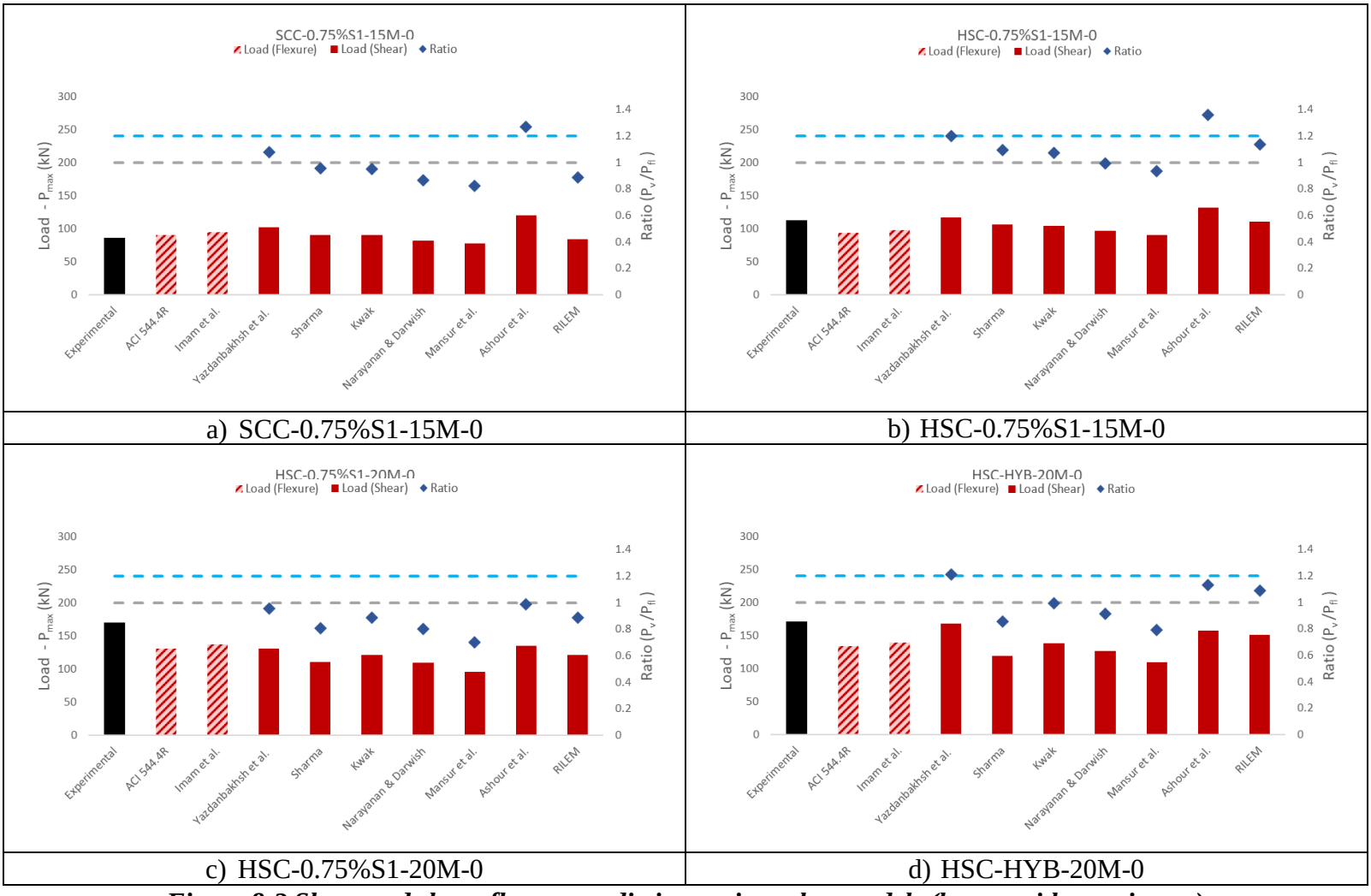

a) SCC-0.75%S1-15M-0

b) HSC-0.75%S1-15M-0

c) HSC-0.75%S1-20M-0

d) HSC-HYB-20M-0

Figure 8-2 Shear and shear-flexure predictions using other models (beams without stirrups)

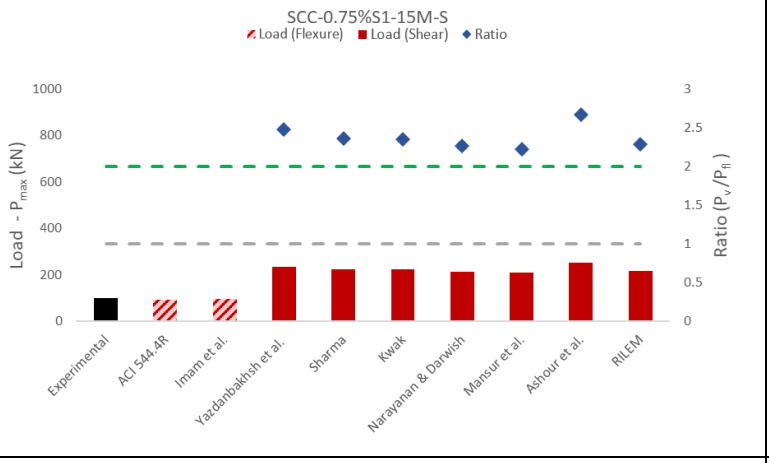

a) SCC-0.75%S1-15M-S

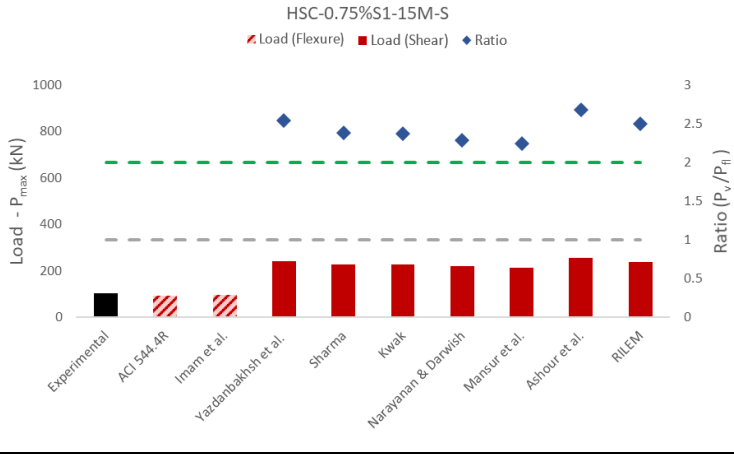

b) HSC-0.75%S1-15M-S

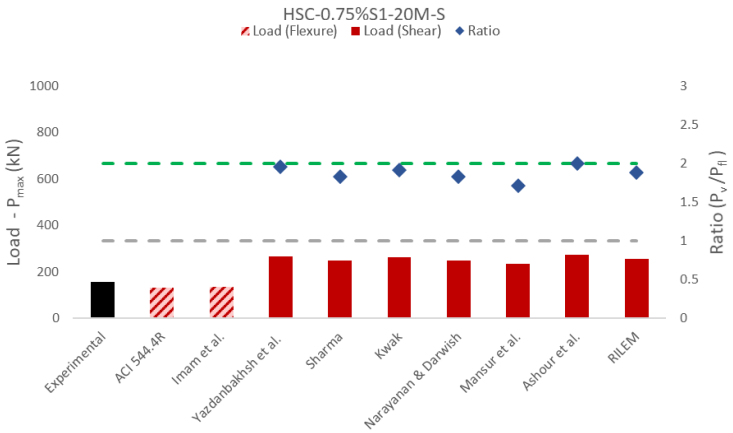

c) HSC-0.75%S1-20M-S

Figure 8-3 Shear and shear-flexure predictions using other models (beams with stirrups)

8.3 Prediction of Static Load-Deflection Curves

8.3.1 Sectional Analysis Procedure

Sectional analysis was the first approach used to predict the static response of the beams. It is worth mentioning that this procedure is only applicable for beams which experience a flexural dominant response. The various constitutive material models for concrete and steel reinforcement used in the analysis are summarized in **Figure 8-5**. To account for the improved behaviour of fiber-reinforced concrete in compression, the model proposed by Lee et al. (2012) was used. It is worth mentioning that most compression models available in the literature have been calibrated for steel fiber FRC. **Figure 8-4** compares the predicted and experimental responses of HSFRC in compression using various models; it can be seen that Lee et al. (2012) model provides a reasonable fit of the experimental FRC response. The use of fibers also improves the tensile response of concrete. To account for this effect, a tri-linear model proposed by Lok and Pei (1998) was used for the tension portion of the FRC stress-strain curve. Next, the behaviour of the normal-strength longitudinal steel in tension was modelled using the model proposed by Jacques et al. (2012) which consists of two linear segments (for elastic and post-yield behaviour) and a parabolic function (for the strain-hardening effect). In the case of the high-strength reinforcement, the model proposed in the ACI ITG-6R-10 guidelines (2011) was used. It is noted that this model provides a lower-bound of the stress-strain response of Grade 690 MPa high-strength steel.

With the material properties described, the moment-curvature relationship ($\boldsymbol{M-\phi}$) for each beam section was generated using sectional analysis as outlined in the procedure shown in **Figure 8-6a**. The sectional analysis begins with discretizing the beam's cross-section into 50 equal horizontal fibers and selecting an initial strain for the top compression fiber. After assuming the depth of the neutral axis, the curvature and stress distribution along the concrete section is obtained. Force equilibrium is then used to determine the bending moment acting on the section, and the first point on the ($\boldsymbol{M-\phi}$) relationship is stored. An iterative procedure is then used to find the complete ($\boldsymbol{M-\phi}$) relationship. Next, the load-deflection relationships were obtained by integrating the curvature along the beam half-span length using the moment-area method ($\Delta= \int_0^{L/2} \boldsymbol{\phi}(x)\cdot x\cdot dx$) as outlined in **Figure 8-6b**. For elastic deformations ($\Delta\leq \Delta_y$), the deflection is obtained by converting curvature using **Equation (8-7**):

$$\Delta_y= \int_0^{L/2} \boldsymbol{\phi}(x)\cdot x\cdot dx = \boldsymbol{\phi}_y\cdot\left(\frac{a^2}{3}\right)+\boldsymbol{\phi}_y\cdot\left(\frac{L_{cm}}{2}\right)\left(\frac{L}{2}-\frac{L_{cm}}{4}\right) \qquad \textbf{(8-7)}$$

In the analysis, non-linear behaviour (cracking and concrete damage) was assumed to be concentrated in the beam plastic hinge region ($\boldsymbol{l_p}$). The inelastic deflection was therefore obtained by adding yield and plastic displacement contributions using **Equation (8-8)**:

$$\Delta_p= \int_0^{L/2} \boldsymbol{\phi}(x)\cdot x\cdot dx = \Delta_y+\left(\boldsymbol{\phi}_u-\boldsymbol{\phi}_y\right)\cdot\left(l_p'\right)\cdot\left(\frac{L}{2}-\frac{l_p'}{2}\right) \qquad \textbf{(8-8)}$$

The length of the plastic hinge in an actual beam can vary and is dependent on several factors. In the case of FRC beams, Ashour and Wafa (1993) have noted that fibers can reduce crack widths which can result in more diffused cracking and an increase in plastic hinge length. Conversely, FRC beams can experience crack localization, which may have the opposite effect (Yoo et al. 2017). To examine the influence of this parameter, two cases of plastic hinge length ($\boldsymbol{l_p}$) were considered in the analysis, including: $\boldsymbol{l_p = l_{cm}}$, where $\boldsymbol{l_{cm}}$ is the length of the constant moment region, and $\boldsymbol{l_p = 2d}$, where $\boldsymbol{d}$ is the section depth**.** The results of this analysis are presented in **Figure 8-9**.

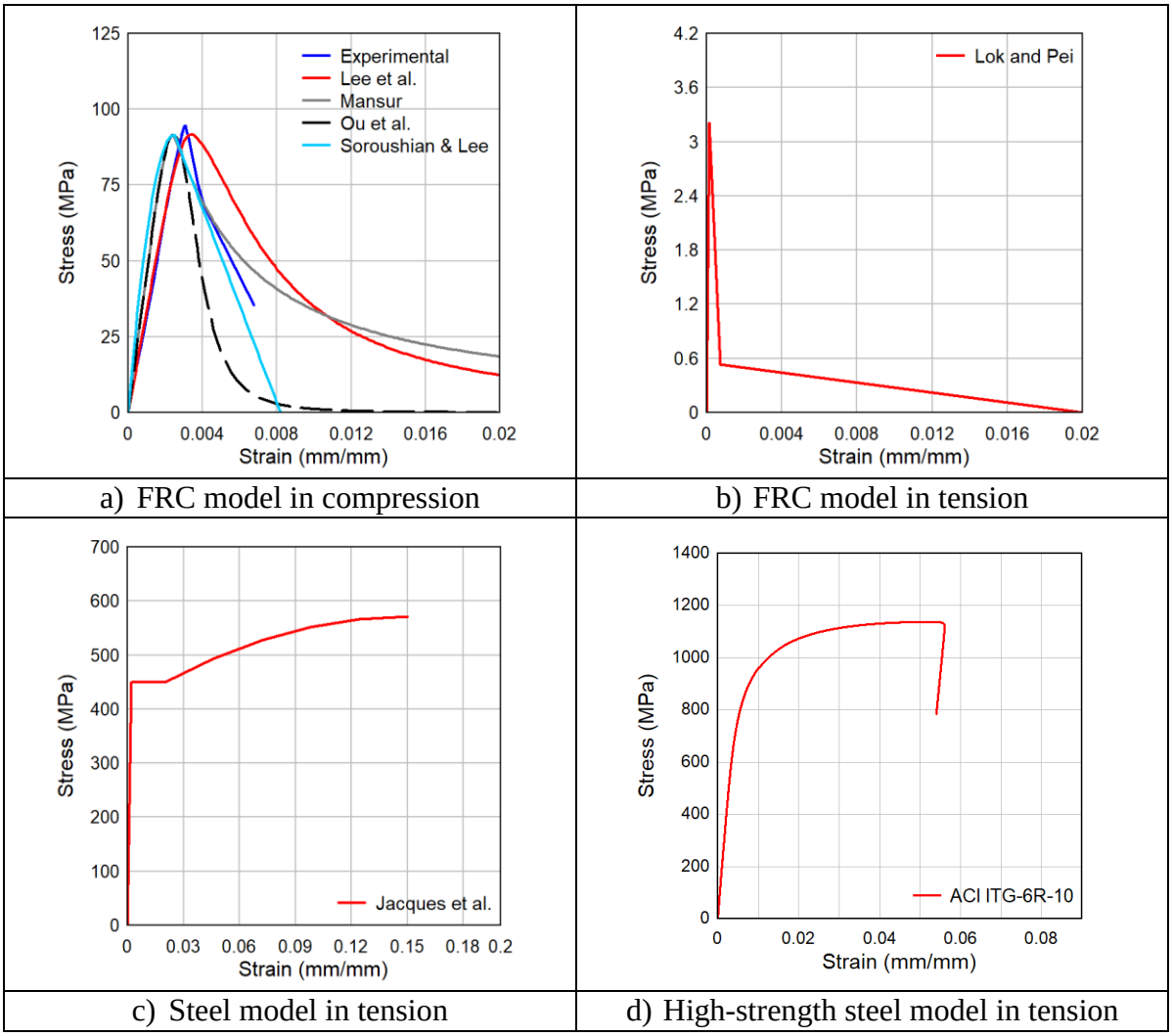

a) FRC model in compression

b) FRC model in tension

c) Steel model in tension

d) High-strength steel model in tension

Figure 8-4 Various constitutive material models for concrete and steel reinforcement

a) Materials models

i. FRC compression model: Lee et al (2012)

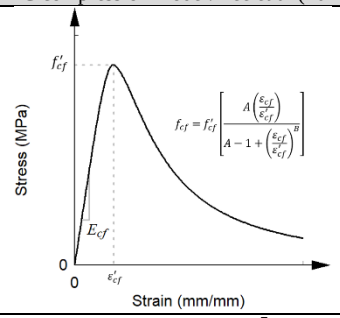

Stress-strain relationship: $f_{cf} = f'_{cf}\left[\frac{A\left(\frac{\varepsilon_{cf}}{\varepsilon'_{cf}}\right)}{A-1+\left(\frac{\varepsilon_{cf}}{\varepsilon'_{cf}}\right)^B}\right]$

$A = B = \frac{1}{1-\left(\frac{f'_{cf}}{\varepsilon'_{cf}E_c}\right)}$ for $\varepsilon_{cf}/\varepsilon'_{cf} \le 1.0$

Where: $A = 1 + 0.723\left(V_f \frac{l_f}{d_f}\right)^{-0.957}$ for $\varepsilon_{cf}/\varepsilon'_{cf} > 1.0$

$B = \left(\frac{f'_{cf}}{50}\right)^{0.064}\left[1 + 0.882\left(V_f \frac{l_f}{d_f}\right)^{-0.882}\right] \ge A$

$\varepsilon'_{cf} = \left(0.0003 V_f \frac{l_f}{d_f} + 0.0018\right) f'^{0.12}_{cf}$; $E_{cf} = \left(-367 V_f \frac{l_f}{d_f} + 5520\right) f'^{0.41}_{cf}$

ii. FRC tension model: Lok & Pei (1998)

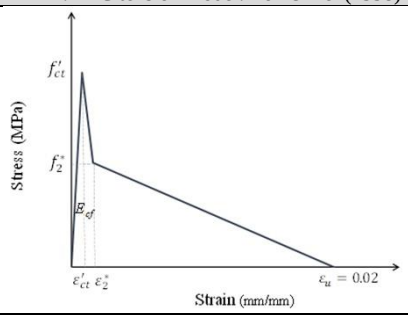

Tri-linear stress-strain relationship:

Branch 1: 0 to stress $f'_{ct} = 0.33 f'^{1/2}_{cf}$; slope = E_{cf}
Branch 2: linear descening to stress f^*_2 and strain ε^*_2
Branch 3: linear to failure stress (f_{ct} = 0 MPa) at strain =0.02

Where: $f^*_2 = \frac{1}{2} V_f \tau_{bond} \frac{l_f}{d_f}$, $\varepsilon^*_2 = \tau_{bond} \frac{l_f}{d_f} \frac{1}{E_{fp}}$ and
$\tau_{bond} = 0.198 \times f'^{1/2}_{cf}$

iii. Steel reinforcement model: Jacques et al. (2012)

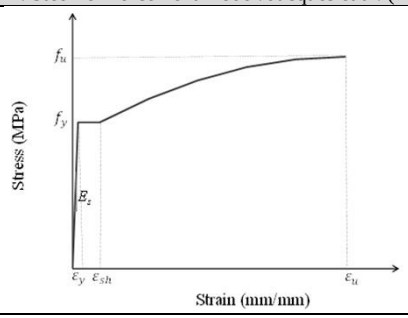

Stress-strain relationship:

$$f_s = \begin{cases} E_s \varepsilon_s & \text{for } \varepsilon_s \le \varepsilon_y \\ f_y + (\varepsilon_s - \varepsilon_y)\left(\frac{f_{sh} - f_y}{\varepsilon_{sh} - \varepsilon_y}\right) & \text{for } \varepsilon_y < \varepsilon_s \le \varepsilon_{sh} \\ f_y + (f_u - f_y)\left[2\left(\frac{\varepsilon_s - \varepsilon_{sh}}{\varepsilon_u - \varepsilon_{sh}}\right) - \left(\frac{\varepsilon_s - \varepsilon_{sh}}{\varepsilon_u - \varepsilon_{sh}}\right)^2\right] & \text{for } \varepsilon_{sh} < \varepsilon_s \le \varepsilon_u \end{cases}$$

iv. HSR model : ACI ITG-6R-10 (2011)

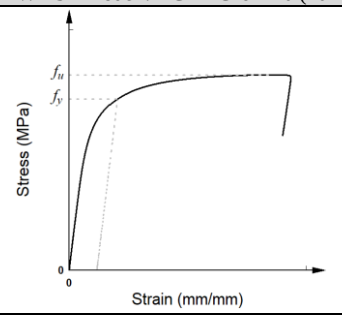

Stress-strain relationship:

$$f_s = \begin{cases} 200{,}000\varepsilon_s & \text{for } \varepsilon_s \le 0.0024 \\ 1170 - \frac{2.96}{\varepsilon_s + 0.0019} & \text{for } 0.0024 < \varepsilon_s \le 0.02 \\ 1040 & \text{for } 0.02 < \varepsilon_s \le 0.06 \end{cases}$$

b) Dynamic Increase factor (DIF) models

i. Concrete in compression

Case 1: Wang et al. (2011):

$$DIF_c = \begin{cases} \left(\frac{\dot{\varepsilon}}{\dot{\varepsilon}_s}\right)^{1.026\alpha} & \text{for } \dot{\varepsilon} \le (30 + 23i)s^{-1} \\ \eta\left(\frac{\dot{\varepsilon}}{\dot{\varepsilon}_s}\right)^{\kappa} & \text{for } \dot{\varepsilon} > (30 + 23i)s^{-1} \end{cases}$$

Where: i =1 and 0 for FRC and plain concrete, respectively;
$\eta = \gamma(1 - 0.3392i)$; $\kappa = (1 + 0.05i)/3$;
$\log\gamma = 6.156\alpha - 2$; $\alpha = \frac{1}{(5+8f'_{cf}/10)}$; and

Case 2: DIF_c = 1.0 (no dynamic factor)

ii. Concrete in tension

Case 1: Malvar and Ross (1998):

$$DIF_t = \begin{cases} \left(\frac{\dot{\varepsilon}}{\dot{\varepsilon}_s}\right)^{\delta}, & \dot{\varepsilon} \le 1s^{-1} \\ \beta^*\left(\frac{\dot{\varepsilon}}{\dot{\varepsilon}_s}\right)^{1/3}, & \dot{\varepsilon} > 1s^{-1} \end{cases}$$

Where:
$\text{Log}\,\beta^* = 6\delta - 2$; $\delta = \frac{1}{(1+8f'_{cf}/10)}$; $\dot{\varepsilon}_s = 10^{-6}s^{-1}$

Case 2: DIF_t = 1.0 (no dynamic factor)

iii. Steel in tension

Case 1: Saatcioglu et al. (2011):

At yield → $DIF_y = 0.034\,ln(\dot{\varepsilon}) + 1.30 \ge 1.0$
At ultimate → $DIF_u = 0.0101\,ln(\dot{\varepsilon}) + 1.10 \ge 1.0$

Case 2: DIF_t = 1.0 (no dynamic factor)

iv. HSR in tension

Case 1: Saatcioglu et al. (2011):

At ultimate → $DIF_u = 0.0101\,ln(\dot{\varepsilon}) + 1.10 \ge 1.0$

Case 2: DIF_t = 1.0 (no dynamic factor)

Note: f_{cf} – FRC stress at strain ε_{cf} ; f'_{cf} – peak FRC stress at strain ε'_{cf}; E_{cf} – FRC elastic modulus; f'_{ct} – peak FRC tensile stress at strain ε'_{ct}; f^*_2– FRC post-cracking stress at strain ε^*_2; τ_{bond} – matrix bond stress; V_f, l_f, d_f and E_{cf}– fiber content, length, diameter and elastic modulus; f_s – steel stress at strain ε_s; f_y – steel yield stress at strain ε_y; f_{sh} – steel hardening stress at strain ε_{sh}; f_u – steel ultimate stress at strain ε_u; $\dot{\varepsilon}_s$ – static strain rate; $\dot{\varepsilon}$ – dynamic strain rate; DIF_c, DIF_t, DIF_y & DIF_u: Dynamic increase factors for concrete in compression & tension and steel at yield & ultimate; α, η, γ, κ, $\beta^*$and δ – various curve fitting parameters; i – fiber parameter taken as = 1 for FRC and 0 for plain concrete.

Figure 8-5 Constitutive material and dynamic increase factor (DIF) models

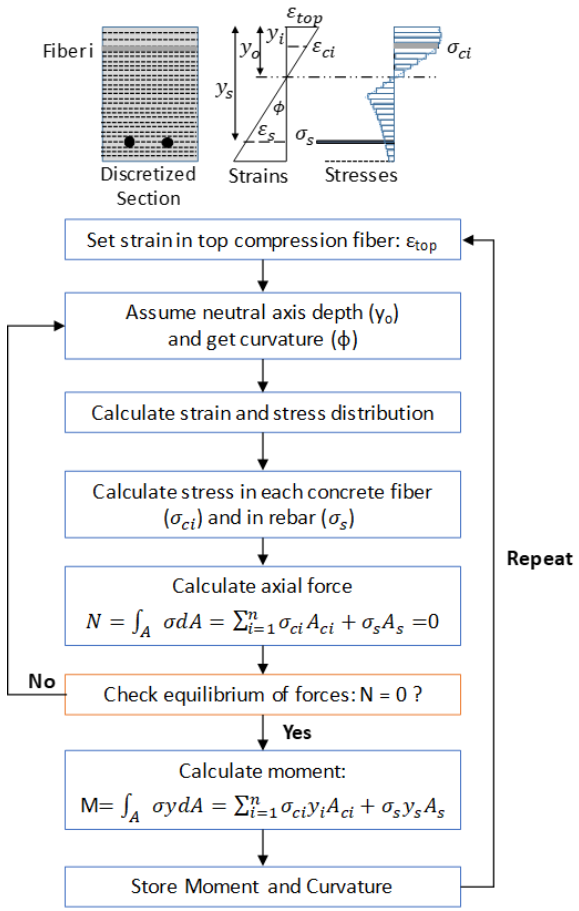

a) Multi-layer sectional analysis procedure to determine M-Φ relationship

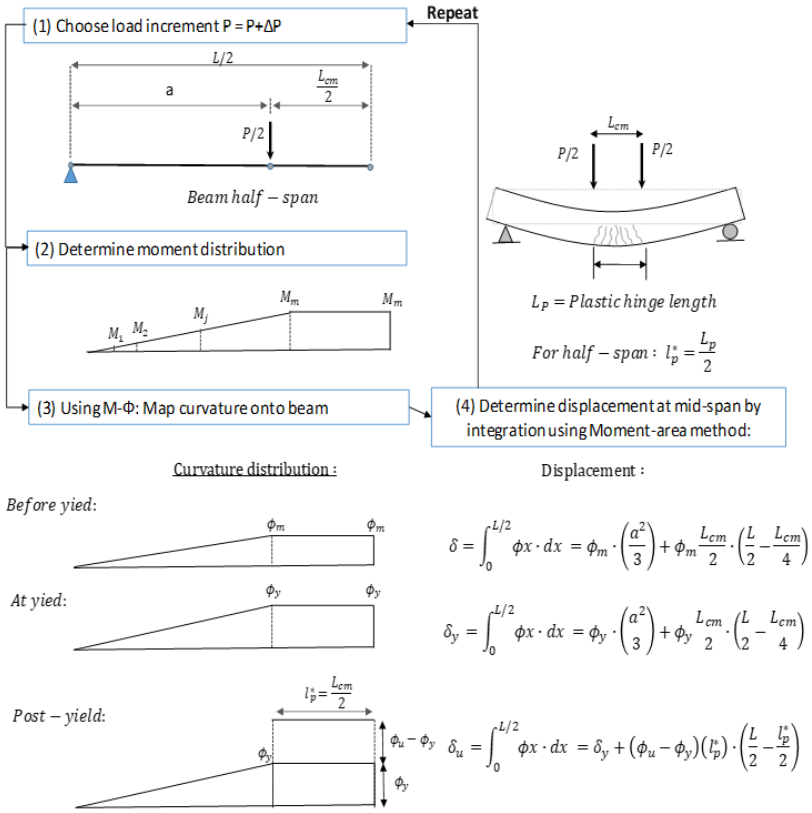

b) Procedure for determining load-displacement relationship

Figure 8-6 Procedure used in the development of analytical resistance curves (Adapted from Algassem et al., 2019)

8.3.2 FEA Procedure

The second approach used to predict the load-deflection response of the beams was finite element (FE) modelling. In this research, analyses were conducted using the two-dimensional nonlinear FE software *VecTor2* which incorporates the Modified Compression Field Theory (Vecchio and Collins, 1986) and the Disturbed Stress Field Method (Vecchio, 2000).

Figure 8-7 shows a schematic of the finite element meshes used in the analysis. Only half of the beam was modelled to account for symmetry. The mesh was generated using the "automatic method" in the software by setting the mesh boundaries and reinforcement locations. A mesh sensitivity analysis was conducted and a final mesh configuration of 10×10 mm for the rectangular elements was found to provide good accuracy. This mesh configuration resulted in a total of 4950 rectangular elements for the concrete and 213 truss elements for the longitudinal reinforcement.

Concrete elements were modelled using rectangular four-node plane stress elements, while two-node truss bar elements were used to model the longitudinal reinforcement. In most cases, transverse shear reinforcement and fibers were smeared within the concrete elements (the exception being the end stirrups in the beams designed without stirrups). Concrete Type 1 (light blue in **Figure 8-7**) was assigned for the regions with concrete and macro-synthetic fibers, while Concrete Type 2 (white in **Figure 8-7**) was assigned to the regions with both fibers and stirrups. For Type 1, *smeared reinforcement* consisted of polypropylene-straight fibers, while two forms of *smeared reinforcement* were used in Type 2 elements: one in the vertical direction to account for stirrups and one with 0.75% polypropylene-straight fibers. For the beam containing hybrid fibers, a third *smeared reinforcement* was added to account for the 0.25% micro-steel fibers. In both concrete types, the maximum crack spacing was set to d_v (effective shear depth) instead of the default value (of 1000 mm). This is based on the observations made by Carnovale (2013), where the default value was found to provide unrealistic results including premature failure.

Table 8-3 presents a summary of all the models used in the analysis. The beams were analyzed using the predefined (default) models in *VecTor2*, with some exceptions. To better model the effect of fibers on the behaviour of FRC in compression, the Lee et al. 2011 (FRC) model was selected for both the pre and post-peak compression response. The Vecchio 1992-A compression softening model was also selected as it has been used in other FRC studies (Susetyo et al., 2013; Hyrynyk & Vecchio, 2016). To better capture the response of FRC in tension, the Simplified Diverse Embedment Model (SDEM) model was used as it considers the effects of frictional bond and mechanical anchorage in fibers, which in turn provides a better prediction of the tensile response of cracked FRC. Likewise, the Lee 2010 (w/Post-Yield) model was selected for tension stiffening as it accounts for the effects of fibers. Concrete strength properties were assigned based on the results from the cylinder tests. The elastic modulus of concrete was calculated using the following equations for HSC (Popovics, 1973) and HSFRC (Lee et al., 2012), respectively:

$$E_c = 3320\sqrt{f'_c} + 6900 \quad \textbf{(8-9)}$$

$$E_{cf} = \left(-367V_f \frac{l_f}{d_f} + 5520\right) f_c'^{0.41} \qquad \textbf{(8-10)}$$

The properties of the normal-strength 15M/20M longitudinal steel reinforcement were assigned using the *ductile reinforcement* reference type in *VecTor2* with the stress and strain parameters obtained from the coupon tests. In the case of high-strength steel, the *MMFX steel* reference type was used. In both cases, the bars were assumed to be perfectly bonded to the concrete. **Figure 8-8** illustrates how these material properties are defined.

All nodes at midspan were restrained from displacement in the x direction while the nodes at the support were restrained from displacement in the y direction. A roller was used for the support since pinned supports would prevent movement in the horizontal direction which in turn would give rise to artificial restraints that are not present experimentally. This in turn was found to increase the stiffness of the beam resulting in higher strength with smaller mid-span deflection. Likewise, Carnovale (2013) reported that steel plates resulted in increased beam stiffness in the numerical results. Hence, they were not included in the model. It is important to note that if local failure occurs at point of load application, "bearing" type elements can be added below the steel plates in the *VecTor2* model. However, this was not the case in the current study. Loading was applied by imposing vertical displacements at the point of load application. The simulations were run in displacement control in increments of 0.5 mm.

The results of this analysis are presented in **Table 8-4** and **Figure 8-9**.

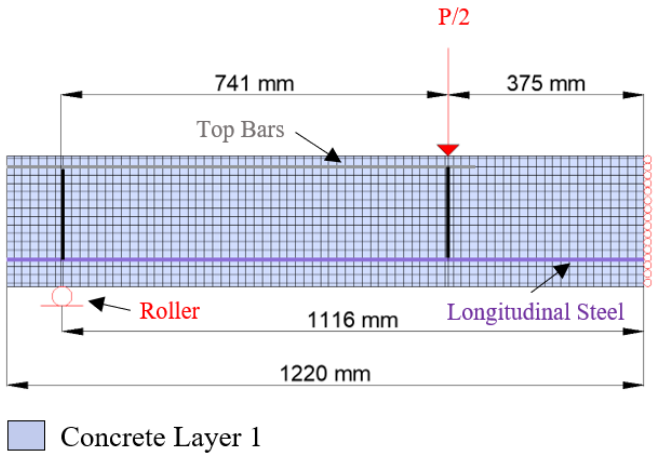

a) Idealized mesh for beamswithout stirrups

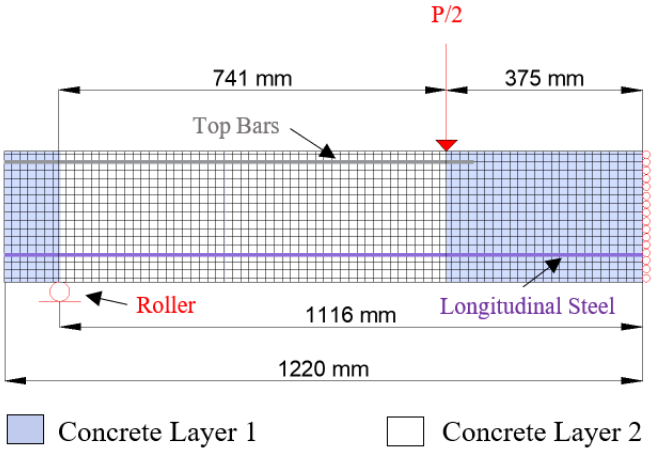

b) Idealized mesh for beams with stirrups

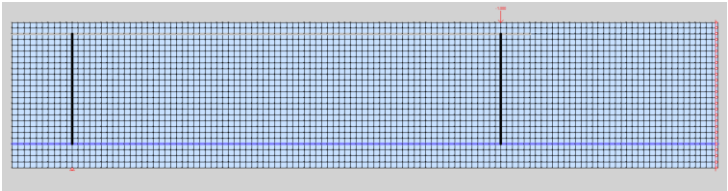

c) Actual model for beams without stirrups

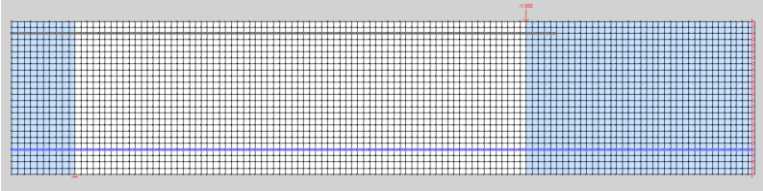

d) Actual model for beams with stirrups

Figure 8-7 Idealized and actual finite mesh for static analysis

Table 8-3 Constitutive models used in the FE analysis

Concrete Constitutive Models			
Compression Pre-Peak	Lee et al 2011 (FRC)	**Dilation**	Variable – Isotropic
Compression Post-Peak	Lee et al 2011 (FRC)	**Cracking Criterion**	Mohr-Coulomb (Stress)
Compression Softening	Vecchio 1992-A (e1/e2-Form)	**Crack Stress Calc**	Basic (DSFM/MCFT)
Tension Stiffening	Lee 2010 (w / Post-Yield)	**Crack Width Check**	Agg/2.5 Max Crack Width
Tension Softening	Exponential	**Crack Slip Calc**	Walraven
FRC Tension	SDEM-Monotonic/Cyclic	**Creep and Relaxation**	Not Considered
Confined Strength	Kupfer / Richart	**Hysteretic Response**	Nonlinear w / Plastic Offsets
Reinforcement Models			
Hysteretic Response	Bauschinger Effect (Seckin)	**Buckling**	Akkaya 2012 (Modified Dhakal-Maekawa)
Dowel Action	Tassios (Crack Slip)	**Concrete Bond**	Perfect Bond

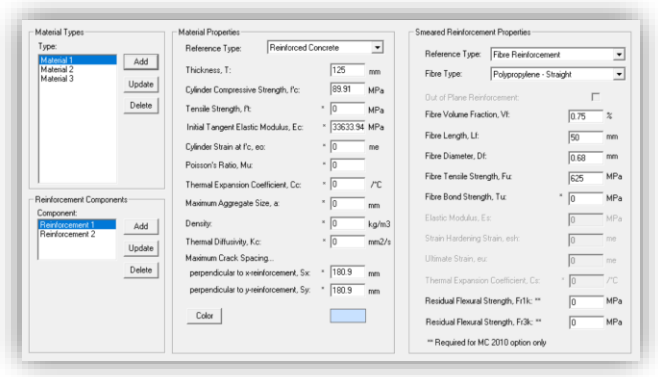

a) Concrete properties with fiber and transverse smeared reinforcement respectively

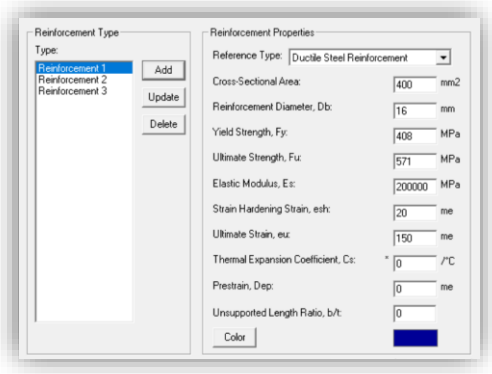

b) Longitudinal steel reinforcement properties

Figure 8-8 Defining material properties in VecTor2

8.3.3 Discussion

Figure 8-9 shows a comparison of the experimental and analytical static load-deflection responses of all the beams tested in this study. **Table 8-4** provides a comparison of maximum loads and displacements obtained in the experiments and in the simulations. Charts showing the accuracy of the predictions are also presented in **Figure 8-11**.

In general, the analytical load-deflection results from both analyses correlate well with the experimental results. However, it is important to note that one of the weaknesses of using sectional analysis is that it is not applicable to beams experiencing shear failure. Examining the initial ascending branches, both models provide good predictions of peak strength, however stiffness was slightly overestimated in both analyses. Considering all the beams, the mean ultimate load ratios (P_{anls}/P_{max}) are found to be 0.918 (with a standard deviation of 0.0337 and coefficient of variation of 3.67%) and 0.978 (with a standard deviation of 0.0556 and coefficient of variation of 5.69%) for the sectional and FE analyses, respectively. On the other hand, the average stiffness was 16% and 18% higher for the sectional and FEA analyses when compared to the experiments. Ababio et al. (2017) previously reported that absence of imperfections like micro cracks and assumed perfect bond between concrete and reinforcement would contribute to a stiffer response in numerical models. In reality, such imperfections lead to higher deflections in experimental testing, thus reducing the stiffness of the beam. Nevertheless, as yielding is approached, the model demonstrates a significant decrease in stiffness.

The maximum displacements were compared at the point of 80% drop in capacity. Considering all beams, the mean analytical-to-experimental displacement ratios ($\delta_{anls}/\delta_{max}$) are found to be 1.425 (with a standard deviation of 0.3574 and coefficient of variation of 25.08%) and 0.972 (with a standard deviation of 0.2066 and coefficient of variation of 21.25%) for the sectional and FE analyses, respectively. Examining the results, it can be observed that the FE modelling was able to better capture the post-peak response and strength decay in the beams, which in turn led to better predictions of δ_{max} when compared to the sectional analysis procedure (see **Figure 8-9i** and **Figure 8-11d**). Focussing on the sectional analysis results, it can also be observed that the choice of plastic hinge length didn't have a noticeable effect on strength or stiffness, however it affected the maximum displacements, which became larger with the increase in hinge length. In general, $\boldsymbol{l_p = l_{cm}}$ was found to better represent the post-peak deflection response in the fiber-reinforced concrete beams, however this is another potential source of error in the analysis.

One of the advantages of conducting finite element modelling is that it can allow for more detailed comparisons of further aspects of experimental behaviour, including crack patterns and failure mode. As shown in **Figure 8-10**, the FE models replicated the crack patterns observed in the experimental tests with reasonable accuracy. More importantly, the failure modes of the beams were well predicted, with diagonal shear crack failures observed in the HSC and FRC beams designed without stirrups and 0.75%S1 fibers as shown in **Figure 8-10a** – **d**. The model was also able to accurately predict the flexural failure and cracking pattern in the beam with 1% hybrid

fibers. Similarly, the FE models accurately predicted the flexural failures, concrete crushing and cracking patterns in the beams built with combined stirrups and fibers.

Table 8-4 Comparison of experimental vs. analytical results

Beam ID	Ultimate Load[1]						Maximum Mid-Span Displacement[2]				Predicted Failure Mechanism (FEA)
	P_{max} (kN)	*Analysis* (Sectional)		*Analysis* (FEA)		δ_{max} (mm)	*Analysis* (Sectional)		*Analysis* (FEA)		
		P_{anls} (kN)	P_{anls}/P_{max}	P_{anls} (kN)	P_{anls}/P_{max}		δ_{anls} (mm)	$\delta_{anls}/\delta_{max}$	δ_{anls} (mm)	$\delta_{anls}/\delta_{max}$	
SCC-0.75%S1-15M-0	85.7	×	--	89.3	1.04	18.3	×	--	18.5	1.01	Shear Failure
SCC-0.75%S1-15M-S	99	91.5	0.92	93.3	0.94	52.3	96.3	1.84	67.6	1.29	Flexural Failure
HSC-0%-15M-0	90	×	--	91.3	1.01	15.3	×	--	15.4	1.01	Shear Failure
HSC-0.75%S1-15M-0	112.2	98.5	0.88	104.0	0.93	67.3	91.4	1.36	63.3	0.94	Shear Failure
HSC-0.75%S1-15M-S	103.7	98.5	0.95	93.8	0.90	85	91.6	1.08	65.2	0.77	Flexural Failure
HSC-0.75%S1-20M-0	170	×	--	160.4	0.94	30	×	--	23.1	0.77	Shear Failure
HSC-0.75%S1-20M-S	156	149.5	0.96	166.7	1.07	31.1	59.0	1.90	38.7	1.24	Flexural Failure
HSC-HYB-20M-0	170.8	150.1	0.88	166.8	0.98	44.5	54.2	1.22	46.0	1.03	Flexural Failure
HSC-0.75%S1-No.5(HS)-S	213.1	195.4	0.92	210.0	0.99	40.7	47	1.15	28.1	0.69	Flexural Failure
		Statistical Data for $\delta_{anls}/\delta_{max}$					Statistical Data for $\delta_{anls}/\delta_{max}$				
		Sectional		*FEA*			*Sectional*		*FEA*		
		Mean	0.918	*Mean*	0.978		*Mean*	1.425	*Mean*	0.972	
		Std. Dev.	0.0337	*Std. Dev.*	0.0556		*Std. Dev.*	0.3574	*Std. Dev.*	0.2066	
		COV	3.67%	*COV*	5.69%		*COV*	25.08%	*COV*	21.25%	
		Max	0.96	*Max*	1.07		*Max*	1.90	*Max*	1.29	
		Min	0.88	*Min*	0.90		*Min*	1.08	*Min*	0.69	

[1]: P_{max} = experimental ultimate load; P_{anls} = analytical ultimate load;
[2]: δ_{max} = experimental mid-span displacement at 80% of peak; δ_{anls} = analytical mid-span displacement at 80% of peak;
× Analysis not applicable

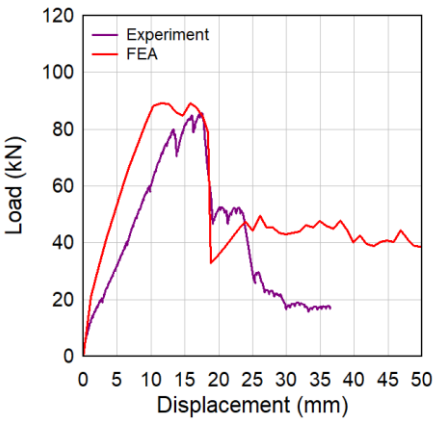

a) SCC-0.75%S1-15M-0

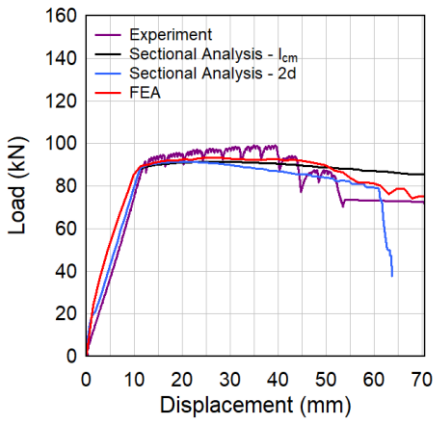

b) SCC-0.75%S1-15M-S

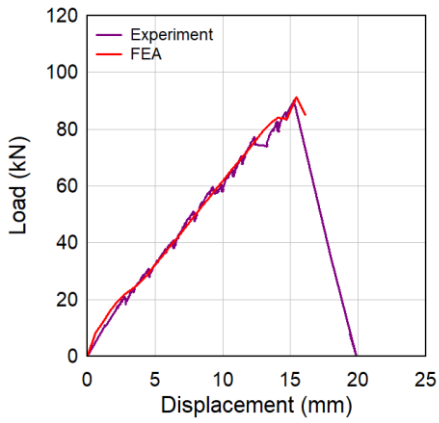

c) HSC-0%-15M-0

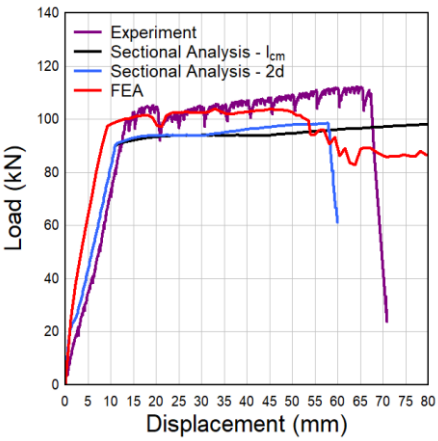

d) HSC-0.75%S1-15M-0

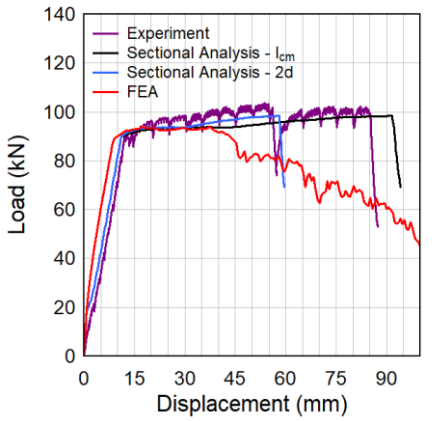

e) HSC-0.75%S1-15M-S

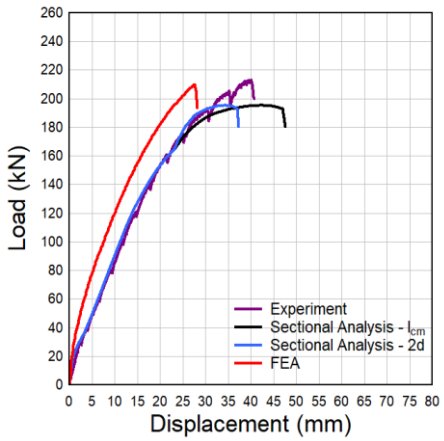

f) HSC-0.75%S1-No.5(HS)-S

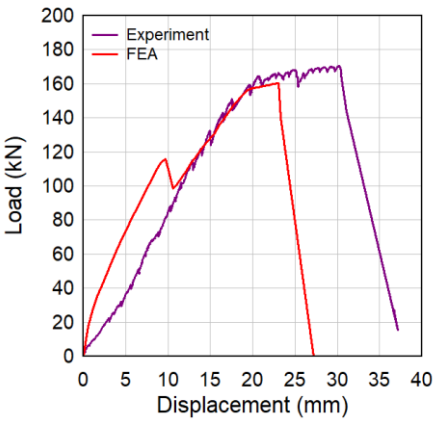

g) HSC-0.75%S1-20M-0

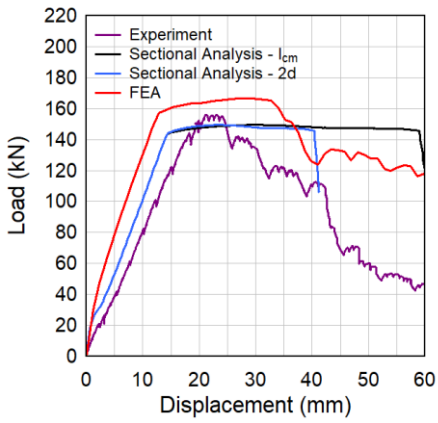

h) HSC-0.75%S1-20M-S

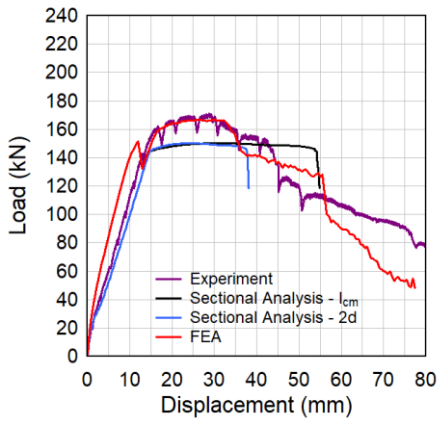

i) HSC-HYB-20M-0

Figure 8-9 Experimental and analytical load-deflection responses

Experimental	FEA
	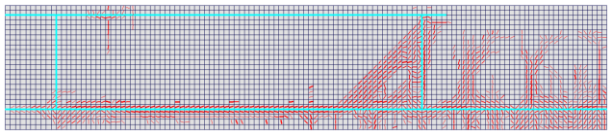
a) HSC-0%-15M-0	
	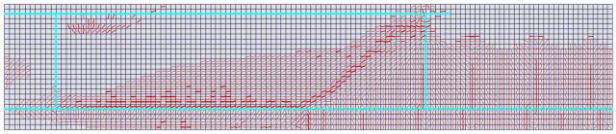
b) SCC-0.75%S1-15M-0	
	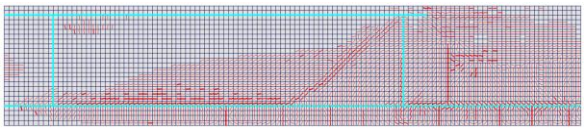
c) HSC-0.75%S1-15M-0	
	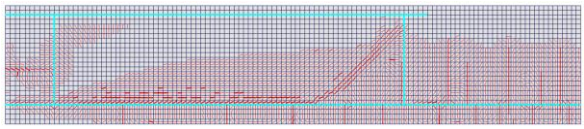
d) HSC-0.75%S1-20M-0	
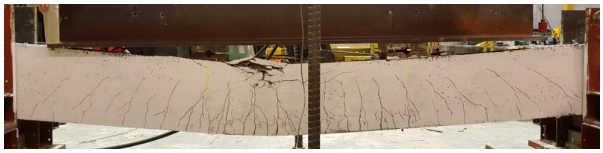	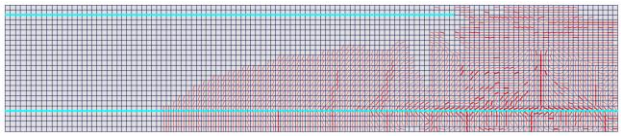
e) SCC-0.75%S1-15M-S	
	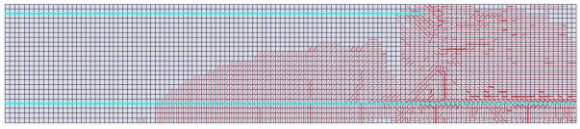
f) HSC-0.75%S1-15M-S	
	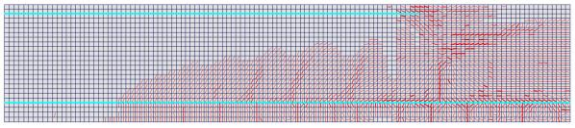
g) HSC-0.75%S1-20M-S	
	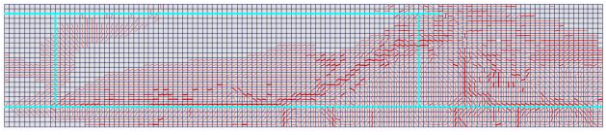
h) HSC-HYB-20M-0	
	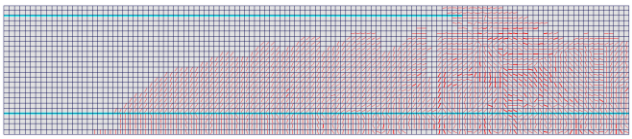
i) HSC-0.75%S1-No.5(HS)-S	

Figure 8-10 Comparison of experimental vs. FEA cracking patterns at end of testing

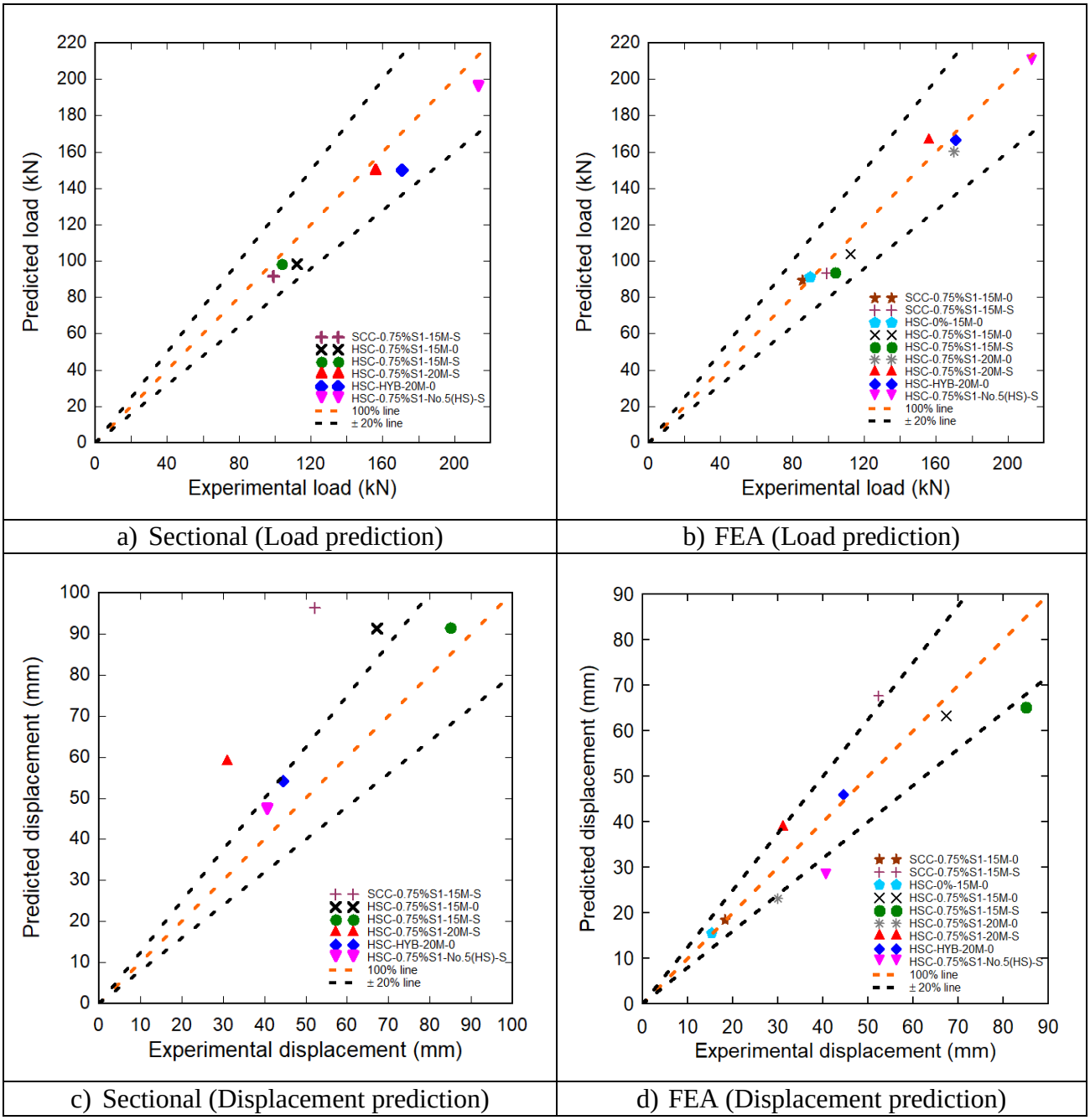

a) Sectional (Load prediction)

b) FEA (Load prediction)

c) Sectional (Displacement prediction)

d) FEA (Displacement prediction)

Figure 8-11 Predicted vs. experimental loads and displacements

8.4 Prediction of Dynamic Results

8.4.1 SDOF Analysis Procedure

The same sectional analysis procedure described in the previous section (**8.3.1**) was used to develop the dynamic resistance curves used in the blast analysis. However, in order to account for the effects of increased strain-rate, dynamic resistance curves were determined by applying dynamic increase factors to the material models described previously. The dynamic increase factors of concrete in compression ($\boldsymbol{DIF_{cf}}$), concrete in tension ($\boldsymbol{DIF_t}$) and longitudinal steel at yield and ultimate stress ($\boldsymbol{DIF_y}$ and $\boldsymbol{DIF_u}$ respectively) were predicted using the expressions proposed by Wang et al. (2011), Malvar & Ross (1998) and Saatcioglu et al. (2011). The equations used in these models are summarized in **Figure 8-5**.

Assuming a constant strain rate ($\dot{\boldsymbol{\varepsilon}}$) of 1 s^{-1} for the shock-tube experiments, the following factors are obtained for the HSC beams designed with normal-strength reinforcement: $\boldsymbol{DIF_c}$= 1.15, $\boldsymbol{DIF_t}$= 1.21, $\boldsymbol{DIF_y}$= 1.30 and $\boldsymbol{DIF_u}$= 1.10. Previous research by Malvar (1998) indicates that steel shows increased strain sensitivity at yield when compared to ultimate. Since the high-strength steel does not exhibit a well-defined yield plateau, the static stress-strain curve for this steel was modified using $\boldsymbol{DIF_u}$= 1.10, which corresponds to the DIF at ultimate in the Saatcioglu et al. (2011) model. **Figure 8-12** shows typical stress-strain curves for HSFRC, normal-strength and high-strength steel before and after incorporating strain-rate effects.

With the dynamic resistance curves determined, single-degree of freedom (SDOF) analysis was used to predict the dynamic response of the beams by solving the equation of motion shown below using the average acceleration numerical integration solution scheme in software *RCBlast*:

$$\boldsymbol{K_{LM} m \ddot{u}(t) + R(u(t)) = A P_r(t)} \qquad \textbf{(8-11)}$$

In this equation K_{LM} is a load-mass transformation factor which is used to transform the real structure into the equivalent SDOF system taking into account the beam loading and boundary conditions. Based on Biggs (1964), these factors were taken as 0.6 and 0.56 before and after yield respectively. The remaining parameters include: m = mass of the system consisting of the weight of the beam and LTD (taken as 450 kg), $u(t)$ and $\ddot{u}(t)$ = beam mid-span displacement and acceleration, $R(u(t))$ = beam resistance function and $AP_r(t)$ = loading function, where A is the impacted area of the LTD (taken as 3.4 m^2) and $P_r(t)$ is an idealized triangular pressure-time history having the same reflected pressure and impulse observed in the experiments.

With these parameters defined, the SDOF equation of motion was solved using the average acceleration numerical integration solution scheme in software *RCBlast*. **Figure 8-13** summarizes the main steps for performing the SDOF analysis.

To further study the influence of the resistance functions, a second set of analyses were conducted using the finite element (FE) load-deformation relationships presented in **Section 8.3.3**. To account for strain-rates effects, the *VecTor2* models were adjusted by increasing the material

strength properties in the simulations using the dynamic increase factor models proposed by Wang et al. (2011) and Saatcioglu et al. (2011) for concrete and longitudinal steel respectively. After determining the dynamic resistance functions, the same equation of motion was solved in *RCBlast* to determine the maximum displacements.

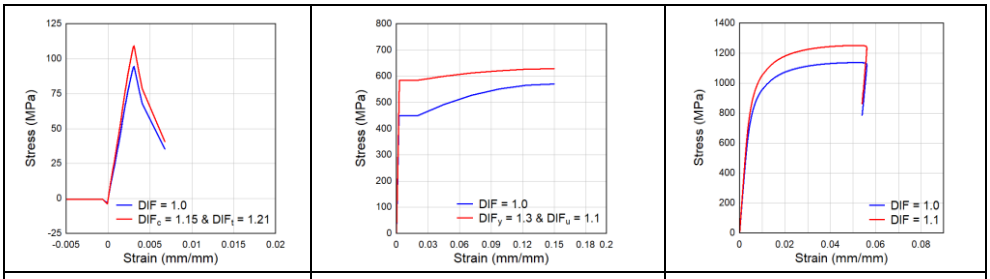

a) HSFRC	b) Normal-strength steel	c) High-strength steel

Figure 8-12 Typical stress-strain relationship with DIF

1st: Define member properties	2nd: Input material properties, section geometry & reinforcement details
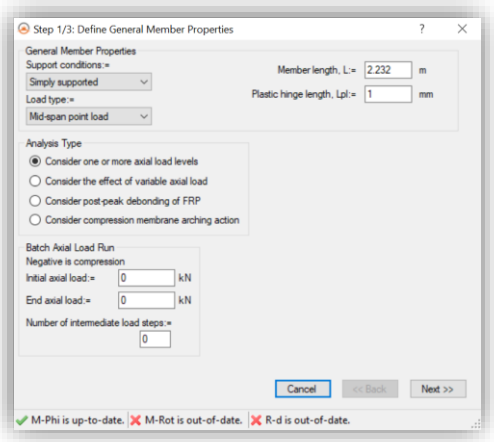	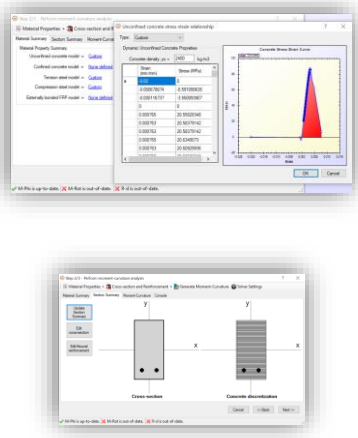
3rd: Generate moment-curvature using *RCBlast* software	4th: Generate load-displacement curve, then input back into *RCBlast*
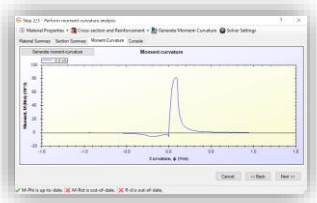	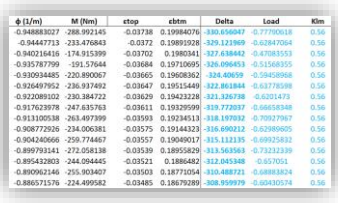

5th: Define the mass of the system and the pressure-time history, then run the SDOF analysis to obtain the maximum displacement

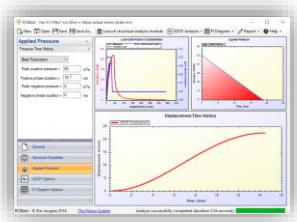

Figure 8-13 Steps for conducting the SDOF analysis

8.4.2 Discussion

Two different approaches were used to predict the dynamic responses of the specimens. In the first approach, sectional analysis (SA) was used to develop resistance functions which were then used to conduct single-degree of freedom (SDOF) analysis and determine maximum mid-span displacements. A similar SDOF analysis was used in the second approach, except that the resistance curves were determined using finite element (FE) modelling. Typical resistance curves developed using both approaches are shown in **Figure 8-14** and **Figure 8-15**. It is important to note that the sectional analysis procedure assumes flexural response and cannot predict shear failure, thus it is not suitable for beams experiencing shear failure (**Figure 8-14d**). When evaluated up to peak, both the sectional analysis and FEA underestimated the dynamic peak loads.

Comparisons between analytical and experimental mid-span displacements vs. time (up to peak) are provided in **Figure 8-16** and **Figure 8-17**. **Table 8-5** and **Figure 8-18** compares the analytical (δ_{anls}) and experimental (δ_{max}) maximum displacement results and their ratio ($\delta_{anls}/\delta_{max}$), along with statistical data related to the accuracy of the predictions.

Considering all the beams, the mean displacement ratio ($\delta_{anls}/\delta_{max}$) is found to be 1.066 (with a standard deviation of 0.1441 and coefficient of variation of 13.52%) when using the sectional analysis SDOF approach. The results indicate good correlations with experimental data confirming that the blast response was well predicted using this procedure. Examining the individual results, larger errors were obtained for beams HSC-0.75%S1-20M-10M-d/2 and HSC-HYB-20M-0 since the models did not specifically account for the effects of confinement and the influence of using hybrid fibers on material properties. Moreover, the results for beam HSC-0.75%S1-No.5(HS)-S are generally conservative ($\delta_{anls}/\delta_{max} > 1$), and this can be explained by the fact that the ACI ITG model provides a lower bound estimate of the actual stress-strain response of the high-strength bars.

Considering the second approach, which used SDOF analysis incorporating the FE derived resistance functions, the mean displacement ratio is found to be 0.976 (with a standard deviation of 0.1617 and coefficient of variation of 16.56%). In general, it can be seen that the analysis predicted blowout failures for some beams ahead of what was recorded experimentally. For instance, beam HSC-HYB-20M-0 fails experimentally at Blast 3a – 80 psi while the analysis predicts failure at Blast 2c – 70 psi. The result can partly be explained by the fact that the dynamic analytical resistance curve shows a smaller maximum displacement, with reduced post-peak ductility, when compared to the static experimental and analytical load-deflection curves as shown in **Figure 8-15f**. This can be attributed to the effects of applying DIF factors on the material models (especially the steel) which may have triggered shear failure in the FE simulations.

Table 8-5 Idealized blast properties and results of analyses

Beam ID	Shot #	Blast I.D.	Idealized Shockwave Properties[1]			Maximum Mid-Span Displacement[2]				
							Analysis (SDOF)		*Analysis* (FEA + SDOF)	
			P_r (kPa)	I_r (kPa·msec)	t_d (msec)	δ_{max} (mm)	δ_{anls} (mm)	$\delta_{anls}/\delta_{max}$	δ_{anls} (mm)	$\delta_{anls}/\delta_{max}$
HSC-0%-15M-0	1	1	35.9	323.6	18.0	16.1	×	--	×	--
HSC-0.75%S1-15M-0	1	1	44.4	377.7	17.0	18.8	19.3	1.03	16.7	0.89
	2	2a	65.6	553.5	16.9	35.6	×	--	×	--
HSC-0.75%S1-15M-S	1	1	35.9	375.5	20.9	16.7	16.3	0.98	14.3	0.86
	2	2a	65.0	484.1	14.9	29.6	32.6	1.10	30.4	1.03
	3	2c	72.0	711.7	19.8	86.7	77.9	0.90	90.5	1.04
HSC-0.75%S1-20M-0	1	1	44.6	378.7	17.0	12.5	14.6	1.17	14.6	1.17
	2	2a	61.0	521.0	17.1	18.5	22.6	1.22	*	--
	3	2b	71.0	653.0	18.4	84.1	×	--	×	--
HSC-0.75%S1-20M-S	1	1	44.0	334.5	15.2	12.2	13.6	1.11	12.3	1.01
	2	2a	55.9	523.4	18.7	23.2	21.0	0.91	19.2	0.83
	3	2c	83.9	723.8	17.3	44.7	41.3	0.92	38.2	0.85
	4	3a	90.9	832.0	18.3	186.6	*	--	*	--
HSC-0.75%S1-20M-10M-d/2	1	1	45.1	405.6	18.0	10.8	14.9	1.38	13.9	1.29
	2	2c	79.8	723.6	18.1	44.2	39.1	0.88	35.9	0.81
	3	3b	90.1	979.8	21.7	86.2	*	--	*	--
HSC-HYB-20M-0	1	1	41.3	377.0	18.3	16.4	14.3	0.87	14.5	0.88
	2	2a	66.9	586.5	17.5	22.9	27.3	1.19	28.6	1.25
	3	2c	76.7	961.8	25.1	41.1	42.4	1.03	*	--
	4	3a	82.8	853.2	20.6	60	*	--	×	--
HSC-0.75%S1-No.5(HS)-S	1	1	45.4	395.4	17.4	16.5	17.9	1.08	13.6	0.82
	2	2a	61.8	520.4	16.8	22.3	25.9	1.16	20.9	0.94
	3	2c	76.3	913.9	23.9	37.8	45.1	1.19	*	--
	4	3b	92.5	876.1	18.9	174.0	*	--	×	--

Statistical Data for $\delta_{anls}/\delta_{max}$			
SDOF		*FEA + SDOF*	
Mean	1.066	*Mean*	0.976
Std. Dev.	0.1441	*Std. Dev.*	0.1617
COV	13.52%	*COV*	16.56%
Max	1.38	*Max*	1.29
Min	0.87	*Min*	0.81

[1]: P_r =reflected pressure; I_r = reflected impulse; t_d = positive phase duration;

[2]: δ_{max} = experimental mid-span displacement; δ_{anls} = analytical mid-span displacement; AD = accumulated damage

***** Analysis predicts blowout failure

× Analysis not applicable

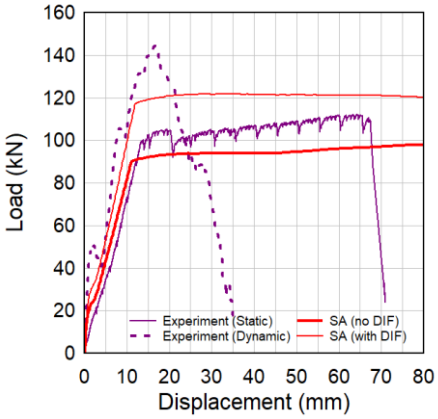

a) HSC-0.75%S1-15M-0

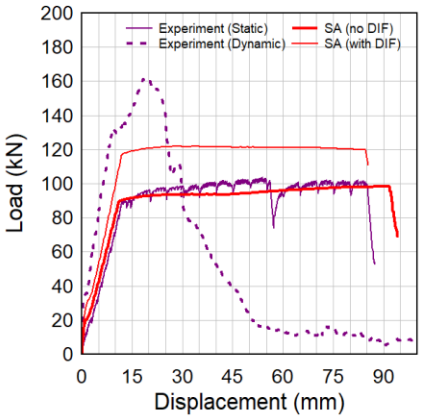

b) HSC-0.75%S1-15M-S

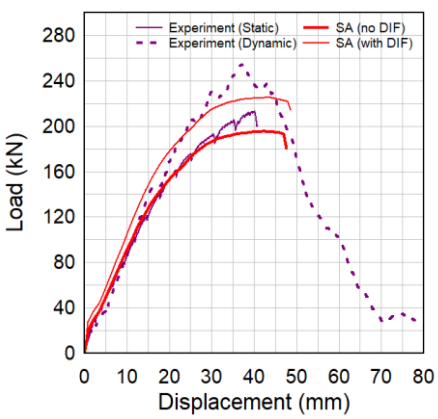

c) HSC-0.75%S1-No.5(HS)-S

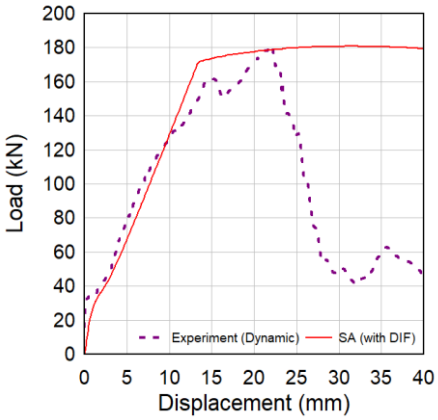

d) HSC-0.75%S1-20M-0

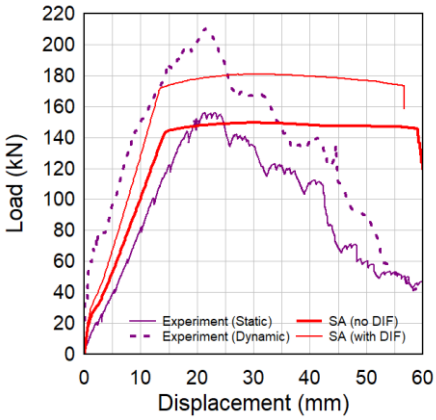

e) HSC-0.75%S1-20M-S

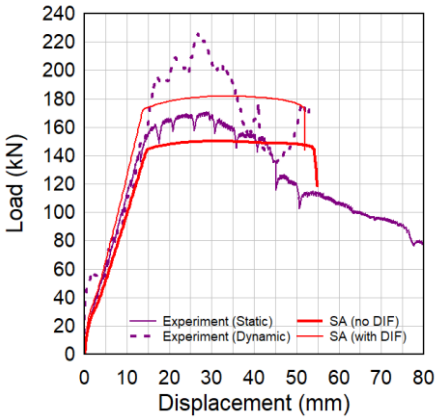

f) HSC-HYB-20M-0

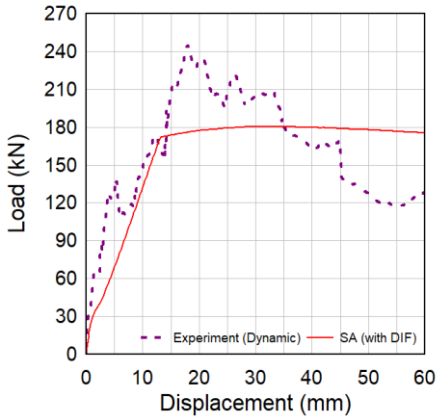

g) HSC-0.75%S1-20M-10M-d/2

Figure 8-14 Sample analytical resistance curves – Sectional analysis procedure

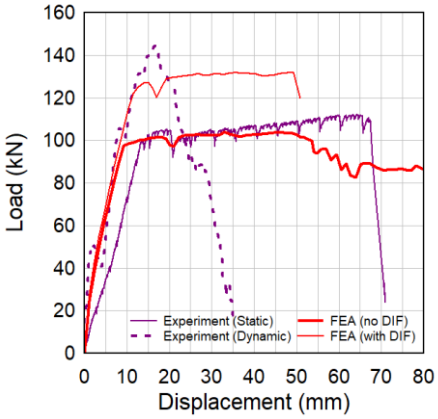

a) HSC-0.75%S1-15M-0

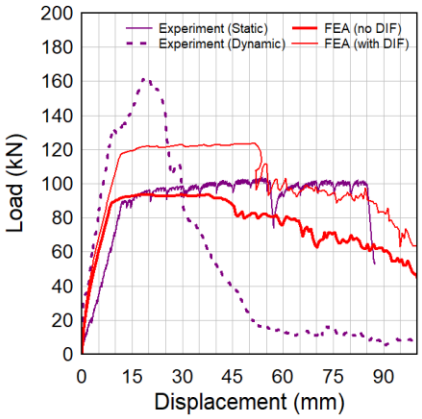

b) HSC-0.75%S1-15M-S

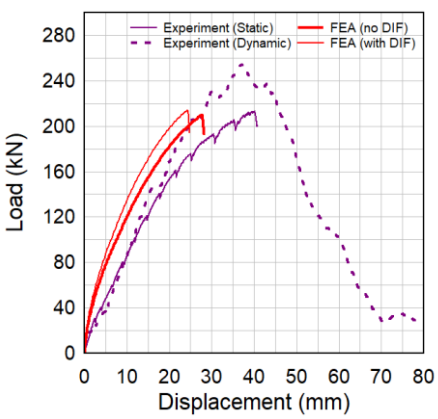

c) HSC-0.75%S1-No.5(HS)-S

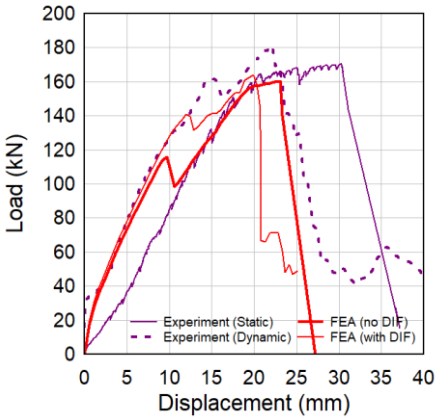

d) HSC-0.75%S1-20M-0

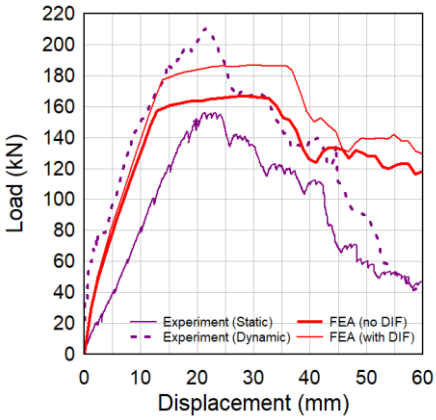

e) HSC-0.75%S1-20M-S

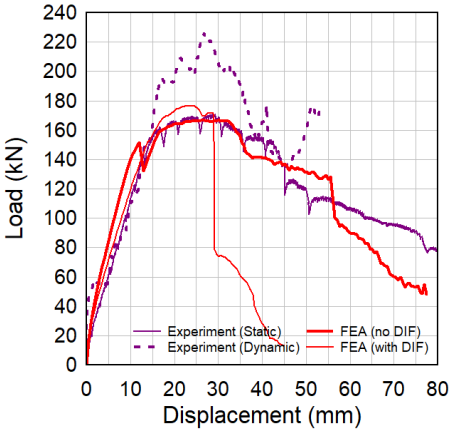

f) HSC-HYB-20M-0

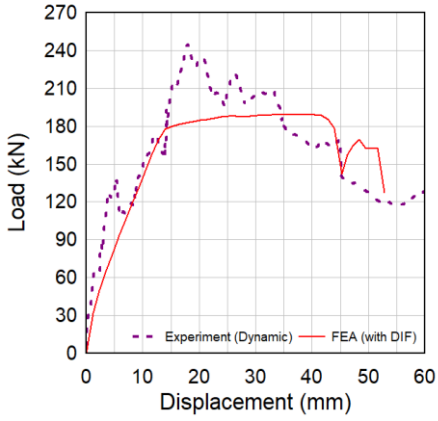

g) HSC-0.75%S1-20M-10M-d/2

Figure 8-15 Sample analytical resistance curves – FEA procedure

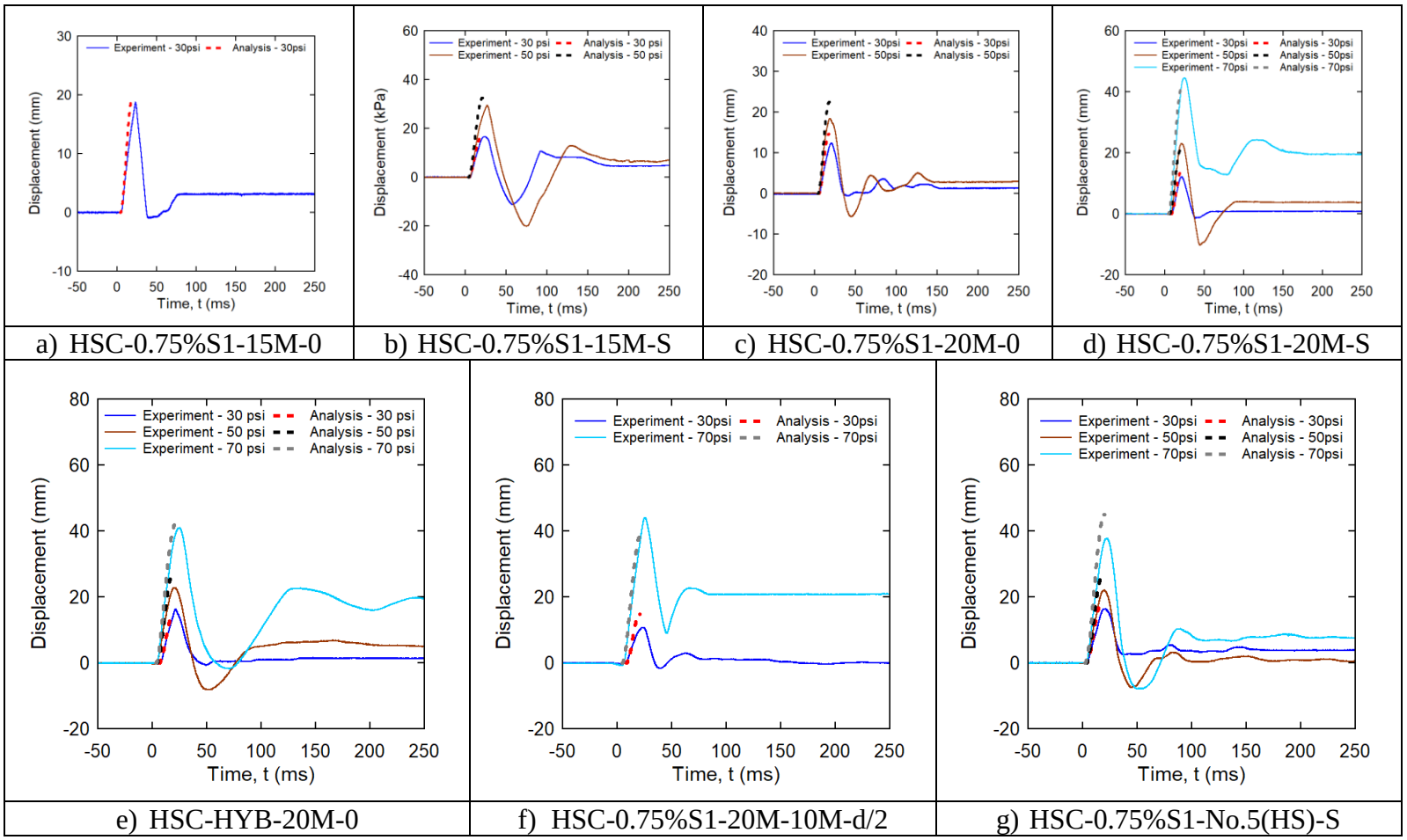

a) HSC-0.75%S1-15M-0 | b) HSC-0.75%S1-15M-S | c) HSC-0.75%S1-20M-0 | d) HSC-0.75%S1-20M-S

e) HSC-HYB-20M-0 | f) HSC-0.75%S1-20M-10M-d/2 | g) HSC-0.75%S1-No.5(HS)-S

Figure 8-16 Predicted (SDOF) vs. maximum mid-span experimental displacement

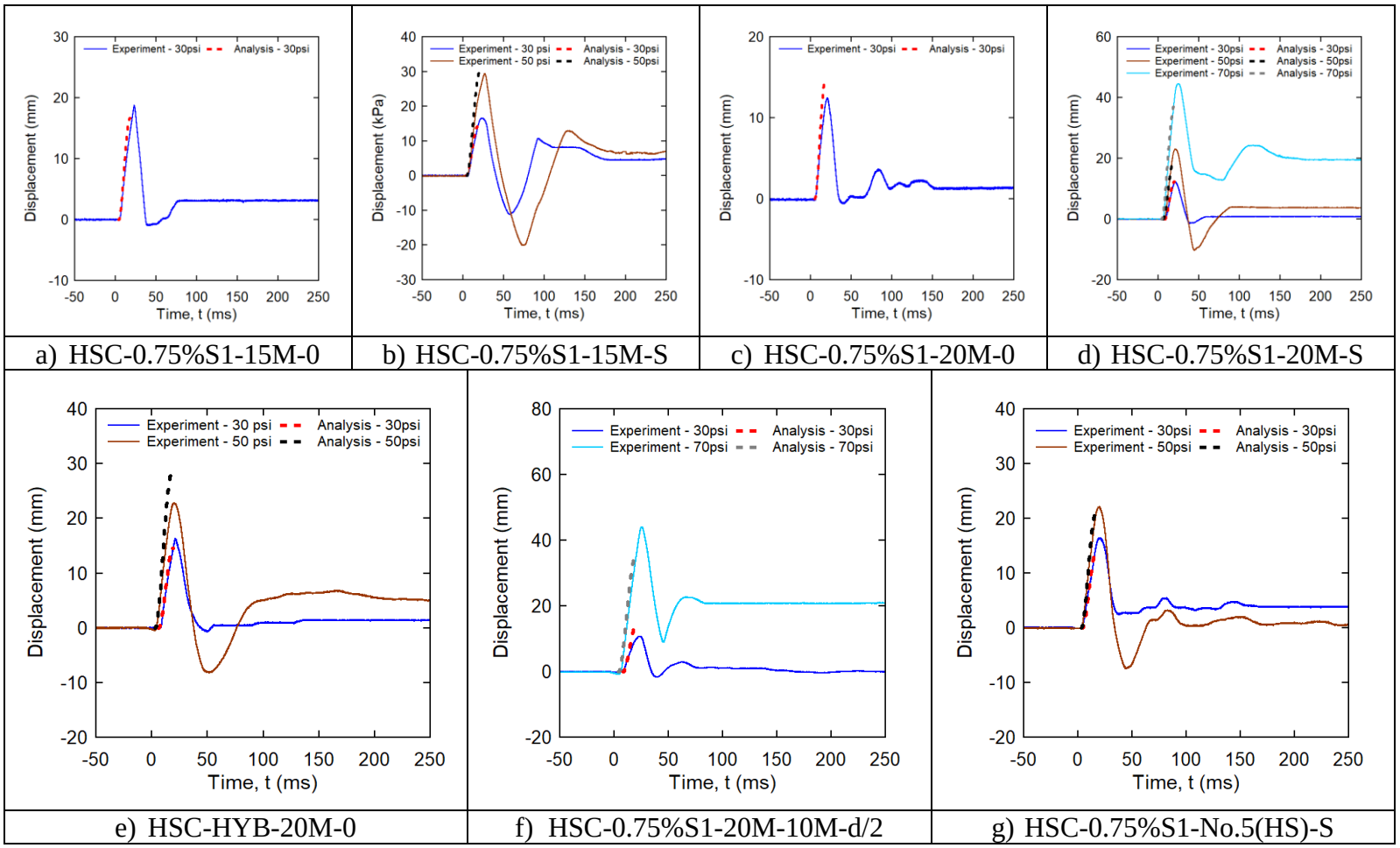

a) HSC-0.75%S1-15M-0 | b) HSC-0.75%S1-15M-S | c) HSC-0.75%S1-20M-0 | d) HSC-0.75%S1-20M-S

e) HSC-HYB-20M-0 | f) HSC-0.75%S1-20M-10M-d/2 | g) HSC-0.75%S1-No.5(HS)-S

Figure 8-17 Predicted (FEA + SDOF) vs. maximum mid-span experimental displacement

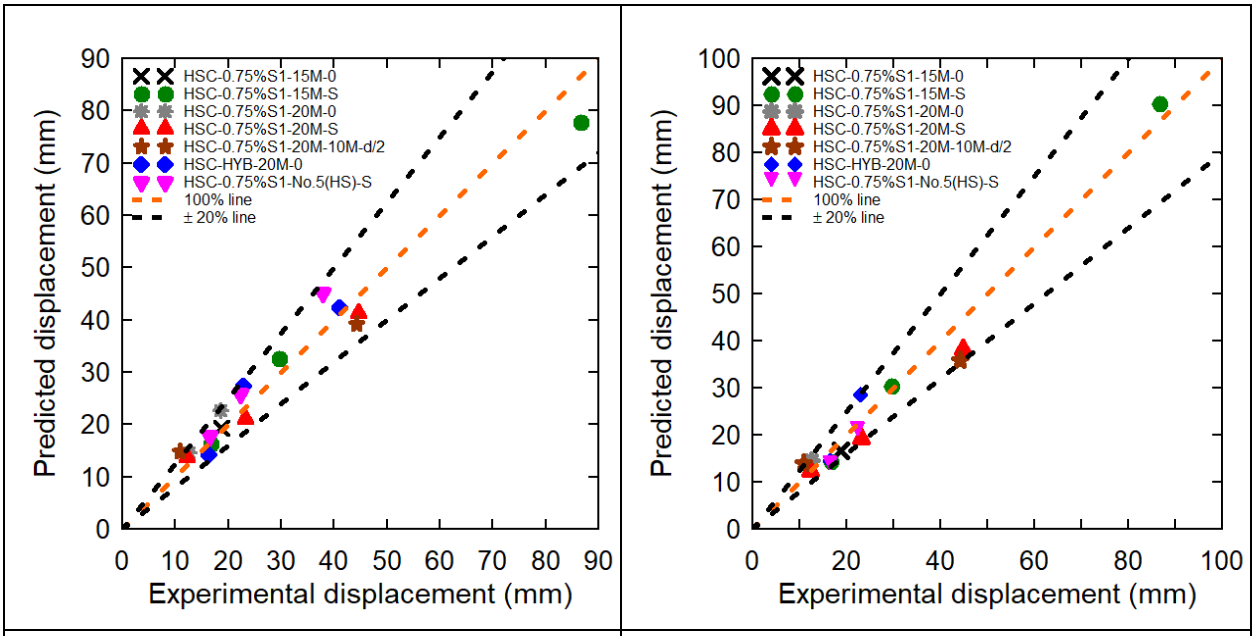

a) SDOF | b) FEA + SDOF

Figure 8-18 Predicted vs. maximum mid-span experimental displacements

Chapter 9: Conclusion & Recommendations

9.1 Conclusion

This thesis presented the results of a combined experimental and analytical research program which examined the effects of macro-synthetic fibers on the shear and flexural behaviour of high-strength concrete beams subjected to static and dynamic loads. The study included seventeen beams, with nine specimens tested under slowly applied four-point bending and eight beams tested under simulated blast loads using a shock-tube. Test parameters included the effects of macro-synthetic fibers, fiber hybridization, combined use of fibers and stirrups, as well as longitudinal steel ratio and type. The following conclusions can be drawn from this study:

- The results indicate that the provision of synthetic fibers increases the shear resistance of high-strength concrete beams tested under both static and blast loads. The use of fibers allowed for the development of yield stresses in the longitudinal rebar due to the fiber bridging effect, which in turn improved the overall behaviour of the beams by delaying shear failure. However, the use of 0.75% fibers was not sufficient to replace transverse reinforcement in beams subjected to both static and blast loading, with a more sudden failure observed under blast conditions due to a loss in fiber efficiency;
- In beams detailed with sufficient shear reinforcement, the use of synthetic fibers was effective in improving ductility and cracking behaviour under static loads. Under blast loading, the use of synthetic fibers improved control of maximum and residual displacements at equivalent blasts and provided increased blast resistance. Moreover, the fibers were very effective in increasing damage tolerance by controlling concrete crushing and reducing secondary fragments;
- The use of 1% hybrid fibers was capable of effectively replacing transverse reinforcement in beams subjected to both static and blast loads, preventing shear failure and promoting ductile flexural response. The use of hybrid fibres also reduced maximum and residual deformations, increased blast capacity, and improved damage tolerance when compared to companion beams built with mono fibers and stirrups;
- When compared to the plain HSC beam, the results confirm that the use of synthetic fibers is better suited for beams detailed with high-strength (HS) reinforcement allowing the steel in such beams to reach post-yield levels under both loading conditions. Adding synthetic fibers was also effective in reducing inbound and rebound mid-span displacements, while also better controlling damage and spalling at failure;
- Substituting normal-strength bars with high-strength bars in HSFRC beams resulted in increased load-carrying capacity under static loads, but at the expense of reduced ductility due to more sudden compression failure. Under blast loading, the use of high-strength bars enhanced control of mid-span displacements and increased blast capacity. However, failure in the HSFRC beam detailed with HS steel was relatively more severe;

- The results show that synthetic fibers can possibly be used to relax blast detailing in HSC beams. Adding fibers in beams with intermediate tie spacing (s = d/2) provided a response that is similar to beams with the reduced tie spacing (s = d/4) required by modern blast codes, both in terms of blast capacity and displacements, with better control of damage.

As part of the analytical study, the response and failure mode of the beams were predicted using various approaches, including sectional analysis, FEA modelling and SDOF analysis. The following conclusions can be drawn from the analytical study:

- The Imam et al. (1995) and Yazdanbakhsh et al. (2015) models provided reasonable predictions of the shear and flexural capacities of the beams tested in this study. Based on the results, a shear-to-flexure load ratio greater than 1.5 is recommended when designing high-strength concrete beams reinforced with synthetic fibers. It is also recommended that such beams be provided with minimum stirrups to prevent brittle shear failure under both static and dynamic conditions;
- The static load-deflection responses of the beams were predicted using both sectional analysis and more advanced FE modelling using software *VecTor2*. Both analytical approaches allowed for reasonable predictions of maximum load and post-peak response in FRC beams having varying design properties. The FE approach was further able to predict the cracking patterns and failure modes of the beams;
- Dynamic resistance functions developed using both sectional analysis and FE modelling were used to predict the dynamic responses of the beams using a SDOF approach. Both methods resulted in good predictions of maximum displacements, with average predicted-to-experimental displacement ratios of 1.066 and 0.976, respectively.

9.2 Recommendations for Future Research

The following recommendations for future studies are suggested in order to improve understanding of the behaviour of HSFRC under quasi-static and blast loads:

- Examining the compressive and tensile response of HSC reinforced with macro-synthetic fibers and hybrid fibers in order to develop reliable models that can be used in the static and dynamic analysis of high-strength FRC structures;
- Examining the effect of synthetic fiber content and type on the static and blast response of reinforced concrete structural members;
- Investigating other forms of fiber hybridization to further understand and enhance the synergy effect observed in such cases;
- Further studying the effect of synthetic fibers in HSC structures reinforced with HSR;
- Performing further analytical studies using 2D and 3D FEA to better capture the blast response of high-strength fiber-reinforced concrete structural components (predicting the dynamic response of the beams with the blast analysis capability of *VecTor2*).

References

AbdelAleem, B. H., Ismail, M. K., & Hassan, A. A. (2018). Effect of Synthetic Fibers on Shear Capacity of Reinforced Rubberized Concrete Beams. *ACI Materials Journal*, *115*(2), 279-288.

ACI Committee 544. (1988). Design considerations for steel-fiber reinforced concrete. *ACI 544.4R-188, American Concrete Institute, Detroit, Mich*.

ACI. (2011). Building Code Requirements for Structural Concrete (ACI 318-11). In *American Concrete Institute*.

Adhikary, S. D., Li, B., & Fujikake, K. (2012). Dynamic behavior of reinforced concrete beams under varying rates of concentrated loading. *International Journal of Impact Engineering*, *47*, 24-38.

Aldabagh, S., Abed, F., & Yehia, S. (2019, March). Flexural Response of RC Beams Reinforced with HSS bars using FEA. In *2019 Advances in Science and Engineering Technology International Conferences (ASET)* (pp. 1-5). IEEE.

Algassem, O. (2016). *Parameters Affecting the Blast Performance of High Strength Fibre Reinforced Concrete Beams* (Masters dissertation, Université d'Ottawa/University of Ottawa).

Algassem, O., Li, Y., & Aoude, H. (2019). Ability of steel fibers to enhance the shear and flexural behavior of high-strength concrete beams subjected to blast loads. *Engineering Structures*, *199*, 109611.

Altoubat, S., Yazdanbakhsh, A., & Rieder, K. A. (2009). Shear behavior of macro-synthetic fiber-reinforced concrete beams without stirrups. *ACI Materials Journal*, *106*(4), 381.

Altoubat, S., Yazdanbakhsh, A., & Rieder, K. A. (2012). Shear strength of beams reinforced with synthetic macro-fibers and stirrups. *BEFIB2012*.

American Society for Testing and Materials. (2001). ASTM C143, Standard Test Method for Slump of Hydraulic-Cement Concrete. Philadelphia: ASTM.

Amin, A., Foster, S. J., Gilbert, R. I., & Kaufmann, W. (2017). Material characterisation of macro synthetic fibre reinforced concrete. *Cement and Concrete Composites*, *84*, 124-133.

Arslan, G., & Keskin, R. S. O. (2019). Influence of polypropylene fibres on the shear strength of RC beams with web reinforcement. *European Journal of Environmental and Civil Engineering*, *23*(10), 1222-1234.

Ashour, S. A., Hasanain, G. S., & Wafa, F. F. (1992). Shear behavior of high-strength fiber reinforced concrete beams. *Structural Journal*, *89*(2), 176-184.

Ashour, S. A., & Wafa, F. F. (1993). Flexural behavior of high-strength fiber reinforced concrete beams. *Structural Journal*, *90*(3), 279-287.

ASTM A1035/A1035M-11. (2011). Standard Specification for Deformed and Plain, Low-Carbon, Chromium, Steel Bars for Concrete Reinforcement.

ASTM. (2012). Standard test method for flexural performance of fiber-reinforced concrete (using beam with third-point loading). *ASTM-C1609*.

ASTM. C1611 (2014). Standard Test Method for Slump Flow of Self-Consolidating Concrete. *ASTM International, West Conshohocken*.

ASTM International. (2014). ASTM C39: Standard Test Method for Compressive Strength of Cylindrical Concrete Specimens.

Athiappan, K. V. S.(2014). Experimental study on flexural behavior of sisal fiber in reinforced concrete beam. *International Journal of Engineering Research & Technology (IJERT), 3*, 1500-1505.

Aulia, T. B. (2015). Bending capacity analysis of high-strength reinforced concrete beams using environmentally friendly synthetic fiber composites. *Procedia Engineering*, *125*, 1121-1128.

Banthia, N. P. (1987). *Impact resistance of concrete* (Doctoral dissertation, University of British Columbia).

Banthia, N., & Mindess, S. (1996). Impact resistance of steel fiber reinforced concrete. *Materials Journal*, *93*(5), 472-479.

Banthia, N., Majdzadeh, F., Wu, J., & Bindiganavile, V. (2014). Fiber synergy in Hybrid Fiber Reinforced Concrete (HyFRC) in flexure and direct shear. *Cement and Concrete Composites*, *48*, 91-97.

Bernard, E. S. (2019). Effect of Synthetic Fibers and Aggregate Size on Flexural Crack Widths. *ACI Structural Journal*, *116*(3).

Biggs, J. M. (1964). Introduction to Structural Dynamics. *McGraw-Hill Inc., New York*.

Biolzi, L., & Cattaneo, S. (2017). Response of steel fiber reinforced high strength concrete beams: Experiments and code predictions. *Cement and Concrete Composites*, *77*, 1-13.

Canadian Standards Association. (2012). Design and assessment of buildings subjected to blast loads, CSA S850-12.

Carnovale, D. J. (2013). *Behaviour and analysis of steel and macro-synthetic fibre reinforced concrete subjected to reversed cyclic loading: a pilot investigation* (Doctoral dissertation).

Castonguay, S. (2017). *Performance of Steel Fiber-Reinforced Concrete Beams Under Shock Tube Induced Blast Loading* (Masters dissertation, Université d'Ottawa/University of Ottawa).

Charles, C. (2019). *Effects of Detailing and Fibers on the Static and Blast Behaviour of High-Strength Concrete Beams* (Masters dissertation, Université d'Ottawa/University of Ottawa).

Chiranjeevi Reddy, K., & Subramaniam, K. V. (2017). Experimental investigation of crack propagation and post-cracking behaviour in macrosynthetic fibre reinforced concrete. *Magazine of Concrete Research*, *69*(9), 467-478.

Chorzepa, M. G., Masud, M., Yaghoobi, A., & Jiang, H. (2017). Impact Test: Multiscale Fiber-

Reinforced Concrete Including Polypropylene and Steel Fibers. *ACI Structural Journal*, *114*(6).

Conforti, A., Minelli, F., Tinini, A., & Plizzari, G. A. (2015). Influence of polypropylene fibre reinforcement and width-to-effective depth ratio in wide-shallow beams. *Engineering Structures*, *88*, 12-21.

Conforti, A., Minelli, F., & Plizzari, G. A. (2017). Shear behaviour of prestressed double tees in self-compacting polypropylene fibre reinforced concrete. *Engineering Structures*, *146*, 93-104.

Coughlin, A. M., Musselman, E. S., Schokker, A. J., & Linzell, D. G. (2010). Behavior of portable fiber reinforced concrete vehicle barriers subject to blasts from contact charges. *International Journal of Impact Engineering*, *37*(5), 521-529.

Di Prisco, M., Plizzari, G., & Vandewalle, L. (2009). Fibre reinforced concrete: new design perspectives. *Materials and structures*, *42*(9), 1261-1281.

Drdlová, M., Popovič, M., & Koutný, O. (2018). Blast resistance of hybrid fibre reinforced concrete containing polyvinyl alcohol, polypropylene and steel fibres with various shape parameters. *The European Physical Journal Special Topics*, *227*(1-2), 111-126.

Euclid Chemical (n.d.). What are the differences between micro and macro-synthetic fibers? *Redwood Road Cleveland, OH*.

fib. (2010). Fib model code for concrete structures 2010. *Lausanne, Switzerland*.

Foglar, M., & Kovar, M. (2013). Conclusions from experimental testing of blast resistance of FRC and RC bridge decks. *International Journal of Impact Engineering*, *59*, 18-28.

Greenough, T., & Nehdi, M. (2008). Shear behavior of fiber-reinforced self-consolidating concrete slender beams. *ACI materials Journal*, *105*(5), 468.

Horska, A., Jiricek, P., & Foglar, M. (2015). Impact performance of FRC slabs under various strain rates. In *EPJ Web of Conferences* (Vol. 94, p. 01057). EDP Sciences.

Hrynyk, T. D., & Vecchio, F. J. (2016). Modeling of Reinforced and Fiber-Reinforced Concrete Slabs under Impact Loads.

Imam, M., Vandewalle, L., & Mortelmans, F. (1995). Shear–moment analysis of reinforced high strength concrete beams containing steel fibres. *Canadian Journal of Civil Engineering*, *22*(3), 462-470.

Jacques, E. (2014). RCBLAST (Version 0.5.1). Retrieved from http://www.rcblast.ca

Jacques, E., Lloyd, A., & Saatcioglu, M. (2012). Predicting reinforced concrete response to blast loads. *Canadian Journal of Civil Engineering*, *40*(5), 427-444.

Jin, L., Zhang, R., Dou, G., Xu, J., & Du, X. (2017). Experimental and numerical study of reinforced concrete beams with steel fibers subjected to impact loading. *International Journal of Damage Mechanics*, *27*(7), 1058-1083.

Joshi, S. S., Thammishetti, N., & Prakash, S. S. (2018). Efficiency of steel and macro-synthetic

structural fibers on the flexure-shear behaviour of prestressed concrete beams. *Engineering Structures*, *171*, 47-55.

Karthik, M. P., & Maruthachalam, D. (2015). Experimental study on shear behaviour of hybrid Fibre Reinforced Concrete beams. *KSCE Journal of Civil Engineering*, *19*(1), 259-264.

Kishi, N., & Mikami, H. (2012). Empirical Formulas for Designing Reinforced Concrete Beams under Impact Loading. *ACI Structural Journal*, *109*(4).

Kwak, Y. K., Eberhard, M. O., Kim, W. S., & Kim, J. (2002). Shear strength of steel fiber-reinforced concrete beams without stirrups. *ACI Structural Journal*, *99*(4), 530-538.

Laning, A. (1992). Synthetic fibers. *Concrete Construction*, 87-90.

Lee, S. C., Oh, J. H., & Cho, J. Y. (2012). Compressive Behavior of Normal and High Strength Concrete with End-Hooked Steel Fibers.

Lee, J. Y., Shin, H. O., Yoo, D. Y., & Yoon, Y. S. (2018). Structural response of steel-fiber-reinforced concrete beams under various loading rates. *Engineering Structures*, *156*, 271-283.

Li, V. C., Ward, R., & Hamza, A. M. (1992). Steel and synthetic fibers as shear reinforcement.

Li, Y. (2016). *Blast Performance of Reinforced Concrete Beams Constructed with High-Strength Concrete and High-Strength Reinforcement* (Masters dissertation, Université d'Ottawa/University of Ottawa).

Li, Y., & Aoude, H. (2019a). Blast response of beams built with high-strength concrete and high-strength ASTM A1035 bars. *International Journal of Impact Engineering*, *130*, 41-67.

Li, Y. and Aoude, H. (2019b). Effect of steel fibers on the static and blast behavior of HSC beams built with Grade 690 MPa high-strength bars. *Engineering Structures*.

Lin, A., & Ostertag, C. P. (2017, September). Multi-Scale Pull-Out Resistance of Steel Reinforcing Bar Embedded in Hybrid Fiber Reinforced Concrete (HYFRC). In *IOP Conference Series: Materials Science and Engineering* (Vol. 246, No. 1, p. 012022). IOP Publishing.

Lok, T. S., & Pei, J. S. (1998). Flexural behavior of steel fiber reinforced concrete. *Journal of Materials in Civil Engineering*, *10*(2), 86-97.

Louw, M. J. (1992). The behaviour of RC columns under impact loading. *Civil Engineering= Siviele Ingenieurswese*, *1992*(v34i11), 371-378.

Magnusson, J., Hallgren, M., & Ansell, A. (2010). Air-blast-loaded, high-strength concrete beams. Part I: Experimental investigation. *Magazine of Concrete Research*, *62*(2), 127-136.

Mahoney, M. (2005). Structural Synthetic Fibers for Precast and Slab-on-Grade Construction. *Construction Canada*, 1-6.

Majdzadeh, F., Soleimani, S. M., & Banthia, N. (2006). Shear strength of reinforced concrete beams with a fiber concrete matrix. *Canadian Journal of Civil Engineering*, *33*(6), 726-734.

Malvar, L. J. (1998). Review of static and dynamic properties of steel reinforcing bars. *Materials Journal*, *95*(5), 609-616.

Malvar, L. J., & Ross, C. A. (1998). Review of strain rate effects for concrete in tension. *ACI Materials Journal*, *95*, 735-739.

Mansur, M. A., Ong, K. C. G., & Paramasivam, P. (1986). Shear strength of fibrous concrete beams without stirrups. *Journal of structural engineering*, *112*(9), 2066-2079.

Mensah Ababio, E., Amegadoe, D., Banahene Osei, J., & Adom-Asamoah, M. (2017). Shear Behaviour of Reinforced Normal Weight Concrete Deep Beams Using Finite Element Analysis.

Min, K. H., Kwon, K. Y., Lee, J. Y., & Yoon, Y. S. (2014). Effects of steel fibre and shear reinforcement on static and impact load resistances of concrete beams. *Magazine of Concrete Research*, *66*(19), 998-1006.

Mindess, S., & Yan, C. (1993). Perforation of plain and fibre reinforced concretes subjected to low-velocity impact loading. *Cement and Concrete Research*, *23*(1), 83-92.

Narayanan, R., & Darwish, I. Y. S. (1987). Use of steel fibers as shear reinforcement. *Structural Journal*, *84*(3), 216-227.

Navas, F. O., Navarro-Gregori, J., Herdocia, G. L., Serna, P., & Cuenca, E. (2018). An experimental study on the shear behaviour of reinforced concrete beams with macro-synthetic fibres. *Construction and Building Materials*, *169*, 888-899.

Nia, A. A., Hedayatian, M., Nili, M., & Sabet, V. A. (2012). An experimental and numerical study on how steel and polypropylene fibers affect the impact resistance in fiber-reinforced concrete. *International Journal of Impact Engineering*, *46*, 62-73.

Ohtsu, M., Uddin, F. A., Tong, W., & Murakami, K. (2007). Dynamics of spall failure in fiber reinforced concrete due to blasting. *Construction and Building Materials*, *21*(3), 511-518.

Ong, K. C. G., Basheerkhan, M., & Paramasivam, P. (1999). Resistance of fibre concrete slabs to low velocity projectile impact. *Cement and Concrete Composites*, *21*(5-6), 391-401.

Pakravan, H. R., Latifi, M., & Jamshidi, M. (2017). Hybrid short fiber reinforcement system in concrete: A review. *Construction and building materials*, *142*, 280-294.

Pantelides, C. P., Garfield, T. T., Richins, W. D., Larson, T. K., & Blakeley, J. E. (2014). Reinforced concrete and fiber reinforced concrete panels subjected to blast detonations and post-blast static tests. *Engineering structures*, *76*, 24-33.

Parra-Montesinos, G. J. (2006). Shear strength of beams with deformed steel fibers. *Concrete International*, *28*(11), 57-66.

Popovics, S. (1973). A numerical approach to the complete stress-strain curve of concrete. *Cement and concrete research*, *3*(5), 583-599.

Rajkumar, K., & Vasumathi, A. M. (2013). Flexural Behavior of Fiber Reinforced Concrete Beams Confined with FRP. In *Applied Mechanics and Materials* (Vol. 256, pp. 938-941). Trans Tech Publications.

Richardson, A., Coventry, K., Lamb, T., & Mackenzie, D. (2016). The addition of synthetic

fibres to concrete to improve impact/ballistic toughness. *Construction and Building Materials*, *121*, 612-621.

Saadun, A., Mutalib, A. A., Hamid, R., & Mussa, M. H. (2016). Behaviour of polypropylene fiber reinforced concrete under dynamic impact load. *Journal of Engineering Science and Technology (JESTEC)*, *11*(5), 684-693.

Saatcioglu, M., Lloyd, A., Jacques, E., Braimah, A., & Doudak, G. (2011). Focused research for development of a CSA standard on design and assessment of buildings subjected to blast loads. *Interim report submitted to Public Works and Government Services Canada, Hazard Mitigation and Disaster Management Research Centre, University of Ottawa, Ottawa, Canada*.

Sahoo, D. R., Solanki, A., & Kumar, A. (2014). Influence of steel and polypropylene fibers on flexural behavior of RC beams. *Journal of Materials in Civil Engineering*, *27*(8), 04014232.

Sharma, A. K. (1986). Shear strength of steel fiber reinforced concrete beams. In *Journal Proceedings* (Vol. 83, No. 4, pp. 624-628).

Suji, D., Natesan, S. C., & Murugesan, R. (2007). Experimental study on behaviors of polypropylene fibrous concrete beams. *Journal of Zhejiang University-Science A*, *8*(7), 1101-1109.

Sundar, R., Sarvanan, G., & Satheesh, V.S. (2017). Flexural Behaviour of Polyproplene Fiber Reinforced Concrete. *IJESC*, *7*(3).

Susetyo, J., Gauvreau, P., & Vecchio, F. J. (2013). Steel fiber-reinforced concrete panels in shear: Analysis and modeling. *ACI Structural Journal*, *110*(2), 285.

Tabatabaei, Z. S., Volz, J. S., Baird, J., Gliha, B. P., & Keener, D. I. (2013). Experimental and numerical analyses of long carbon fiber reinforced concrete panels exposed to blast loading. *International Journal of Impact Engineering*, *57*, 70-80.

Tahenni, T., Chemrouk, M., & Lecompte, T. (2016). Effect of steel fibers on the shear behavior of high strength concrete beams. *Construction and Building Materials*, *105*, 14-28.

Trottier, J. F., Mahoney, M., & Forgeron, D. (2002). Can synthetic fibers replace welded-wire mesh in slabs-on-ground?. *Concrete international*, *24*(11), 59-68.

Ulzurrun, G. S., & Zanuy, C. (2017). Enhancement of impact performance of reinforced concrete beams without stirrups by adding steel fibers. *Construction and Building Materials*, *145*, 166-182.

Vandewalle, L., Nemegeer, D., Balazs, L., Barr, B., Barros, J., Bartos, P., ... & Falkner, H. (2003). RILEM TC 162-TDF: Test and design methods for steel fibre reinforced concrete'-sigma-epsilon-design method-Final Recommendation. *Materials and Structures*, *36*(262), 560-567.

Vecchio, F. J., & Collins, M. P. (1986). The modified compression-field theory for reinforced concrete elements subjected to shear. *ACI J.*, *83*(2), 219-231.

Vecchio, F. J. (2000). Disturbed stress field model for reinforced concrete: formulation. *Journal of structural engineering*, *126*(9), 1070-1077.

Wang, H., & Belarbi, A. (2005). Flexural behavior of fiber-reinforced-concrete beams reinforced with FRP rebars. *ACI Structural Journal*, *SP230*, *51*(230), 895-914.

Wang, S., Zhang, M. H., & Quek, S. T. (2011). Effect of high strain rate loading on compressive behaviour of fibre-reinforced high-strength concrete. *Magazine of Concrete Research*, *63*(11), 813-827.

Weidner, A. M., Pantelides, C. P., & Richins, W. D. (2012). *Dynamic Tests of High Strength Concrete Cylinders* (No. INL/EXT-13-28118). Idaho National Laboratory (INL).

Wong, P. S., Vecchio, F. J., & Trommels, H. (2013). VecTor2 & Formworks user's manual second edition. *University of Toronto, Canada*.

Xu, H., Mindess, S., & Duca, I. J. (2004, September). Performance of plain and fiber reinforced concrete panels subjected to low velocity impact loading. In *Proceedings of RILEM conference on fiber reinforced concrete, BEFIB, Varenna, Italy* (pp. 1257-68).

Yang, J. M., Min, K. H., Shin, H. O., & Yoon, Y. S. (2012). Effect of steel and synthetic fibers on flexural behavior of high-strength concrete beams reinforced with FRP bars. *Composites Part B: Engineering*, *43*(3), 1077-1086.

Yang, J. M., Kim, J. K., & Yoo, D. Y. (2018). Flexural and shear behaviour of high-strength SFRC beams without stirrups. *Magazine of Concrete Research*, *71*(10), 503-518.

Yazdanbakhsh, A., Altoubat, S., & Rieder, K. A. (2015). Analytical study on shear strength of macro synthetic fiber reinforced concrete beams. *Engineering Structures*, *100*, 622-632.

Yin, S., Tuladhar, R., Shi, F., Combe, M., Collister, T., & Sivakugan, N. (2015). Use of macro plastic fibres in concrete: A review. *Construction and Building Materials*, *93*, 180-188.

Yoo, D. Y., Banthia, N., Kim, S. W., & Yoon, Y. S. (2015). Response of ultra-high-performance fiber-reinforced concrete beams with continuous steel reinforcement subjected to low-velocity impact loading. *Composite Structures*, *126*, 233-245.

Yoo, D. Y., Banthia, N., & Yoon, Y. S. (2017). Impact Resistance of Reinforced Ultra-High-Performance Concrete Beams with Different Steel Fibers. *ACI Structural Journal*, *114*(1).

Zhan, T., Wang, Z., & Ning, J. (2015). Failure behaviors of reinforced concrete beams subjected to high impact loading. *Engineering Failure Analysis*, *56*, 233-243.

Zhang, L. (2008). *Impact resistance of high strength fiber reinforced concrete* (Doctoral dissertation, University of British Columbia).

Zhang, C., Han, S., & Hua, Y. (2018). Flexural performance of reinforced self-consolidating concrete beams containing hybrid fibers. *Construction and Building Materials*, *174*, 11-23.

Zhang, H., Wang, L., Bai, L., Addae, M., & Neupane, A. (2019). Research on the impact response and model of hybrid basalt-macro synthetic polypropylene fiber reinforced concrete. *Construction and Building Materials*, *204*, 303-316.

Zheng, Z., & Feldman, D. (1995). Synthetic fibre-reinforced concrete. *Progress in Polymer Science, 20*(2), 185-210.